MicroRNAs in brown and white adipocytes

Federica Dimitri

A thesis presented in partial fulfilment for the degree of

Doctor of Philosophy in Medical Sciences

University of Warwick, Medical School,
Division of Cell and Developmental Biology
July 2017

Table of Contents

List of Figures

List of Tables

Acknowledgments

I would like to thank Dr Mark Christian for allowing me to undertake my Ph.D. in his laboratory. His guide through the scientific research has been fundamental for my professional growth. His passion for science and willingness to share the knowledge, have been for me what I consider as an excellent example to follow for becoming a great scientist. I am grateful for all his brilliant suggestions and constant help and support. Thanks to the University of Warwick for funding my research and for providing an amazing environment. I also would like to thank Dr Mohammad Tauqeer Alam for his great help and collaboration in the bioinformatics analysis and Dr Nigel Dyer for his contribution to it. I acknowledge Professor Fredrik Karpe for kindly donating the human cell lines and Dr Sean James for gently performing the tissue histology. Thanks to Dr Aled Clyton for welcoming me in his lab and Dr Jason Webber for his great assistance during the experiments on vesicle characterisation. I am thankful to Professor Victor Zammit and my second supervisor Dr Claire Bastie for their suggestions during the constructive meetings enthusiastically organised by Prof Zammit.

My special thanks go to the post docs and great friends Dr Lea Dib and Dr Zehra Irshad. Lea, besides taking part in some experiments, has been an enlightening guide for me. I am sincerely grateful to Zehra for her great cooperation and precious help. Their support has been priceless. I am also thankful to all my friends for always being there.

Lastly, but definitely not least, I immensely thank my family for their support and for believing in me. This helped me reach where I am today.

Declaration

This thesis is submitted to the University of Warwick in support of my application for the degree of Doctor of Philosophy. It has been composed by myself and has not been submitted in any previous application for any degree. The work presented (including data generated and data analysis) was carried out by me unless otherwise stated in the text.

Federica Dimitri

Abstract

The adipose tissue has an important role in maintaining the energy homeostasis balance. Understanding its physiology is important for the development of treatments against diseases where this equilibrium is compromised, such as obesity and associated metabolic disorders. MicroRNAs (miRNAs) are important gene regulators and an increasing body of evidence suggests their involvement in adipogenesis and adipose metabolism. MiRNAs can also be secreted into the extracellular environment and be taken up by distal cells, mediating cell-to-cell communication. However, very little is known about adipose tissue-derived circulating miRNAs. Through miRNA PCR array analysis we identified several miRNAs that are differentially secreted among mouse undifferentiated and differentiated brown and white adipocytes, among which, miR-196a and miR-378a-3p showed a conservative pattern of secretion in different adipocyte models. MiR-138-5p was identified as the unique miRNA differentially secreted between human brown and white adipocytes. Bioinformatics target prediction revealed that these miRNAs are potentially involved in important processes regulating the functioning of adipose tissue and its cross-talk with distal cells. By ultracentrifugation of adipose conditioned media and Nanosight technology, we investigated vesicle and vesicle-free miRNA carriers and characterized adipose derived vesicles. Finally, through microRNA array and mRNA sequencing we identified genes, miRNAs and pathways differentially enriched in human brown and white adipocytes contributing to improve the knowledge on the nature of human adipocytes, hampered by the scarce availability of human brown adipose samples. Through integration of the two analyses, we identify poorly known or novel miRNAs, potentially involved in the pathways associated with the genes differentially expressed between human brown and white adipocytes. Among the significantly downregulated miRNAs in brown versus white adipocytes we highlighted miR-513a-3p, miR-4511 and miR-4328. While, among the significantly upregulated miRNAs in brown versus white we highlighted miR-4698, miR-4516, miR-4531, miR-29a-3p and miR-3915.

List of abbreviations

ACC	Acetyl-CoA Carboxylase
ACOX1	Acyl- CoA oxidase 1
ACSL1	Acyl-CoA synthase 1
ADAM	ADAM metallopeptidase domain
ADIPOQ	Adiponectin
ADMSC	Adipose derived stem cells
Ago	Argonaute
aP2	Adipocyte protein 2
ATGL	Adipose triglyceride lipase
ATP	Adenosine triphosphate
B	Brown
BAT	brown adipose tissue
BMP	Bone morphogenetic protein
C/EBPs	CCAAT/enancher binding proteins
C57BL/6	C57 black mouse 6
CACT	Carnitine/acylcarnitine translocase
cAMP	Cyclic adenosine monophosphate
CARD	Caspase recruitment domain
CCL2	C-C Motif Chemokine Ligand 2
CD	Cluster of differentiattion
CDK6	Cyclin Dependent Kinase 6
cDNA	Complementary DNA
CG-I58	ATGL-coactivator comparative gene identification-58
ChIP	Chromatin Immunoprecipitation assays
CIDEA	Cell death-inducing DFFA-like effector a
CL	CL 316,243
COX-2	Cyclooxygenase-2
CPT	Carnitine palmitoyltransferase
Cq	Quantification cycle
CREB	cAMP response element binding protein
Cre-LBD	Cre-ligand binding domain
CXCL16	Chemokine (C-X-C motif) ligand 16
CXCR6	Chemokine (C-X-C Motif) Receptor 6
DAMPs	Damage associated molecular patterns
DB	Differentiated brown adipocytes
DCP1	Decapping protein 1
DCP2	Decapping protein 2
DC-SIGN	Dendritic ell-specific intercellular adhesion molecule-3-grabbing non-integrin
ddCq	Delta delta Cq
Dex	Dexamethasone
DGCR8	DiGeorge syndrome critical region 8

DLS	Dynamic Light Scattering
DMEM/F12	Dulbecco's Modified Eagle Medium/Nutrient Mixture F-12
DMSO	Dimethyl sulfoxide
DNA	Deoxyribonucleic acid
DNMT3A	DNA methyltransferase 3 (DNMT3A)
dsRBD	Double-stranded RNA binding domain
DW	Differentiated white adipocytes
EC	Endothelial cells
ECAR	Extracellular acidification rate
ECM	Extracellular matrix
EDC4	Enhancer of mRNA decapping 4
EDTA	Ethylenediaminetetraacetic acid
EID1	EP300 inhibitor of differentiation 1
eIF4E	Eukaryotic translation initiation factor 4E
eIF4F	Eukaryotic translation initiation factor 4F
Eif4g	Eukaryotic translation initiation factor 4G
Elovl3	Elongation of very long chain fatty acids protein
ERK	Extracellular signal-regulated protein kinase
EXO5	Exportin 5
FA	Fatty acid
FABPs	Fatty acid binding proteins
FADH	Flavin adenine dinucleotide + H
FADS2	Fatty acid desaturase 2
FAS	Fatty acid synthase
FATP	Fatty Acid Transporter Proteins
FBS	Fetal bovine serum
FC	Fold change
FGF-21	Fibroblast growth factor 21
G0S2	G0/G1 switch gene 2
G418	Geneticin 418
GDP	Guanosine diphosphate
GLUT4	Glucose transporter type 4
GSK3β	Glycogen synthase kinase-3 β
GTP	Guanosine-5'-triphosphate
GW182	Glycine-tryptophan protein of 182 kDa
H	Hydrogen
HB-EGF	Heparin-binding EGF-like growth factor
HD	Huntington Disease
HDL	High density lipoprotein
HEK	human foreskin fibroblast
HFD	High fat diet
HIF1	Hypoxia-inducible factor
HOXC	Homeobox cluster

HOXC8	Homeobox C8
HS	Heparan Sulphate
HSA	Homo Sapiens
HSL	Hormone sensitive lipase
HSP	Heparan sulfate proteoglycans
HSP	Heat shock protein
HSP70	Heat shock proteins 70
HSP90	Heat shock proteins 90
HSPG	Heparan Sulphate proteoglycans
IBMX	3-isobutil-1-methylxanthine
IgG	Immunoglobulin G
IKBA	NF-kB inhibitor alpha
IKKαß	IkB kinase alpha/beta
IKKβ–NF-κB	IκB kinase-β–NF-κB
IL	Interleukin
IL1RA	Interleukin-1 receptor antagonist
IL6R	Interleukin-6 receptor
ILV	Intraluminal vesicle
Indo	Indomethacin
INF	Interferon
IRS	Insulin receptor substrate
IRS	Insulin receptors substrates
ISO	Isoproterenol
IκB	Inhibitor of NF-κB
JNK–AP1	Jun N-terminal kinase–activator protein-1
KEGG	Kyoto encyclopaedia of genes and genome
KLF5	Kruppel-like factor 5
KO	Knock Out
KO	Knocked Out
LBD ER	Ligand-binding domain of the estrogen receptor
LBP	LPS Binding Protein
LCFA	Long chain fatty acids
LDHA	Lactate dehydrogenase A
LNA	Locked nucleic acid
lncRNA	Long non-coding genes
Lowess	LOcally WEighted Scatterplot Smoothing
LPL	Lipoprotein Lipase
LRR	Leucine-Rich Repeat
MAPK	Mitogen-activated protein kinase
MD2	Differentiation factor 2 also known as lymphocyte antigen 96
MEF2C	Myocyte enhancer factor 2
MEF2D	Myocyte enhancer eactor 2D
MGL	Monoacylglycerol lipase

MID88	Myeloid differentiation primary response gene 88
miRNA	MicroRNA
MLV	Multi-lamellar vesicle
M-MLV	Moloney murine leukemia virus reverse transcriptase
MMPs	Matrix metalloproteinases
Mmu	Mus musculus
MREs	miRNA response elements
MRI	Magnetic Resonance Imaging
mRNA	messenger RNA
MSC	Multipotent stem-cells
MUC1	Mucin 1
MVB	Multi-vesicular bodies
MVs	Multi-vesicles
NADH	Nicotinamide adenine dinucleotide + H
NAFLD	Non-alcoholic-fatty liver disease
ND	Non-detectable
NF-kB	Nuclear factor
NGS	Next generation sequencing
NLRP3	NLR containing protein 3
NLRs	NOD-like receptors
NOD	Nucleotide-binding Oligomerization Domain
NPMI	Nucleophosmin I
NRP-1	Neuropilin-1
nSMase2	Sphingomyelinase 2
NTA	Nanoparticle tracking analysis
OCR	Oxygen consumption rate
OPN	Osteopontin
ORO	Red Oil O
P2	Purinergic receptor
PAMPs	Pathogen associated molecular patterns
PAZ	Pwi Argonaute Zwille
PC1	Principal component 1
PC2	Principal component 2
PCA	Principal component analysis
PCR	Polymerase chain reaction
PDGRF-α	Platelet-derived growth factor receptor-α
PED1B	Phosphodiesterase 1B
pen/strep	Penicillin/streptomycin
PET/CT	Positron Emission Tomography associated with Computer Tomography
PG	Prostaglandin
PGC-1α	PPARγ activator 1α
PI3k	Phosphoinositide 3-kinase
PKA	Protein kinase A

PKA	Protein kinase A
PKB	Protein kinase B
Poly (A)	Poly-adenosine
Poly (T)	Poly-thymine
PPAR	Peroxisome proliferator-activated receptor
PRDM16	PR domain zinc-finger protein 16
Pref-1	pre-adipocyte factor-1
PYD	Pyrin domain
Q-RT PCR	Quantitative real-time polymerase chain reaction
Rb	Retinoblastoma
RBL	Retinoblastoma like protein
RIP140	Receptor-interacting protein 140
RIP140	Nuclear co-repressor receptor 140
RISC	RNA-induced silencing complex
RNA pol	RNA polymerase
ROS	Reactive oxygen species
Rosi	Rosiglitazone
RT	Room temperature
RUNX1	Runt-related transcription factor 1
RUNX1T1	RUNX1 Translocation Partner 1
RXR	Retinoid acid receptor
SAT	Subcutaneous adipose tissue
SCD	Stearoyl-CoA desaturase
SEM	Standard error mean
SEPN1	Selenoprotein N1
SNS	Sympathetic Nervous System
SRC	Steroid receptor co-activator
ß-ARs	ß-adrenergic receptors
ssRNA	Single-stranded RNA
SULF1	Sulfatase 1
SV40	Simian virus 40
SVF	Stromal vascular fraction
T2D	Type 2 diabetes
T3	Triiodothyronine
TAR	Trans-activator
Tbx15	Transcription factor 15
TGF-β1	Transforming growth factor beta 1
TIMPs	Tissue inhibitors of metalloproteinases
TIRAP	Toll-IL-1 receptor (TIR) domain-containing adapter protein
TLRs	Toll-like receptors
TMEM26	Transmembrane protein 26
TNFα	Tumor necrosis factor α
TRAM	Translocating Chain-Associated Membrane Protein

TRBP	Trans-activator RNA binding protein
TRF	Time resolved fluorometry
TRIF	TIR Domain Containing Adaptor Inducing Interferon-ß
TZD	Thiazolidine
UB	Undifferentiated brown adipocytes
UCP1	Uncoupling Protein 1
UTR	Untranslated region
UV	Ultraviolet
UW	Undifferentiated white
VEGF	Vascular endothelial growth factor
VEGFR	VEGF receptor
VLCFA	Very long chain fatty acid
W	White
WAT	White adipose tissue
XIAP	X-linked inhibitor of apoptosis
XRN1	Exoribonuclease 1
ΔCq	Normalised Cqs

Chapter 1- Introduction

1.1 The adipose tissue

Adipose tissue is the main site for storing energy and in healthy conditions it constitutes 20% of the body weight [1]. Different types of adipose tissue exist and can be subdivided into two main categories, brown adipose tissue (BAT) and white adipose tissue (WAT). WAT and BAT cooperate in maintaining a delicate equilibrium between fat accumulation and energy dissipation, thus they present different structure, functions and location. However, both consist of a heterogeneous population of cells including endothelial cells, immune cells and pre-adipocytes. The pre-adipocytes, under differentiation stimuli, develop into mature brown or white, adipocytes that constitute the major cellular component of the tissue. Both tissues are innervated by the sympathetic nervous system (SNS) [2] even though at a different grade, with BAT being more highly innervated and vascularized than WAT.

Depending on its location, WAT is classified either as subcutaneous (SAT, under the skin) or visceral (mesenteric, gonadal, perirenal and omental). White adipocytes present a diameter comprised between 30-200 μm. Larger adipocytes are generally more highly metabolic and release more factors attracting immune cells [3]. WAT functions as an endocrine organ [4, 5] and a store of energy by accumulating triglycerides into a single large lipid droplet that occupies a central position in the mature adipocytes. The periphery includes the nucleus and few mitochondria.

In contrast, brown adipocytes are much smaller (15-60 μm in diameter) [6], their nucleus occupies a central position and triglycerides are stored in small multilocular lipid droplets. This increases the surface exposed to lipases to allowing easy access to the lipids that can be rapidly catabolised [7]. Brown adipocytes also contain a large number of mitochondria expressing high levels of uncoupling protein 1 (UCP1) in the inner membrane. This protein is responsible for non-shivering heat production in the brown adipocytes thus playing an important role in body temperature regulation [8]. BAT is present in mammals, in mice and human newborns it is principally located in the interscapular area. In humans its amount strongly decreases with the growth [9]. However recent PET/CT-scans (Positron Emission Tomography associated with Computed Tomography) demonstrated the presence of BAT in the supraclavicular, suprarenal, paravertebral areas and in the neck of healthy men exposed to cold temperature [10-12]. These data were then confirmed with the safer magnetic resonance imaging (MRI)

technique. [13] Moreover, cells with high thermogenic activity were found within white depots [14]. In murine experiments, Petrovic et al., induced epididymal fat cells to express high level of UCP1 enabling these cells to dissipate energy and present a brown-like phenotype, though, still keeping some classical white fat gene expression [15]. This introduced the concept of brite/beige adipocytes, which means brown in white. Lately beige adipocytes have been demonstrated to be distinct from classic brown adipocytes [16] and to arise from white adipocyte transdifferentiation [17].

1.1.1 *Fat tissue development*

WAT develops soon after birth, while, BAT starts to form during the prenatal stage, in order to provide an immediate protection from the extrauterine colder temperature [18]. Both BAT and WAT derive from the mesoderm, which originates from mesenchymal (MSC) stem-cells, where the microenvironment contributes to the generation of mature adipocytes. MSCs are multipotent stem-cells which can self-renew and originate myocytes, chondrocytes, osteocytes, neurons, besides adipocytes [19]. White adipocytes derive from the Myf5-negative lineage, while classical brown adipocytes come from the Myf5-positive precursor, which is in common with myocytes. In these common precursors, PR-domain zinc-finger protein 16 (PRDM16) and CCAAT/enancher binding protein ß (C/EBPß) are the major players for suppression of muscle phenotype in favour of the brown phenotype [20]. However, in a recent study, white adipocytes in the interscapular and retroperitoneal area were found to be descended from Myf5-positive progenitors as well [13].

1.1.1.1 *Adipogenesis: determination and differentiation*

Although they have opposing functions and morphologic differences, the processes underling BAT and WAT development is regulated by an initial common cascade of events that takes different directions in the later stages of differentiation. Adipogenesis can be divided in two main phases: determination and differentiation. The first stage, determination, ends with the irreversible conversion of the pluripotent stem-cells into committed pre-adipocytes that have partially lost the differentiation potential [21]. In *vivo*, the events occurring between these two stages are still unknown. However, in *vitro*, committed pre-adipocyte proliferation is strongly reduced due to contact inhibition, as long as no stimuli occur to induce the final differentiation [22]. These cells

express the pre-adipocyte factor-1 (Pref-1) that, in its soluble active form, prevents adipocyte differentiation [23]. The re-entry in the cell cycle is then induced by hormonal stimuli and differentiation is reached upon activation of a cascade of transcriptional factors where, the most important protagonists are peroxisome proliferator-activated receptor γ (PPARγ) and CCAAT/enhancer binding proteins (C/EBPs) [22]. Some proteins responsible for cell-cycle regulation have been found to also control adipocyte differentiation. In particular, E2F transcription factor is inhibited by C/EBPα and also indirectly by PPARγ [24]. E2F inhibition leads to a second growth arrest that allows cells to undergo the final stages of differentiation. E2F is also inhibited by the retinoblastoma proteins Rb, Rb-like proteins 1 and 2 (RBL1 and RBL2) also known as p107 and p130 respectively [22] . More interesting, Rb and p107 have been proposed to be involved in the switch of white versus brown adipogenesis [25].

1.1.1.2 *PPARγ and C/EBPs*

PPARγ is a nuclear receptor and ligand-activated transcription factor and it is activated by thiazolidinedione (TZD) drugs, oxidized and unsaturated fatty acids, prostaglandins and eicosanoids. However, no endogenous ligands have been identified to induce PPARγ activation with comparable or higher efficiency than TZDs [26]. In addition to its crucial role in activation of adipogenesis, PPARγ expression is also fundamental for the maintenance of mature adipocytes [15]. Three different isoforms of PPARγ exist: PPARγ1, 2 and 3. The most expressed isoform in adipocytes is PPARγ2, which heterodimerizes with the retinoid X receptor (RXR), recruits cofactor proteins and in concert with these, unfolds the DNA structure in determined regions. This enable gene transcription and adipocyte differentiation [15].

C/EBPs are members of the C/EBP basic-leucine zipper protein family. C/EBPβ and C/EBPδ are induced at the early stage of adipocyte differentiation and in turn, increase the expression of C/EBPα. C/EBPβ is induced by the phosphorylated form of cyclic adenosine monophosphate (cAMP) response element binding protein (CREB) [27] and is activated by mitogen-activated protein kinase (MAPK) and glycogen synthase kinase-3 β (GSK3β) [28]. Phosphorylated C/EBPβ dimerizes with another C/EBPβ monomer forming a DNA binding domain which promotes the expression of other genes including C/EBPα and PPARγ. C/EBPα expression leads to cell proliferation arrest and transcription of several adipocyte genes such as adipocyte protein 2 (aP2) and glucose

transporter 4 (GLUT4) [29]. Most important, C/EBPα maintains PPARγ expression and vice versa. C/EBPβ and C/EBPδ action is likely to be redundant since adipocyte differentiation is strongly affected only upon concurrent deletion of the two genes [30]. Moreover, C/EBPβ may compensate C/EBPα absence in brown adipocytes development. Indeed, C/EBPα ablation in mice prevented WAT development but did not impair BAT adipogenesis [22].

1.1.1.3 *Brown adipose tissue and beige adipocyte differentiation*

BAT has been proposed as a potential alternative strategy to fight obesity since its activation would increase lipolysis preventing fat deposition in peripheral tissues non specialized in fat storage [31]. Indeed, mice with high brown/beige fat depots present elevated insulin sensitivity, glucose tolerance and obesity resistance [32]. Interestingly, beige adipocytes activated upon cold exposure or β-adrenergic stimuli, have been shown to play a more consistent role in this process than pre-existing interscapular brown adipocytes [33]. Among the different types of white adipose tissues, subcutaneous depots are more predisposed for acquisition of thermogenic characteristics [34]. Beige cells show molecular signatures distinct from both white and brown adipocytes. Among beige-selective genes, there are the developmental transcription factor 15 (Tbx15) and plasma membrane proteins such as transmembrane protein 26 (TMEM26) and CD137 [16, 35]. In addition, platelet-derived growth factor receptor-α (Pdgfr-α) has been found to be a marker for white precursor with potential ability of differentiation into beige adipocytes [36]. However, one of the most evident differences between constitutive brown and inducible beige adipocytes is that the former express UCP1 at high extent even in absence of stimuli, while beige adipocytes activate UCP1 and the thermogenic program only after cold exposure or β-adrenergic stimulation [15, 37]. Several proposals regarding beige cells origins have been suggested, such as derivation from resident stem cells in WAT depot [36], recruitment of stem cells in WAT from other tissues [38] or trans-differentiation of mature white adipocytes [39]. However, one hypothesis does not necessary exclude the other ones. Despite descending from two different lineages, thermogenic activity in brown and beige adipocytes is apparently promoted by the same cascade of events that leads to UCP1 expression. In *vivo*, activation of the thermogenic program in fat cells is predominantly under the control of the SNS. SNS activated by cold temperatures, through norepinephrine release, triggers activation of specific genes

reputed to promote the program for heat production. This signalling pathway is mediated by ß-adrenergic receptors, described more in details below. One of the pathways involved in recruiting beige cells upon β3-adrenergic stimulation is represented by Cyclooxygenase-2 (COX-2) activation. Up-regulation of this enzyme induces the synthesis of Prostaglandins (PGs), which are able to promote the browning effect in WAT [40].

Another protein downstream of β-adrenergic signalling and involved in the thermogenic program is the Fibroblast growth factor 21 (FGF-21). It positively regulates glucose uptake in adipocytes and is generally produced and secreted by the liver [41]. However, activation of protein kinase A (PKA) and p38 MAPK, following β-adrenergic stimulation, induces brown adipocytes to became a source of FGF-21 as well [42]. FGF-21 importance in non-shivering heat production is demonstrated by the fact that FGF-21 Knock Out (KO) mice fail to activate an appropriate thermogenic program when exposed to cold temperatures [43].

A combination of all the pathways discussed above leads to a molecular cascade of numerous transcription factors that induce fat cells to acquire the specific characteristics for cold adaptation [44].

The presence of PPARγ and C/EBPs is a prerequisite for brown and beige adipogenesis and their sustained expression plays a key role in maintaining the characteristics of mature adipocytes. Though, PPARγ and C/EBPα co-expression leads mesenchymal stem cells to only develop into white adipocytes [45]. Hence, PPARγ and C/EBPs, even if necessary, are not brown/beige-specific determinant factors. Indeed, brown/beige cell fate is subject to PRDM16 and PPARγ activator 1α (PGC-1α). However, while PGC-1α plays an important role in thermogenesis but is not decisive in phenotype determination, PRDM16 is strictly necessary for both the phenomena. In fact, in the absence of PGC-1α, several classical-brown genes are normally expressed, even though, thermogenesis activity is strongly impaired [46, 47]. On the contrary, in mice, lack of PRDM16 leads to the expression of a myocyte phenotype in BAT and negatively affects thermogenic activity [48].

PGC-1α is induced under cold exposure through activation of the PKA-CREB (cAMP response element binding protein) pathway [49, 50] and by FGF-21 [43] and regulates mitochondria biogenesis [43]. Its expression in white adipocytes, triggers the

transcription of genes involved in thermogenic activity, in particular UCP1 [51]. On the other hand, a factor responsible for PGC-1α inhibition through direct interaction is the corepressor RIP140 [52]. Another level of PGC-1α regulation is represented by several steroid receptor coactivators (SRC) such as SRC-1 and SRC-2, which respectively, promotes and inhibits PGC-1α- PPARγ interactions [53]. Interestingly, as discovered recently, PGC-1α in muscle cells regulates the expression of Irisin, a membrane protein that is secreted in the plasma, especially upon physical exercise. In mice, released Irisin, induced high thermogenic activity and beige cell formation in WAT depots [54].

PRDM16 is a protein with seven zinc-finger domains through which it binds specific DNA regions [55]. However, Seale et al., demonstrated that its predominant mechanism of action in adipocytes is by direct interaction with proteins such as PGC-1α, PGC-1β, PPARα and PPARγ [56]. PRDM16, besides directly promoting the classical-brown fat genes, such as PGC-1α, UCP1 and cell death-inducing DFFA-like effector A (CIDEA) [48, 56, 57], inhibits specific white fat and muscle gene expression [57]. PRDM16 gene ablation resulted in primary brown pre-adipocyte differentiation into skeletal muscle [57]. Signaling stimulated by bone morphogenetic protein BMPs inhibit myogenesis [58]. Tseng et *al,* demonstrated that PRDM16 expression is positively regulated by BMP7 in brown precursor derived from mice [59].

1.1.2 *Fatty acid biosynthesis lipolysis and beta oxidation*

The ability to accumulate lipids can be considered as an evolutionary strategy to store energy in order to encounter relatively long periods of food scarcity. Animals such as C. elegans, Drosophila and sharks store lipids in gut cells, fat body and liver respectively [60-62]. The development of specialised fat depots in mammals implicates a high level of coordination among these tissues and other organs to regulate food intake, lipid absorption and transport, fatty acid biosynthesis and oxidation in order to maintain the homeostatic balance. Adipose tissue secretes a large number of hormones and cytokines, grouped under the name of adipokines [63] that contribute to the cross-talk among fat depots and distal tissues/organs. For example, leptin, also known as satiety hormone, is released in response to food intake by the adipose tissue and stimulates the hypothalamus to suppress appetite [64-66]. Mice with leptin mutation *ob/ob* or leptin receptor mutation *db*/*db* are phenotypically indistinguishable from wild type littermates at birth, but become obese because of uncontrolled appetite and consequent excess food

intake [67, 68]. Paradoxically, obese subjects present high concentrations of this hormone in the circulation. However, in obesity, hypothalamic resistance to leptin abolishes the beneficial effect of the satiety hormone [66].

Another important adipokine released by adipocytes in the blood stream is adiponectin [69]. This protein, encoded by the ADIPOQ gene, has anti-inflammatory functions and promotes lipid oxidation. Therefore, it promotes insulin sensitivity and protects against obesity [70-72], indeed, levels of circulating adiponectin is reduced in obese subjects and increase after weight loss [73].

Several other factors control fatty acid oxidation, that takes place mainly in brown adipocytes and is accelerated in the thermogenic process activated by ß-adrenergic stimuli or promoted by diet [10]. The two main sources of fuel for brown adipocytes consist of lipids taken from the circulation and lipids synthesised *de novo* by the lipogenesis process.

1.1.2.1 *Fatty acid uptake*

After absorption in the intestine, lipids are transported into the blood stream via the lymphatic system, packed into lipoproteins such as chylomicrons to reduce hydrophobicity. In the blood streams the Lipoprotein Lipase (LPL) catalyses the hydrolysis of the triglycerides from the chylomicrons into monoacylglycerol and free fatty acids that can be internalized by the brown adipocytes by different fatty acid transporter proteins (FATPs) and cluster of differentiation (CD) 36 (CD36) expressed on the cytoplasmic membrane [74]. In the cytoplasm, fatty acid binding proteins (FABP) such as FABP3, FABP5 and FABP4, also known as aP2, bind to the internalized fatty acids to prevent their lipotoxicity on cellular structures [75, 76]. Fatty acids (FAs) can then be oxidised or alternatively stored (figure 1).

1.1.2.2 *Lipogenesis*

De novo fatty acid synthesis is initiated by acetyl coenzyme A (acetyl-CoA) carboxylase (ACC), which, from Acetyl-CoA, forms Malonyl-CoA, that, in turn, is converted into palmitate, a 16 carbon saturated fatty acid, by the fatty acid synthase (FAS). Fatty acid chains of palmitate molecules are elongated by elongase enzymes such as elongation of very long chain fatty acids protein 3 (ELOVL3), which are located on the membrane of the endoplasmic reticulum. Fatty acids are then desaturated through the introduction of double bonds in determined positions of the chain by desaturase enzymes

such as stearoyl-CoA desaturase (SCD). At this stage, fatty acids are esterified and either stored into lipid droplets in the form of triacylglycerides or oxidised [77].

1.1.2.3 *Lipid storage*

Triacylglycerides are packaged into lipid droplets surrounded by a phospholipidic layer where specific proteins, such as CIDEA and adipose triglyceride lipase (ATGL), control lipid droplet enlargement and lipolysis, respectively. As mentioned before, CIDEA mRNA is upregulated during adipogenesis and is considered as a brown marker. However its expression is downregulated after cold stimuli [78] and mice lacking the CIDEA gene are resistant to diet induced obesity [79].

1.1.2.4 *Lipolysis and fatty acid oxidation*

Release of lipids from the lipid droplets is permitted by the lipolysis process that can be catalysed either by acid lysosomal lipases or by enzymes that work at neutral pH (neutral lipolysis). The most important lipases involved in neutral lipolysis are the adipose triglyceride lipase (ATGL), the hormone sensitive lipase (HSL) and the monoacylglycerol lipase (MGL) which control three different steps of the process and catalyse the formation of three different types of free fatty acids (FFAs): diacylglycerol (DG), monoacylglycerol (MG) and deglycerinated FFA respectively (reviewed in [77]). Long chain fatty acids (LCFA) can then be oxidized in the mitochondria and the very long chain fatty acid (VLCFA) in the peroxisome. However, the major contribution for thermogenesis is given by the mitochondrial fatty acid oxidation. This process is mediated by the acyl-CoA synthase 1 (ACSL1) and the carnitine palmitoyltransferase (CPT) system. Briefly, ACSL converts LCFAs into LCFAs-CoA which are in turn converted into LCFAs-carnitine by CPT-1ß through a trans-esterification reaction of the fatty acyl group. The carnitine/acylcarnitine translocase (CACT) transports the acylcarnitines into the mitochondrial matrix. Here, CPT-2 reconverts the LCFA-acylcarnitine into LCFA-CoA which are then transferred into the mitochondrial inner membrane space and ß-oxidized. This results in nicotinamide adenine dinucleotide (NAD) + hydrogen (H) (NADH) and flavin adenine dinucleotide + H (FADH) generation which transfer the electrons to the electron transport chain allowing the proton pumps to create the proton gradient for adenosine triphosphate (ATP) production or thermogenesis.

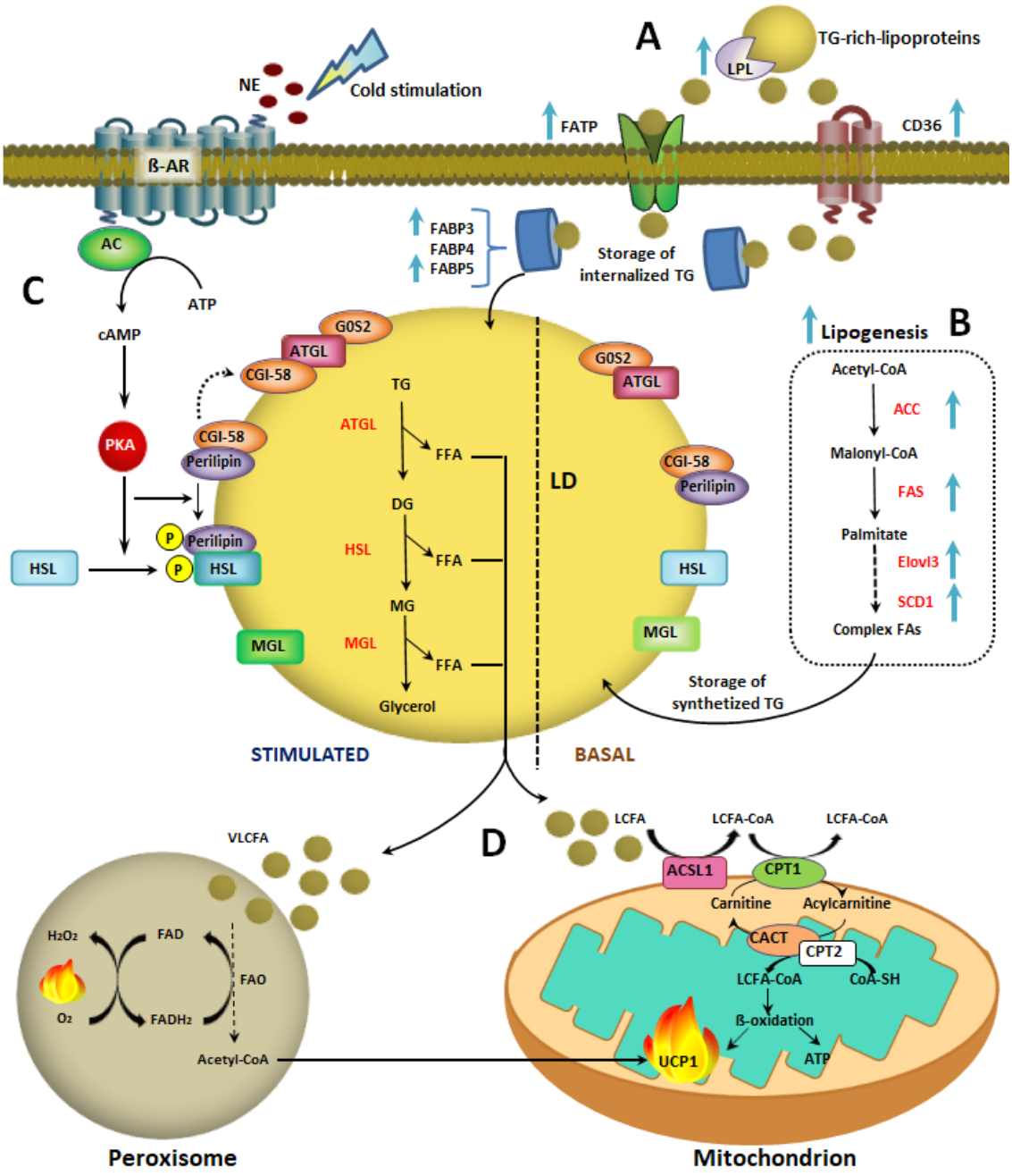

Figure 1 Lipid metabolism in adipocytes.
Figure modified from [77]. **A)** Fatty acid uptake in brown adipocytes. LPL catalyses the release of free fatty acids (FFAs) from lipoproteins. FFAs are taken up by proteins such as cluster of differentiation 36 (CD63), FA transport proteins transport FFAs. Once in the cytoplasm, FFAs are transported by fatty acid binding proteins (FABPs) into lipid droplets (LD). **B)** Lipogenesis. Alternatively to FFAs uptake, the cell can synthesise lipids by lipogenesis, which occurs in the cytoplasm. Product/substrate are indicated in black, while enzymes catalysing the transformation of substrates into the following products are in red. Fatty acid synthase (FAS) catalyses multiple reactions, resulting in the final product of palmitate (dashed arrow). Synthetized FFAs can be esterified for fatty acid oxidation or stored into lipid droplets. Enhancement of processes or protein expression upon ß-adrenergic stimuli are indicated by blue arrows. **C)** Fatty acid mobilization (neutral lipolysis) for oxidation, upon cold stimuli. With neutral lipolysis the hydrolysis of triglycerides triggers to release of glycerol and 3 FFAs that are used for thermogenesis. The enzymes involved in this proces are: adipose triglyceride lipase (ATGL), the hormone sensitive lipase (HSL) and the monoacylglycerol lipase (MGL). In basal conditions, G0/G1 switch gene 2 (G0S2) inhibits

ATGL and ATGL-coactivator comparative gene identification-58 (CG-I58) is sequestered by perilipin. Upon ß-adrenergic stimuli, activated PKA phosphorylates HSL, that translocates onto the membrane of LDs. Perilipin, phosphorylated by PKA releases CG-I58, which, in turn fully activates ATGL. D) Mobilized long chain fatty acids (LCFA) are then oxidised for heat production in mitochondria, while very long chain fatty acids are oxidised in the peroxisome.

1.1.2.5 *Thermogenesis*

Thermogenesis is the process of heat generation by burning calories and can be obligatory or adaptive. In the obligatory thermogenesis, heat is the result of the metabolic activity necessary for the basic functioning of the organism [80]. Adaptive thermogenesis is a regulated process for active heat production in response to external temperature and it can be classified as shivering and non-shivering [81]. The first one takes place in muscles, while, the latter one occurs in BAT and/or in WAT upon acquisition of brown-like features. Non-shivering thermogenesis can be induced either by temperature or diet [82, 83]. As mentioned before, the key factor for non-shivering heat production is UCP1, also known as Slc25a7 and thermogenin, located in the inner membrane of mitochondria principally in BAT and beige adipocytes. UCP1 belongs to the UCP family which comprises 5 members of anionic carrier transporters with similar structure but different tissue distribution. UCP2 is ubiquitous, UCP3 is mainly expressed in muscles, while UCP4 and 5 are in the brain. Whereas ATP is the final product of coupled respiration, energy dissipation can be facilitated by the uncoupling of respiration by UCP1 and other inner membrane proteins, which creates a gap in the oxidative respiratory chain so that the protons pumped in the intermembrane area return in the mitochondrial matrix. Therefore the proton flux cannot reach the ATP synthase machinery resulting in heat generation instead of ATP synthesis [84]. This mechanism and therefore lipid consumption can be protracted at higher rate and independently of ATP saturating concentration [85]. UCP1 activity is under the control of ß-adrenergic receptors (ß-ARs).

The β-adrenergic receptors, which are classified as β1, β2 and β3 are expressed on the cell membrane, coupled with Gαs-proteins. β1-adrenergic receptor stimulation triggers constitutive BAT precursor proliferation, while, β3-adrenergic signalling is responsible for beige adipocyte differentiation and activation in WAT depots [86]. The β3-adrenergic receptors are expressed on fat cells rather than other type of cells, but their stimulation in humans did not lead to a significant recruitment of beige cells in white tissues [8]. The ß2-adrenergic receptors are mainly expressed in the vasculature of the adipose tissue but not on the adipocytes [87].

Under stimuli, such as cold temperature exposure, norepinephrine is released by the SNS, and binds to the ß-AR. This causes a conformational change in the receptor and consequent activation of the coupled G protein. The Gαs subunit of the coupled G protein can exchange guanosine diphosphate (GDP) with guanosine triphosphate (GTP) and dissociate from the Gßɣ subunits, activating the adenylate cyclase, which triggers an increase in cAMP and PKA activation. PKA phosphorylates the Hormone-Sensitive Lipase, which in turn converts triacylglycerol into free fatty acids activating UCP1 and thermogenesis. This process also increases LPL activity in order to provide further fuel [88], indeed lipids absorbed via LPL were demonstrated to be is the major source of fatty acids in BAT [89]. However, ß-adrenergic stimulation also enhances de novo lipogenesis [90]

The coordination of BAT and WAT functions is a prerogative for the balance between energy storage and consumption of excessive fatty acids. The major factor compromising this equilibrium, nowadays, is represented by excessive food intake which leads to obesity and associated metabolic disorders such as insulin resistance, type 2 diabetes (T2D) [91] and atherosclerosis [92]. The brown adipose tissue plays an important function in controlling fatty acid metabolism and counteracting obesity and it was shown that it is reduced in obese patients [10]

1.1.3 *Obesity and adipose tissue dysfunction*

Obesity is among the pathologies with the highest incidence in developed countries, mostly due to factors such a large availability of food, unhealthy diet rich in fat and carbohydrate and sedentary life style. Upon high fat intake WAT mass increases as adipocytes store excessive lipid. The two existing mechanism for adipose tissue expansion consist of increasing adipocytes size, defined as hypertrophy and increasing adipocytes number or hyperplasia. Studies on mice suggested that increased adipogenesis and therefore increased number of adipocytes occurs after achievement of the maximal size expansion of the pre-existing adipocytes [93, 94]. The coexistence of adipocyte hypertrophy and adipocyte hyperplasia is mainly observed in obese children [95, 96] . In contrast, as lean and obese human adults present a similar adipocyte turnover, adipocyte hypertrophy is thought to be the main mechanism occurring in adulthood for WAT mass growth, as well as the one causing adipose tissue dysfunction and related disorders [97, 98].

During AT development or gain/loss of weight, different component of the adipose tissue contribute to the correct remodelling of the adipose depots. The major players involved in providing the conditions necessary for adipocyte growth and de novo adipogenesis are the extracellular matrix, endothelial cells and the immune cells, which functions are compromised in obesity.

1.1.3.1 *Angiogenesis in the adipose tissue*

Compared to other tissues, which size remain almost unvaried after completing the development, the adipose tissue has a striking ability to expand and regress through the whole course of the life, depending on the caloric availability. This plasticity requires a dynamic vascularization support ensuring the appropriated oxygen and nutrient supply as well as the clearance of toxic waste products. This mechanism has to be accompanied by re-modelling of the extracellular matrix (ECM) and requires communication between adipocytes and endothelial cells. Angiogenesis occurs during tissue development/repair by formation of new vessels that sprout form pre-existing ones. Briefly: the process starts with endothelial cell (EC) proliferation triggered by pro-angiogenic stimuli and followed by EC migration through the ECM to the site of new vessel formation where the capillary wall is degraded by extracellular proteinases. The cells establish intercellular junctions and organise themselves to form the lumen and connect to other new forming tubes (anastomosis). Each step requires a high degree of regulation that may be different from tissue to tissue. Vascular Endothelial Growth Factor A (VEGFA) is considered the master regulator of angiogenesis in adipose tissue and hypoxia is a potent stimulus that triggers its transcription. In normoxic conditions, oxygen-dependent enzymes, such as oxygen-dependent prolyl hydroxylases induce degradation of hypoxia-inducible factor 1- alpha (HIF1α) preventing dimerization with HIF1ß. Hypoxia inactivates the oxygen-dependent enzymes and HIF1α dimerizes with HIF1ß forming the complex HIF1, which induces the transcription of vascular endothelial growth factor (VEGF). Studies on rodents have reported that high fat diet (HFD) is associated with hypoxia in adipose tissues [99, 100]. However, as reviewed in [101], studies in humans have shown that the differences in oxygen tension between adipose tissue in lean and obese subjects is not as prominent and consistent as in mice [102, 103]. The additional finding that blood flow in obese subjects was not increased proportionally to fat mass expansion [104] suggests that hypoxia in humans fails to induce sufficiently adequate angiogenesis. It has been demonstrated that

overexpression of active HIF1α elicits fibrosis and inflammation rather than an appropriate angiogenic response [105]. Beneficial effects of VEGF in adipose tissue were observed as its forced overexpression reduced inflammation and insulin-resistance associated with HFD besides increasing vascularization [106-110]. However, contrasting results have been reported regarding VEGF levels in obese, as its expression was found to be lower in adipose tissue (contra lateral abdomen) from obese compared to lean, while another study showed that VEGFA expression was greater in adipose tissues (omental and subcutaneous) from insulin-sensitive obese versus lean and insulin-resistant subjects [109]. All together, these results suggest that increased levels of VEGF in obese subjects may be a consequence of the activation of a mechanism for VEGF production independent from hypoxia or at least from HIF-1α [111, 112]. For example, PGC-1α activation by adrenergic stimuli is known to induce VEGFA [110, 113]. Therefore, obese subjects whose white adipose tissues have not lost the ability to acquire brown-like features might be able to induce VEGF expression in the adipose depots more efficiently than obese individual with white fat unresponsive to ß-adrenergic stimuli. However, this has to be proven. A relevant mechanism regulating VEGF expression is represented by activation of PPARɣ. Interestingly, expression of PPARɣ in endothelial cells results in the block of proliferation of these cells, while activation of PPARɣ in adipocytes stimulates adipogenesis in parallel with pro-angiogenic factor expression VEGFA [114].

1.1.3.2 *Extracellular matrix and its role in adipose tissue plasticity*

The extracellular matrix provides the structural support to adipocytes and mediates many actions essential for the correct functioning, development and remodelling of the adipose tissue, such as cell adhesion and migration, interaction of ligands with cellular receptors, tissue repair after injury etc. There exist a large variety of ECM components, however, only the most relevant for the purpose of this study will be discussed.

Collagen is the major component of the ECM and the different types of this fibrotic protein are involved in a large number of functions [115]. Abnormalities in the expression of the different types of collagen compromise the functionality of the tissue. Obesity is characterized by an excessive presence of collagens in the adipose tissue [116] and collagen VI has been recognized as one of the most important collagen types involved in the development of fibrosis [117].]. Its ablation in mouse obese models improves AT

expansion and shows a protective effect against the development of diabetic phenotype [118]. Also collagenase V is increased in human obesity and it seems to exert an antiangiogenic function [119]. Additionally, adipose tissue fibrosis was found to be associated with increased insulin-resistance [120]

Another component of the ECM which expression is altered in obesity is Osteopontin (OPN) or secreted phosphoprotein 1. In obesity, macrophages display high expression of this glycoprotein, which mediates their infiltration in the adipose tissue in combination with integrins and CD44 [121, 122]. CD44 is a cell membrane receptor that interacts with different components of the ECM besides OPN [123]. It is widely expressed in many types of tissue and has different isoforms [124]. Its involvement in inflammation and insulin-resistance [125] is attracting scientists' interest.

Integrins anchor cells to the extracellular matrix interacting with the cytoskeleton and ECM components and together with other focal adhesion proteins control cellular motility. There exist two families of integrins, α and ß which comprise eighteen and eight subunits respectively that form different combinations of integrin heterodimers [126]. Alteration of the integrin pattern of expression can result in insulin-resistance and impaired vascularization [122]. For example, mutation of ß2 integrin in mice was associated with insulin-resistance and recruitment of neutrophils in adipose tissue [127], while deletion of α2ß1 integrin enhanced vascularization in the muscles of obese mice [128].

Proteoglycans are proteins that are highly glycosylated and abundant in the ECM and are involved in a large number of processes. Among the different types, Heparan Sulphate (HS) proteoglycans (HSPG), containing mono or pluri HS chains, play an important role in creating chemokine gradients for cell attraction and contribute to the binding of ligands and their specific receptors expressed on the cell surface [129]. HSPG were found to play an important role in fatty acid transport across the plasma membrane of adipocytes [130]. HSPG structure is under the control of specific enzymes such as heparanases and sulfatases, secreted by resident cells, that modify the HP chains allowing or inhibiting the transport of vesicles and ligands through the extracellular matrix to the receptor targets [131, 132].

Remodelling of the EMC is permitted by the action of different enzymes that degrade and regulate modifications of the ECM components [133]. These include matrix

metalloproteinases (MMPs) and tissue inhibitors of metalloproteinases (TIMPs). MMPs are classified based on their ECM component substrate, and therefore categorized as collagenase, gelatinase, elastase etc. [134]. TIMPs and MMPs involvement in the pathogenesis of obesity was suggested by the differential pattern of expression of MMPs and TIMPs in two different mouse models of obesity [135]. Moreover, Adam metalloproteinase domain 10 (ADAM10), a disintegrin metalloprotease known to inhibit angiogenesis by modulating Notch signalling [136] was found to be upregulated in obese mice and its silencing ameliorated insulin sensitivity [137]

In summary it is believed that in obesity, plasmatic membrane rupture of hypertrophic adipocytes and accumulation of ECM components cause necrotic adipocyte death. This results in lipid leakage and release of molecules, that recall macrophages, which, in turn sustain inflammation and promote insulin-resistance [122, 138].

1.1.3.3 *Obesity and insulin resistance*

The precise mechanism that leads in obesity to the development of insulin resistance and T2D is still poorly understood. Insulin resistance in skeletal muscle and the inability of pancreatic ß-cells to release adequate levels of insulin into the circulation to regulate glycaemia, are the two prerequisites for the establishment of the diabetic status [139-141]. However not all obese individuals develop T2D, highlighting the great contribution of genetic/environmental predisposition to the disease.

The link between the development of insulin resistance and obesity resides in the high level of circulating fatty acids and the consequential low grade inflammation observable in hypertrophic adipose depots. Adipocytes are responsible for storing, synthesizing and releasing lipids to maintain appropriate circulating levels of fatty acids that can be up-taken and oxidized by distal tissues, principally skeletal muscles during fasting. In prolonged hyperphagia, adipocytes enlarge proportionally to the caloric intake. Initially, adipocytes respond to high food intake by increasing expression of enzymes involved in lipid storage processes and muscle still show normal sensitivity to insulin despite the slight increase of circulating fatty acids [142, 143]. With perpetuation of this condition adipocytes become hypertrophic and their endocrine activity is progressively impaired resulting in secretion of pro-inflammatory adipokines such as C-C Motif Chemokine Ligand 2 (CCL2), tumor necrosis factor alpha (TNFα) and interleukin-6 (IL-6) [144] that recruit and activate immune cells which sustain the inflammatory state

contributing to insulin resistance. Activated macrophages in turn start secreting cytokines [145] among which, TNFα plays a pivotal role in the process. TNFα transcription is activated through the IKKβ–NF-κB (inhibitor of nuclear factor (NF)-κB (IκB) kinase-β–NF-κB) and the JNK–AP1 (Jun N- terminal kinase–activator protein-1) signalling pathways and has been found to inhibit PPARɣ activity via MAP4K4 or other kinases [146, 147], repressing the expression of adipogenic genes such as C/EBPs. This results in further impaired equilibrium between fatty acid storage and release in the circulation. Additionally TNFα induces PPARɣ degradation by activating caspases [148]. Consequently, free fatty acids circulating in high levels accumulate in peripheral tissues such as liver, arteries and muscles causing secondary diseases such as atherosclerosis, non-alcoholic-fatty liver disease (NAFLD) and muscle insulin resistance which sustain and further enhance the pathological condition. However, many other cytokines and mechanisms have now been found to contribute to the development of insulin resistance associated to obesity (reviewed in [149]).

Cytokine production and release is the downstream effect of activation of different signalling pathways that are mainly activated by free fatty acids [150], reactive oxygen species (ROS) [151], and cytokines themselves [152]. One mechanism responsible for cytokine production that takes part in inflammation and impairing the insulin signalling pathway is represented by activation of Toll-like receptors (TLR) among which TLR4 has been found to play an important role in this process (reviewed in [152]) . TLR4 is expressed on the surface of the cellular component of different organs and tissues such as brain [153], liver [154], endometrial cells [155], vasculature [156], pancreatic ß-cells [157], thyroid [158], skeletal muscles [159], immune cells, and adipose tissue [160]. Lipopolysaccharide (LPS) is one of the strongest TLR4 agonist among the TLR4 ligands [161-163] and is expressed on the membrane of gram-negative bacteria [164]. HFD is associated with altered gut flora growth and permeability leading to excessive release of LPS in the blood stream [165-167]. As summarized in figure 2, LPS binds to TLR4, helped by accessory proteins such as LPS Binding Protein (LBP), CD14 and MD2 (differentiation factor 2), activating two pathways initialized by MID88/TIRAP (myeloid differentiation primary response gene 88/Toll-IL-1 receptor (TIR) domain-containing adapter protein) and TRAM/TRIF (translocating chain-associated membrane protein/ TIR domain containing adaptor inducing Interferon-ß). In the former, downstream factor

such as NF-*K*B, CREB, activator protein 1 (AP-1) induce transcription of pro-inflammatory molecules among which, TNFα and IL-6, that in turn activate further pathways sustaining the pro-inflammatory cascade. On the other side the TRAM/TRIF triggers activation of interferon 1 (INF-1) genes and via IkB inhibits NF-kB activity in a negative feedback loop. Mediators of these cascades such as suppressor of cytokine 3 (SOCS3), P38, IKKαß and JNK are involved in insulin receptor substrate (IRS) phosphorylation, impairing the insulin signalling cascade.

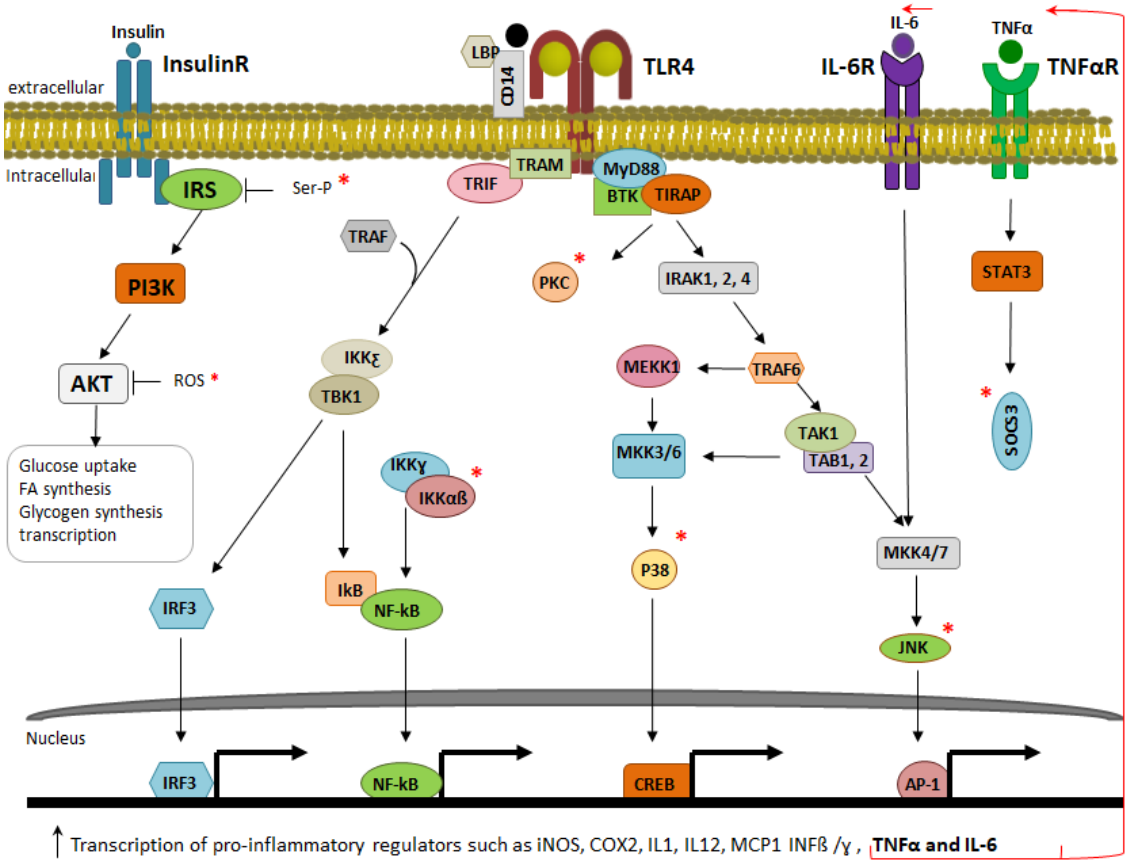

Figure 2 TLR4 signalling cascades and insulin resistance
TLR4 stimulated by LPS and aided by CD14 and MD2 accessory proteins triggers signalling cascades of TRAM/TRIF and MyD88/TIRAP pathways resulting in the final activation of NF-kB and other factors. This leads to pro-inflammatory regulator production such as IL-6 and TNFα, which in turn further sustain insulin resistance. Molecules and mediators of these cascades interfering with insulin pathway transduction through IRS-serine phosphorylation are indicated with a red star (*).

1.1.3.4 *NOD-Like Receptors*

Another mechanism mediating inflammation and involved in insulin resistance development is represented by activation of the Nucleotide-binding Oligomerization Domain (NOD)-Like Receptors. NLRs consist of three domains: a C-terminal Leucine-Rich Repeat (LRR) responsible for recognition of damage and pathogen associated molecular patterns (PAMPs and DAMPs), a central NACHT domain that mediates ATP-dependent self-oligomerization, fundamental for NLR activation and an N-terminal domain which includes a caspase recruitment domain (CARD) and a pyrin domain (PYD) that mediates homotypic protein-protein interactions [168, 169]. NLRs are involved in the formation of inflammasomes, which are multiprotein complexes, located in the cytoplasm, that process pro-inflammatory cytokines triggering their maturation [170]. Different types of inflammasome have been identified and generally their structure consists of a sensor NLR protein, a protease caspase 1 and an ASC protein containing PYD and CARD domains that function as adaptor between the NLR protein and the protease caspase 1 [171]. Depending on the type, NLRs recognize molecules derived from gram-positive and/or gram-negative bacteria as well as endogenous ligands such as saturated FFAs [172, 173] and lead to NF-kB pathway activation or maturation of the pro-inflammatory cytokine via the inflammasome machinery. Similar to the toll-like receptors, activated mediators of this process impair the insulin signalling pathway (figure 3) [174, 175].

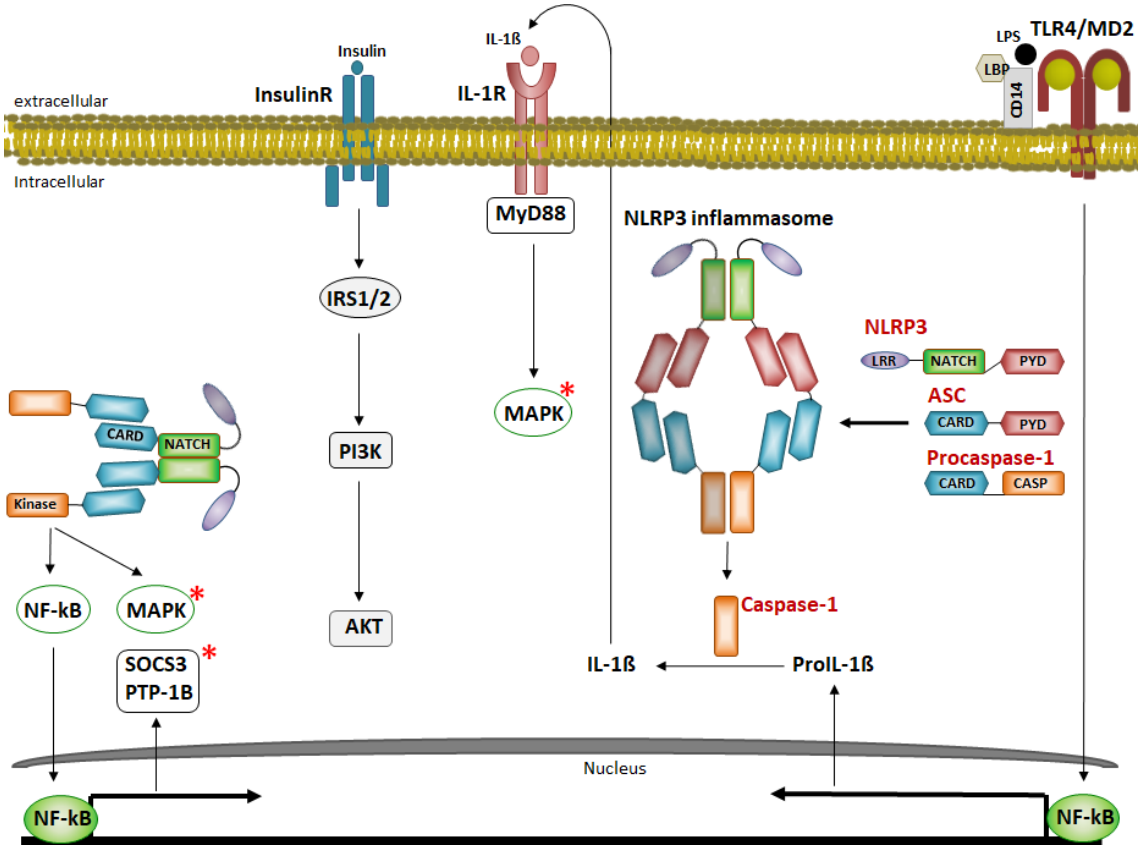

Figure 3 NOD-like receptors and insulin resistance
The figure shows a schematic representation of nucleotide-binding domain (NOD1/2) and NOD-like receptors family, pyrin domain containing protein 3 (NLRP3) inflammasome. NOD1/2 oligomerization upon activation by FFAs occurs by recruitment of receptor-interacting protein2 (RIP2) and triggers activation of NF-kB and MAPK. NF-kB is also activated by stimulated TLR4 and leads to expression of NLRP3 and precursors of IL-1β. NLRP3 oligomerizes upon recognition of DAMPs and triggers activation of procaspase-1 which catalyses maturation of IL-1ß. Secreted IL-1ß and mediators of the NOD signalling cascade impair insulin pathway by IRS1/2 inhibition (indicated by red star *).

1.2 MicroRNAs

MicroRNAs (miRNAs) are small non-coding single stranded RNAs (ssRNAs), of about 18-25 nucleotides in length, that regulate gene expression at a post-transcriptional level. In particular they recognise specific sequences in the messenger RNA (mRNA) targets and inhibit them through two mechanisms: perfect pairing, which elicits direct mRNA cleavage and imperfect pairing, that blocks mRNA translation [177].

1.2.1 *MicroRNA nomenclature*

MicroRNA nomenclature consists of a prefix that specifies the species of origin, such as ‘mmu-’ for *Mus musculus*, ‘hsa-’ for *Homo sapiens* etc., followed by the three letters ‘miR-’ or ‘mir-’ and a number assigned sequentially. MicroRNAs of different species but with identical sequence have the same numbering but different prefix. ‘miR-

’ refers to the mature miRNA whereas ‘mir-’ refers to the miRNA gene. MiRNAs can be grouped into families when closely related to each other, so that they have the same numbering but different suffixes. Lettered suffixes indicate miRNAs with very similar sequences that generate from distinct genes, such as hsa-miR-121a and hsa-miR-121b. MiRNA genes on different genomic locations generating identical mature miRNA sequence but distinct precursor sequences are distinguished by the addition of a numerical suffix such as mir-121-1 and mir-121-2. Mature miRNAs originating from opposite arms of the same precursor hairpin structure are referred as lead and passenger strand, where the lead is the most abundant strand and the passenger strand is indicated with the star symbol (e.g. miR-56*). When there is no clear evidence that one strand is more abundant than the other one the two miRNAs are distinguished by specifying 5p for the 5’ arm or 3p for the 3’ arm (example: miR-142-5p and miR-142-3p). There are some miRNAs that do not fit into these conventions, either for historical reasons such as Let-7 and Lin-4 or because they are named by adopting a slightly different scheme, such as in the case of plants and viral miRNAs.

1.2.2 *miRNA Biogenesis*

MiRNA genes have been found in every chromosome, Y included [178], which was previously thought not to have any miRNA. In 50% of cases the miRNA and mRNA loci are side by side, organised in clusters, which are concurrently transcribed in a unique primary polycistonic transcript and usually functionally correlated. MiRNA genes can also be located in intergenic regions. Their transcription is generally under the control of the host gene promoter, but sometimes they have their own independent promoters [179]. In mammals, miRNA transcription is mediated by the RNA polymerase II (RNA pol II) [180] (in most of the cases), or the RNA polymerase III (RNA pol III) when miRNAs genes are located in the proximity of Alu repeat sequences [181] . Transcription generates a pri-microRNA of variable sizes, generally several thousands of bases in length with a 7-methylguanosine cap on the 5’ termini and a poly (A) (poly-adenosine) tail at the 3’ end. In the transcript, the central core relative to each miRNA folds up forming a hairpin structure presenting one or two loops. In the nucleus, pri-miRNAs are recognised and processed by the endonucleases Drosha and Pasha, which, in association with other proteins, such as DEAD box, p27, p68 and some ribonuclease proteins form the Microprocessor complex. Pasha, also known as DiGeorge syndrome critical region 8

(DGCR8), and Drosha present specific RNase III catalytic domains (RIIIDa, RRIIDb). Pasha ties the hairpin structure through its two double stranded RNA binding domains (dsRBDs). This allows Drosha to cleave the 5' and 3' strands of the miRNA at about 11 bases after the junction between the double strand and the single strands of the hairpin structure. The pre-miRNA so formed is of about 70 nucleotides in length and presents a 5' phosphate group and a 2 nucleotide 3' overhanging end [182, 183]. MiRNAs do not always need to be processed by the microprocessor complex. When miRNA genes are situated in short introns, with the termini in the splice donor and acceptor sequences, the pre-miRNA is directly obtained through the splicing process and transferred into the cytoplasm. These particular miRNAs are called "mirtrons". Pre-miRNA transport across the nuclear pores is mediated by the nuclear receptor protein Exportin 5 (EXPO5) (figure 4) which selectively recognizes dsRNA structures containing a number of base pairs over 14 and a 3'overhang [184]. EXPO5 binds to the pre-miRNA in a GTP-dependent way inside the nucleus and releases it in the cytoplasm consequently to GTP hydrolysis [185].

In the cytoplasm, pre-miRNA is processed by the RNase III Dicer1 that presents several domains: an N-terminal DEXH-box helicase domain, a DUF283 domain which function is unknown, a Pwi Argonaute Zwille (PAZ) domain, two RNase III domain and finally a double stranded RNA binding domain (dsRBD) [186]. The 3' of the pre-miRNA is recognized by the PAZ domain, while the RNase III domain facilitates a cleavage event that generates a ~ 22 bp dsRNA with a 2 nucleotides 3' overhanging end [187].

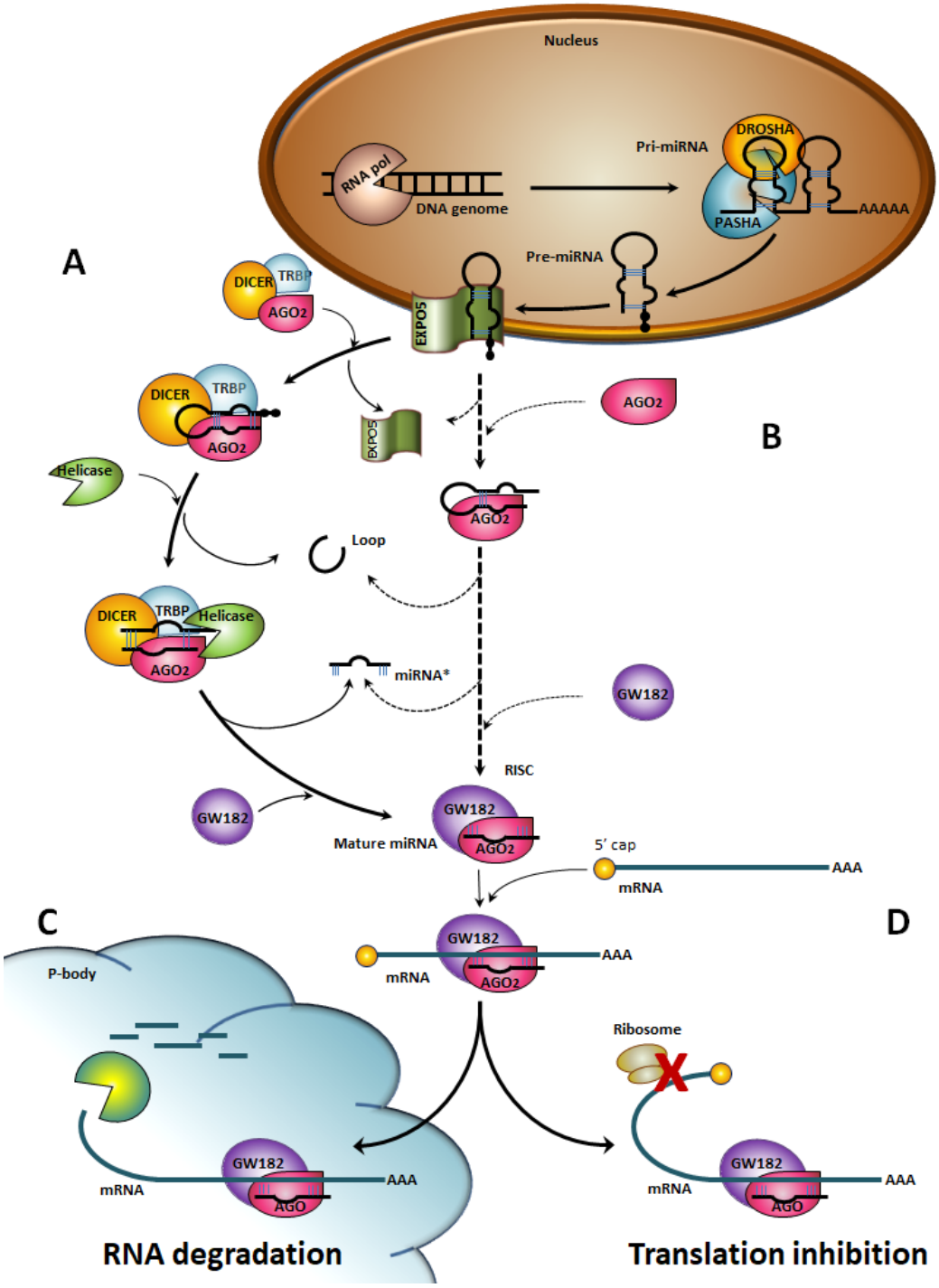

Figure 4 The biogenesis of miRNAs.
The RNA polymerase generates a pri-miRNA. The pri-miRNA is cleaved into a 70–100 nt pre-miRNA with a hairpin structure and 2–3 nt 3'overhang by Drosha and DGCR8/Pasha complex. Then exportin5 exports the pre-miRNA to the cytoplasm via the nucleus core. A) Dicer, with its partner TRBP2, binds to the pre-miRNA and shears it to form a dsRNA. Ago2 is ready to load a mature miRNA after the conformational change of Dicer and TRBP2 complex. B) Another pathway for miRNA maturation is dependent on Ago2 instead of Dicer complex. Ago2 loading a mature miRNA binds to GW182 to form the core components of RISC. The RISC binds to the mRNA . The target mRNA can undergo two different fates: C) degradation into the P-body by an exonuclease Xran1 following mRNA decapping and deadenylation; D) inhibition of protein translation based on the imperfect complementarity.

Trans-activator RNA-binding protein (TRBP) is phosphorylated by MAPK extracellular signal-regulated protein kinase (ERK) upon stimuli such as cell growth and confers stability to the DICER complex, relating the miRNA maturation process to the MAPK pathway [189].

In mammals, DICER interacts with argonaute proteins (Ago) that load the mature miRNA and in association with TRBP and other proteins, such as the accessory heat shock proteins 70 and 90 (HSP70 and HSP90), to form the miRNA Induced Silencing Complex RISC [190]. These proteins facilitate and permit the ATP-dependent process of miRNA loading onto Argonaute (Ago) proteins [191]. Ago proteins are present in all eukaryotic organisms and 4 isoforms exist: Ago1-4. All of them show similar efficiency in miRNAs recognition, but only Ago2 also presents endonuclease activity [186]. Only one strand of the mature miRNA is incorporated in the RISC complex, generally the one with a lower thermodynamic stability at the 5' extremity. The other one, called passenger strand (miRNA*) is generally degraded [192, 193] If both the strands present a similar stability either strand can be selected for incorporation with the same probability. MiRNA incorporation in the Dicer complex was previously thought to be necessary for miRNA maturation, but an alternative way has been observed for miR-451 [194]. Once processed by Drosha, the pre-miR-451 consists of a small hairpin where the stem is made of 18 bp. Since Dicer is unable to process such short structures, miR-451 maturation is completed by Ago2, skipping the Dicer step [194]. A similar mechanism is likely to be adopted by brown adipocytes for miRNA maturation. In fact, a study showed that Dicer KO in Dicer-conditional aP2-Cre transgenic mice did not affect BAT development in vivo, even though it impaired the expression of several genes [195]. Moreover, a study suggested that some miRNAs could be accumulated in inactive form and activated when needed [196]. The level of expression of these miRNAs might show only a little variation upon DICER1 ablation via Cre-recombinase induction. MiRNA loading onto Ago protein is widely considered to occur during miRNA biogenesis [197, 198]. However, in a recent study a pool of inactive mature miR-34, lacking a 5' phosphate and not loaded on Ago2, was found in four human cell lines in the absence of DNA damage insult. MiR-34 is known to be induced by p53 and functions as a tumor suppressor. The miRNA pool was activated by 5' end phosphorylation and loaded onto Ago2 only after exposure to ionizing

radiation. This mechanism could provide a miRNA response to specific stimuli more rapidly than the classic de novo miRNA biogenesis as observed in this study [196].

1.2.3 *MicroRNAs and mechanism of action*

The 5' end of the miRNA sequence is referred to as the seed region and it is essential in the silencing process, as also supported by the fact that it is the most conserved sequence in miRNAs of multicellular organisms [199]. The seed sequence is generally 6-8 nucleotides in length starting from the second nucleotide at the 5'end. The typical miRNA-target interactions are shown in figure 5. The first nucleotide is not a determinant for the pairing and thus is not necessarily complementary to the 3' untranslated region (UTR) of the target. In the mRNA sequence, the presence of an adenosine not complementary to the correspondent first nucleotide in the 5' end of the miRNA can increase miRNA activity [200]. The 3' end of the miRNA, albeit not perfectly complementary to the target, can compensate mismatches in the seed region [186]. In some cases, the pairing of miRNA with the 5' UTR of the mRNA targets can promote translation into protein instead of inhibiting it [201]. Several other types of miRNA:mRNA interactions different from the canonical ones have been recently reported to occur (figure 5). Based on the complementarity of miRNA sequences to the 3' UTR sequence of mRNAs, several algorithms have been developed to calculate miRNA-mRNA affinity and predict miRNA potential targets. These algorithms are designed to reduce the possibility of obtaining false results and take into account conservation of the sequences across species, free energy and accessibility to the target sequence. The most commonly used algorithms are miRANDA, PicTar, DIANA, miRdb and Target Scan. M*iRanda* algorithm [202] searches for complementarity between miRNAs and the mRNA 3' UTRs without considering cross-species conservation of binding sites. Scores are assigned considering thermodynamic stability of the miRNA:mRNA duplex and grade of complementarity. One wobble pairing in the seed region compensated by matches in the 3' region is allowed. *Targetscan* (http://www.targetscan.org/) searches for sites that are fully complementary to the seed region (nucleotides 2-7). Scores are calculated based on the length of perfect matching regions and the presence of adenosine nucleotide in the first position of the mRNA target sequence. It considers conservation of targets and miRNA families [200]. *Pictar* (http://pictar.mdc-berlin.de/) [203, 204] is similar to *targetscan* with the difference that it

searches for nearly perfect matches with regions of conservative 3' UTRs. It calculates the free energy of the duplexes and considers multiple 3' UTR binding sites. *Diana* (http://diana.imis.athena-innovation.gr/DianaTools/index.php) is a website that offers several types of bioinformatics tools. For miRNA target predictions it uses the *Diana-microT* algorithm [205] which searches for MREs on 3' UTRs of human mRNAs deposited in the RefSeq database. In a frame of 38 nt in the mRNA sequence, it calculates the minimum binding energy between the miRNAs and mRNA sequence for every shift on the mRNA sequence consisting of six nucleotides each.

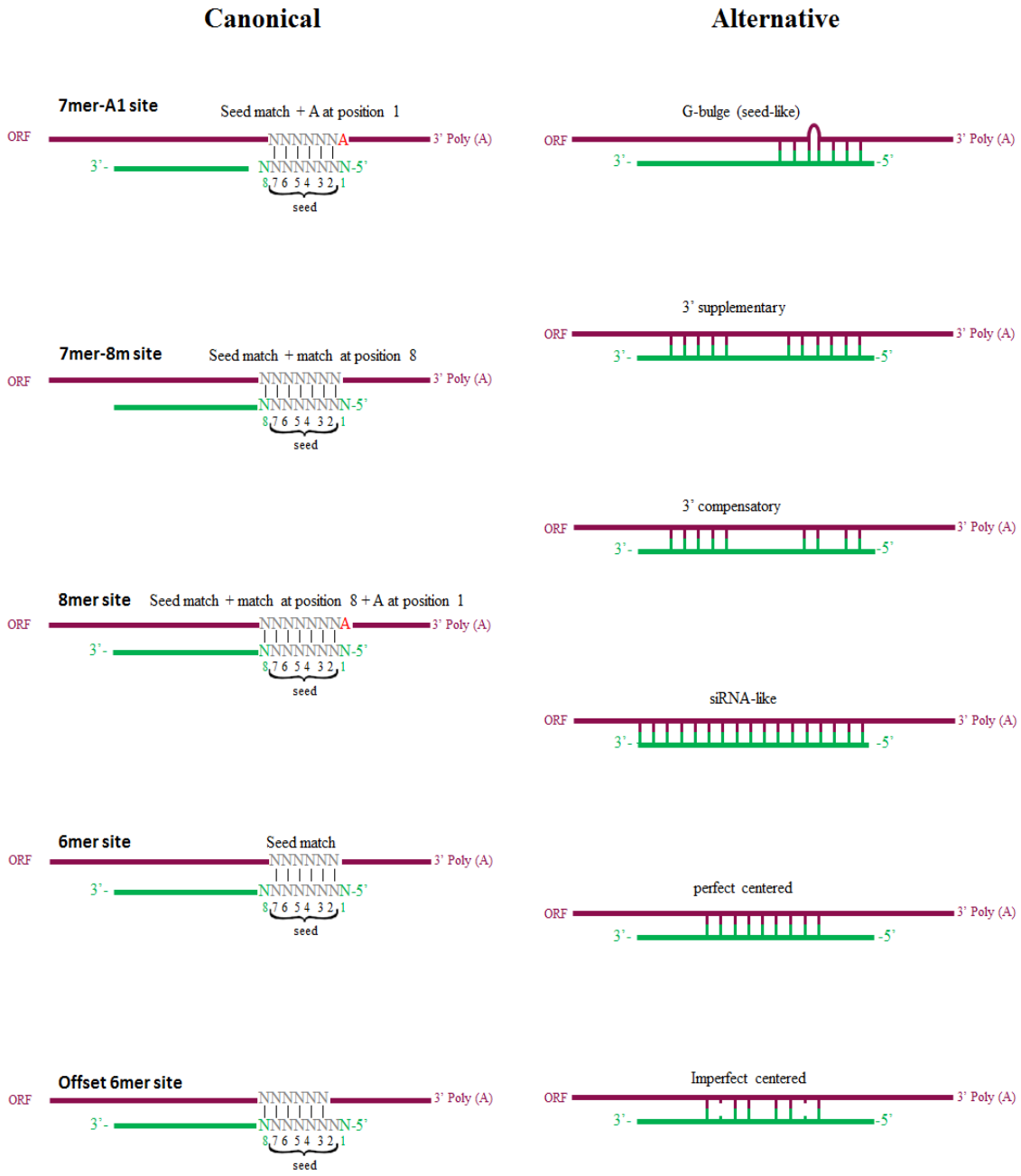

Figure 5 Types of miRNA:mRNA interactions.
On the left panel are shown canonical miRNA:mRNA interactions having the highest efficacy, with 8mer >>> 7mer-8m >> 7mer-A1 > 6mer. Less effective sites, such as 6mer or lower, can sometimes be compensated by interactions between the 3' region of the miRNA and the mRNA as shown on the right panel (Alternative miRNA:mRNA interactions). ORF: open reading frame.

1.2.3.1 *The silencing process*

Argonaute proteins present three conserved domains: PAZ, MID and PIWI [206]. The PAZ domain interacts with the 3' end of the miRNA while the PIWI and the MID domains with the 5' end of the miRNA (figure 6) in which nucleotides are positioned in a way to favour interaction with the mRNA target. An RNase-like fold in the PIWI domain confers the catalytic ability of Ago2 to cleave the mRNA target. However, mRNA cleavage by Ago2 occurs predominantly in mRNA inhibition mediated by siRNAs, which share the same machinery for gene silencing. Indeed, numerous mismatches in miRNA:mRNA interactions impede Ago2 to cleave the mRNA [207]. The silencing process requires the participation of additional proteins, including GW182 which interacts with the PIWI domain of Ago2. Several proteins belong to GW182 protein family, such as TNRC6A/B/C. These proteins present Glycine (G) and Tryptophan (W) repeats through which they play an important role in the silencing process. Inhibition of mRNA translation into protein can occur either at the initiation of protein production or during the elongation stages, as a consequence of mRNA degradation, dropping off the ribosome or proteolytic degradation of the forming polypeptide (figure 7) [208, 209]. There is evidence that reduced expression of protein is not necessarily accompanied by reduced expression of mRNA [210, 211].

mRNA degradation in this process is triggered by decapping and deadenylation events. mRNA stability and translation into protein in eukaryotes is permitted by several factors that induce its circularization and hence protection from degradation [212, 213]. Specifically, the complex eukaryotic translation initiation factor 4E (eIF4F) includes two proteins: eIF4E and eIF4G, with the former interacting with the 5' cap and the latter binding to poly A binding protein (PABP), which, as suggested by the name, interacts with the poly A tail. Subsequently, CAF1-CCR4-NOT, recruited by GW182, catalyses the adenosine residues removal [214] impeding mRNA circularization and translation initiation [215]. The DCP1-DCP2 (decapping protein1-2) in association with enhancer of mRNA decapping 4 (EDC4) and DEAD-Box Helicase 6 (DDX6) catalyses 5' decapping exposing mRNA to the 3' and 5' RNase activity of the exoribonuclease 1 (XRN1) [186].

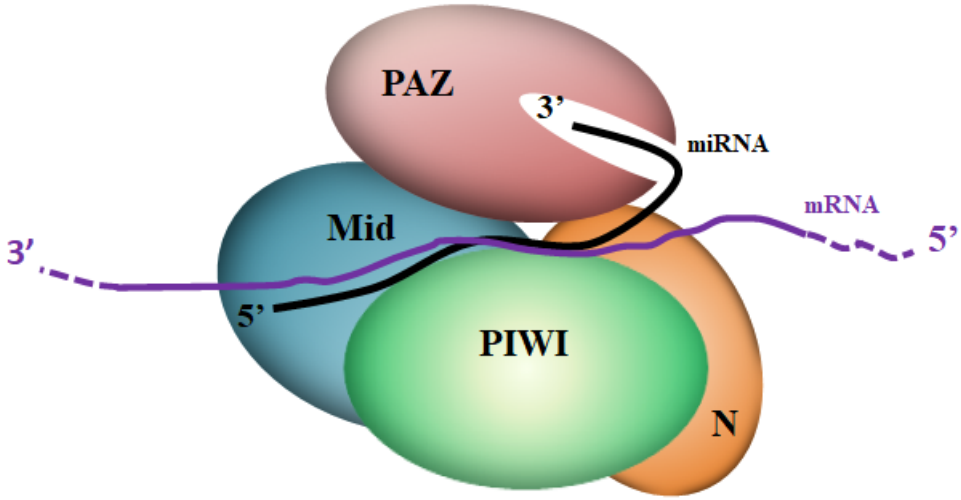

Figure 6 Argonaute protein structure and miRNA:mRNA interaction
The figure shows PAZ, PIWI Mid and N-terminal domains of argonaute protein. The 3'end of the miRNA interacts with the PAZ domain, while the 5' end is held by MID and PIWI domains favouring miRNA:mRNA interaction.

Decapping, deadenylation and mRNA degradation occur in P-bodies [216, 217], also known as GW-bodies. These compartments contain a high amount of vesicles (MLVs) on which membrane dissociation of GW182 and RISC takes place. GW182 is embedded in intraluminal vesicles (ILV) and degraded after ILV fusion with lysosomes [218]. Ago2 is then delivered back into the cytoplasm by binding HSP90 that acts as a carrier. The whole mechanism of RISC dissociation and miRNA release are still to be clearly elucidated. However, Simons et al., demonstrated that miRNAs [219] during this process can be included into MLVB and then secreted in association with proteins or inside exosomes [220, 221]. Ago2 has been found in association with several circulating miRNAs and GW182 inhibition resulted in impaired exosome production. This suggests an involvement of Ago2 and GW182 in miRNA secretion. Investigation of their role in this process would be of great interest for elucidating the mechanisms through which miRNAs are released in the extracellular environment and mediate cell-to-cell communication.

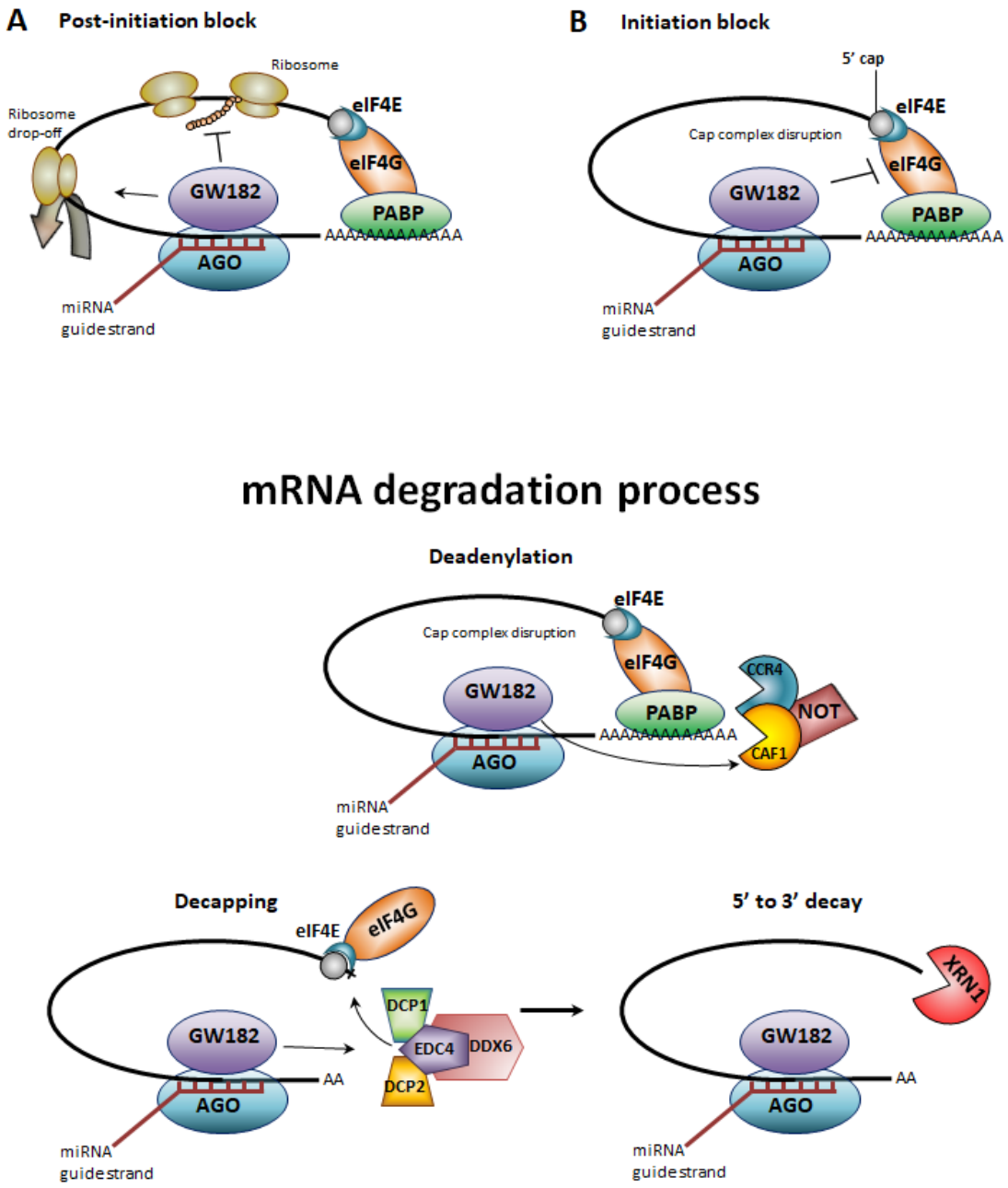

Figure 7 The silencing mechanism mediated by miRNAs in animals
mRNA circularization, for polysomes loading and translation, is mediated by the proteins PABP, eIF4G and eIF4E containing miRNA. The RISC complex containing GW182, AGO2 and the miRNA interacting with the 3' UTR of the mRNA prevents mRNA translation into protein in different possible ways: B) post initiation block by promoting proteolytic degradation of the nascent polypeptide or ribosome drop-off; A) disruption of the cap complex (initiation block). mRNA degradation occurs upon deadenylation, and decapping. In sequence, GW182 recruits CAF1-CCR4-NOT complex, which removes the poly A tail. The 5' cap of the deadenylated mRNA is then removed by the DCP1-DCP2 complex in cooperation with EDC4 and DDX6 also recruited by GW182 (decapping). The exonuclease XRN1 degrades the unstable mRNA (5' to 3' decay).

1.2.4 *Mechanism of gene regulation*

An increasing body of evidences suggests that gene regulation mediated by miRNAs is not a simple mechanism but rather the result of a complex network where miRNAs, coding and non-coding genes "talk" to each other through the language of miRNA response elements (MREs). MREs are those sequences on mRNAs responsible for miRNA-mRNA interactions. The principle of this mechanism, hypothesized by Salmena and colleagues, resumes previous observations and is based on the existence of pseudogenes and long non-coding genes, that possess the same MREs of coding genes and can potentially compete for the same set of miRNAs influencing protein translation [222]. Pseudogenes are genomic DNA sequences similar to the ones of real genes but that are not functional, as they generally do not code for proteins, have premature stop codons or present some sort of mutations [223]. With their expression level differing among diverse types of tissue or altered in certain pathologies [224], pseudogenes may influence miRNA activity on a real gene in a tissue-specific way. Long non-coding genes (lncRNA) do not code for proteins and their transcription results in RNAs with a length of over 200 nucleotides. As demonstrated, lncRNAs can interact with miRNAs [225, 226]. The presence of competitors for miRNAs, results in decreased miRNA detection and activity [227-229]. Therefore, at a post-transcriptional level, miRNAs regulate RNAs and vice versa. An example of miRNA regulated Post-transcriptionally by RNA molecules is represented by a non-coding RNA of herpesvirus saimiri which sequesters human miR-27 and induces its degradation [227]. This new logic of gene expression regulation resembles in a certain way the dynamics of competition observed in proteins, where the concentration of competitors and degree of affinity are determinant factors. The high number of combinatorial events, reflect the complexity of the regulatory mechanism of gene expression. Affinity between miRNAs and RNA competitors or RNAs and miRNA competitors relies in the existence of different modalities for miRNA-mRNA interaction and the resulting bound efficacy (figure 5). Recent studies have shown that also miRNA-miRNA interactions occur [230, 231], remarking the complexity in the post-transcriptional gene regulation network.

1.2.5 *MicroRNA secretion*

The complexity of multicellular organisms requires every cellular member to work harmoniously in synchrony with all other cells in order to ensure the correct functioning of the organism. Communication between organs, tissues and cells is fundamental to accomplish this aim. Several molecules can be delivered in different ways from one cell to another where they transmit signals and modify the program in the acceptor cell. This regulates numerous processes like apoptosis, cell growth, proliferation, and differentiation [232]. Many messenger molecules are well known and only relatively few have been discovered recently [232]. Among these, circulating miRNAs have attracted interest in the last few years.

RNA molecules are very susceptible to degradation since the extracellular environment is enriched in RNase enzymes that work as a defence against exogenous nucleic acids, such as viruses genes [233]. Even so, miRNA presence has been detected in many body fluids [232]. They also show strong resistance to non-physiological conditions like drastic pHs and temperature variations [234, 235]. This necessarily implicates the existence of protection systems. So far, three different ways by which miRNAs are released in the extracellular environment have been identified. These include: spontaneous spill out as a consequence of cellular damage, active incorporation into delivery systems consisting of membranes (exosomes, micovesicles), and through protein/lipoprotein association [188]. The principle mechanisms for miRNAs secretion are represented in figure 8.

1.2.5.1 *MicroRNA vesicles-mediated* **s***ecretion*

Incorporation of molecules into messenger systems allows exchange of information between cells. The process can be divided into three main stages: incorporation/release, travelling toward the acceptor cell and finally cellular uptake. During each phase, molecules have to overcome numerous obstacles to successfully reach the target [236]. Lipid membranes constitute an efficient system for this purpose since they can easily fuse cellular membranes and reach different organelles or cellular compartments [236]. The release of membranous particles through fusion with the plasma membrane is known as exocytosis and can be constitutive or inducible [237]. In the first instance, release occurs soon after the vesicle has formed, while, the second one requires particular stimuli that increases Ca^{2+} concentration. One mechanisms underlying this process is mediated by the

adenosine triphosphate (ATP)-gated ion channel P2X7 receptor which is activated by extracellular ATP and is involved in inflammatory processes [238].

Circulating membranous microparticles can be divided into exosomes and microvesicles. Both of them, as demonstrated in many studies, facilitate extracellular miRNA transport [188]. For some miRNAs identified as circulating through vesicles, the distinction between the two systems is not always specified. In fact, Microvesicles (MVs) are derived from direct blebbing of the plasma membrane with heterogeneous size (1nm to 1000 um) [239, 240]. Exosome dimensions vary between 30-150 nm [241, 242], but they differ in composition, biogenesis and way of secretion. However, the two are mixed in the extracellular environment, and without specific marker analysis, it is not possible to discriminate one from the other [243].

Exosomes originate by subsequential intralumen invaginations (ILV) of the multi-vesicular bodies (MVBs) membrane [244], which in turn originate in the GW-bodies . The GW-bodies are cellular compartments similar to the P-bodies in terms of structure and function [245]. MVBs are intracellular compartments that mediate transfer of molecules between early-endosomes and late-endosomes, which together regulate the fate of incoming and/or outgoing molecules [244]. Exosome release into the extracellular environment follows the fusion of the MVBs membrane with the plasma membrane [246]. MiRNA incorporation into exosomes can occur during RISC complex dissociation in the MVBs [219, 243]. Many markers have been identified, among these, there are the heat shock proteins involved in miRNA maturation HSP70 and HSP90 which might constitute a link between miRNA biogenesis and their release through exosomes [246].

Another mechanism underlying exosome and miRNA secretion may be represented by the ceramide-dependent secretory machinery as reported by Kosaka in 2010 [247] and confirmed by Mittelbrunn et al. [248]. In their work, inhibition of the regulator for ceramide biogenesis, sphingomyelinase 2 (nSMase2), negatively affected exosome formation and miRNA secretion from T cells.

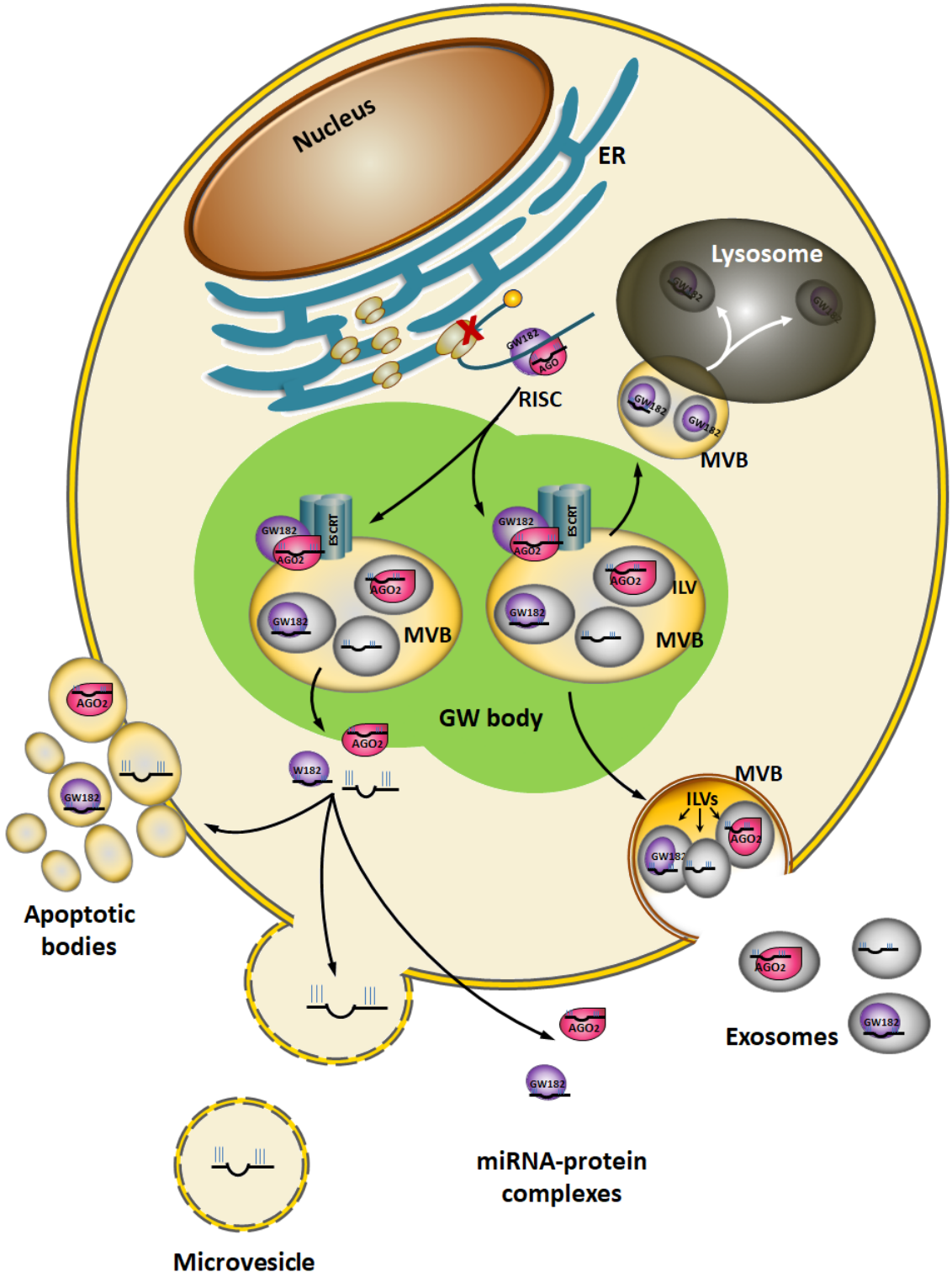

Figure 8 Different transporters for miRNA transport.
The RISC in the GW-body is dissociated from the membrane of MVBs by the ESCRT, and the GW182 is eliminated from the RISC and sorted into the ILVs for degradation by entering the lysosome. MiRNAs are transported in exosomes by the fusion between MVB sand plasma membrane or in microvesicles through budding of plasma membrane. Protein complexes and apoptotic bodies could also carry miRNA in extracellular environment.

1.2.5.2 *MicroRNA-protein secretion*

The first protein proposed as carrier for miRNA was nucleophosmin I (NPMI). This nucleolar phosphoprotein is responsible for RNA and ribosomal protein transfer from nucleolus to cytoplasm. Its incubation with a synthetic miR-122 prevented miRNA degradation by RNaseA [188]. In human plasma, High Density Proteins (HDL) have been found in association with several miRNAs [249].

One of the most intriguing proteins involved in extracellular miRNA transport is represented by Ago2, which is fundamental in miRNA maturation and mRNA silencing. It was found associated with several miRNAs in human plasma [188]. However, it is still not clear if the association occurs inside the cells or after secretion. It was also demonstrated that most of the miRNAs detected in the extracellular environment were bound to proteins rather than included in vesicles [250]. The contrary was showed by Gallo et al., where miRNA were principally inside exosomes [251]. However, there is evidence that miRNA-proteins complexes can be incorporated into and released as circulating vesicles. Li et al., could in fact detect Ago2-miRNA presence into microvesicles [252]. They also proposed that miRNA included in vesicles but not associated with Ago2 might be degraded once absorbed by the acceptor cells. Different cells might have different mechanisms for secretion of the same molecules [188]. This could justify the presence of both miRNA-Ago2 complexes inside vesicles and alone in extracellular fluids [188, 252].

1.2.5.3 *miRNA delivery*

The discovery of exosomes containing miRNAs has aroused great excitement in the scientific community for the implication of this novel potential mechanism of miRNA delivery in the cross talk between cells. However, a quantitative and stoichiometric analysis of miRNA content in exosomes from human blood samples has revealed that a single exosome contains on average, less than one molecule of a specific miRNA [253] for which functionality is therefore biologically insignificant. However, this conclusion was made on the assumption that miRNAs are equally distributed in the exosome population of human blood. In contrast, in *vitro* studies show that different types of cells/tissues present differential expression of exosomal miRNAs demonstrating that miRNAs are not equally distributed in the exosome population. Therefore, more significant concentrations of a specific miRNA could be contained in a single exosome

as well as no copies at all of that miRNA might be present in exosomes derived from a different type of cell. The ability of exosomes to deliver their cargo to selective target cells would further improve the achievement of a substantial concentration of a given miRNA in a specific cell/tissue type. Whether exosomes can selectively target specific cells is still unclear. Some studies show that exosomes can virtually target any type of cells [254], while others suggest that expression of specific molecules on the cellular and exosomal surfaces are required for exosome uptake [131]. An example of specific interaction is given by monocyte-derived dendritic cells that were showed to selectively internalised exosomes from breast milk expressing MUC1 (Cell Surface Associated Mucin 1) via DC-SIGN (Dendritic Cell-Specific Intercellular adhesion molecule-3-Grabbing Non-integrin) and MUC1 interaction [255]. Derivation from other sources or absence of MUC1 resulted in failed exosome uptake by these cells. Another study revealed that more than one mechanism for exosome internalization, are likely to exist. Indeed, treatment with a blocker of integrin-mediator receptor internalization resulted in decreased exosome uptake by macrophages and dendritic cells but not microglia [255]. In vitro studies also suggest that miRNAs delivered into distal cells are functional and can effectively modulate acceptor cell pathways. Initial evidence was reported by Zernecke et al., who demonstrated that miR-126, delivered by apoptotic bodies, reduced expression of RGS16 in recipient HUVEC cells [256]. Successively, the results of many other in *vitro* studies supported the functionality of delivered miRNAs into recipient cells [257-260]. A study conducted recently, exhaustively addressed the question whether this process actually occurs in *vivo.* Thomou T. and colleagues discovered that BAT-derived exosomes containing miR-92b suppress FGF-21 in liver and also reduce its circulating levels [261]. This effect was observed selectively for exosomes released by BAT, although other fat depots contribute to miR-92-exosome release, supporting the fact that exosome uptake can be tissue specific. Moreover, this demonstrates that miRNAs packaged into exosomes can travel long distances and their function is not limited to autocrine and paracrine actions. In contrast, this is still not clear for miRNAs associated to vesicle-free system. However, evidence show that also these carriers are able to deliver functional miRNAs into recipient cells [262]. Neuropilin-1 (NRP-1) is a cell surface receptor expressed on different type of cells and involved in the internalization of several types of ligand [263]. It was demonstrated to efficiently mediate uptake of miRNAs

complexed with Ago2. NRP1 was found to have high affinity for miRNAs either in association with Ago2 or Ago2-free. Vice versa, NRP1 bound with high affinity to Ago2 either associated to miRNAs or alone. Internalised miRNAs promoted migration and proliferation in human ACHN cells (kidney adenocarcinoma cell line). As NRP-1 is widely expressed in different cell types, it would be logic to assume that miRNA internalization is not a selective process. However, a population of ACHN cells was found to be naturally NRP1-negative [262] and did not internalise the miRNA tested. Moreover, even though circulating vesicle-free miRNAs are mainly associated with Ago2, other types of proteins carrying miRNAs could exist. Finally, components of the ECM that are not present in in vitro studies, should be considered in this process, as they are known to favour or inhibit ligand-receptor binding [264] and their expression could be tissue-specific.

1.2.6 *MicroRNAs in adipocyte differentiation and metabolic disorders*

An increasing body of studies has revealed that miRNAs play important roles in the different steps of adipogenesis. Some miRNAs have been identified as regulators of the commitment of MSC to the adipocyte lineage while others have been found to play a major role in the later stage of the pre-adipocyte differentiation into mature adipocytes. Additionally, some of these miRNAs are specific promoters of the brown, white or beige phenotype. An example of miRNA regulating early stages of adipogenesis is mmu-miR-204, which has a homologue in humans, namely hsa-miR-211. This miRNA targets runt-related transcription factor 1 (RUNX1) in MSCs inhibiting the osteogenic lineage in favour of the adipogenic program [265]. Another miRNA with similar function is miR-103a-3p as its overexpression in human adipose derived stem cells (hADSCs) inhibited osteogenic proliferation and differentiation. Cyclin Dependent Kinase 6 CDK6 and DICER1 were identified as miR-103a-3p targets [266] .

MiRNAs such as miR-10b, miR-15, miR-26a, miR-34c, miR-101 miR-185 miR-224 and others were found to be upregulated in the late stages of differentiation suggesting their potential involvement, not only in adipogenesis but also in the metabolic activities pertinent of mature adipocytes [267].

Among the miRNAs that were found to promote adipogenesis there are: miR-371, the cluster miR-17-92, miR-21 miR-103 miR-143 and miR-378. The former was reported

to induce the expression of FABP4 and adiponectin, the cluster miR-17-92 downregulates Rb2/p130 and miR-21 modulates the anti-adipogenic pathway mediated by Transforming growth factor beta (TGF-ß) [268]. MiR-143 showed opposing functions depending on the stage of differentiation. In fact, ADSCs differentiation was inhibited by overexpression of miR-143 during clonal proliferation stage and promoted it in the terminal phase, during growth arrest. In this study MAP2K5 was identified as a miR-143 target [268]. MiR-103 promotes 3T3-L1 adipogenesis by inhibiting myocyte enhancer eactor 2D (MEF2D), a suppressor of differentiation [269], besides targeting CDK6 and DICER in hADSC, as mentioned previously.

MiR-378, besides promoting adipocytes differentiation, was found to be involved in a large number of functions, not only restricted to the adipocytes, such as metabolism, lipid storage, cell differentiation/proliferation [270] and angiogenesis [271], many of which have been reviewed by Bart Krist *et al*., [272]. Mir-378a is located in the intron of the Ppargc1b gene [273], and it was reported to be co-expressed with PGC-1 during cell differentiation, suggesting their involvement in similar processes [270]. From mir-378a the mature miR-378a-3p and miR-378a-5p are generated, situated in the opposite arms forming the pre-miR378a stem loop. These miRNAs were previously identified under different names: miR-422b, miR-378 and miR-378-3p for miR-378a-3p and miR-378 and miR-378* for miR-378a-5p, both in human and mouse. MiRNAs with very similar sequences to miR-378a have been identified in different locations of the genome and have been named as: miR-378b, c, d1, d2, e, f, g, h, i and j in mouse and human [274-278]. However, a large body of study has mainly focussed on miR-378a-3p and its opposite strand miR-378a-5p. The sequence of miR-378a-5p is identical in mouse and human, while, mmu-miR-378a-3p and hsa-miR-378a-3p differ by one nucleotide [278, 279]. MiR-378a-3p and miR-378a-5p generally take part in similar processes [270] despite showing in certain cases opposite functions. For instance, in the cardiac cells H9c2, the enzyme lactate dehydrogenase A (LDHA), a direct target of miR-378a, was downregulated by miR-378a-3p but upregulated by miR-378a-5p [280]. The existence of different names for these miRNAs can generate confusion and sometimes the precise strand of miR-378a is not specified [281]. In mice, removal of the intron region containing mir-378a leads to HFD-induced obesity resistance and high mitochondrial activity and oxygen consumption [279]. MiR-378a has been demonstrated to promote adipogenesis

by positively regulating the activity of CEBPα and CEBPß which in turn results in enhanced transactivation of GLUT4 [270]. Pan, D., et al., reported that ectopic expression of miR-378a-3p in mice promotes enlargement of interscapular BAT but not of WAT, [282] suggesting that determined functions of miR-378a are tissue specific.

Another miRNA that was found to be mainly involved in brown adipogenesis is miR-365 which is transcribed in cluster with miR-193 [283]. However, they have been proposed as necessary not only for the late brown differentiation but also for early brown and white adipogenesis. MiR-193/365 were found to directly target and negatively regulate RUNX1 Translocation Partner 1 (RUNX1T1), an inhibitor of adipogenesis [284]. MiR-193/365 inhibition in the stromal vascular fraction of interscapular BAT of C57BL/6 mice, affected lipid accumulation and the expression of genes such as aP2, C/EBPα and PPARγ [283] that are crucial for both white and brown adipogenesis. However, the most important evidence in this work was that miR-196/365 specifically promotes the brown phenotype by targeting genes that activate the myogenic program such as CDON [285] and the insulin-like growth factor-binding protein 5 (IGFBP5) [286]. This was confirmed by a significant decrease of classical-brown proteins like UCP1, PPARγ, PGC1α PRDM16, and CIDEA when miR-193/365 inhibition was induced by locked nucleic acid (LNA) technology. Indeed, UCP1 over-expression was obtained when miR-193/365 was ectopically expressed in vitro in C2C12 myoblasts. Interestingly, after forcing PRDM16 expression in these same cell lines, miR-193/365 was up-regulated, probably, as a result of PPARα induction promoted by PRDM16. However, a later study showed contrasting results demonstrating that development and function of BAT in mice, was not affected by the absence of miR-193/365 cluster [287].

MiR-26a and miR-26b are up-regulated in the early phases of adipogenesis and miR-26a has been associated with promoting energy dissipation in brown adipocytes by targeting ADAM metallopeptidase domain 17 (ADAM17) also known as tumor necrosis factor-α-converting enzyme [288]. This protein is responsible for the cleavage of the membrane protein Pref-1 that generates soluble form of protein Pref-1 (50kD) previously discussed, which inhibits adipocyte differentiation [289]. In the same study, MiR-26a and miR-26b were found to upregulate UCP1 mRNA expression at the early and late stage of white and also at the late brite stages [288].

Also miR-133 has been associated with human and mouse BAT development versus myogenic differentiation. MiR-133, initially believed to be muscle specific was later found to be also expressed in BAT [290]. It directly targets PRDM16 and, at high levels, inhibits the brown phenotype [291]. In fact, all its variants present in the seed portion a complementary sequence to the 3' UTR of PRDM16. MiR-133 transcription is positively regulated by myocyte specific enhancer factor 2 (MEF2C) expression of which is reduced after cold acclimatization or adrenergic stimulation as a consequence of increased cAMP levels [283]. However, miR-133 decrease in muscles or promotion of brown phenotype in muscle progenitors was only achieved when cold exposure was prolonged for more than one week [292].

Also miR-155 is a negative regulator of brown adipogenesis. Its expression inhibits and is inhibited by C/EBPβ [293], while, its induction is promoted by TGF-β1 [294]. This is further supported by chromatin immunoprecipitation assay data which revealed the presence of TGF-β1 on the enhancer sequence of miR-155. Moreover, miR-155 expression strongly decreased when BAT pre-adipocytes were induced to differentiate, while, inhibition of C/EBPβ resulted in over-expression of miR-155 [295].

MiR-33 is involved in the control of lipid metabolism gene expression [296, 297] and regulates fatty acid and cholesterol homeostasis by targeting receptor-interacting protein 140 (RIP140), a nuclear corepressor that inhibits the brown phenotype [298]. Thus, miR-33 might also be involved in promotion of brown adipogenesis. [296, 297].

Another miRNA, miR-27, has been described recently as negative regulator of brown adipogenesis by directly targeting PRDM16, PPARα, CREB [299] and PPARγ [300].

MiR-455 is up-regulated during brown adipogenesis [290], and modulates thermogenesis. This miRNA promotes differentiation by suppressing anti-adipogenic genes such as RUNX1T1 and NECDIN. Moreover, it inhibits HIF1α activating MAPKα1 and mitochondrial biogenesis [301].

One of the most intriguing miRNAs in adipogenic differentiation is represented by miR-196a. This miRNA is involved in the acquisition of classic brown characteristics by white pre-adipocytes after β-adrenergic stimuli or cold exposure, the so called "browning" effect [302]. MiR-196a is encoded by two genes, mir-196a-1 and mir-196a-2, both embedded in homeobox (HOX) gene clusters (HOXC) on chromosome 17 and

12, respectively and present a complimentary sequence to the HOXC8 transcript [302, 303]. Thus, their strict correlation in adipogenesis regulation is not surprising. HOXC8 is a member of HOX family present at high levels in white progenitors and strongly decreases during brown differentiation. Indeed, it acts as a brown adipogenesis inhibitor and is directly repressed by miR-196a. In addition, HOXC8 regulates C/EBPβ expression by binding the C/EBPβ locus, as shown by chromatin immunoprecipitation assay (ChIP) in mouse. A role for miR-196a in promoting brown-like differentiation is supported by the in vivo experiments where transgenic mice for this miRNA demonstrate high energy consumption and resistance to obesity [302].

MiR-138 is encoded by mir-138-1 and mir-138-2 genes located on the chromosomes 3 and 16 respectively [304]. MiR-138 was reported to inhibit human adipose derived stem cell (ADMSC) differentiation and to target EP300 inhibitor of differentiation 1 (EID1) [305]. EID1 was reported to inhibit 3T3-L1 differentiation into white adipocytes by decreasing PPARɣ expression via pRb inhibition. EID1 was associated with decreased lipid droplet formation and increased expression of brown genes such as UCP1 and PGC-1α [306]. Similarly, other studies showed that treatment with EID1 leads to ADMSC differentiation into highly metabolic adipocytes expressing high levels of UCP1 and CITED1 (Cbp/P300 interacting transactivator with Glu/Asp rich Carboxy-terminal Domain 1) [307], while EID1 suppression inhibited ADMSC differentiation [305]. EID1 was proposed as a promoter of white adipocyte transdifferentiation into beige adipocytes [307]. According with these findings, at least partially, miR-138 was downregulated in differentiating ADMSC and its overexpression resulted in reduced fat accumulation and downregulation of CEBPα, PPARɣ2, FABP4 and LPL [305]. Therefore, miR-138 is likely to inhibit brown/beige adipogenesis in favour of the white phenotype by repressing EID1. MiR-138 was found to be overexpressed in amniotic MSC (hAMSC) from obese mothers compared to lean controls [308] while it was overexpressed in serum from non-diabetic obese subjects compared to lean controls [309]. This suggests that the intracellular and extracellular role of miR-138 in obesity may differ depending on the cell type in which it is synthesised or taken up.

Some other miRNAs have been identified as suppressor of adipose differentiation. MiR-448 inhibits adipogenesis by negatively regulating Kruppel-like factor 5 (KLF5) [310], miR-369-5p by targeting FABP4 and reducing levels of adiponectin [311], while

miR-130 by targeting PPARɣ [312]. MiR-29a/b/c was found to be downregulated during the contact inhibition stage and its overexpression inhibited adipogenesis by targeting DNA methyltransferase 3 (DNMT3A) [313] which is involved in the epigenetic modification of DNA during adipogenesis [314].

1.3 Hypothesis & Aims

The adipose tissue has an important role in maintaining the energy homeostasis balance. Understanding its physiology is important for the development of treatments against diseases where this equilibrium is compromised, such as obesity and associated metabolic disorders. MiRNAs are important gene regulators and an increasing body of evidence suggests their involvement in adipogenesis and adipose metabolism. MiRNAs can also be secreted in the extracellular environment and be taken up by distal cells, mediating cell-to-cell communication. Exosomes secreted by the adipose tissue were found to contain miRNAs capable of regulating gene expression in distal organs. However, a large part of the data derive from analysis of miRNAs in blood samples or miRNAs released by adipose tissues, where it is not possible to identify the specific cellular component secreting miRNAs. Circulating miRNAs are transported by different types of carriers, however, most of the studies have focussed either on total adipose miRNAs or specifically on adipose exosomal miRNAs, leaving the other typology of miRNA carriers largely unexplored. Therefore, we hypothesise that brown and white adipocytes secrete different miRNAs that can potentially mediate cell-to-cell communication and that also vesicle-free systems contribute to adipose-miRNA transport. Stimulation of ß-adrenergic receptors in adipocytes triggers a cascade that induces transcription of several factors and activation of the beta oxidative program; therefore, we hypothesise that it can also affect miRNA expression and secretion.

The high degree of cell heterogeneity of human BAT and its scarce availability for scientific research, slow the progresses on comprehending the differences between human brown and white adipocytes. We hypothesise that as in the mouse, human brown and white adipocytes, besides having substantial differences in terms of gene and miRNA expression, secrete different miRNAs for cell-to-cell communication. For all these reasons we aimed:

1) To identify microRNAs differentially secreted between undifferentiated and differentiated brown and white adipocytes in mouse.

2) To test extracellular and intracellular level of expression of the selected miRNAs among the ones identified as differentially expressed among undifferentiated and mature

brown and white adipocytes, in different adipose models in order to verify consistency/inconsistency between mouse and human adipocytes.

3) To identify microRNAs differentially secreted by mature brown and white adipocytes in human cells.

4) To predict miRNA targets of the secreted microRNAs which display a pattern of expression that is consistent across the adipose models for further investigations on the role of miRNAs in the cross-talk between adipocytes and distal cells.

5) To define whether the selected miRNAs are released by adipocytes in the extracellular environment preferentially through incorporation into vesicles or in association with vesicle-free systems.

7) To assess whether ß-adrenergic stimulation affects miRNA release.

6) To identify genes differentially expressed between human mature brown and white adipocytes.

7) To identify pathways enriched in human brown versus white adipocytes.

8) To identify miRNAs potentially involved in the pathways associated with the genes differentially expressed between human brown and white adipocytes.

Chapter 2 – Materials & Methods

2.1 Materials

2.1.1 *Cell Culture Reagents*

DMEM/F12 (Gibco, Fisher Scientific, Loughborough, UK)

Advanced DMEM (Gibco, Fisher Scientific, Loughborough, UK)

Seahorse XF Base Media (Agilent Technologies, Stockport, UK)

Heat Inactivated Foetal Bovine Serum (Fisher Scientific, Loughborough, UK)

Penicillin/Streptomycin (100X) (Fisher Scientific, Loughborough, UK)

L-Glutamine (100x) (Invitrogen, Fisher Scientific, Loughborough, UK)

Bovine Serum Albumin (Sigma-Aldrich, Haverhill, UK)

Krebs-Ringer Bicarbonate Buffer (Sigma-Aldrich, Haverhill, UK)

Collagenase, Type 1 (Sigma-Aldrich, Haverhill, UK)

Insulin (10 mg/ml) (Sigma-Aldrich, Haverhill, UK)

Dexamethasone (Sigma-Aldrich, Haverhill, UK)

3-Isobutyl-1-methylxanthine (Sigma-Aldrich, Haverhill, UK)

Indomethacin (Sigma-Aldrich, Haverhill, UK)

Rosiglitazone (Cayman Chemical, Cambridge, UK)

Triiodo-L-thyronine (Sigma-Aldrich, Haverhill, UK), Haverhill, UK)

0.05% Trypsin-EDTA (Invitrogen, Fisher Scientific, Loughborough, UK)

2.1.2 *Europium-based like Elisa Reagents*

Primary antibodies

CD9 (Monoclonal Mouse IgG_{2B}) (R&D, Bio-Techne, Abingdon, UK)

CD81 (Monoclonal Mouse IgG1) (Bio-Rad AbD Serotec, Kidlington, UK)

CD63 (Monoclonal Mouse IgG1) (Bio-Rad AbD Serotec, Kidlington, UK)

Human Serum Albumin (Monoclonal Mouse IgG_{2A}) (R&D, Bio-Techne, Abingdon, UK)

IgG2b (eBioscience, Fisher Scientific, Loughborough, UK)

IgG1 (eBioscience, Fisher Scientific, Loughborough, UK)

Secondary antibodies

Anti-mouse IgG (Goat) biotin labelled (Perkin Elmer, Shropshire, UK)

Reagents

DELFIA Eu-N1 Streptavidin (Perkin Elmer, Shropshire, UK)

DELFIA Wash Buffer (Perkin Elmer, Shropshire, UK)

DELFIA Assay Buffer (Perkin Elmer, Shropshire, UK)

Enhancement Solution (Perkin Elmer, Shropshire, UK)

Reagent Diluent (R&D, Bio-Techne, Abingdon, UK)

2.1.3 *Chemicals and reagents*

Ethanol (Sigma-Aldrich, Haverhill, UK)

Chloroform (Sigma-Aldrich, Haverhill, UK)

Random Hexamers (Invitrogen, Fisher Scientific, Loughborough, UK)

JumpStart SYBR Green I Mix (Sigma-Aldrich, Haverhill, UK)

MMLV Reverse Transcriptase (Sigma-Aldrich, Haverhill, UK)

RNAse OUT Ribonuclease Inhibitor (Invitrogen, Fisher Scientific, Loughborough, UK)

TRI reagent® (Sigma-Aldrich, Haverhill, UK)

100x ROX reference dye (Sigma-Aldrich, Haverhill, UK)

Dimethyl sulfoxide (DMSO) (Sigma-Aldrich, Haverhill, UK)

DNase I, amplification grade (Sigma-Aldrich, Haverhill, UK)

10x MMLV buffer (Sigma-Aldrich, Haverhill, UK)

Glucose powder (Sigma-Aldrich, Haverhill, UK)

Sodium Pyruvate (100mM) (Fisher Scientific, Loughborough, UK)

Oil Red O (Sigma-Aldrich, Haverhill, UK)

10mM dNTP mix (Invitrogen, Fisher Scientific, Loughborough, UK)

5x Reaction BF (Exiqon, Vedbaek, Denmark)

Enzyme mix (Exiqon, Vedbaek, Denmark)

Particle-free water (Fresenius Kabi, Runcorn, UK)

RNase-free water (Invitrogen, Fisher Scientific, Loughborough, UK)

2.1.4 *Kits*

miRCURY^{TM} RNA Isolation Kit-Biofluids (Exiqon, Vedbaek, Denmark)

miRCURY LNA^{TM} Universal RT microRNA PCR (Exiqon, Vedbaek, Denmark)

Amplification grade DNase I kit (Sigma-Aldrich, Haverhill, UK)

DNA extraction REDExtract-N-Amp (Sigma-Aldrich, Haverhill, UK)
miRNeasyR Mini Kit (Qiagen, Manchester, UK)
miRCURY LNA^{TM} Hi-Power Labeling Kit Hy3^{TM}/ Hy5^{TM} (Exiqon, Vedbaek, Denmark)
Illumina TruSeq Stranded mRNA Library Prep Kit (Exiqon, Vedbaek, Denmark)

2.1.5 *Media formulations*

DMEM/10 Media (Fisher Scientific, Loughborough, UK)
DMEM/F12 with phenol red supplemented with 10% v/v FBS and 1% (v/v) Penicillin/Streptomycin

A-DMEM/3 Media (Fisher Scientific, Loughborough, UK)
Advanced DMEM/F12 with phenol red supplemented with 3% (v/v) FBS, 1% (v/v) Penicillin/Streptomycin and 1% (v/v) L-Glutamine

Seahorse Media for Oxygen Consumption assay (Agilent Technologies, Stockport, UK)
Seahorse XF base media, Glucose (25mM), Sodium Pyruvate (1mM), pH 7.4

2.1.6 *Buffers*

10x Dnase I Reaction buffer (Sigma-Aldrich, Haverhill, UK)
200 mM Tris-HCl, pH 8.3, 20 mM MgCl2

DNase Stop solution (Sigma-Aldrich, Haverhill, UK)
50 mM EDTA

MMLV 10x reaction buffer (Sigma-Aldrich, Haverhill, UK)
500 mM Tris-HCl, pH 8.3, with 500 mM KCl, 30 mM MgCl2, 50 mM DTT

Phosphate Buffered Saline (PBS)
140mM NaCl, 2.5mM KCl, 1.5mM KH_2PO_4 pH7.2, 10mM Na_2HPO_4 ,pH7.2

Kreb-Ringer bicarbonate buffer (Sigma-Aldrich, Haverhill, UK)

1.8 g/L D-Glucose, 0.0468 g/L Magnesium Chloride [Anhydrous], 0.34 g/L Potassium Chloride, 7 g/L Sodium Chloride, 0.1 g/L Sodium Phosphate Dibasic [Anhydrous], 0.18 Sodium Phosphate Monobasic [Anhydrous], 1.26g/L Sodium Bicarbonate, pH 7.4.

2.1.7 *Solutions*

Seahorse Calibrant Solution (Agilent Technologies, Stockport, UK)
Paraformaldehyde 4% in PBS (1X) (Affymetrix, Buckinghamshire, UK)
Harris Haematoxylin Solution (Sigma-Aldrich, Haverhill, UK)
Extracting Solution (Sigma-Aldrich, Haverhill, UK)
Tissue Preparation Solution (Sigma-Aldrich, Haverhill, UK)
Neutralization Solution (Sigma-Aldrich, Haverhill, UK)
Lysis Solution BF (Exiqon, Vedbaek, Denmark)
Protein Precipitation Solution BF (Exiqon, Vedbaek, Denmark)
Wash Solution 1 BF
Wash Solution 2 BF
Acid Ethanol: 1 ml concentrated Hydrochloric Acid in 400 ml 70% ethanol
Eosin (Sigma-Aldrich, Haverhill, UK)
Eosin Yellowish (1g) in 100 ml of distilled water

Stock Oro Solution (Sigma-Aldrich, Haverhill, UK)
Stock Oil Red O powder (0.5g) in 100 ml of absolute isopropanol

Working Oro Solution
Stock Oro solution diluted in distilled water 3:2

2.1.8 *Primers and oligonucleotides*

ʎ-Bacteriophage RNA (Sigma-Aldrich, Haverhill, UK)
Unisp6 and all Spike-ins (Exiqon, Vedbaek, Denmark)
LNA miRNA Primers (Exiqon, Vedbaek, Denmark)

Table 1 Primer sequences for human genes

Gene Name	Forward primer	Reverse primer
L19	GCGGAAGGGTACAGCCAA	GCAGCCGGCGCAAAA
UCP1	GTGTGCCCAACTGTGCAATG	CCAGGATCCAAGTCGCAAGA
FABP4	TGTTGCAGAAATGGGATGGAAA	CAACGTTCCCTTGGCTTATGCT
HOXC9	CCGGCAGCAAGCACAAAGAG	AGCGGGCGTGAATCCAGTT
CIDEA	CATGTATGAGATGTACTCCGTGTC	GAGTAGGACAGGAACCGCAG
PGC1a	TGAAGAGCGCCGTGTGATT	CAGTTCTGTCCGTGTTGTGTCA
FABP3	CTGGAAGCTAGTGGACAGCAA	CACCTGCCTGGTAGCAAAAC
AGO2	CCAGCTACACTCAGACCAACAGA	GAAAACGGAGAATCTAATAAAATCATGAC
DICER1	TTGCTTGAAATGGAACCAGAAA	ACTCTGACCTTCCCGTCGTAAG
GW182	TACTGTGCGGGAAGTTGAC	CCAGGCACTAGTTGAAGGCA
SLC27A2	AAGGCCCCGGTTTCTAAGAA	TTAAAGCCCTCCTCCTCCACCAG
CPT-1B	AGGAGCCCTCTCATGGTGAA	TGGCGTGGATGATGTTTCCC
CYT-B	ACAACCCCCTAGGAATCACC	GAGGGCGTCTTTGATTGTGT
RIP140	ACATTTGGAGGGAGGCTTCAT	GCTTTCGTTTCTGCAGTAGGAAGTA

Table 2 Primer sequences for mouse genes

Gene Name	Forward primer	Reverse primer
L19	GGAAAAAGAAGGTCTGGTTGGA	TGATCTGCTGACGGGAGTTG
Ucp1	TACCCAAGCGTACCAAGCTG	ACCCGAGTCGCAGAAAAGAA
aP2	ACACCGAGATTTCCTTCAAACTG	CCATCTAGGGTTATGATGCTCTTCA
Cidea	CACGCATTTCATGATCTTGGA	GTTGCTTGCAGACTGGGACAT
Dicer1	TTTGCACGTACCCTGATGCT	TTGCCAAGGCGATACAGGTT
Ago2	CCATCTAGCTGTGAAGGCTCTGA	TTCTTAGGGCCAGGCTTTAAAA
Gw182	GACAATGTCATGCCCCACACT	CAAGCCTATAGGAAAGTTGCTGAAA

2.1.9 *Miscellaneous*

Oil Red O (Sigma-Aldrich, Haverhill, UK)

Cell strainer (40 μm) (Fisher)

Syringe filters (0.22 μm) (MicroScience)

Seahorse XF24 cell culture microplates and cartridges (Agilent, Technologies, Stockport, UK)

Cell culture plates (Fisher Scientific)

OptiSeal 32.4 ml tubes system (Beckman Coulter)

RNase-free tubes (Sigma-Aldrich, Haverhill, UK)

Elisa Strip Plate, F16, highbinding (Greiner Bio One)

Permount (Invitrogen, Fisher Scientific, Loughborough, UK)

Optically clear adhesive seals (Appleton Woods)

miRCURY LNA^{TM} microRNA Array 7th Gean (Exiqon)

RNeasyR Mini Spin Columns (Quiagen)

MicroRNA Mini Spin Columns (Exiqon)

100 nm Polystyrene Latex Beads (Sigma-Aldrich, Haverhill, UK)

2.2 Methods

2.2.1 *Cell culture and differentiation*

Adipose tissue consists of a heterogeneous population of cells including pre-adipocytes and mature adipocytes. Even though the mature adipocytes represent the major component of the tissue, being differentiated cells they have lost mitotic properties and cannot proliferate. Therefore, to obtain a sufficient number of cells to perform experiments or create an immortalised cell line it is necessary to isolate pre-adipocytes which can be grown and successively differentiated *in vitro*.

2.2.1.1 *In vitro differentiation*

Several protocols have been developed to induce *in vitro* adipocyte differentiation. Treatments generally consist of the same set of drugs with concentrations and length of treatment being adapted to the different cells of interest in order to optimise differentiation. The differentiation cocktail usually contains triiodothyronine (T_3), dexamethasone, indomethacin (Indo), insulin, 3-isobutyl-1-methylxanthine (IBMX), hydrocortisone and a thiazolidinedione (TZD) drug, like rosiglitazone. TZDs are a group of drugs that are known to activate PPARγ, hence, stimulating adipogenesis and differentiation [26]. However, some brown adipocyte cell lines do not require rosiglitazone for differentiation, while, in white adipocytes rosiglitazone is normally included to induce differentiation. Insulin is a potent hormone able to induce adipogenesis by activating a signal transduction cascade that culminates with adipose-specific gene transcription, although the precise mechanism is still not fully clarified. However, insulin has been proposed to act through insulin receptor substrates 1 and 2 (IRS1 and IRS2) by promoting CREB and MAPK phosphorylation [316, 317]. Dexamethasone (Dex) is a synthetic glucocorticoid and has been demonstrated to synergistically act with insulin in adipose differentiation through glucocorticoid receptors [318]. IBMX, a non-specific inhibitor of phosphodiesterases [319], acts on differentiation by increasing intracellular cAMP levels that is a crucial event for differentiation as previously discussed in the introduction. T3 is a thyroid hormone that promotes adipose gene expression through nuclear T3 receptors [320]. T3 has also been demonstrated able to induce UCP1 expression in primary adipocytes [321]. Indomethacin is a non-steroidal anti-inflammatory drug able to inhibit cyclooxygenases (COX). However, as proposed by

Styner et al., indomethacin exerts a pro-adipogenic effect by increasing C/EBP and PPARγ expression in a prostaglandin-independent way [322].

2.2.1.2 *Mouse interscapular brown and subcutaneous white primary adipocytes*

Primary adipocytes were obtained and differentiated as previously described [323]. Briefly, interscapular BAT and subcutaneous WAT were dissected from 4 to 10-week old mice. The tissues were digested in a Krebs-Ringer bicarbonate buffer (KRB) solution containing 0.2% collagenase Type I and 2% BSA. After 45 minutes, 8 ml of KRB solution containing 2% BSA was added to every 3 ml of digested tissue to stop the enzymatic activity of collagenase. The tissues were centrifuged at 1000 rpm for 7 min at RT and the supernatant was discarded. The stromal fraction was resuspended in DMEM/F12, penicillin/streptomycin 1% and FBS 10% (DMEM10), filtered through a 40 µm strainer and plated in tissue culture flasks. Media was replaced every other day and cells were allowed to grow until 80/90% confluent. Following trypsinization, 4 – 5 x 10^4 cells per well were reseeded in a 12-well dish. At 100% confluence differentiation was started. Concentrations of components contained in induction and maintenance media for differentiation protocol are listed in table 4. Induction media was added and left for 96 hours, at the end of which, it was replaced with maintenance media 1. After 48 hours cells were switched to maintenance 2 and kept for at least 48 hours prior to start experiments.

Table 3 Media for mouse brown and white primary cells differentiation (in DMEM/10)

Compound	Induction Media (96 h)	Maintenance media 1 (48 h)	Maintenance media 2
Insulin	1 µg/ml	1 µg/ml	1 µg/ml
T_3	1 nM	1 nM	1 nM
Rosiglitazone	2 µM	2 µM	-
IBMX	250 µM	-	-
Indomethacin	30 µM	-	-
Dexamethasone	0.5 µM	-	-

2.2.2 Explants

Interscapular BAT and subcutaneous WAT explants were obtained from 4 to 10-week old mice. The dissected tissues were cut into 2 mm pieces using scissors in order to increase the tissue surface in contact with the media for gaseous exchange, thereby minimising the necrosis process. The explants were placed into cell culture inserts in 6-well plates and incubated for 2 hours in DMEM10 at 37 °C, 5% CO_2. After 5 washes

with DMEM/F12 to remove debris and serum traces, explants were left in serum-free media (2 ml) for 6 hours either in the presence of CL316,243 (CL) (10 μM) or DMSO for control wells. Media was collected for miRNA detection. Tissues were frozen in liquid nitrogen, weighed and homogenised in 1 ml of TRI reagent® for total RNA extraction.

2.2.2.1 *Mouse immortalised adipocytes*

Brown and white adipose tissue cell lines were generated previously [324]. Briefly, interscapular BAT and subcutaneous WAT of four 10-week old female 129Sv mice were digested and centrifuged. The cells collected from the stromal vascular fraction were cultured and immortalized with retroviral-mediated expression of temperature-sensitive simian virus 40 (SV40) large T-antigen (H-2Kb-tsA58). Cells were grown at 33 °C in DMEM10, and selected for 2 weeks in the presence of 100mg/ml Geneticin (G418) [324]. Afterwards, G418 concentration was decreased to 50 μg/ml [5]. Cells were passaged at 80% confluence and experiments were conducted between 12-26 passages. Cells were seeded in plates pre-coated with 0.1% gelatin and at 80% confluency differentiation was started. Two different protocols were used to differentiate brown and white adipocytes. Components and their concentration in induction and maintenance media for white and brown adipocytes are listed in table 5 and 6 respectively. Induction media and maintenance media were administered for 96 and 48 hours respectively to differentiate white adipocytes. Next, cells were kept in maintenance media 2 before starting experiments. For brown adipocytes, differentiation induction media was added and kept for 48 hours. Subsequently, cells were cultured in maintenance 1 until experiments were started.

Table 4 Media for mouse white adipose cell lines differentiation (in DMEM/10)

Compound	Induction Media (96 h)	Maintenance media 1 (48 h)	Maintenance media 2
Insulin	5 µg/ml	1 µg/ml	1 µg/ml
T_3	0.1 nM	0.1 nM	0.1 nM
Rosiglitazone	5 µM	1 µM	-
Biotin	16 µM	16 µM	-
Pantothenic acid	1.8 µM	1.8 µM	-
Ascorbic acid	100 µM	100 µM	-
IBMX	500 µM	-	-
Dexamethasone	0.25 µM	-	-

Table 5 Media for mouse brown cell line differentiation (in DMEM/10)

Compound	Induction Media (48 h)	Maintenance media
Insulin	1 µg/ml	1 µg/ml
T_3	1 nM	1 nM
Indomethacin	125 µM	-
IBMX	500 µM	-
Dexamethasone	0.25M	-

2.2.2.2 *Human immortalised brown and white adipocytes*

Human brown and white adipose cell lines were a kind gift from Prof Fredrik Karpe (University of Oxford). Preadipocytes were obtained from abdominal subcutaneous adipose tissues of a lean and healthy male volunteer as reported by *Collins at al.,* [325] and immortalized by using the pLenti6.3/V5-DEST lentiviral expression system to coexpress human telomerase reverse transcriptase (hTERT) and human papillomavirus type-16 E7 oncoprotein (HPV16-E7) as described by Pinnick *et al.,* [326]. The brown/beige cell line was generated from adipose tissue obtained from a neck dissection using the same methodology (data not published).

Cells were seeded in 12-well gelatin pre-coated plates and grown at 37 °C, 5% CO_2 in DMEM10. At 80% confluency, differentiation was started. Induction and maintenance media were prepared in Advanced DMEM/F12, FBS 3%, penicillin/streptomycin and L-Glutamine 1% (A-DMEM3) as illustrated in table 7. Induction media was added to the cells and refreshed every 3 days. Starting from day 12, concentration of all the compounds was serially decreased by 2-fold every two days for brown adipocytes while, on day 12, white adipocytes were switched to maintenance media 1. In both cases media was refreshed every 2 days for the next 6 days to reach full

differentiation. Prior to any experiment, brown and white adipocytes were kept for 48 hours in maintenance media 2.

Table 6 Media for human brown and white adipocyte differentiation (in A-DMEM3)

Compound	Induction Media	Maintenance media 1 (white adipocytes only)	Maintenance media 2
Insulin	1 µg/ml	1 µg/ml	1 µg/ml
T_3	10 nM	0.1nM	0.1nM
Rosiglitazone	5 µM	5 µM	-
IBMX	500 µM	-	-
Dexamethasone	0.25 µM	-	-
Indomethacin	125 µM	-	-

2.2.3 Haematoxylin-eosin *stain* for histology

Haematoxylin and eosin staining of brown and white adipose tissues was performed by Dr Sean James (University of Warwick). Briefly: dissected tissues, with a thickness of about 3 mm, were immediately placed into 4% paraformaldehyde for fixation. After a maximum of 48 hours, tissues were moved into 70% ethanol. Next, casseting and wax infiltration steps were performed prior to embedding into paraffin block. Tissue sections were cut, so that width was approximatively 4 µm, and collected onto glasses slides. Wax ribbons were transferred onto a warm water bath (43-45°C) and spread on the microscope glass slide before drying at least for one hour at 45°C. To perform haematoxylin stain, the slides were deparaffinised by bathing three times in Xylene, three times in ethanol (sequentially: 100%, 95% and 80%) for 3 minutes each and rinsed in deionized water for 5 minutes. Subsequently, the slides were stained with Haematoxylin for 3 to 10 minutes, and rinsed in tap water. Next, the slides were quickly dipped 12 times in acid ethanol for destaining, rinsed twice in tap water and once in deionized water, for 2 minutes each time. The slides were then stained with eosin for 30 seconds and bathed 3 times in 95% ethanol, 3 times in 100% for 5 minutes each time and 3 times in Xylene for 15 minutes. Tissue sections were covered with coverslip slides Permount and dried overnight under hood prior to histology analysis.

2.2.4 *Oil Red O staining*

A stock solution of Oil Red O (ORO) was made by dissolving 0.5 g of ORO powder in 100 ml of absolute isopropanol and stirred overnight. Stock ORO solution was further diluted in distilled water 3:2, stirred for 10 minutes and passed through a 0.22 µm filter. Medium was removed from adipocytes and cells were washed with PBS. Cells were fixed with 4% paraformaldehyde for 15 min. Paraformaldehyde was removed and cells were washed twice with PBS for 5 min. Working ORO solution (500µl) was added to each well and incubated for 1h. Afterwards, the ORO solution was discarded and cells were quickly washed with 60% isopropanol. Cells were further washed with PBS and examined by microscopy. All steps were performed at RT. Stained cells were stored at 4 °C in PBS.

2.2.5 *DNA isolation*

DNA from human adipocytes was isolated using the DNA extraction REDExtract-N-Amp^{TM} Tissue PCR Kit protocol. A mix containing Extraction Solution and Tissue Preparation solution 4:1 was prepared for n+1 samples. To lyse the cells, 60 µl of this mix was added into each well of a 12-well plate. After scraping and homogenising, the lysates were placed into fresh nuclease-free tubes and incubated at RT for 10 min and at 95 °C for 3 min. Neutralization Solution B (50 µl) was added to each tube. Samples were vortex mixed and diluted 1:4 in nuclease-free water. DNA concentration was measured using a NANOdrop. To perform relative mitochondrial DNA quantification, 10ng of DNA was amplified through Real Time qPCR.

2.2.6 *Total RNA isolation from cells*

Medium was removed and cells were washed with PBS, lysed in 1 ml of T RI reagent® and transferred into RNase-free tubes. Samples were incubated at room temperature (RT) for 5 minutes to allow the complete dissociation of the nucleoprotein complex. Chloroform (0.2 ml, TRI reagent®:Chloroform 5:1 v/v) was added and samples were vigorously shaken for 15 seconds, incubated at RT for 3 min and centrifuged at 12,000 x g for 15 minutes at 4 °C. The lower red phenolchloroform phase and the interphase, resulting from phase separation, were discarded. The upper aqueous phase was transferred into a new RNase-free tube and 100% Isopropanol (0.5 ml, TRI reagent®: Isopropanol 2:1 v/v) was added. Samples were incubated for 10 minutes at RT to allow

RNA precipitation followed by centrifuging at 12,000xg for 15 minutes at 4 °C. The supernatant was removed; the pellet was washed with 75% Ethanol (1 ml) and centrifuged at 7,500xg for 5 minutes at 4 °C. The supernatant was discarded, the pellet was air-dried and resuspended in 10 µl of RNase-free water. RNA concentration was measured using a NANOdrop (lab-tech).

2.2.7 *Medium sample collection and exosome precipitation*

Medium was removed from cells or explants. Cells were washed five times with PBS and cultured in serum-free medium. Media samples were collected after 5/24/96 hours or 5 days and transferred into 15 ml tubes. A series of centrifugation steps was then performed: to eliminate non-adherent cells, samples were centrifuged at 300xg for 10 min and the pellet was discarded; samples were than centrifuged at 16,000xg for 25 min, passed through 0.22 µm filters and either stored at -80 °C, directly processed for miRNA analysis or ultra-centrifuged at 120,000xg for 2 hours with OptimaL-100 XP ultracentrifuge (Beckman) rotor SW32Ti to isolate vesicles. The pellet was gently washed with PBS and resuspended in 2.5 ml of PBS or unconditioned serum-free media. Samples were analysed for vesicle characterization.

2.2.8 *RNA isolation from media and serum samples*

Total RNA was extracted from serum or media samples using the MIRCURY™ isolation kit-biofluids. An aliquot of 250 µl per sample was transferred to a new microcentrifuge tube. Lysis solution BF (60 µl) containing 16.67 µg/mL of RNA carrier (ʎ or MS2-bacteriophage RNA) and 1 µL of spike-in template mixture or Unisp6 spike-in alone was added to each sample. After mixing, samples were incubated for 3 min at RT. Next, 20 µl of Protein Precipitation solution BF were added. After 1 minute of incubation at RT samples were centrifuged at 11,000 x g for 3 min. The clear supernatant was transferred to a new collection tube and 270 µl isopropanol was added to the spin column. The solutions were mixed and transferred to a binding column. The column was incubated for 2 min at RT and emptied using a vacuum-manifold or centrifuged for 30 sec at 11,000xg followed by flow-through discard. Wash solution 1 BF (100 µl) was added to the spin column and emptied or centrifuged as before. The same operation was performed with 700 µl and successively 250 µl of wash solution 2 BF. To dry the column entirely the last vacuum or centrifugation was extended to 2 min. The dry spin columns

were transferred to a new collection tube and 50 µl of RNase free water was added directly on the membrane of the spin column. The column was incubated for 1 min at room temperature prior to centrifugation at 11,000xg. The RNA was stored at -80 °C or directly reverse transcribed into cDNA.

2.2.9 *Reverse transcription*

Principle

In reverse transcription, total RNA is converted into cDNA by a reverse transcriptase enzyme (DNA polymerase RNA-dependent) in the presence of nucleotides and a primer. The primer can be non-specific or specific for the gene of interest. The reaction results in RNA-DNA hybrid products. The newly polymerized DNA will work as template in the next amplification through classic PCR or Quantitative Real-Time PCR reaction (q-PCR). The product amplified is proportional to the initial amount of RNA (Figure 9 panel A).

In this study the reagents for reverse transcription reaction were: Moloney Murine Leukemia Virus Reverse Transcriptase (M-MLV) and random hexamers for total RNA reverse transcription. To reverse transcribe microRNAs the miRCURY LNA™ Universal RT Kit has been used. A poly (A) tail is ligated to the mature microRNA template. A poly thymine (T) primer with a 3' degenerate anchor, consisting of bases that can bind to any base and a 5' universal tag is used to synthesize the cDNA. The latter can be successively amplified in the Q RT-PCR reaction (figure 9 panel B).

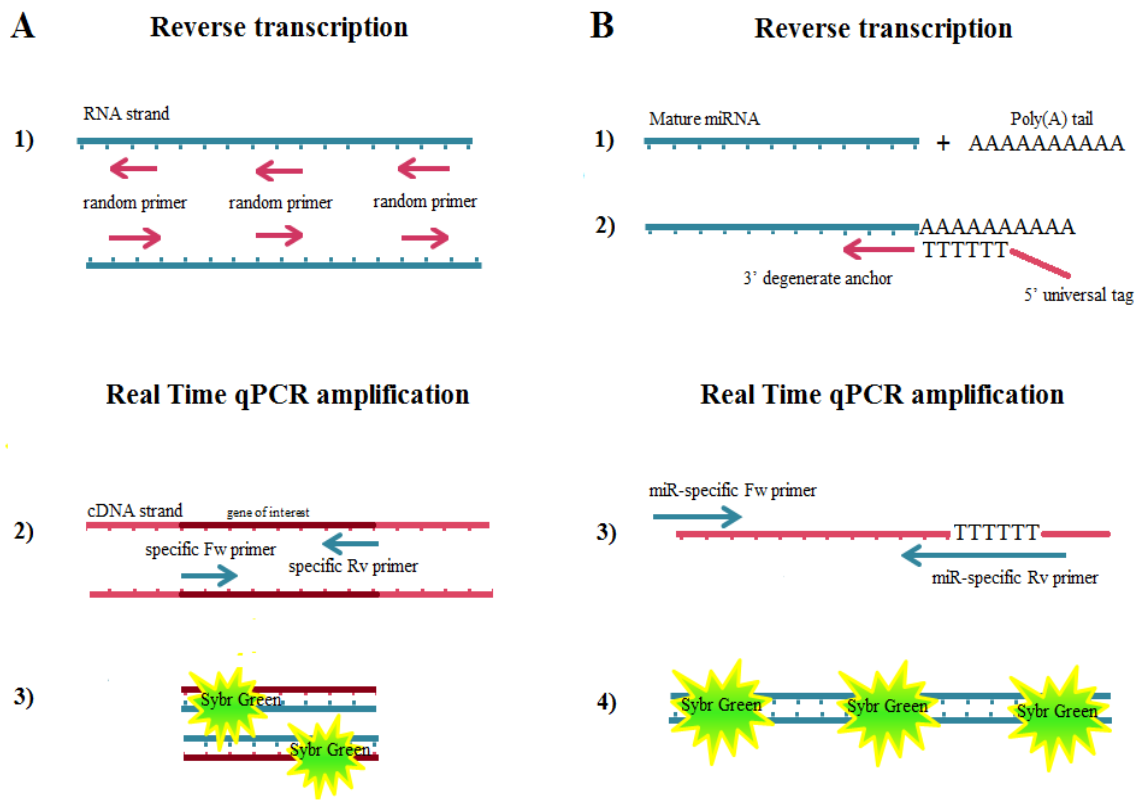

Figure 9 Representation of reverse transcription and Real-Time qPCR.
A) Reverse transcription using random hexamer. 1) Random primers anneal to complementary mRNA sequences and total RNA is converted into cDNA. 2) The gene of interest is amplified by the use of forward and reverse primers specific for that gene. Sybr green molecules intercalate the double stranded cDNA and the signal increases with the amplification of the gene. B) Reverse transcription using Universal MIRCURY LNA RT. 1) Poly(A) tails are ligated to the mature miRNAs. 2)The primer for the reverse transcription consists of a 3' degenerate anchor able to bind to any base, a poly(T) portion that anneals to the poly(A) tail of the mature miRNA and that is attached to a 5' universal tag allowing miRNA reverse transcription into cDNA. 3) These regions in the cDNA synthesized will be complementary to the miR-specific reverse primer and will work as a template in the Real Time qPCR. The miR-specific reverse and forward primers anneal to the miRNA of interest and allow miRNA amplification, 4) which is the quantified by the Sybr Green signal.

2.2.9.1 *DNase treatment*

To remove DNA contamination, 200 ng of cellular RNA were dissolved into 4 µl of free-RNase water and treated with 0.5 µl of amplification grade DNase I and 0.5 µl of 10x DNase I buffer. After 15 min of incubation at RT, the reaction was stopped by adding 0.5 µl of stop solution and incubating at 65 °C for 10 min to inactivate the DNase I.

2.2.9.2 *Cellular total RNA RT*

To reverse transcribe total cellular RNA, 1 µl of Random Hexamers and 1 µl of dNTPs were added to the DNase-treated samples. The reactions were made up to 12 µl with water, incubated at 70 °C for 10 min and cooled in ice for 2 min. Afterwards, a master mix for n+1 samples was prepared and added to the samples. It contained for each sample: M-MLV Buffer (2 µl), M-MLV (1 µl), RNase OUT (0.5 µl) and RNase-free water up to 20 µl final volume of reaction. Reverse transcription reaction conditions were 25 °C for 10 min, 37 °C for 50 min and 80 °C for 10 min. The obtained cDNA was diluted by adding 150 µl of nuclease-free water and stored at -20 °C.

2.2.9.3 *MicroRNA Reverse Transcription (miRCURY LNATM Universal RT)*

The concentration of DNase treated-cellular RNA was adjusted to 5ng/µl in RNase-free water and 2 µl of this solution or total RNA from serum/media samples were reverse transcribed in a 10 µl final volume of total reaction, containing 5x Reaction Buffer (2 µl), nuclease-free water (5 µl) and enzyme mix (1 µl). For cellular RNA reverse transcription, 1 µl of water was substituted with 0.5 µl of Synthetic Unisp6 RNA spike-in and 0.5 µl of random hexamers. To ensure the same concentration of all the reagents for each reaction, a mix for n+1 sample was prepared and 8 µl of this was added to each RNA sample. The reaction was gently vortexed and incubated for 60 min at 42 °C. The reverse transcriptase was heat-inactivated for 5 min at 95 °C. The newly formed cDNA was immediately cooled at 4 °C and directly amplified or stored at -20 °C. Before PCR, cDNA was diluted 1:80 in nuclease free water.

2.2.10 *Real Time Quantitative PCR (qPCR)*

2.2.10.1 *Principle*

Quantitative Real-Time PCR allows relative DNA amplification and its simultaneous quantification by the use of particular fluorescent systems. It is based on a classic PCR, where, during the exponential phase, the amount of amplified DNA copies is proportional to the initial cDNA quantity and to the fluorescence emitted by the fluorophore. Through this technique it is possible to measure the absolute or relative expression/amount of a particular gene using respectively cDNA or genomic DNA as input for the amplification reaction.

In Real Time PCR systems, the user sets the thermal cycles specific for the optimal functioning of the enzyme. During the amplification a laser light, sent through optical fibres, excites the fluorophore's light emission, collected back by the optical fibres, is directed to a spectrophotometer. The signal is detected by a charged coupled device (CCD) camera and analysed by the software. The output results consist of a graphic where the fluorescence signal, ΔRn, at each time point, is plotted versus the cycle number. The software calculates ΔRn by subtracting Rn^- to Rn^+ ($\Delta Rn = Rn^+ - Rn^-$) where the normalized reporter value (Rn) is the ratio between the fluorescence intensity of the reporter dye and the passive reference dye. The Rn values, obtained during the first cycles, are used to determine the baseline Rn-, which represents the background. Indeed, initially, the amount of cDNA template is very low and only the background signal is detectable. Proceeding with the reaction, the DNA copies increase and so do the Rn^+ values. The cycle at which the change of intensity exceeds the threshold of the baseline is referred as threshold cycle (Ct). Therefore, the higher the amount of amplified DNA the lower is the cycle. This reflects the level of expression of the gene and can be used for statistical comparisons, considering that a lower Ct corresponds to a higher amount of amplified DNA.

2.2.10.2 *Primer design*

Primers for mRNA were synthesised by Sigma Aldrich and 100 μM stocks were prepared by dissolving the dried nucleic acids in nucleic acid nuclease-free water and stored at -20 °C. Design was performed using Ensemble Genome Browser Primers tool (http://www.ensembl.org/index.html) or Primer 3 (http://simgene.com/Primer3). Primer characteristics were evaluated through USCS Genome In-silico PCR (http://genome.uscs.edu/cgi-bin/hgPcr). These include: size of product between 70-150 nucleotides, melting temperature and GC content around 60 °C and 55% respectively. Primers for mRNAs of specific proteins were designed so that one was complementary to a sequence of an exon-exon junction, in order to exclude amplification of eventual contaminating genomic DNA.

For mature microRNAs, locked nucleic acid LNA primers were used. LNA primers are oligonucleotides containing one or more locked nucleic acids where the ribose ring is "locked" by a bridge connecting the 2' oxygen and the 4' carbon (figure 10). The presence of these modified nucleotides induces an increase in the melting temperature of

the primer from +2 to +10 °C per each LNA base [327] allowing higher specific complementarity and a shorter length of the sequence compared to unmodified primers. Primer mixes were purchased from Exiqon, dissolved into 400 µl of nuclease-free water, aliquoted and stored at -20 °C.

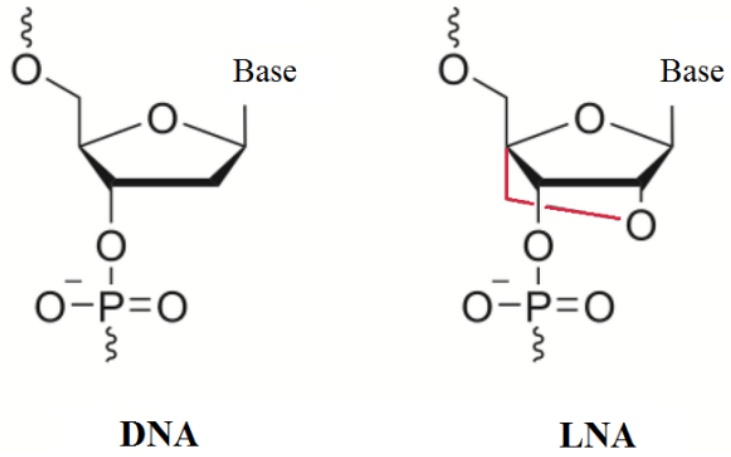

Figure 10 Illustration of DNA and LNA nucleotides.
Left panel shows the structure of a standard deoxyribonnucleotide. In the right panel is represented an LNA monomer which ribose ring present a bridge connecting the 2' oxygen to the 4' carbon.

2.2.10.3 *SYBR Green I PCR*

In this study, Real-Time PCR analysis has been performed by using SYBR Green I. This fluorophore is an asymmetrical cyanine dye able to bind the DNA. The DNA-dye-complex absorbs blue light with a maximum wavelength (λ) of 497 nm and emits green light (λ_{max}= 520 nm). SYBR Green molecules preferentially bind to double stranded DNA intercalating in its minor grooves, hence, fluorescence intensity increases with PCR product accumulation at every cycle.

For genomic or protein-encoding genes 2 µl of cellular DNA/cDNA sample or nuclease-free water non-template control were mixed in a 96 well plate with 18 µl of a master mix previously made and aliquoted in the wells. Master mixes were prepared in different tubes for every target and reference gene with a volume for n+1samples. Each one contained the following reagents at the following final concentrations in 20 µl final volume: 1X Jumpstart SYBR Green I mix, 300 nM forward and reverse primer, ROX reference dye 0.1X and nuclease free-water up to the 20 µl final volume.

Real Time PCRs for microRNA detection were performed similarly. In this case, 4 µl of cDNA or non-template control was used as input. The master mix contained 1X

Jumpstart SYBR Green 1 mix, 0.5 µl of primer mix, ROX reference 0.1X and water up to 10 µl final volume reaction.

Every DNA/cDNA and non-template sample was tested in duplicate. The plates were centrifuged to avoid bubbles and sealed with clear optical seals. PCR reactions were run in the 7500 Real-Time PCR machine (Applied Biosystems). Thermocycler conditions consisted of an initial denaturation at 95 °C for 2 min followed by 40 cycles at 94 °C for 34 s, 60 °C for 34 s and a final step at 72 °C for 30 seconds at which data were collected. A step for melting curves was added to evaluate the presence of single or multiple products.

2.2.10.4 *MiRNA profiling in media from mouse and human adipocytes*

Experiments were conducted at Exiqon Services, Denmark. MiRNA real-time qPCR mouse&rat panel was used for mouse samples and miRNA real-time qPCR human panel for human samples.

RNA isolation from mouse samples was performed as per MIRCURY^{TM} isolation kit-biofluids instructions and as described in paragraph 2.2.8.

Total RNA was extracted from human samples using the Qiagen miRNeasyR Mini Kit. Media was lysed in 700 µl Qiazol lysis reagent in a Qiagen TissueLyzer with one 5mm stainless steel bead. The lysate was transferred into a fresh tube containing 140 µl chloroform, mixed, incubated for 2 min at RT and centrifuged at 12.000xg for 15 min in a 4 °C microcentrifuge. The upper aqueous phase was transferred to a new microcentrifuge tube and 1.5 x volume of 100 % ethanol was added. After mixing gently, 750 µl of the sample was transferred to a Qiagen RNeasyR Mini spin column in a collection tube and centrifuged at 8.000 x g for 15 sec at RT. The process was repeated until all remaining sample had been loaded. The Qiagen RNeasyR Mini spin column was rinsed with 700 µl Qiagen RWT buffer and centrifuged at 8.000xg for 15 sec at RT followed by another rinse with 500 µl Qiagen RPE buffer and centrifuged at 8.000xg for 15 sec at RT. A rinse step (500 µl Qiagen RPE buffer) was repeated twice. The Qiagen RNeasyR Mini spin column was transferred to a new collection tube and centrifuged at 15,000xg for 2 min at RT. The Qiagen RNeasyR Mini spin column was transferred to a new microcentrifuge tube and air dried for 1 min. Total RNA was eluted by adding 50 µl of RNase-free water to the membrane of the Qiagen RNeasyR mini spin column and

incubated for 1 min before centrifugation at 15,000xg for 1 min at room temperature. The RNA was stored in a -80 °C freezer.

The spike-ins used for quality control RNA isolation of both human and mouse samples were Unisp2, Unisp4 and Unisp5.

2.2.10.5 *MiRNA real-time qPCR Panels*

RNA (19 µl) was reverse transcribed in 95 µl reactions using the miRCURY LNA™ Universal RT microRNA PCR, Polyadenylation and cDNA synthesis kit (Exiqon). Each RT was performed in duplicate, including an artificial RNA spike-in (UniSp6). The obtained cDNA was diluted 50x and using a pipetting robot it was transferred together with Exilent SYBR Green mastermix to qPCR panels preloaded with primers in 10 µl PCR reactions, according to the protocol for miRCURY LNA™ Universal RT microRNA PCR; each microRNA was assayed once. For quality controls miR-23a, miR-30c, miR-103, miR-142-3p, miR-451 and the spike-ins were pre-assayed. Negative controls were performed excluding template from the reverse transcription reaction and profiled like the samples. The amplification was performed in a LightCycler® 480 Real-Time PCR System (Roche) in 384 well plates. The amplification curves were analysed using the Roche LC software, both for determination of Cq (by the 2nd derivative method) and for melting curve analysis.

2.2.10.6 *Data analysis*

The raw data was extracted from the Lightcycler 480 software. PCR reactions that gave rise to multiple melting curve peaks or single peaks with melting temperature inconsistent with the specifications for the corresponding assay (in-house database) or with amplification efficiency below 1.6 were removed from the dataset. For Spike-ins and quality control miRNAs an average Cq (quantification cycle) was calculated for the duplicate RT's, and evaluation of expression levels was performed based on raw Cq-values. Only assays that detected 5 Cqs lower than the negative control were included in the data analysis. For assays that did not yield any signal on the negative control, the upper limit of detection was Cq equal to 37. Normalization of raw values after background filtration was performed based on the average of the assays detected in all samples as this is shown to be the best normalization for qPCR studies involving numerous assays [328]. Indeed, the stability value of the average Cq of the assays (143

in mouse and 34 in human) detected in all samples ($n_{(mouse)} = 16$, $n_{(human)} = 8$) calculated through the Normfinder algorithm was the lowest compared the ones of each single miRNA. Therefore ΔCq values were obtained as follows:

Normalized Cq = average Cq – assay Cq (sample)

Principal Component Analysis was performed prior to differential expression analysis to evaluate variation among the assays. Briefly, PCA is a method used to reduce the dimension of large data sets by considering only those variables that inflict large variance to the data. The component accounting for the largest variation is plotted along the X-axis; the second largest is plotted on the Y-axis etc. If samples present pronounced differences in terms of one particular biological characteristic, for example level of differentiation or cell type, this will be a primary component of variance. Each sample will scatter in different areas of the PCA plot corresponding to their biology eventually clustering with samples presenting similarity for that characteristic. This method is particularly useful also to assess the quality of the samples and therefore the reliability of the results that can be obtained by their analysis for a specific experiment. For instance, if RNA quality inflicts further variation to the samples, these last will no longer cluster based on their biology and can be removed from the data analysis. PCA plot for mouse and human experiments was obtained by including the top 50 or 30 microRNAs, respectively, that had the largest variation across all samples.

Normalised Cqs (ΔCq) were used for differential expression analysis. T-test was performed for microRNAs detected in at least three samples per group, to identify differences in miRNA expression between two groups. Raw p-values were adjusted for multiple testing by the Benjamini-Hochberg procedure. The normal distribution of the data was assessed by a Shapiro-Wilk normality test.

2.2.10.7 *MicroRNA array*

RNA from human differentiated brown and white immortalised adipocytes was sent to Exiqon Services, Denmark, where all the experiments were performed. RNA quality was verified by an Agilent 2100 Bioanalyzer profile.

The miRCURY LNA™ microRNA Hi-Power Labeling Kit, Hy3™/Hy5™ (Exiqon, Denmark) was used as per the manufacturer instructions. Total RNA (550 ng) from the samples was labelled with Hy3™ and reference with Hy5™ fluorescent label. The Hy3™

labelled samples and a Hy5™-labelled reference RNA sample were mixed pair-wise and hybridized to the miRCURY LNA™ microRNA Array 7th Gen (Exiqon, Denmark), which contains capture probes targeting all microRNAs for human, mouse or rat registered in the miRBASE 18.0. The hybridization was performed according to the miRCURY LNA™ microRNA Array Instruction manual using a Tecan HS4800™ hybridization station (Tecan, Austria). Next, to avoid decolourization of the fluorescent dyes, microarray slides were scanned and stored in an ozone free environment (ozone level below 2.0 ppb). The scanning was performed using the Agilent G2565BA Microarray Scanner System (Agilent Technologies, Inc., USA) and the image analysis was carried out through the ImaGeneR 9 (miRCURY LNA™ microRNA Array Analysis Software, Exiqon, Denmark).

To evaluate the labelling reaction, hybridization

, and the performance of the array experiment in general 52 different spike-in controls were added in concentrations covering the full signal range in both the Hy3™ and the Hy5™ labelling reactions. For correlation (R2) of the signal intensities across all slides >0.95 hybridization was considered successful.

The threshold of detection was calculated for each individual microarray slide multiplying by 1.2 the 25th percentile of the overall signal intensity of the slide. MicroRNAs with intensities above threshold in less than 20% (or 2) of the samples were removed from the final dataset used for the expression analysis.

The quantified signals were corrected to the background (Normexp with offset value 10, [329]) and normalized using the global LOWESS (LOcally WEighted Scatterplot Smoothing) regression algorithm. Normalized values were used to calculate the log median of the ratio for each of the four spots (M) on slide. The log2 (fold change), corresponding to the deltaLogMedianRatios, was calculated to analyse differential miRNA expression between brown and white adipocytes. Statistical analysis was performed using R/Bioconductor limma package as described in paragraph 2.2.10.9.

2.2.10.8 *Next generation (mRNA) sequencing*

Next generation sequencing methods include different high throughput technologies progressively improved from the first sequencing technique developed by Frederick Sanger in 1997 [330]. The advantages offered by the NGS compared to previous sequencing methods consists mainly in the possibility to sequence not only a

restricted number of selected genes of interest, but instead to provide a complete view of the coding transcriptome allowing identification of novel genes isoforms, besides being highly efficient and cost effective. All these techniques have in common three main steps: library preparation, sequencing and data analysis. In this study, mRNA sequencing technique was performed to sequence the transcriptome of human brown and white adipocytes using the Illumina TruSeq Stranded mRNA Library Prep Kit. This system targets all polyadenylated transcripts of the transcriptome with a size above or equal to 170 nucleotides, which are selected using an Oligo-dT magnetic bead strategy and fragmented using divalent cations at high temperature. The fragments are then reverse transcribed into cDNA. In this phase, first strand cDNA is obtained using reverse transcriptase and random primers. The second cDNA strand is synthesized using DNA Polymerase I and RNase H. The second strand is converted into NGS cDNA libraries. The sequencing is then performed through the Illumina platform. A description of the process is schematized in figure 11. For this experiment 1x50bp cut fragments (single read) and Illumina TruSeq Stranded mRNA Library Prep Kit were used running 50 million reads per sample. Read alignments and counts were performed using TopHat and HTseq-count packages in R.

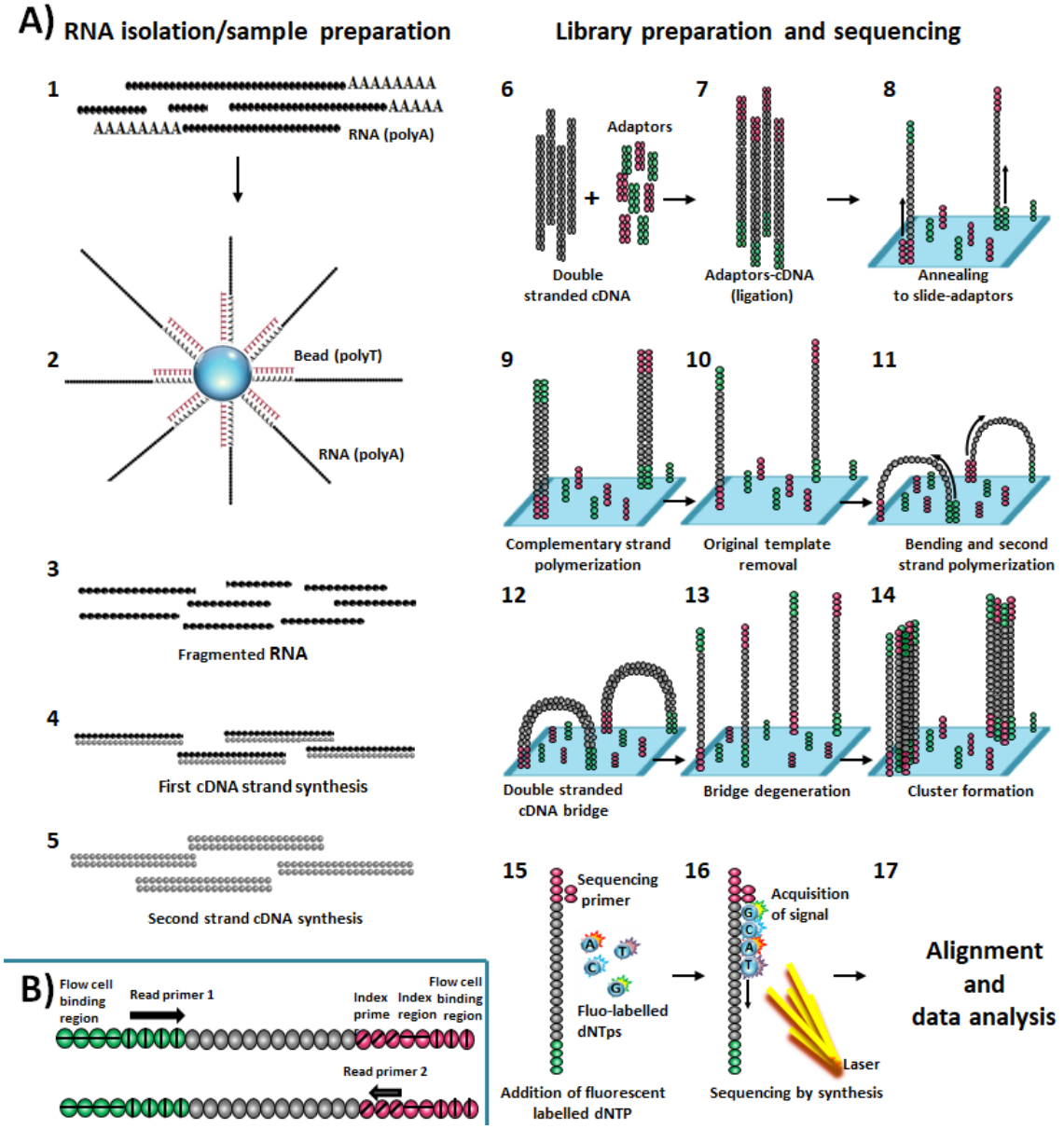

Figure 11 mRNA sequencing (Illumina)
The figure shows **A) the steps of mRNA sequencing**. 1) Total RNA is extracted and 2) poly-A tailed fragments are isolated using beads on which poly-T strands are anchored to the surface. 3) Isolated RNA is fragmented and 4-5) reverse transcribed into cDNA. 6-7) Adaptors are ligated to the cDNA. These contain indexes, sequencing primer regions and sequences designed for hybridization with the oligos attached on the cell flow surface of the slide. 8) The cDNA is thermally denatured and the single strands anneal to the oligos attached on the surface of the slide through the complementary sequence of the adaptor. 9) Complementary cDNA is polymerized and the original template is removed. 11) The remaining filament bends over and the adaptor region hybridizes to the second type of oligo present on the flow cell forming a bridge structure. 12) The complementary strand is polymerized and 13) the bridge denatured. The process is then repeated over and over from step 10. The simultaneous amplification of all the fragments originally attached to different areas of the slides results in the formation of 14) millions of clusters. Afterwards, the reverse strands are cleaved and washed away. 16) Sequencing by synthesis of the forward strand starts by 15) adding the primer specific for the sequencing primer region 1 of the adaptors and 4 fluorescent labelled and blocked nucleotides. At each cycle, only one nucleotide is incorporated in the forming strand based on the complementarity to the template. The clusters are excited by a laser light and 16) the characteristic signal is emitted by the specific nucleotides incorporated. Signal is acquired and the lock removed from the nucleotide so that the next nucleotide can be incorporated. The process is repeated until the first read is completed. The number of cycles determines the length of the read. The base call is determined by the signal intensity and the wave length. For each cluster all identical strands are read simultaneously. Successively, the read product is removed and the index is read by adding the index primer. At the end of the entire

process, reads with similar length and base calls are clustered together, obtaining contiguous sequences which are then 17) aligned to a reference genome. **B) Adapter structure for single and paired end reading.** The function of the index is to associate the reads to the different samples. In single end-reading, strands are read only in one direction and only read primer 1 sequence are included in the adapters along with flow cell binding, index primer and primer regions. In paired end reading, strands are read in both directions. To do so, read primer2 sequence is added to the adapters.

2.2.10.9 *Unsupervised and supervised analysis of mRNA sequencing and microRNA array data*

Variation among samples was analysed by principal component analysis, performed on all samples and all sequencing read count data or miRNA data. The significance of differentially expressed genes and miRNAs between brown and white adipocytes was assigned using Student's t-test and p values were adjusted with Benjamini-Hochberg correction. Gene targets of the differentially expressed miRNAs were predicted using Bioconductor (R) package miRNAtap which performs target prediction aggregation from the prediction algorithms: DIANA [331], Miranda [202], PicTar [204] and TargetScan [332]. We set a minimum of two sources through the command: getPredictedTargets(mir, species = 'hsa',method = 'geom', min_src = 2), so that targets were considered only when predicted by at least two out of the four aforementioned algorithms. Identification of the pathways (from Kyoto Encyclopedia of Genes and Genomes (KEGG) database) associated to differential expressed genes between brown and white adipocytes were identified using hypergeometric test (phyper function in R)

2.2.11 *Vesicle characterization*

Sample preparation and analysis were performed at the Velindre Cancer Centre, Division of Cancer & Genetics, and Cardiff University.

2.2.11.1 *Nanoparticle tracking analysis (NanoSight™)*

Vesicle characteristics were analysed by Nanoparticle tracking through the NanoSight NS300 system (NanoSight Ltd, UK) similarly to as described previously [333]. This technology enables the visualization in real time of nanoparticles (10-1000nm) present in liquid suspensions and provides information on their size distribution and concentration analysing dynamic light scattering and Brownian motion characteristics. The system consists of a laser module inside a sealed housing on top of which an optical flat element is fixed. A flow-cell top-plate is assembled on the flat element, forming the sample chamber connected to a tubing system. The sample is

injected through a syringe connected to the inlet tube and a syringe pump dispositive allows its flow into the chamber at a constant controlled rate. When the sample reaches the chamber the laser beam illuminates the particles suspended in the fluid. By scattering the laser light, each particle and their motion can be visualised and monitored by a high sensitivity camera. The particles are seen as small points moving randomly upon collision with atoms or other molecules suspended in the fluid. This type of movement is referred as Brownian motion and is related to the viscosity of the liquid, the temperature and the size of particles but not to particle density or refractive index. The nanoparticle tracking analysis (NTA) software calculates each particle diameter using the Stokes-Einstein equation. Especially for those samples containing a largely heterogeneous population of particles, this particle-by-particle approach results in a more sensitive analysis compared to classical Light Scattering techniques such as Dynamic Light Scattering (DLS), which provide an average of particle size. The sample is let out from the chamber to a discharge container via another tube.

For this analysis, the instrument was configured with a 532 nm laser. For each sample, administrated under controlled flow, six replicate videos of 30s were taken at 25 °C by the high sensitivity digital camera sCMOS system and the speed of the syringe pump was set to 80. For data collection the NTA-software was used with minimal expected particle size, minimum track length, and blur settings in automatic mode and detection threshold set to 5. Samples were diluted in particle-free water (Fresenius Kabi, Runcorn, UK) adjusting concentration to 2×10^8 - 9×10^8 particles/ml and run after calibration with 100 nm standard polystyrene latex beads. Data were analysed adjusting for the dilutions applied.

2.2.11.2 *Europium-based ELISA-like assay for exosome marker detection*

Europium is a lanthanide metal used in Time Resolved Fluorometry (TRF) as a chelate label for several types of assays, especially immunoassays. In standard fluorometry, excitation of the fluorophore and detection of the fluorescence emitted by the exited fluorophore occur simultaneously, generating a high autofluorescent background signal. The fluorescence lifespan of lanthanides is much longer than traditional fluorophores; therefore, fluorescence measurements can be taken in a delayed time after excitation, reducing the background signal. Lanthanides present some additional properties contributing to improved efficiency and sensitivity of the system,

such as: narrow emission peak and large difference between excitation and emission wavelengths, known as Stokes' shift. In this study, for the detection of exosome markers, Delfia reagents have been used. The addition of the enhancement solution induces the dissociation of the Europium which is then incorporated into protective micelles. In this way, the fluorescence signal can be further amplified.

The assay was performed as following: isolated vesicles were resuspended in 2 ml of PBS and immobilized on high-protein-binding ELISA plates by adding 100 µl of sample per well and incubating overnight at RT. The wells were washed 3 times with 1x Delfia Wash Buffer using a plate washer. Non-specific sites were blocked with 300 µl of 1% (w/v) BSA/PBS at RT for 2h. After washing as before, vesicles were incubated for 2h at RT with 100 µl of primary mouse monoclonal antibodies (IgG2b) anti-human CD9, CD81, CD63 in parallel with the controls for IgG2b and IgG1, all diluted in 0.1% (wt/v) BSA in PBS at the concentration 1 µg/ml. Wells were washed as previously and incubated for 1h at RT with secondary goat anti-mouse (IgG) biotinylated antibodies (PerkinElmer Life) at a working concentration of 0.2 µg/ml. Samples were washed as previously and incubated for 45 min at RT with 100 µl of Europium-Streptavidin conjugate in red assay buffer 1:1000 (v/v). After washing 6 times, 100 µl of Enhancement Solution was added to each well. Samples were incubated at RT for 5 min and readings through TRF were taken on a BMG Pherastar plate reader with excitation filter set on UV (TRF340) dug11 + wg320, filter emission at 615 nm, delay time and window of 200 and 500 µs, respectively.

2.2.12 *Oxygen consumption*

Cellular respiration can be either anaerobic or aerobic. In the first case ATP is generated via the glycolysis which produces lactic acid and protons. With aerobic respiration oxygen is used to oxidise fatty acids for ATP and /or heat generation through UCP1. The Seahorse XF Analyzer provides information on these metabolic events by monitoring the changes in oxygen and proton concentrations in the extracellular media. The system consists of a 24/96 cell culture plate where cells are seeded and a sensor cartridge that is placed on top of the plate. The cartridge, pre-incubated overnight or for a minimum of 4 hours with the calibrant solution at 37 °C without CO_2, is inserted first in the instrument to allow the calibration of the probes. At the end of the calibration the

cell culture plate is inserted as well. The cartridge has an individual sensor for each well. Two different fluorophore probes are embedded in polymers at the bottom of each sensor, one quenchable by oxygen and the other one by protons (H^+). Inside the instrument, the sensor is lowered to 200 μm above the cell monolayer (figure 12), creating a micro chamber, which allows the small changes in oxygen and proton concentrations to be detected almost immediately, instead of hours. The detection, based on the quenching chemistry, occurs upon stimulation of the fluorophores by a light diffused by optic fibres that insert themselves into each sensor sleeve during the measurements. The emission of the excited fluorophores is captured back via the optical fibres. When the sensor detects a 10% drop of oxygen or proton concentration the instrument lifts the sensor allowing the media to mix, restoring the cells baseline and avoiding cell damage. The measurements can be repeated several times and the oxygen consumption rate (OCR) and extracellular acidification rate (ECAR) can be calculated. Surrounding the sensor probe sleeve, there are 4 ports in which different drugs can be preloaded and injected sequentially in the same experiment, in order to study their effect on cell metabolism. The protocol can be personalised, setting the desired times of drug injections and measurements.

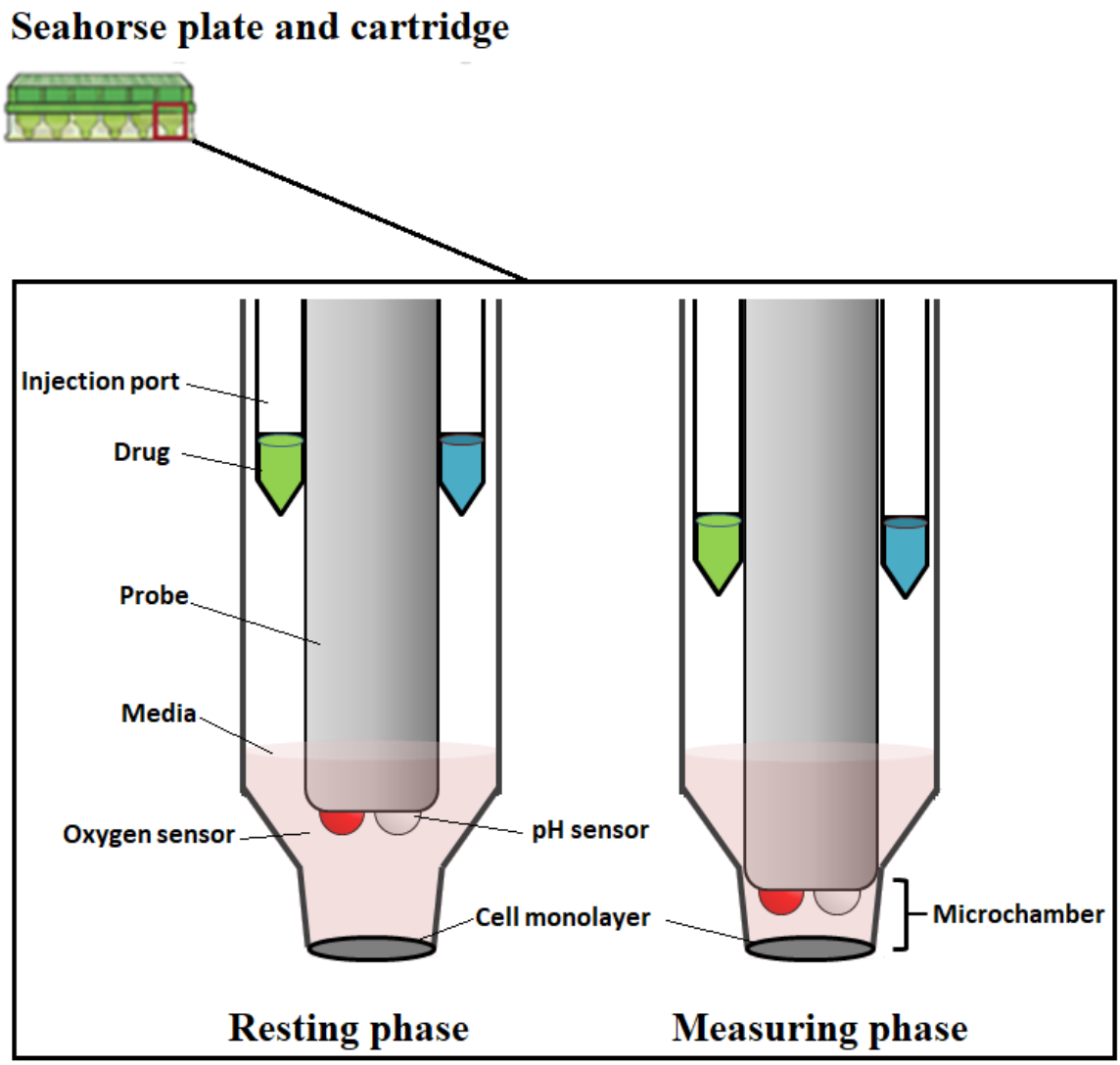

Figure 12 Seahorse XF analyzer plate for OCR and ECAR measurments
On the top left is shown a seahorse cell culture well plate covered by the green cartridge. In the magnification of a well of the seahorse plate are represented the resting and measuring phases. During the measuring phase the cartridge probe is lowered 200 µm above the cell monolayer, creating the microchamber environment, where the oxygen and proton concentration are measure by the oxygen and pH sensors. The sensor is surrounded by 4 ports that can be used for drug injection.

Base line OCR and ECAR were measured in Isoproterenol (ISO)-treated/untreated human adipose cell lines as follows. Differentiated human brown and white adipocytes were trypsinised and 50,000 cells per well were reseeded into a 24-well seahorse plate. Cells were left in maintenance media containing insulin and T3 for 24 h to recover from trypsinization. Media was removed and cells were gently washed with seahorse media. Afterwards, 675 µl of pre-warmed seahorse media containing glucose (25mM) and Sodium Pyruvate (1mM) (pH 7.4) was added to each well. Cells were incubated at 37 °C in a non-CO_2 incubator in the presence of either Isoproterenol (10 µM)

or dimethyl sulfoxide (DMSO) for control wells for 40 minutes, both to allow media temperature and pH to reach equilibrium before measurement and isoproterenol to induce UCP1 function. The plate was run in the Agilent Seahorse XF24 Analyzer to measure the base line OCR. The assay protocol was set so that in a 3 times loop, media was mixed for 3 minutes and measurements were taken for 2 minutes after a delay time of 2 minutes, to allow the oxygen partial pressure to reach equilibrium.

2.2.13 *Statistical methodology for hypothesis testing*

To provide a comprehensive understanding of the choice of methodology undertaken the principles of the different statistical tests utilized in this study and specified in the results section, relative to each experiment, will be briefly described in this section. Indeed, there exist different types of statistical tests that can be used to analyze data in testing a determinate hypothesis. The choice should be taken accounting for different situations relative to the number of samples (one, two or more than two) involved and the assumption that the data come or do not come from a known distribution. Based on the last criterion, the test to perform could be parametric, in the cases that data (interval or ratio types) are known or assumed to follow a determined distribution, or non-parametric when no a priori knowledge on data distribution is available or not applicable.

2.2.13.1 *Student's t-test*

The t-test, also referred as Student's t-test, is one of the most frequently used parametric tests in medical/biological science. It is performed to compare the means of two and no more than two groups, in order to verify whether they are different from each other. There exist different types of t-test depending on the groups to compare. For instance, the one- sample t-test is used to compare a single group sample mean with the mean of a known population, the paired t-test, which compares the mean of two groups dependent one to each other. The independent or unpaired t-test that is used to compare the mean of two independent groups. To give some examples, the one-sample t-test could be performed to compare the mean of intelligence quotient (IQ) of 30 subjects treated with a drug, with the average of the IQ of the population, which is known to be 100, in order to investigate whether the drug increases or decreases the IQ. Therefore, the mean IQ of this group is compared to 100, the mean of the population. If the IQ of 30 individuals was measured before and after the treatment in the same subjects and the comparison

were to be done between the mean IQ of pre-treatment and the mean IQ of post-treatment, the paired t-test would be more appropriated. In the case that the IQ is measured on a sample of untreated subjects and a sample of different subjects treated with the drug, an independent t-test should be performed. To perform a t-test the samples must satisfy the conditions of normality, random sampling and equal variances of populations. In the one-sample case, where the mean c of the sample is compared to the mean μ of a known population, the null hypothesis (H0) and the relative alternative hypothesis (Hα), which can be anything but H0, could be stated in three different ways:

$$H_0 : \mu = c, H_a : \mu \neq c$$

$$H_0 : \mu > c, H_a : \mu < c$$

$$H_0 : \mu > c, H_a: \mu > c$$

Assuming that the sample follows the normal distribution, the formula of the t test formula can be extracted from the standardized normal distribution Z test by substituting the sample standard deviation s to the population standard deviation σ as shown below:

$$Z = \frac{\overline{X} - \mu}{\frac{\sigma}{\sqrt{n}}} \qquad\qquad t = \frac{\overline{X} - \mu}{\frac{s}{\sqrt{n}}}$$

Where $\overline{X}$ is the mean of the sample, μ the mean of the population and n the number of the measurements. The t value is then used to calculate the p value, which represents the probability, under the null hypothesis, of obtaining the observed value of the statistic test (in this case t-test) or a "more extreme" one, depending on the hypothesis stated. It defines whether it is possible to reject the null hypothesis after establishing the critical value α, obtained by subtracting the level of confidence from 100. Commonly the level of confidence is established as 95%, therefore, in this case, α is 0.05. Depending on the hypothesis stated among the three reported above the test will be a two-tailed or one tailed t-test. In the first case, where there is no a priori knowledge, a two tailed (both tails of the t-distribution curve are considered) t-test must be performed. In the second and the third cases, the sample mean c is expected to be greater and lower than μ respectively, therefore a one-tail t-test (only right and left tail respectively considered) would be the correct test. According to this, the appropriate table of t distribution is consulted. Based on the critical

value determined and the degrees of freedom (n-1), the p value or the range of the area in which the p value falls is calculated.

In the *independent t-test*, under the assumption of equal variances and normal distribution of the two populations, as the comparison is between the two sample means, the formula becomes:

$$t = \frac{(\overline{X}_1 - \overline{X}_2) - (\mu_1 - \mu_2)}{s_{(1+2)}\sqrt{\frac{1}{n_1} + \frac{2}{n_2}}}$$

Because the samples are assumed to come from an identical population with a normal distribution, the mean of the two populations are assumed to be 0 and the t formula becomes:

$$t = \frac{(\overline{X}_1 - \overline{X}_2)}{s_{(1+2)}\sqrt{\frac{1}{n_1} + \frac{2}{n_2}}}$$

where the pooled variance of the samples is used and calculated as follows, as the variance of the population is not known

$$s_{(1+2)} = \frac{(n_1 - 1){s_1}^2 + (n_2 - 1){s_2}^2}{n_1 + n_2 - 2}$$

and the degrees of freedom are:

$$df = n_1 - n_2 - 2$$

In the case that the condition of equality of variances is violated, the t test formula remains the same but the degrees of freedom are calculated as:

$$df = \frac{\left(\frac{{s_1}^2}{n_1} + \frac{{s_2}^2}{n_2}\right)}{\frac{\left(\frac{{s_1}^2}{n_1}\right)^2}{n_1 - 1} + \frac{\left(\frac{{s_2}^2}{n_2}\right)^2}{n_2 - 1}}$$

The equality of variances can be assessed using the F test and the tables of the F distribution. The degrees of freedom are calculated for each group as $df = n - 1$.

$$F = \frac{Larger\ s^2}{Smaller\ s^2}$$

The *paired t-test* is very similar to the one sample t-test as the samples are dependent. The t value is calculated as:

$$t = \frac{\overline{d}}{\frac{s_d}{\sqrt{n}}}$$

Where $\overline{d}$ is the mean of all the differences between the two observations on each pair and s_d is the standard deviation of the differences. Under the null hypothesis, the degrees of freedom are, also in this case, $df = n - 1$.

All the t-tests performed in this study were independent t-tests except when measuring miRNA content in media before and after ultracentrifugation as the samples were not independent. Indeed the miRNA content was measure in the same sample before and after vesicle precipitation. In this case, paired t-test was used.

2.2.13.2 *The Shapiro-Wilk test*

The Shapiro-Wilk test is a test used to assess whether a sample actually comes from normally distributed population. The statistical null and alternative hypotheses are stated as:

H_0 : the sample (of size n) is drawn from a normally distributed population

H_α : the sample is drawn from a not normally distributed population.

The formula of the Wilko-Shapiro test is:

$$W = \frac{(\sum a_i x_i)^2}{\sum (x_i - \overline{x})^2}$$

where, x_i is the i^{th} smallest value of x (single observation) and a is the Shapiro-Wilk constant. Through the use of the Shapiro-Wilk tables the null hypothesis is rejected if W < W_α. Therefore, for p values smaller than the critical value α there is evidence that the data do not follow a normal distribution. In the opposite situation, a large p value does not mean that that the data are normally distributed, but rather that there is not enough evidence proving that the data are not normally distributed (failure to reject the null hypothesis).

2.2.13.3 *The Benjamini-Hochberg correction for p-value adjustment*

When performing a large number of statistical tests, some of these will give significant results purely by chance. For example, when performing one statistical test where the p-value threshold has been determined as 0.05, there is a chance of one in twenty times (5%) that result is a false positive. If a larger number of tests are performed, let us say 20000 tests, such as it happens in microRNA array where there are more than 20000 of probe sets, the probability of obtaining false positives becomes 1000 (20000*0.05), which is extremely high to be accepted. The Benjamini-Hochberg correction adjusts the p-values in order to reduce the false positive results under the condition that the individual tests are independent from each other. In other words, this is a method of error type I (false positives) controls. In this procedure, the p value obtained by the different tests performed are sorted from smallest to largest and ranked (the smallest rank will be rank 1, the second smallest rank 2 until the largest n rank). Then each p-value is multiplied by the total number tests (largest rank n) and divided by its rank number.

2.2.13.4 *The ANOVA*

In comparisons involving more than one sample, the analysis of variance ANOVA should be used, in order to control the error type I that is given by multiple testing [334]. The null hypothesis can be formulated as following:

$$H_0 : \mu_1 = \mu_2 = \ldots = \mu_k$$

If multiple t-tests are performed, their outcomes cannot be used to draw a single conclusion and, therefore, when verifying whether the aforementioned H_0 is rejected or we fail to reject it. There exist different types of ANOVA. However here we will only consider the one-way and the two way ANOVA focussing on the last one as it was the only type performed in this study. The one-way ANOVA is designed for investigating data in which only one factor is considered, for example when verifying the effect of a drug on a number k of independent samples. The null hypothesis would be that all the groups present the same mean, and the alternative hypothesis, that at least one of the k population means differs from all of the others. If a second factor is introduced, for example a second drug, then two-ways ANOVA is more appropriate. The null hypothesis will be that there is no significant variability between the k groups, and the alternative hypothesis is that there is such variability. The variability of the sample is well represented by the variance of the sample (s^2):

$$s^2 = \frac{\sum(x - \mu)^2}{n - 1}$$

where x is a data point and μ is the population mean. The numerator of the variance is the sum of squares and is indicated as SS. The principle of the ANOVA is to partition the overall variance of a larger population from which the individual populations of the different conditions (for example observations of drug A in each of the sample groups) are drawn, into different parts, and one of these parts is always error/noise. Therefore, by partitioning the overall sum of squares, the total sum of squares in one-way ANOVA and the relative degrees of freedom will be:

$$SS_{Total} = SS_{condition} + SS_{error}$$

$$N - 1 = (k - 1) + (N - k)$$

Subsequently, the error mean squares (MS_{error}) and the condition mean squares ($MS_{condition}$) are calculated:

$$MS_{error} = \frac{SS_{error}}{N - k} \qquad MS_{condition} = \frac{SS_{condition}}{k - 1}$$

The ratio of these two values is used to test the null hypothesis and follows an F distribution with $v_1 = k-1$ and

$$F = \frac{MS_{condition}}{MS_{error}}$$

This is a one-tail test as the statistic value can either be equal to or larger than 1. In the first case the null hypothesis is true and in the second it is rejected.

The two-way ANOVA, allows us to also account for the variation of additional factors or grouping of the experimental units, which are defined as blocks. The two- way ANOVA without repetitions is also called randomized block experiment. The partitioning of the overall sum of squares and its degrees of freedom below will be in this case:

$$SS_{Total} = SS_{treatment} + SS_{block} + SS_{error}$$
$$bk - 1 = (k - 1) + (b - 1) + (b-1)(k - 1)$$

where k is the number of the samples and b of the blocks. Then the MS of the partitions are calculated:

$$MS_{treatment} = \frac{SS_{treatment}}{k-1};\ MS_{block} = \frac{SS_{block}}{b-1};\ MS_{error} = \frac{SS_{error}}{(b-1)(k-1)}$$

The F statistics of the treatment and the blocks will be:

$$F = \frac{MS_{treatent}}{MS_{error}} \qquad F = \frac{MS_{block}}{MS_{error}}$$

The null hypothesis is rejected if $F > 1$.

The two-way ANOVA can also be with replications. In our study it was with replications as we had triple biological replicate for each group. In this case an additional type of measurement is introduced, that is the interaction between factors. The two-way ANOVA with replication is also referred as factorial experiment as it allows to investigating the effect of a factor A and simultaneously of a factor B on a dependent variable y (which could be the expression of a gene of interest), alongside with the

interactions between different levels of the factors on the dependent variable y. An interaction occurs when the effect of one factor varies for different levels of the other factors. An example could be the synergic or antagonistic effect of two drugs on the expression of a gene. The partitioning of the SS_{Total} is in this case:

$$SS_{Total} = \overbrace{SS_A + SS_B + SS_{A\times B}}^{SS_{cells}} + SS_{error}$$

$$\underbrace{abn - 1}_{N-1} = \underbrace{(a-1) + (b-1) + (a-1)(b-1)}_{ab-1} + ab(n-1)$$

When designing such a factorial experiment, the lay-out of the data can be imagined as a three-dimensional matrix, where, the first index/dimension represents the factor A, the second represents the factor B, and the third represents the position of the observation within the ij cell, where, αi is the i-th unit of factor A and ßj is the j-th unit of factor B. Each cell represents the set of observations under factor A_i and B_j. As before the MS of the partitions are calculated as the sum of square of the partition divided by the relative degrees of freedom. First, is tested the interaction between factors where the hypothesis are:

H_0 : $(\alpha ß)_{ij} = 0$ for all i, j

H_a : there is at least one pair i, j for which $(\alpha ß)_{ij} \neq 0$

and the F statistics is:

$$F_{A\times B} = \frac{MS_{A\times B}}{MS_{error}}$$

If $MS_{A\times B}$ is significantly larger than MS_{error}, the null hypothesis is rejected. In this case pairwise t-tests are performed using multiple comparisons tests which correct for the error type I, such as the Bonferroni, Tukey's tests etc.

If we fail to reject the null hypothesis at this stage, the following hypothesis are tested:

1) H_0 : $\alpha_1 = \alpha_2 = \ldots \alpha_a = 0$

   H_a : there is at least one pair of factors A presenting unequal means

and

2) $H_0 : ß_1 = ß_2 = \ldots ß_b = 0$

H_a : there is at least one pair of factors B presenting unequal means.

The F statistics for testing the null hypothesis are respectively:

$$F_{\mathrm{A}} = \frac{MS_{\mathrm{A}}}{MS_{error}}$$

and

$$F_{\mathrm{B}} = \frac{MS_{\mathrm{B}}}{MS_{error}}$$

The assumptions in the factorial two way ANOVA are that the n samples in each cell are independent and drawn from a population with μ_{ij} and normally distributed. Such populations are assumed to present the same variance.

2.2.13.5 *Tukey's test*

As the ANOVA only allows to test whether the results are significant but does not provide information on among which group's mean are the significant differences, additional post-hoc tests need to be used when performing multiple comparisons. The Tukey's HSD (honest significant difference) test [335], compares every mean with every other mean. It was employed in this study to perform multiple comparisons after factorial two-way ANOVA. The HSD represents the least amount that means must vary from each other to be significantly different. The HSD is first calculated as:

$$HSD = q\sqrt{\frac{MSerror}{n_k}}$$

where q is the constant that is determined from the studentized range q table by using and n_k is the sample size, which is assumed to be equal in each group. The HSD value obtained is then compared to each mean difference. If HSD is smaller than the difference between the means considered, such means are significantly different. The assumptions for the use of this test are the same of the t-test, such as the observations are independent among and within groups, such groups are normally distributed, the groups of the compared means present equal within variance. The sample size is assumed to be equal

for each groups, but if this assumption is violated, the Tukey-Kramer test can be used instead [336].

2.2.13.6 *KEGG database and the hypergeometric test*

The KEGG is a database (http://www.genome.jp/kegg/or http://www.kegg.jp/) in which genes are mapped into pathways, integrating systemic, chemical, genomic and functional information deriving from experimental knowledge [337]. In order to have an overview of the potential function of the genes differentially expressed between brown and white adipocytes, the hypergeometric test was performed to identify the KEGG pathways enrichment in brown and white adipocytes. The hypergeometric distribution is a discrete probability distribution and describes the probability that k objects (genes) and exactly k, have a determined property (are associated with the KEGG category) in a sample of n objects (differentially expressed genes) drawn from the given set. When a random variable x follows a hypergeometric distribution, the cumulative distribution function formula is given as follows:

$$P = \sum_{k=1}^{x} \frac{\binom{m}{k}\binom{N-m}{n-k}}{\binom{N}{n}}$$

where N is the number of objects and would represent the number of gene that have a KEGG annotation and m is the number of objects having a determined property and would correspond to the number of genes annotated to specific pathways. The assumptions made to perform the hypergeometric test, are that the population is discrete and defined with a known value and trials are done without replacement.

Chapter 3 – Results

Intracellular and extracellular miRNAs in different adipocyte models

3.1 Introduction

MiRNAs are important gene regulators. Their presence in several biological fluids has recently raised the hypothesis that they could also mediate cell to cell communication, besides being used as biological markers. Several studies have investigated miRNA function in adipogenesis and the different profiles of miRNA expression presented by brown and white adipose tissues highlights their importance [338]. However, very little is known about the miRNAs secreted by adipocytes. In this study we have profiled the miRNAs secreted into media by mouse differentiated and undifferentiated brown and white adipocytes, seeking to identify differences in the miRNA secretome among these groups of cells. The differentially secreted miRNAs could have key local or distal actions intrinsic to the functions of white and brown adipocytes. Therefore, some of the most significantly differentially secreted miRNAs were selected and their intracellular and extracellular level of expression were analysed in different adipose models. In this chapter we also show the results obtained by profiling miRNA secreted by human mature brown and white adipocytes and the effect of ß-adrenergic stimulation on the intracellular and extracellular expression of the selected miRNAs in the different adipose models. Prior to analysis of miRNA expression, the adipose systems were characterized to evaluate their reliability as brown and white models. The immortalised human and mouse adipocytes will be referred for simplicity as human and mouse cell lines, even though they do not come from a monoclonal population.

3.2 Mouse adipocyte cell lines differentiation

Mouse brown and white pre-adipocytes were seeded in 6-well plates and differentiated as described in the methods section. Pictures of differentiated adipocytes were taken with a Nikon DS-L3 camera. RNA was isolated and gene expression was analysed by Real-Time qPCR. Statistical analysis was performed using two-way ANOVA and significance assigned for $p\text{-value}<0.05$. Differentiation observed at the microscope, was confirmed by the increased mRNA level of aP2 in mature adipocytes compared to pre-adipocytes (figure 13). Indeed, aP2, also called FABP4, is known to increase during adipogenesis and is considered a marker of differentiation. The mRNA of UCP1, the most relevant marker of brown phenotype, was overexpressed in brown preadipocytes compared to the white preadipocytes and significantly increased (about 100 fold) with the differentiation in both cell types. As expected, it was 10 fold higher in

mature brown compared to white adipocytes. Similarly, CIDEA, another brown marker gene, was upregulated during differentiation and 100-fold overexpressed in mature brown adipocytes compared to differentiated white adipocytes.

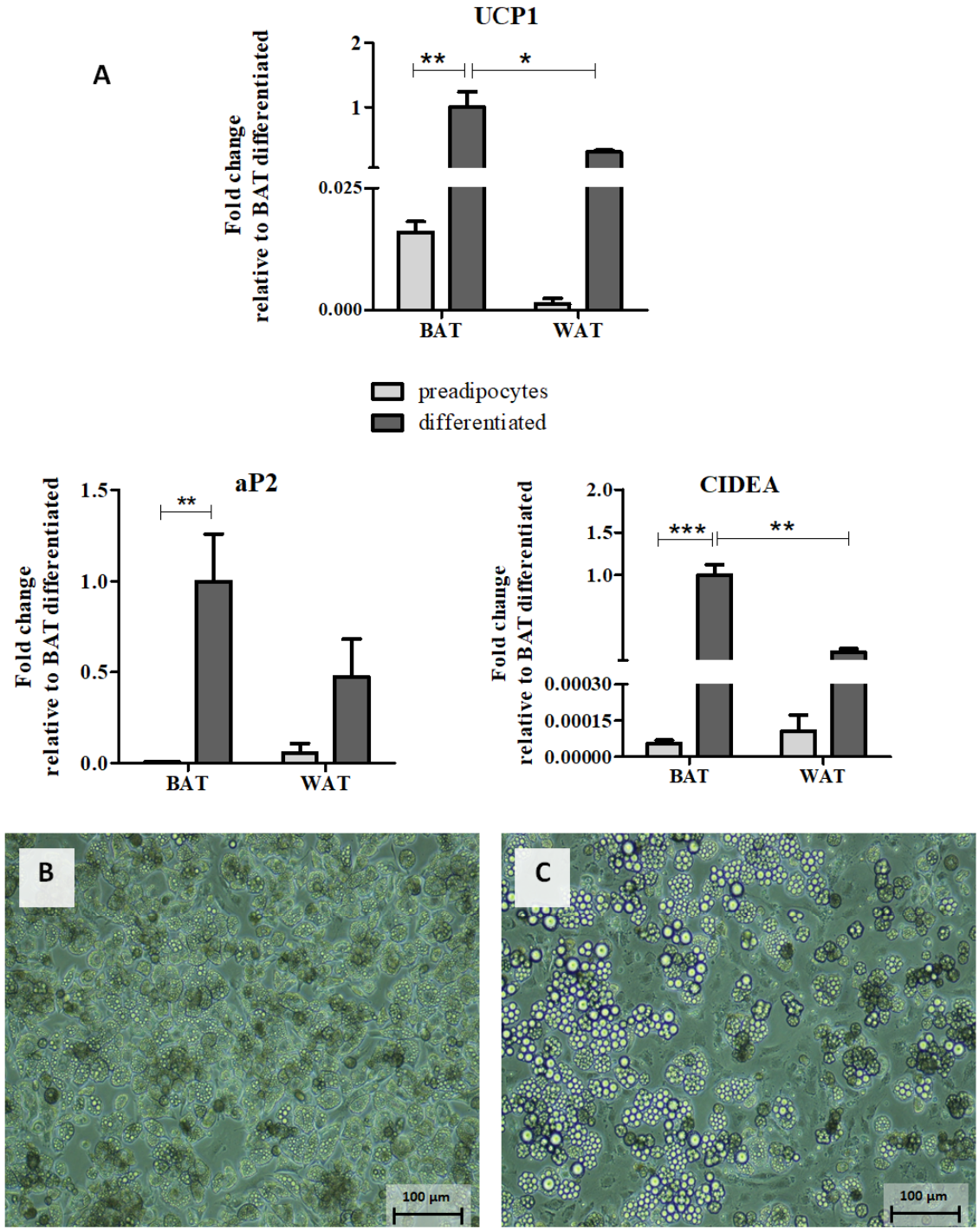

Figure 13 Gene expression and lipid droplets accumulation in mouse brown and white adipose cell lines.

(A) mRNA expression of aP2, UCP1 and CIDEA of interscapular brown and subcutaneous white adipose cell lines before and after differentiation normalised to L19. Bars represent fold change means ±SEM of the biological triplicates and compared to differentiated brown adipocytes. * indicates $p \leq 0.05$, ** $p \leq 0.01$

and *** p≤0.001 according to multiple comparisons in two-way ANOVA test. Differentiated brown (B) and white (C) mouse adipose cell lines.

3.2.1 *UCP1 mRNA induction upon CL treatment in differentiated brown and white adipose cell lines*

To verify the ability of the cells to induce UCP1 transcription upon ß-adrenergic stimulation, differentiated brown and white adipocytes were treated for 6 hours with CL (10 µM), a highly selective ß3-AR agonist, or DMSO for controls. UCP1 mRNA levels were then compared between untreated and CL-treated adipocytes. As shown in figure 14, both BAT and WAT responded to CL raising UCP1 expression. The mRNA levels were 12-fold increased in BAT and only three times higher in WAT. Functional studies on uncoupled respiration of this brown adipocyte cell line has been documented previously in Jaimiao Hu et al., [339].

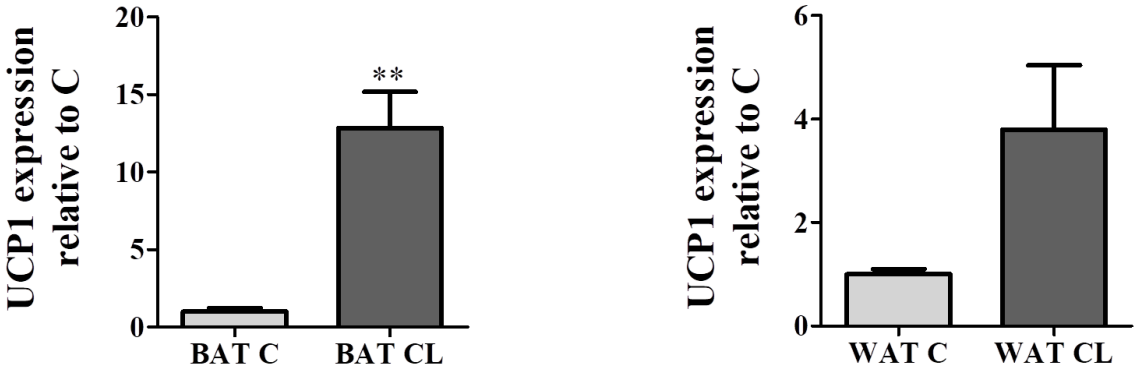

Figure 14 UCP1 mRNA induction upon CL treatment in differentiated brown and white adipose cell lines
Graphs show UCP1 mRNA level of expression in interscapular BAT (left panel) and subcutaneous WAT adipose cell lines (right panel) untreated I and treated with CL (CL) for 6 hours. Expression levels were normalised to L19 and bars represent the fold changes means of the triplicates ± SEM compared to brown or white adipocyte controls (BAT C and WAT C). ** indicates p≤0.01, according to t-test.

3.2.2 *Regulation of genes involved in miRNA maturation during differentiation of mouse adipose cell lines*

The transition from an undifferentiated stage towards a more differentiated one requires a profound change in gene expression that will define the fate of a cell. MiRNAs are known for their important contributions to gene regulation and an increased demand

for these small RNAs, consequently, would require a raised availability of the molecules responsible for their maturation. Therefore, we analysed the changes in mRNA expression of Dicer1, Ago2 and GW182 genes in brown and white undifferentiated and mature adipocytes. Differentiation of mature adipocytes was confirmed by the increased level of aP2 compared to preadipocytes (Figure 15).

All the genes tested were upregulated in mature brown adipocytes even though the changes in mRNA expression were only significant for Dicer1 and Ago2. The latter showed a similar trend of expression in white adipocytes. On the contrary, Dicer1 and GW182 levels remained unvaried between undifferentiated and mature white adipocytes.

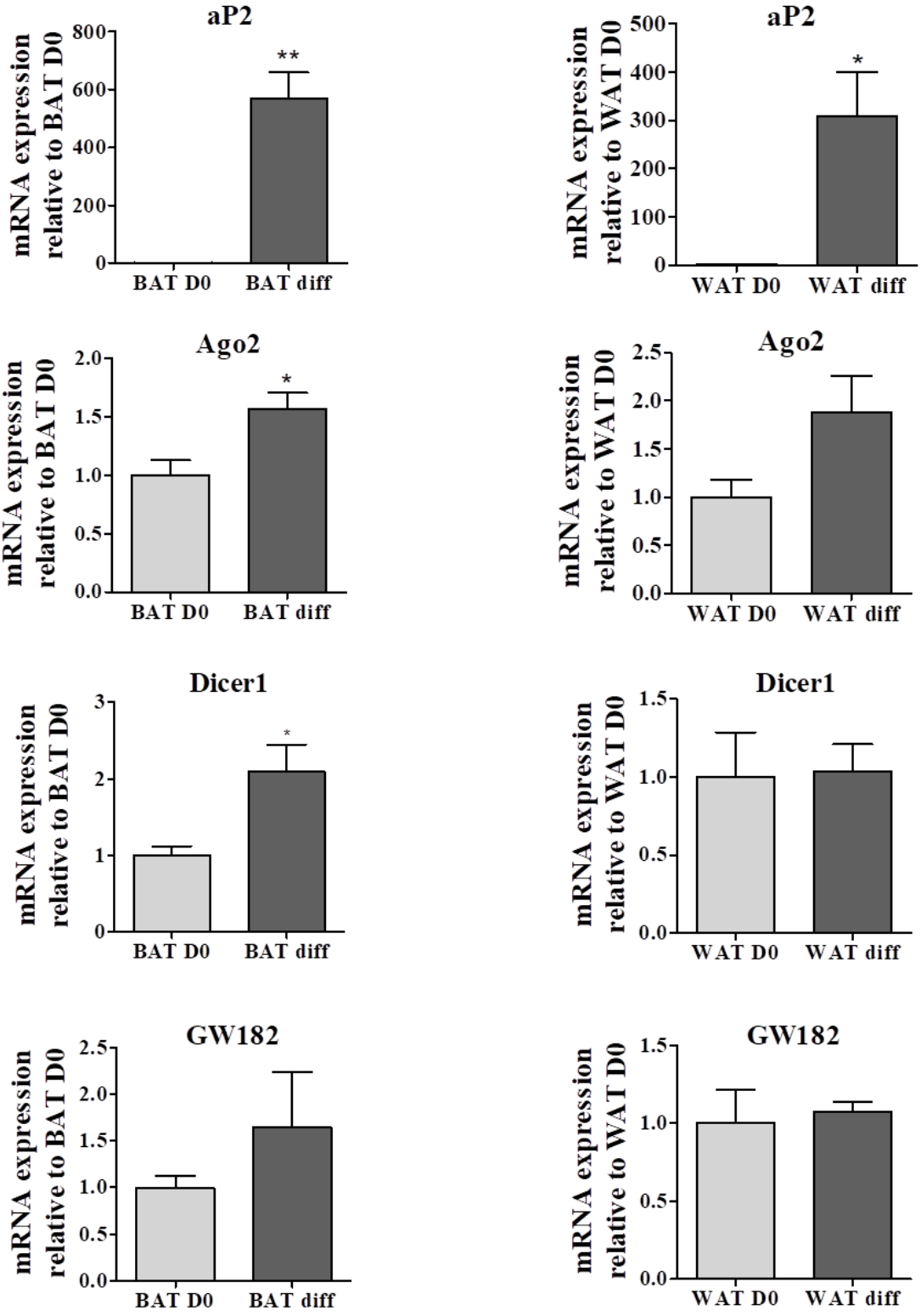

Figure 15 Regulation of genes involved in miRNA maturation during differentiation of mouse brown and white adipose cells

The graphs show mRNA expression of aP2, Ago2, Dicer1 and GW182 in undifferentiated and differentiated brown and white adipocytes. The mRNA levels of each gene were normalised to L19. Bars

represent average fold changes of the biological triplicates ± SEM compared to preadipocytes (BAT D0 and WAT D0). Significance was assessed according to Student's T-test, $p \leq 0.05$ (*) and $p \leq 0.01$(**).

3.2.3 *MiRNA PCR Array*

To identify miRNAs differentially secreted among undifferentiated and differentiated brown and white adipocytes we profiled miRNA expression of media from undifferentiated and differentiated brown and white adipocytes using miRCURY LNA™ Universal RT microRNA PCR Mouse&Rat panel I+II comprehensive for 752 miRNA assays. Because in media samples housekeeping genes cannot be used for normalisation, the same number (1.2×10^6) of differentiated and undifferentiated brown and white adipocytes was seeded into each well of a 6-well plate. Because miRNA concentration in the media can be low, cells were left in serum-free media for 24 hours to allow miRNA accumulation and simultaneously avoiding cell sickness due to a long time in serum-free conditions. Media samples (4 biological replicates for each group) were collected, processed for serial centrifugations, filtered and stored at -80 °C. The next steps were performed at Exiqon Service. RNA was isolated and reverse transcribed. The cDNA obtained was run on the miRCURY LNA™ Universal RT microRNA PCR Mouse&Rat panel I+II. Data were collected through Lightcycler Software. The controls performed (non-templates and RNA spike-ins) proved good technical performance of the profiling experiment and data were analysed.

Variation among the assays was analysed by unsupervised two-way hierarchical clustering (figure 17), Principal Component Analysis (PCA) (figure 16) and pairwise volcano plots (data not showed).

The PCA plot shows that samples clustered into the 4 expected groups. The biggest contributor to the observed variance appeared to be the differentiation status of the cells. The white vs brown adipocytes factor was robust but in this sample set a secondary contributor.

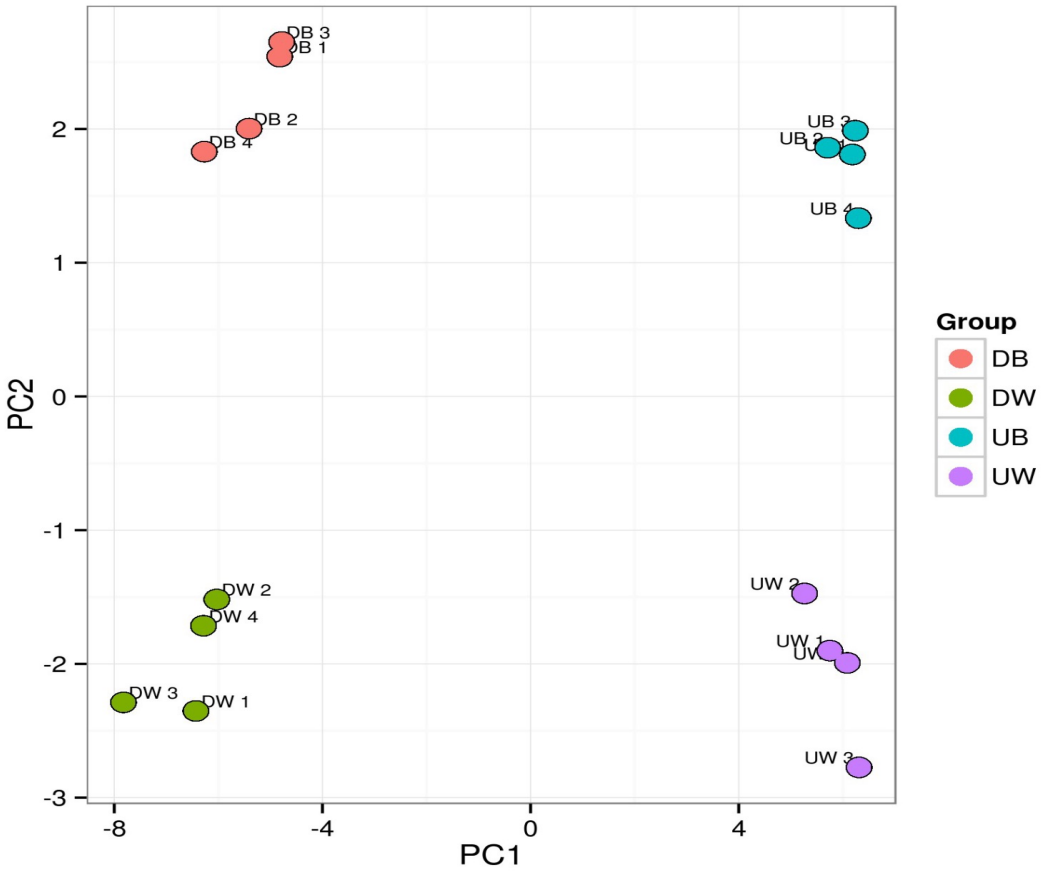

Figure 16 PCA plot (miRNA PCR array analysis on media from mouse adipocytes)
The principal component analysis performed on all samples and on the top 50 miRNAs with highest standard deviation.

Figure 17 shows the heat map diagram obtained by the two-way hierarchical clustering performed on all samples and on the top 50 microRNAs with highest standard deviation. The shade of colours in the red-green scale of each spot represents the relative level of each miRNA (rows) expressed for the corresponding sample (columns). The differences in miRNA expression between media from undifferentiated and mature cells as largest contributor to variance previously observed in the PCA plot, is marked by the red and green squares. The diagram provides an alternative graphical visualization of the clear differences that exist among the 4 groups of cells. To identify miRNAs differentially secreted among the groups, data were analysed pairwise using t-test with cut-off of p-value <0.05 and filtered for Benjamini-Hochberg correction to exclude false positives (cut-off value < 0.05). The results revealed that 45 miRNAs were differentially secreted between undifferentiated brown (UB) and undifferentiated white (UW), 118 in UW

versus differentiated white (DW), 123 in UB versus differentiated brown (DB) and 12 between DB and DW (table 8)

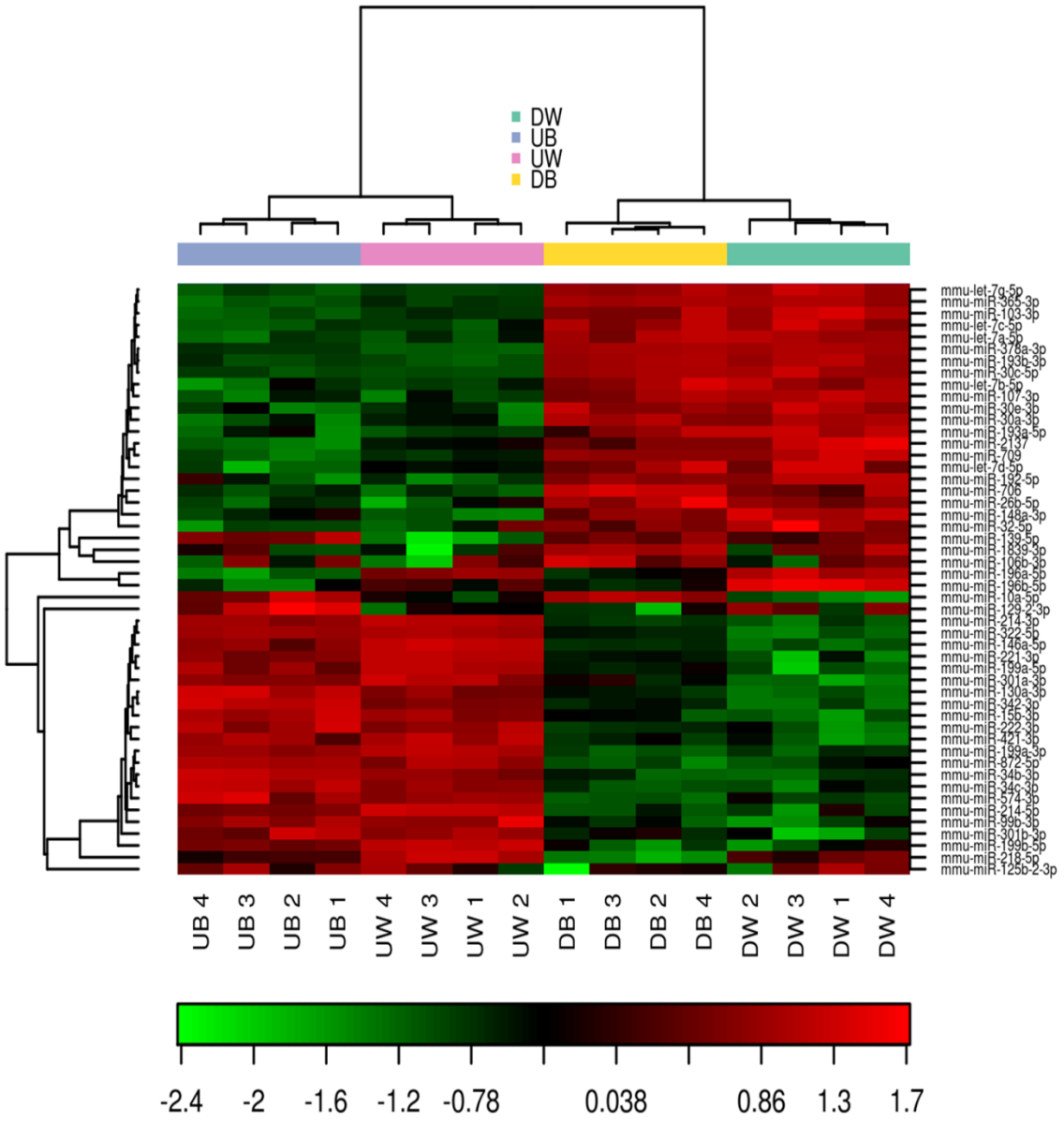

Figure 17 Heat map and unsupervised hierarchical clustering
The clustering was performed on all samples, and on the top 50 microRNAs with highest standard deviation. The normalized (dCq) values have been used for the analysis. The heat map diagram shows the result of the two-way hierarchical clustering of microRNAs and samples. Each row represents one microRNA, and each column represents one sample. The microRNA clustering tree is shown on the left. The colour scale shown at the bottom illustrates the relative expression level of a microRNA across all samples: red colour represents an expression level above mean, green colour represents expression lower than the mean.

.

Table 7 miRNA differentially secreted among undifferentiated and differentiated brown and white mouse adipocytes in pairwise analysis

	UW vs UB	UB vs DB	UW vs DW	DW vs DB
Tot n	45	123	118	12
Selected miRNAs	miR-378a-3p	miR-378a-3p	miR-378a-3p	miR-10b
	miR-196a-5p	miR-322-5p	miR-365-3p	miR-196a-5p
	miR-10b	miR-365-3p	miR-322-55p	

Legend. UW: undifferentiated white adipocytes; UB: undifferentiated brown adipocytes; DB: differentiated brown adipocytes; DW: differentiated white adipocytes

Among these, we selected some of the most significantly differentially secreted miRNAs (table 8) to test in other in vitro adipose models both for intracellular and extracellular levels. Details of standard deviations (SD), average ΔCqs, fold changes, p-values and Benjamini-Hochberg correction (BH adj. p-value) are reported in tables 9-12. MiR-378a-3p and miR-365-3p levels were significantly higher in media from differentiated brown and white adipocytes (DB and DW) compared to the undifferentiated (UB and UW) while, miR-322-5p levels went in the opposite direction (tables 10 and 11). MiR-378 was previously found to induce differentiation of preadipocytes by increasing lipid droplet size and to be specifically involved in brown adipogenesis and metabolism [282, 340, 341]. Also miR-365 was identified as a key regulator of BAT [342] even though it was subsequently found not to be essential for its development [343] and further investigation are needed to clarify these conflicting results. Several studies have been conducted on miR-322, which has an ortholog in humans referred to as miR-424. This miRNA has been found to regulate osteogenesis [344], inflammation [345] and protects against metabolic syndrome-induced cardiac dysfunction in mice [346]. As these three miRNAs were differentially secreted primarily between undifferentiated and differentiated adipocytes and they were identified as regulators of adipogenesis and other processes strictly linked to it, they were selected because of their possible involvement in the cross talk between cells during the differentiation process. MiR-10b was at the top of the list of miRNAs differentially secreted between DB and DW, being very highly expressed in media from BAT. Conversely, miR-196a-5p was higher in UW vs UB (table 9), DW vs DB (table 12)

and increased in UW vs DW (data not showed). MiR-196a promotes browning of the white adipose tissue [302] but to our knowledge no studies have been carried out to investigate its secretion.

Table 8 miRNA differentially secreted between Undifferentiated White and Brown (UW vs UB) adipocytes

miRname	SD UW	SD UB	Average ΔCq UW	Average ΔCq UB	Fold Change	P-value	BH adj.p-value
miR-378a-3p	0.16	0.17	-0.120	1.2	-2.4	0.000033	0.0024
miR-196a-5p	0.26	0.46	0.020	-3.2	9.5	0.000091	0.0036
miR-10b-5p	1.10	0.25	-4.400	2.5	-1.2e+2	0.000610	0.0083

Legend. SD UW: standard deviation of undifferentiated white adipocytes; SD UB: standard deviation of undifferentiated brown adipocytes; Average ΔCq UW: average of normalised quantification cycle in undifferentiated white adipocytes; Average ΔCq UB: average of normalised quantification cycle in undifferentiated brown adipocytes; P-value: p-value obtained using pairwise t-test; BH adj.p-value: p-value adjusted using Benjamini-Hochberg correction.

Table 9 miRNA differentially secreted between Undifferentiated and Differentiated Brown (UB vs DB) adipocytes

miRname	SD UB	SD DB	Average ΔCq UB	Average ΔCq DB	Fold Change	P-value	BH adj. p-Value
miR-378a-3p	0.17	0.20	1.20	7.4	-73	7.8e-9	0.0000016
miR-322-5p	0.12	0.23	3.90	-0.3	18	0.0000018	0.0000630
miR-365-3p	0.28	0.11	-0.36	4.1	-23	0.0000093	0.0001700

Legend. SD UB: standard deviation of undifferentiated brown adipocytes; SD DB: standard deviation of differentiated brown adipocytes; Average ΔCq UB: average of normalised quantification cycle in undifferentiated brown adipocytes; Average ΔCq DB: average of normalised quantification cycle in differentiated brown adipocytes; P-value: p-value obtained using pairwise t-test; BH adj.p-value: p-value adjusted using Benjamini-Hochberg correction.

Table 10 miRNA differentially secreted between Undifferentiated and Differentiated White (UW vs DW) adipocytes

miRname	SD UW	SD DW	Average ΔCq UW	Average ΔCq DW	Fold Change	P-value	BH adj. p-value
miR-378a-3p	0.16	0.19	-0.12	7.4	-1.9e-9	1.9e-9	4.2e-7
miR-365-3p	0.25	0.23	0.30	4.2	-15	4.7e-7	0.00005
miR-322-5p	0.20	0.57	4.10	-2.1	70	0.0000590	0.00100

Legend SD UW: standard deviation of undifferentiated white adipocytes; SD DW: standard deviation of differentiated white adipocytes; Average ΔCq UW: average of normalised quantification cycle in undifferentiated white adipocytes; Average ΔCq DW: average of normalised quantification cycle in differentiated white adipocytes; BH adj.p-value: p-value adjusted using Benjamini-Hochberg correction.

Table 11 miRNA differentially secreted between Differentiated White and Brown (DW vs DB) adipocytes

miRname	SD DW	SD DB	Average ΔCq DW	Average ΔCq DB	Fold Change	P-value	BH adj. p-value
miR-10b-5p	0.42	0.20	-4.40	2.1	-90	0.0000058	0.0013
miR-196a-5p	0.31	0.42	0.54	-1.9	5.4	0.0001500	0.0056

Legend. SD DW: standard deviation of differentiated white adipocytes; SD DB: standard deviation of differentiated brown adipocytes; Average ΔCq DW: average of normalised quantification cycle in differentiated white adipocytes; Average ΔCq DB: average of normalised quantification cycle in differentiated brown adipocytes; BH adj.p-value: p-value adjusted using Benjamini-Hochberg correction

3.2.4 *Extracellular miRNA expression in mouse adipose cell lines*

To validate the results obtained by the miRCURY LNA™ Universal RT microRNA PCR Mouse&Rat panel I+II we repeated the experiment and analysed the expression of the selected miRNAs in unconditioned and conditioned media samples by Real Time qPCR as described in paragraphs 4.4 - 4.7. Multiple comparisons two-way ANOVA test with cut-off of p-value < 0.05 was performed to analyse the data.

None of the selected miRNA was detected in unconditioned media (data not shown). MiR-103 was among the miRNAs significantly differentially expressed between preadipocytes and differentiated adipocytes even though it did not pass the Benjamini-Hochberg test in the initial screen. This miRNA was found to negatively regulate insulin sensitivity in fat and liver cells [347]. Moreover, circulating miR-103 was identified among the miRNAs involved in metabolic disorders [348]. However, these studies were based on blood sample analysis and therefore it is not possible to determine the cellular component responsible for their secretion. For these reasons, we explored miR-103 levels of expression in media from adipocytes. Figure 18 shows that, in accordance with the miRNA profiling data (data not shown), miR-103 was significantly overexpressed in mature brown adipocytes. MiR-322 secretion, in contrast to previous results (table 10 and 11), was upregulated in differentiating adipocytes. Except for this miRNA, the data obtained in this experiment confirmed the profiling results. Indeed, miR-365 levels significantly increased in brown differentiated adipocytes, miR-10b was predominantly secreted by mature brown adipocytes, miR-196a by mature white adipocytes and miR-378 levels increased in differentiated adipocytes.

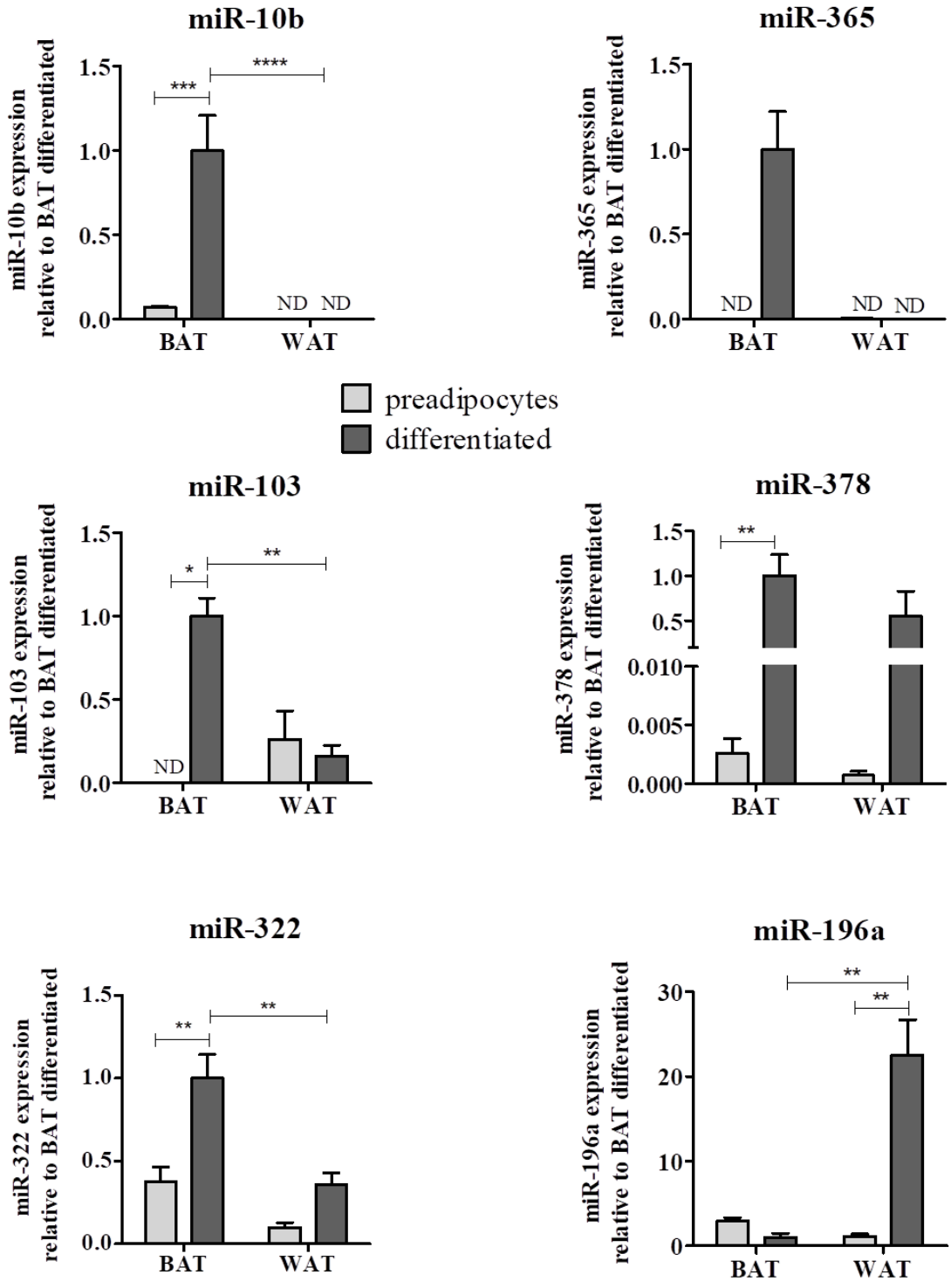

Figure 18 MiRNA expresssion in media samples from mouse undifferentiated and differentiated adipose cell lines

Graphs show miRNA expression in serum-free media from subcutaneous white and interscapular brown preadipocytes and mature brown and white adipocytes seeded all at the same cellular density. Expression levels were normalised to Unisp6 spiked-in at RNA isolation stage. Bars represent the fold changes means of triplicates ± SEM compared to BAT differentiated. ND indicates not detectable. * indicates $p \leq 0.05$, ** $p \leq 0.01$, *** $p \leq 0.001$ and **** $p \leq 0.0001$ according to multiple comparisons in two-way ANOVA test

3.2.5 *CL treatment affects extracellular levels of miRNAs released by differentiated mouse adipose cell lines*

We investigated the effect of ß3-AR activation on miRNA secretion by CL treatment. The same number of differentiated adipocytes were seeded into 12-well plates and left for 24 hours in serum-free media in the presence of CL (10 μM) or DMSO (vehicle) for control wells. After 24 hours, media samples were collected and processed for miRNA expression by Real-Time qPCR. Significance was assessed using t-test analysis for p-values <0.05. The CL treatment was able to significantly affect the secretion of 3 out of 6 miRNAs (figure 19). MiR-322 and miR-196a levels significantly increased in BAT media samples after treatment, while, miR-103 was significantly reduced. In WAT, the level of secretion of these miRNAs upon CL administration had an opposite direction to the one observed in BAT even though this was significant only for miR-196a. MiR-10b and miR-365 were only detectable in BAT samples and were not particularly affected by CL.

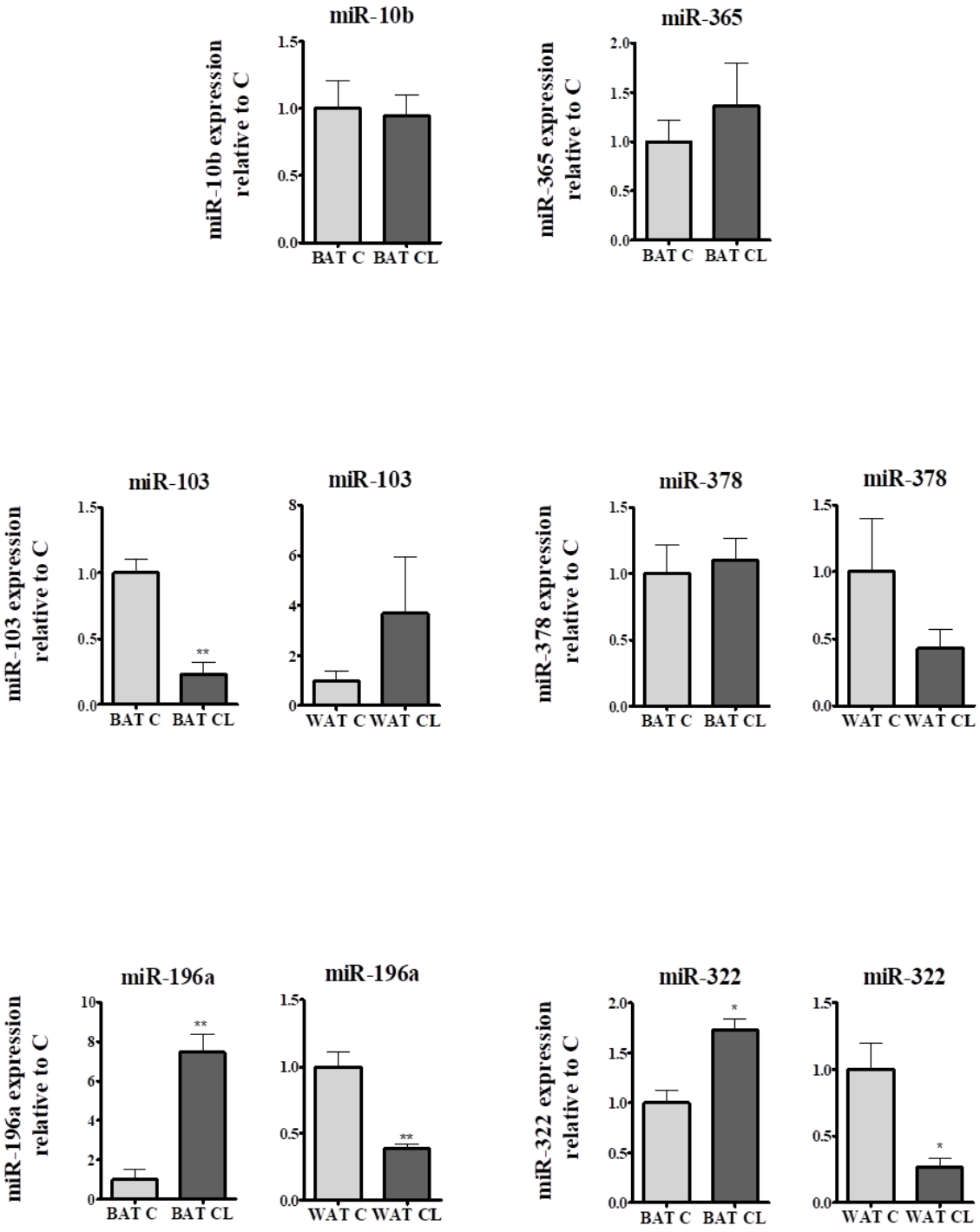

Figure 19 CL treatment affects extracellular levels of miRNAs released by differentiated mouse adipose cell lines.

Graphs show miRNA expression in serum-free media from interscapular brown (BAT) and subcutaneous white (WAT) mature adipocytes untreated (C) or treated with CL (10µM) for 24 hours. The same number of differentiated cells were seeded for each biological triplicate. Expression levels were normalised to Unisp6 spiked-in at the RNA isolation stage. Bars represent the fold changes means of the triplicates ± SEM compared to BAT or WAT controls (BAT C and WAT C). * indicates $p \leq 0.05$ and ** is for $p \leq 0.01$, according to t-test.

3.2.6 *Intracellular miRNA expression in mouse adipose cell lines*

In this section the intracellular expression of the selected miRNAs was monitored in undifferentiated and differentiated white and brown mouse cell lines. Interestingly, the intracellular miRNA patterns of expression (figure 20) did not always reflect the ones observed for extracellular miRNAs (figure 18). The increase in differentiated brown adipocyte intracellular miR-10b compared to preadipocyte levels corresponded to its induction in media from the same group of cells and miR-378 intracellular level increased with the differentiation in parallel with its extracellular levels. Also, the pattern of miR-196a intracellular expression was similar to that observed for its secretion, being downregulated in differentiated BAT versus preadipocytes and more highly expressed in mature WAT compared to mature BAT. In contrast, miR-322 secretion increased in differentiated cells while its intracellular level decreased. MiR-365 was almost undetectable in media from white adipocytes while its intracellular level was much higher in WAT than in BAT besides increasing with differentiation in both cell lines. Finally, miR-103 was mostly secreted by mature brown adipocytes even if it was predominantly expressed in white adipocytes. Moreover, intracellular upregulation of miR-103 corresponded to its extracellular downregulation in differentiated WAT. These results suggest that miRNA release by adipocytes is not necessarily directly proportional to the intracellular expression and therefore it may not simply be a passive process.

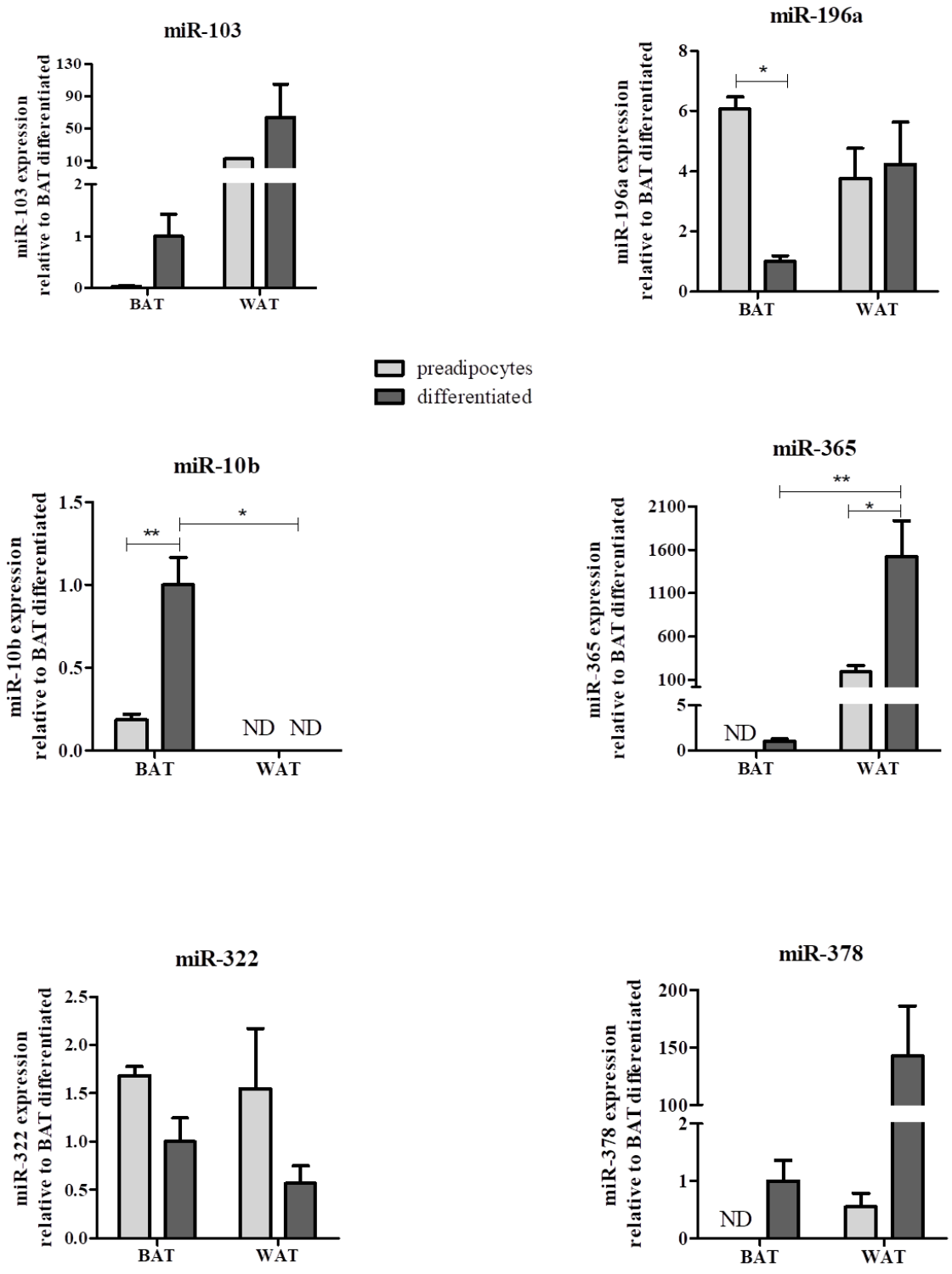

Figure 20 Intracellular miRNA expression in mouse adipose cell lines.

Graphs show miRNA expression in differentiated and undifferentiated interscapular brown and subcutaneous white adipocyte cell lines. Expression levels were normalised to Unisp6 spiked-in at the reverse transcription stage. Bars represent the fold change means of triplicates ± SEM compared to differentiated brown adipocytes. ND indicates not detectable. Significance is indicated with * for $p \leq 0.05$ and ** for $p \leq 0.01$ according to multiple comparisons in two-way ANOVA analysis.

3.2.7 *Effect of ß3-adrenergic activation on intracellular miRNA expression in mouse adipose cell lines*

Differentiated brown and white adipocytes were treated for 6 hours with 10 μM CL or DMSO for control replicates. Cells were harvested for RNA isolation and miRNA expression was analysed by Real-Time q-PCR. The results obtained are reported in figure 21. CL significantly induced miR-103 expression in brown adipocytes which was about 20-fold higher compared to untreated cells, while in white adipocytes an opposite trend of expression was observed. Upon CL treatment miR-10b was strongly induced in white adipocytes but only slightly in brown adipocytes. MiR-322 was expressed at lower levels in CL treated samples compared to untreated, while, miR-365 and miR-196a levels increased in both CL-treated brown and white adipocytes. However, only miR-365 upregulation in BAT was statistically significant.

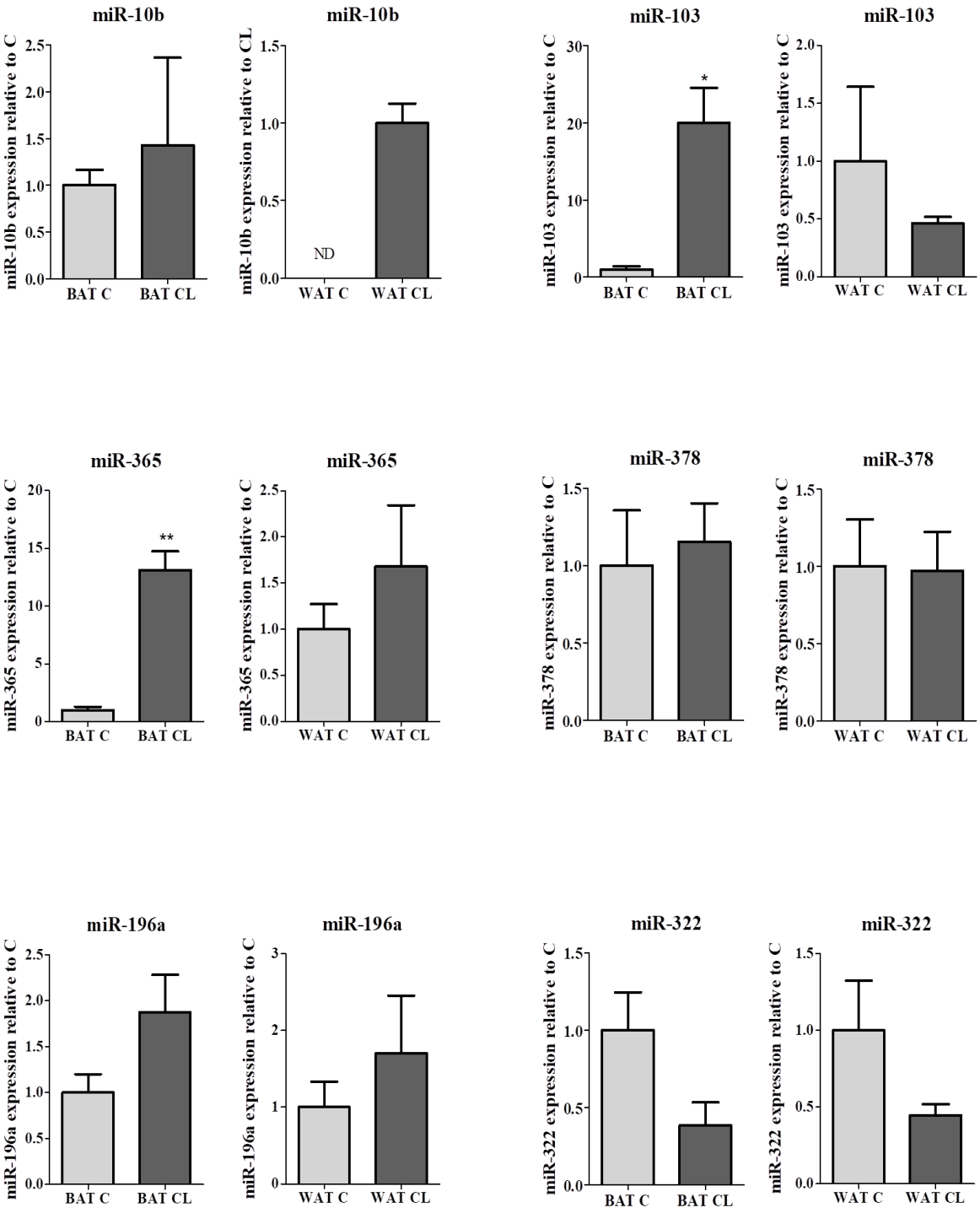

Figure 21 Effect of CL on intracellular miRNA expression in mouse adipose cell lines.

Differentiated adipocytes were treated for 6 hours with CL (10µM). Graphs show miRNA expression in untreated (C) and CL-treated (CL) differentiated interscapular brown and subcutaneous white adipocytes. MiRNA levels were normalised to Unisp6 spiked-in at the reverse transcription stage. Bars represent fold change means ± SEM of the biological triplicates compared to the controls BAT C or WAT C. Significance is indicated with * for $p \leq 0.05$ or ** for $p \leq 0.01$ according to Student's t-test.

3.3 Mouse primary adipocyte differentiation

Mouse primary brown and white cells were differentiated in vitro from the purified cells of the SVF isolated from interscapular BAT and subcutaneous WAT. The cells efficiently differentiated into adipocytes, as lipid accumulation was apparent in the cells imaged prior to RNA isolation (figure 22, panels B and C).

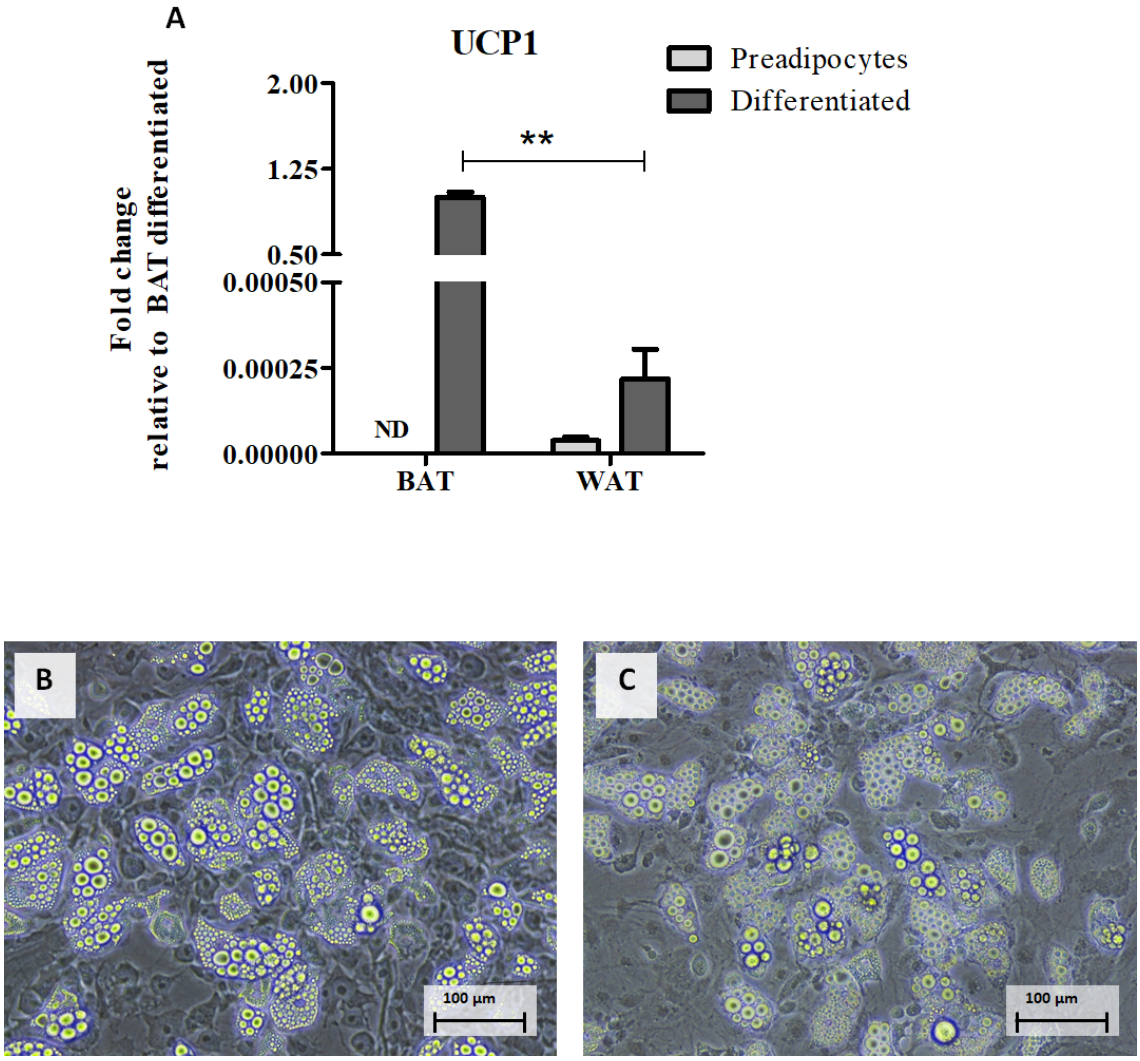

Figure 22 UCP1 expression and lipid droplet accumulation in mouse differentiating primary adipocytes
(A) UCP1 mRNA levels in primary preadipocytes and differentiated adipocytes from interscapular brown and subcutaneous white were normalised to L19 and expressed as fold changes compared to differentiated brown adipocytes. Bars represent means ± SEM of the biological triplicates. ND indicates not detectable. Significance is indicated with * for $p \leq 0.05$ and ** for $p \leq 0.01$ according to multiple comparisons in two-way ANOVA analysis. Bottom panels show 20x magnification of primary differentiated brown (B) and white (C).

After reverse transcription into cDNA and Real-Time qPCR amplification, samples were analysed for gene expression. Significance was assed using two-way ANOVA with a cut-off of p-value < 0.05. Panel A of figure 22 shows UCP1 mRNA expression relative to differentiated brown adipocytes. As predicted, this brown marker was overexpressed in differentiated brown adipocytes compared to white adipocytes and increased in both cell types with the differentiation. Subsequently, differentiated primary adipocytes were treated for 6 hours with CL (10 μM) and data analysed using t-test. As shown in figure 23, UCP1 transcription was enhanced by the ß3-agonist around 8000-fold in BAT compared to untreated and about 30-fold in WAT.

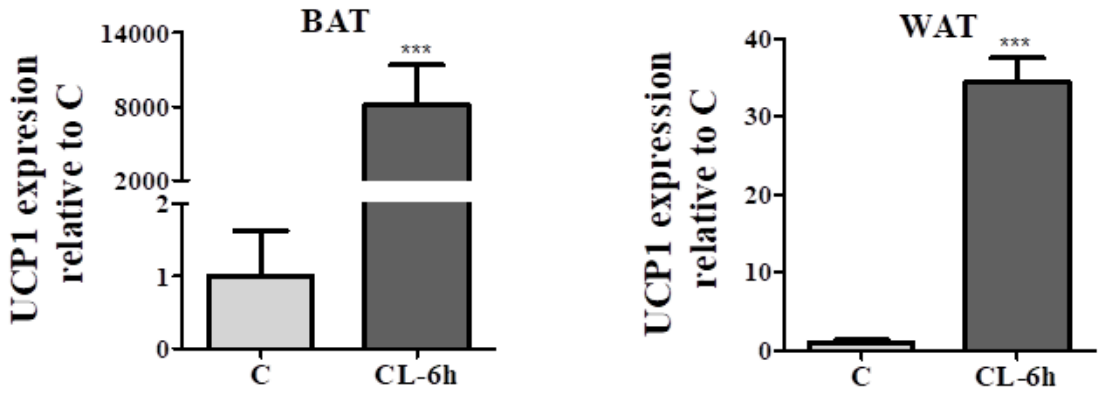

Figure 23 UCP1 mRNA induction upon CL treatment in differentiated primary adipocytes.
Graphs show UCP1 mRNA level of expression in interscapular brown adipocytes (left panel) and subcutaneous white adipocytes (right panel) untreated (C) and treated with 10 M CL (CL) for 6 hours. Expression levels were normalised to L19 and bars represent the fold changes means of the triplicates ± SEM compared to the relative controls (C). * indicates p≤0.05, ** p≤0.01 and *** p≤0.001 according to Student t-test.

3.3.1 *Extracellular miRNA secreted by primary cells*

Extracellular levels of the selected miRNAs were analysed in media from mouse primary cells. The same number of differentiated or undifferentiated adipocytes was seeded into 12-well plates and incubated in serum-free media for 24 hours. Media samples were processed as before and analysed for miRNA detection by Real-time qPCR. Significance was assessed using multiple comparisons two-way ANOVA analysis with cut-off of p-value <0.05 and results are shown in figure 24. MiR-103 was not detectable. Expression of all the miRNAs increased in differentiated cells compared to preadipocytes except for miR-322 in white adipocytes, which remained unchanged, and miR-196a that was not detectable in brown adipocytes. Different from what was

observed in mouse cell lines, miR-10b was equally expressed in media from differentiated brown and white adipocyte primary cultures.

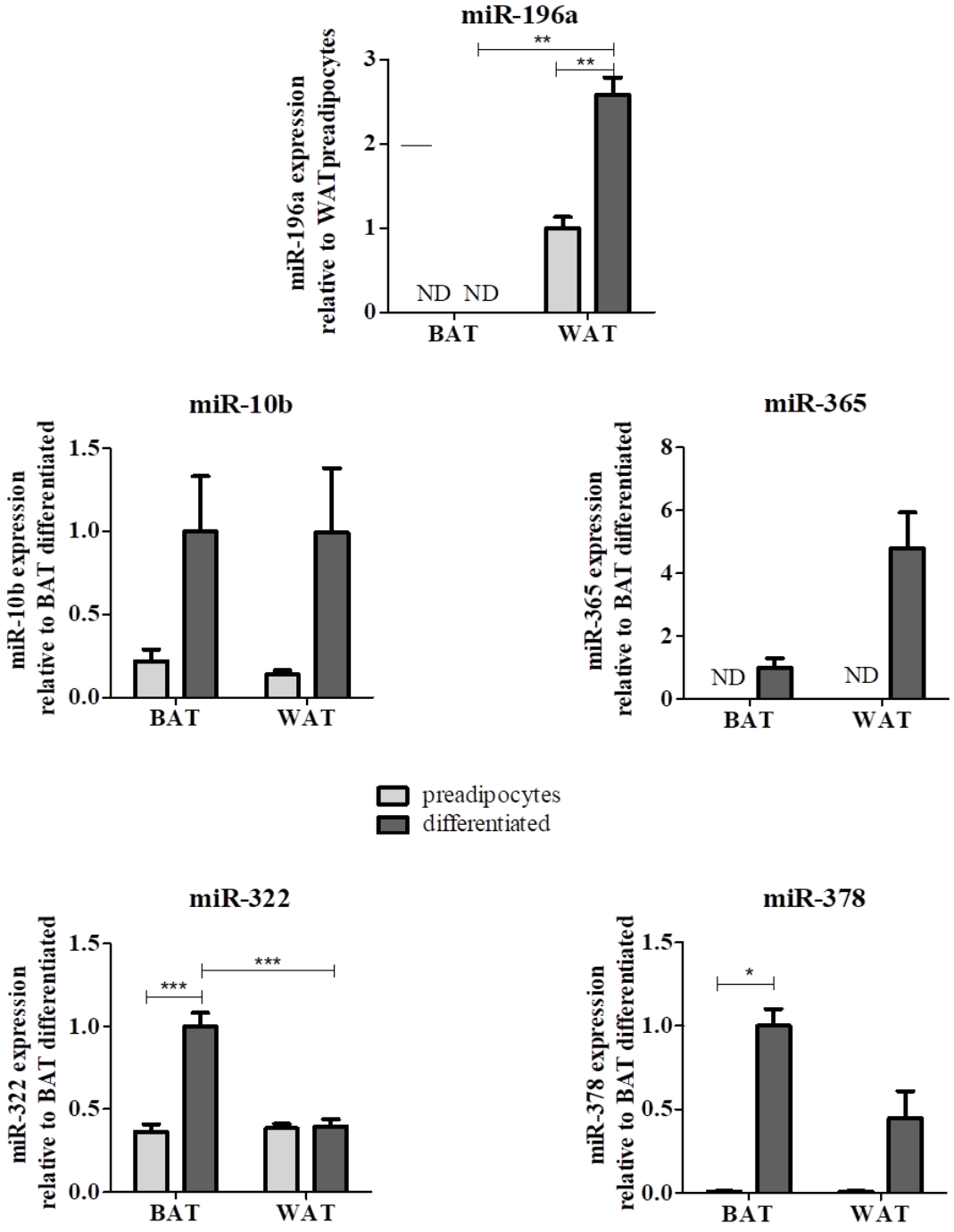

Figure 24 Extracellular miRNA expression in primary adipocytes.
Graphs show miRNA expression in serum-free media from undifferentiated and differentiated interscapular brown (BAT) and subcutaneous white (WAT) adipocytes. The same number of cells was seeded per each well. Expression levels were normalised to Unisp6 spiked-in at the RNA isolation stage. Bars represent the fold changes means of triplicates ± SEM compared to BAT differentiated. ND stays for not detectable. * indicates $p \leq 0.05$, ** $p \leq 0.01$ and *** $p \leq 0.001$ according to multiple comparisons in two-way ANOVA test.

3.3.2 *Effect of ß3-adrenergic activation on miRNA secretion in primary mouse adipocytes*

Undifferentiated and mature primary adipocytes were maintained for 24 hours in serum-free media in the presence of CL (10 µM) or DMSO vehicle control. MiRNA expression in media samples was evaluated by Real-Time qPCR and data analysed using student's t-test (figure 25). MiR-103 was not detectable once again. The treatment did not strongly affect miRNA secretion except for miR-322 and miR-196a. The latter was only detectable in white adipocyte samples and significantly decreased upon CL-treatment. Upon CL treatment MiR-322 was slightly increased in white adipocytes and significantly decreased in brown adipocytes.

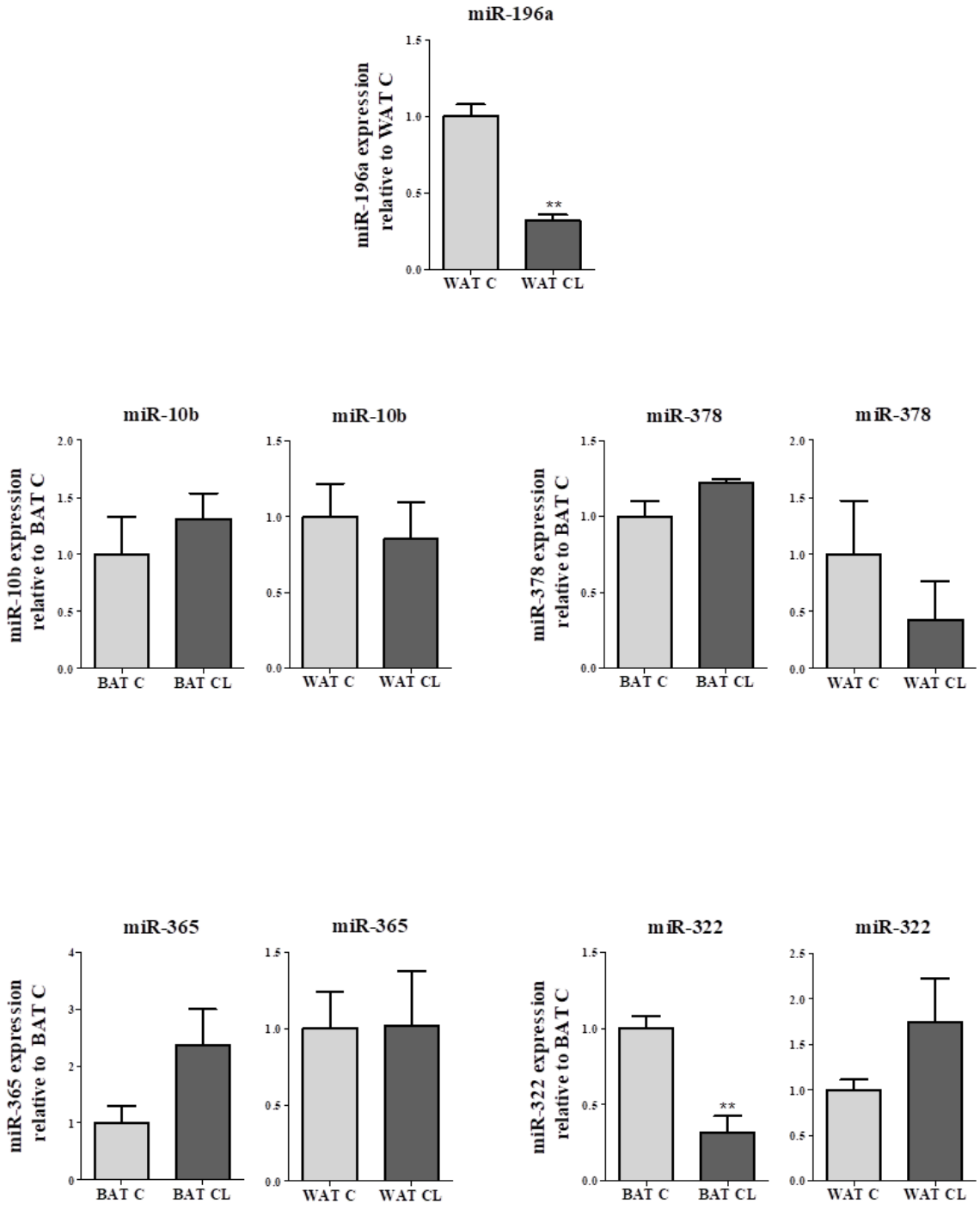

Figure 25 Effect of ß3-adrenergic activation on miRNA release in differentiated primary adipocytes. Graphs show miRNA expression in serum-free media from interscapular brown (BAT) and subcutaneous white (WAT) mature adipocytes untreated (C) and treated with 10μM CL for 24 hours. The same number of differentiated cells was seeded for each biological triplicate. Expression levels were normalised to Unisp6 spiked-in in RNA isolation stage. Bars represent the fold changes means of the triplicates ± SEMcompared to BAT or WAT controls (BAT C and WAT C). ** indicates $p \leq 0.01$, according to t-test.

3.3.3 *Intracellular miRNA expression in primary cells*

The intracellular miRNA expression in mouse primary cells analysed by Real-Time qPCR revealed that miR-10b was upregulated in differentiated brown adipocytes (figure 26) in accordance with the findings in the mouse cell lines. MiR-378 and miR-365 were significantly upregulated in differentiated cells compared to pre-adipocytes and more highly expressed in white adipocytes, confirming the observations in the cell lines. MiR-196a was undetectable in preadipocytes and highly induced following differentiation in both white and brown adipocytes. MiR-322 increased in differentiated brown adipocytes and was more highly expressed in white adipocyte samples, where it was equally expressed between undifferentiated and mature adipocytes. MiR-103 showed a similar pattern of expression to that found in the mouse cell lines, being upregulated during differentiation and significantly higher in white compared to brown adipocytes. Also in this case, the intracellular expression pattern of the miRNAs did not reflect the extracellular one, except for miR-365 and miR-378.

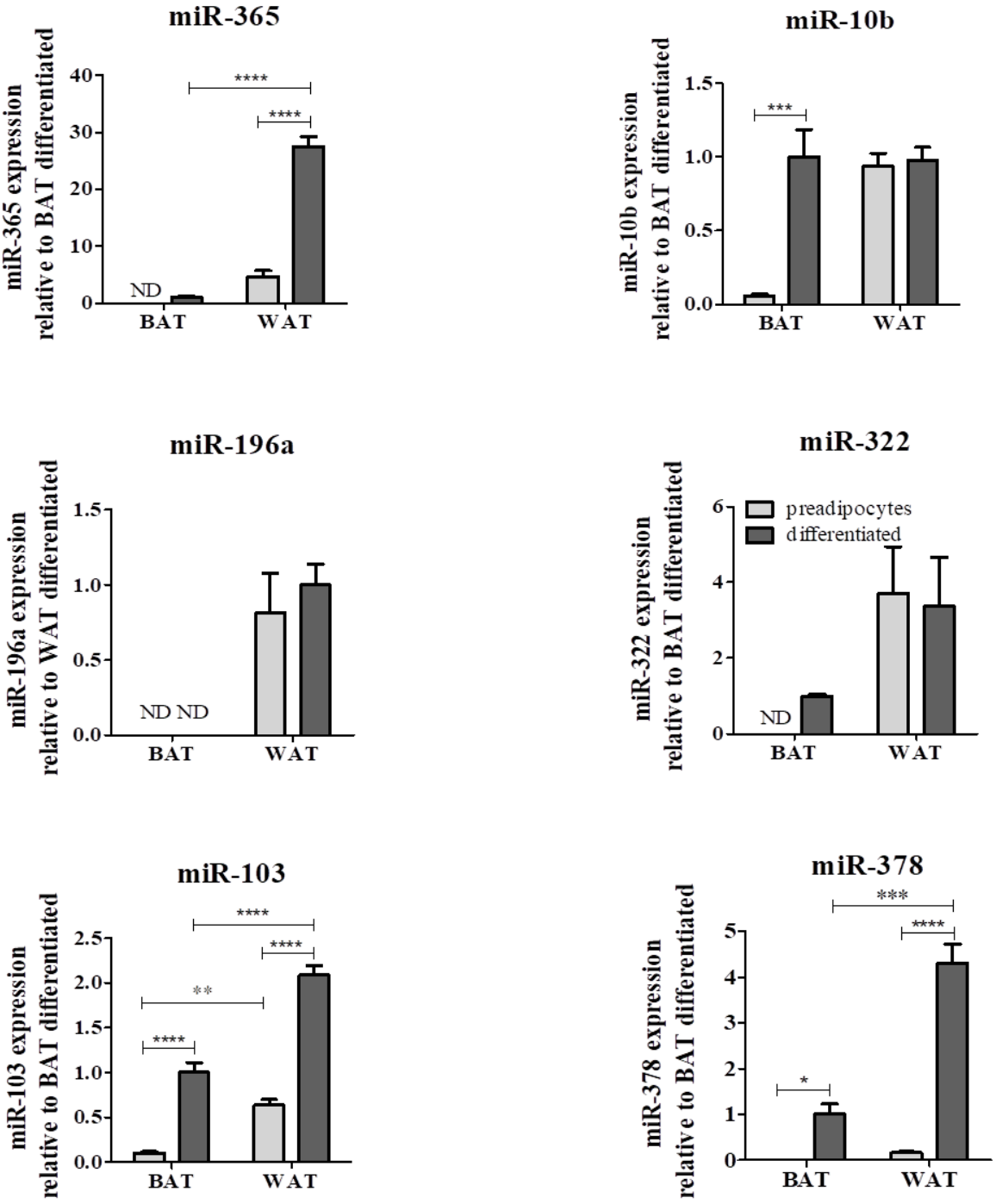

Figure 26 Intracellular miRNA expresssion in mouse primary adipocytes.
Graphs show miRNA expression in differentiated and undifferentiated interscapular brown and white adipocyte primary cultures. Expression levels were normalised to Unisp6 spiked-in at the reverse transcription stage. Bars represent the fold change means of triplicates ± SEM compared to BAT differentiated. ND indicates not detectable. Significance is indicated with * for $p \leq 0.05$ and ** for $p \leq 0.01$, *** for $p \leq 0.001$ and **** for $p \leq 0.0001$ according to multiple comparisons in two-way ANOVA analysis.

3.3.4 *Effect of ß3-adrenergic activation on intracellular miRNA expression in primary cells*

Differentiated primary adipocytes were treated for 6 hours with CL and intracellular miRNA content was analysed by Real-Time qPCR. Student's T-test was performed and significance assigned for $p<0.05$. As shown in figure 27, miR-103 was not affected by CL treatment, while, all the other miRNAs were induced. Significant fold changes of miRNA expression in CL-treated cells compared to controls went from a minimum of 1.5 of miR-378 in BAT and a maximum of 10 for miR-196a observed in white adipocytes. The latter was not detectable in brown adipocytes.

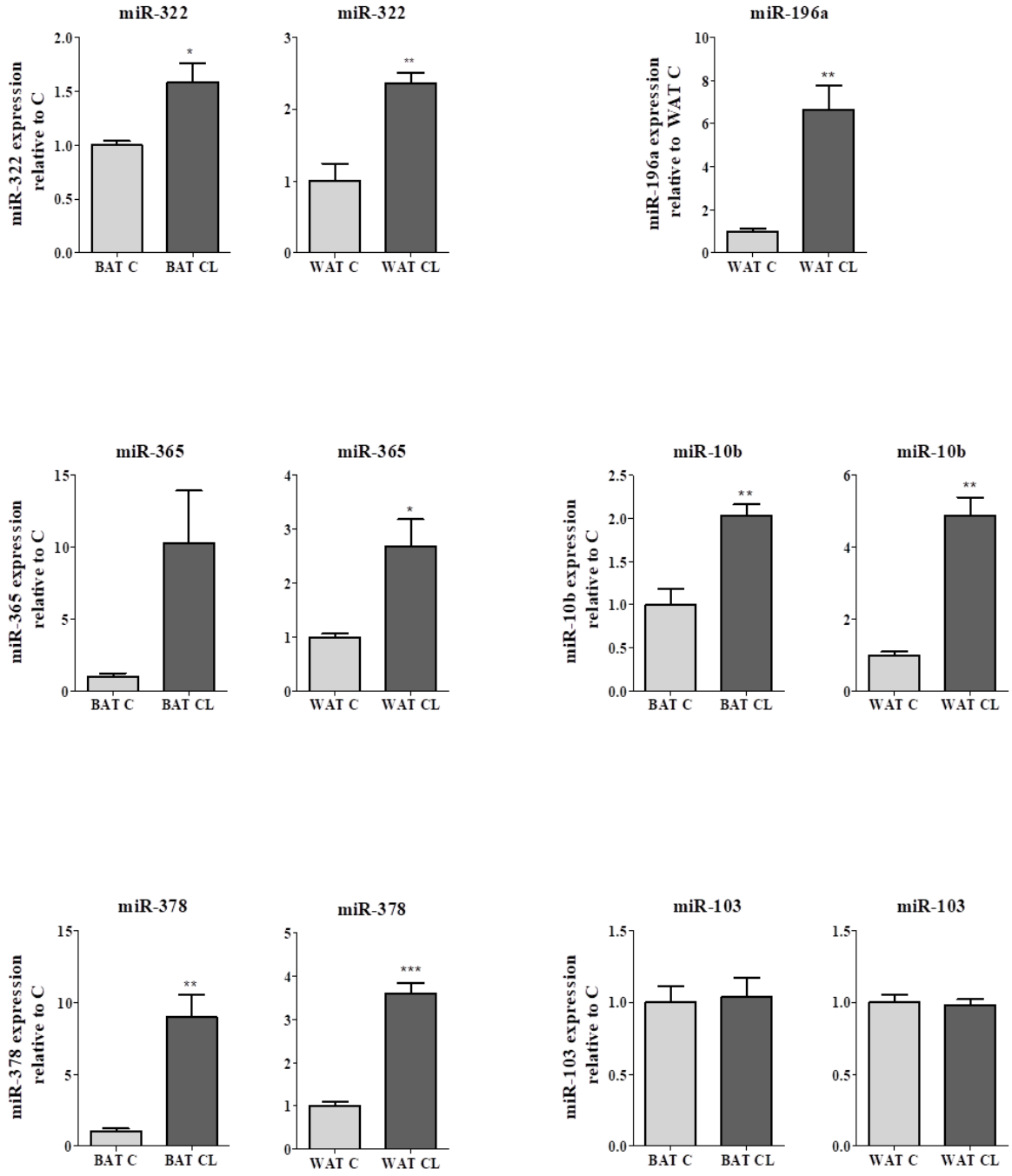

Figure 27 Effect of ß3-adrenergic activation on intracellular miRNA expression in mouse primary adipocytes.

Differentiated adipocytes were treated for 6 hours with CL (10µM). Graphs show miRNA expression in untreated (C) and CL-treated (CL) interscapular brown and subcutaneous white primary adipocytes. MiRNA levels were normalised to Unisp6 spiked-in at reverse transcription stage. Bars represent fold change means ± SEM of the biological triplicates compared to the controls BAT C or WAT C. Significance is indicated with * for p≤0.05, ** for p≤0.01 and *** for p≤0.001 according to Student's T-test.

3.3.5 *Explants: mRNA expression and tissue histology*

Explants were obtained by dissecting interscapular BAT and subcutaneous WAT from 4-6 week old mice. Dissected tissues were washed several times with DMEM to remove debris and serum traces. Experiments were run in quadruplicates. Explants were maintained in serum-free media for 6 hours to reduce mRNA degradation due to necrosis factors production occurring after dissection. Both, tissue and media samples were collected and processed for mRNA and/or miRNA expression analysis. The aim of this experiment was to investigate intracellular and extracellular miRNA expression in BAT and WAT where the adipocytes are integrated in the tissue and therefore in an environment resembling the physiological condition occurring in vivo.

White adipose tissue starts developing after birth and depending on the age of the mouse or the temperature to which the mouse has been exposed, it can present brown-like feature in terms of morphology and gene expression. The interscapular brown adipose depot appears as a dark red butterfly which edges are relatively easily distinguishable from the surrounding muscular tissue in young mice. However, with growth, the edges start becoming of a paler colour as the beige/white cellular component increases. This area, if present, was removed from the tissues during dissection. In this section histology of the dissected tissues, obtained through haematoxylin-eosin stain and their mRNA expression of UCP1 are reported in figure 28 Panel B shows the histology of BAT, rich in cells containing multilocular lipid droplets. Panel C shows WAT section where the major cellular component consists of adipocytes presenting unilocular lipid droplets. The analysis of mRNA expression shows that UCP1 was significantly greater in BAT than in WAT (panel A)

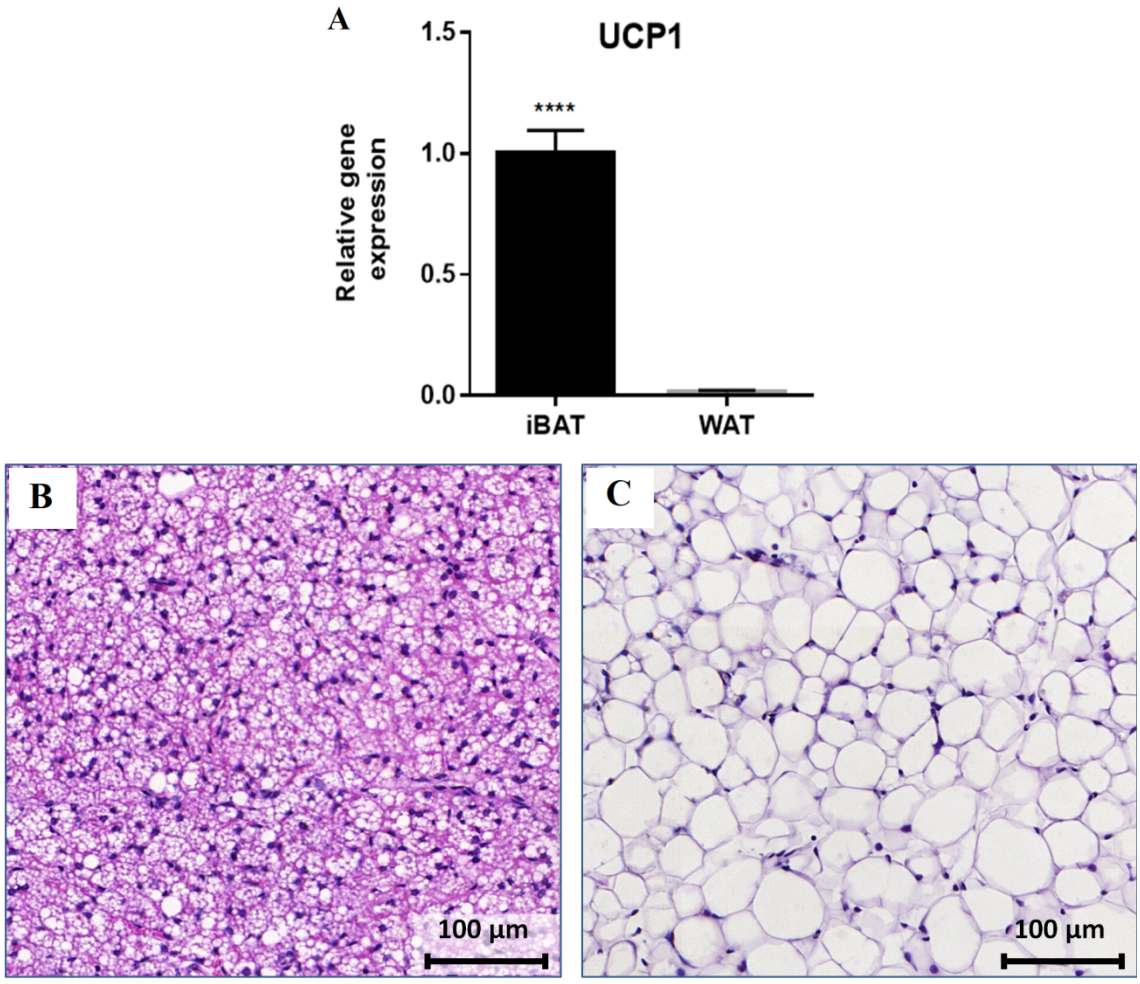

Figure 28 UCP1 mRNA expression and histology of mouse adipose tissues.
(A) UCP1 mRNA expression in interscapular BAT and subcutaneous WAT explants. Bars represent mean ±≤ SEM of UCP1 levels of biological quadrulicates normalised to L19 and expressed in fold change compared iBAT. Significance was assessed by Student's t-test analysis and **** indicates p≤0.0001. Panels at the bottom show haematoxylin-eosin stain of BAT (B) and WAT (C).

3.3.6 *MiRNA expression in media from explants*

MiRNA expression in media samples was normalised for tissue weight (figure 29). Consistent with previous results in mouse primary cells and cell lines, miR-196a was selectively secreted by WAT, mir-322 and miR-378 mostly by BAT. Similar to the findings in primary cells, secreted miR-103 was not detectable in media from explants. MiR-365, differed from primary cells but in accordance to the data obtained in mouse cell lines, was significantly more highly expressed in media from BAT. Surprisingly, miR-10b was 100 times higher in media from WAT. Inconsistency between these results and the ones observed in mouse primary adipocytes and/or cell lines may be explained

by the fact that, in explants, different cellular components alongside with adipocytes are present and all of them contribute to miRNA secretion.

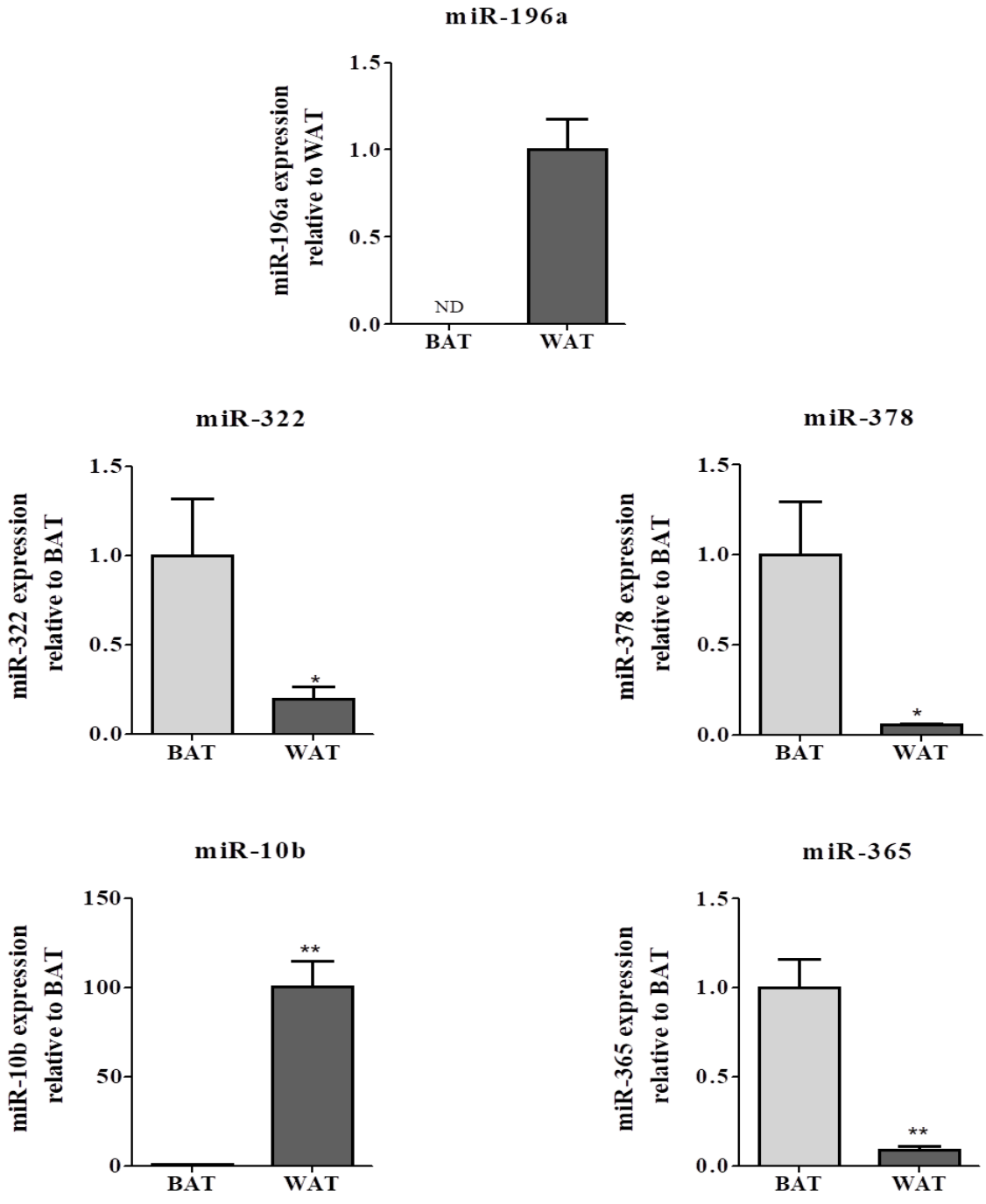

Figure 29 miRNA expression in media samples from mouse explants.
Graphs show extracellular miRNA expression in BAT and WAT explants incubated in serum-free media for 6 hours. Expression levels in the media were normalised to Unisp6 spiked-in at RNA isolation stage. Bars represent the fold changes means of quadruplicates or triplicates divided by the tissues weight ± SEM compared to BAT differentiated. ND indicates not detectable. Significance is indicated with * $p \leq 0.05$ and ** for $p \leq 0.01$ according to Student's t-test analysis.

3.3.7 *MiRNA expression in explant tissues*

The analysis of intracellular miRNA expression by Real-time PCR in BAT and WAT explants (figure 30) revealed that miR-103 was present in both tissues and more highly expressed in WAT. MiR-365 was significantly overexpressed in BAT and miR-322 showed a trend of expression similar to miR-365. MiR-196a was only detectable in WAT and there were no differences in miR-10b and miR-378 expression between BAT and WAT.

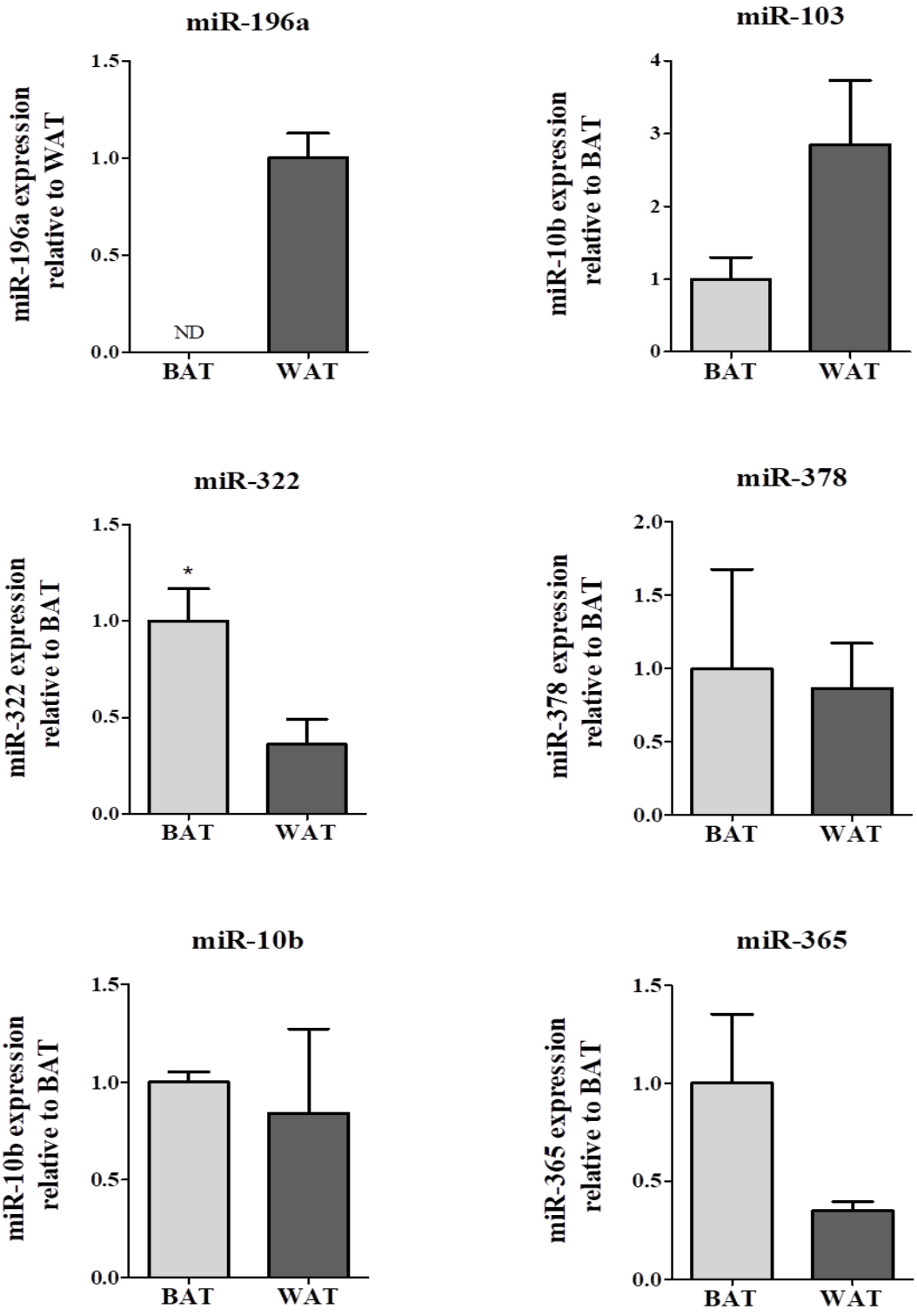

Figure 30 miRNA expression in BAT and WAT explants.
Graphs show miRNA expression in BAT and WAT explants. MiRNA levels were normalised to L19. Bars represent the fold changes means of quadruplicates or triplicates ± SEM compared to BAT explants. ND indicates not detectable. Significance is indicated with * $p \leq 0.05$ according to Student's t-test analysis.

3.4 Human adipocyte characterization

In *vitro* studies on adipocytes have led to rapidly increase the knowledge on many molecular mechanisms underlying the physiological metabolism of the adipose tissue and its pathologies. However, while human white adipocytes are largely available, procedures to obtain human BAT samples require invasive surgery, making human primary brown pre-adipocytes and the relevant cell lines very rare. So far, only few human brown adipose cell lines have been created [349-351] and they have been reported to resemble characteristics more similar to the beige mouse adipocytes rather than to the brown mouse adipocytes [351, 352]. In addition, human brown adipose depots present a more heterogeneous cellular population than mouse BAT and selection of the brown preadipocyte clones is very difficult. The human adipose cell lines used for this study were provided by Prof Fredrik Karpe (University of Oxford). Before performing any experiments to investigate miRNA expression or secretion, cells were characterised to ensure their reliability as brown and white adipocyte models.

3.4.1 *Oil Red O Staining*

The human adipocyte cell lines were differentiated and stained with Oil Red O. Images were captured at day 0 and 22 of differentiation. On the very first day, after only few hours of administration of induction media, cells assumed a flatter and more compact shape. Small lipid droplets started to appear at day 4 becoming larger and more numerous with the progression of differentiation, until cell edges were no longer distinguishable (figure 31, panels C and D). As shown in figure 31, cell size dramatically decreased upon increased confluency and progressed differentiation.

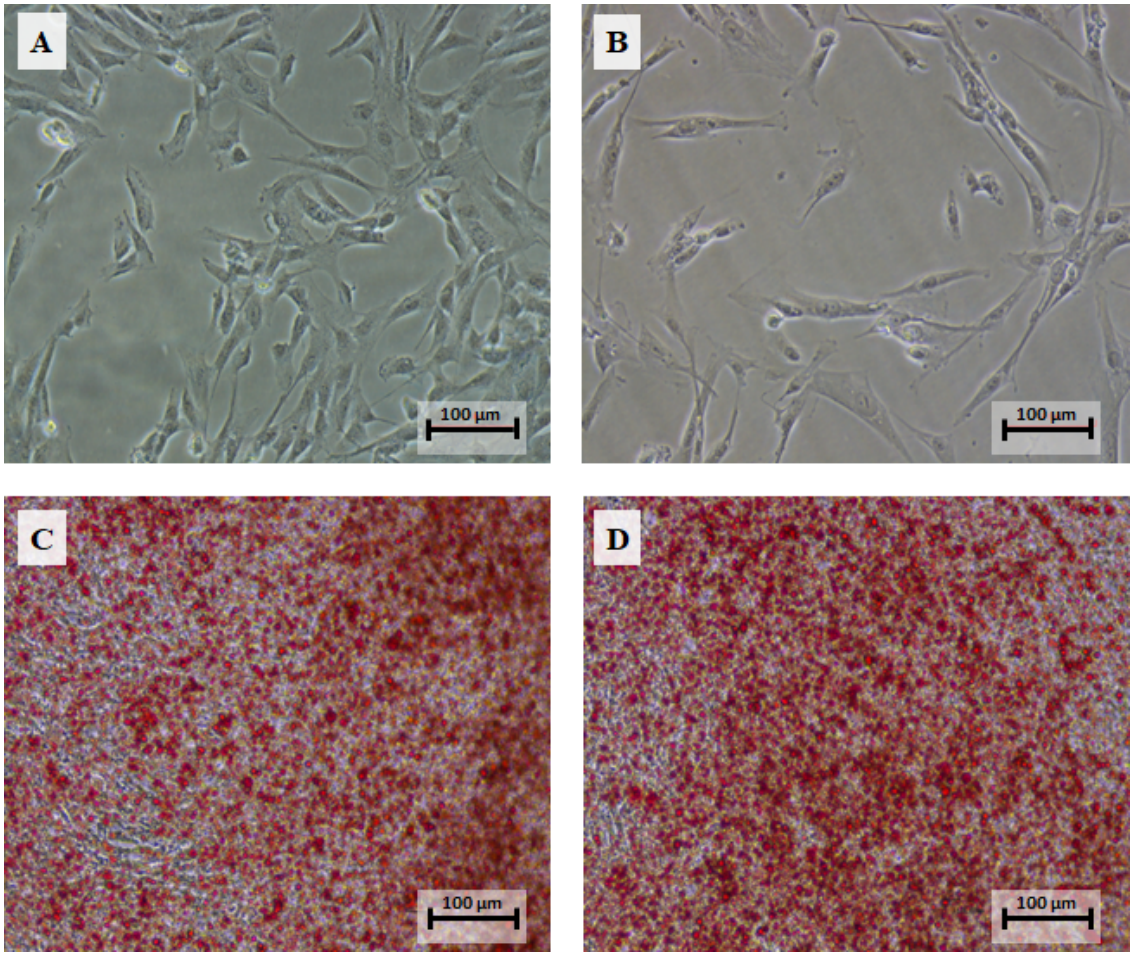

Figure 31 Oil Red O staining of human brown and white adipocytes.
Human undifferentiated and differentiated brown and white and brown adipose cell lines were stained with Oil Red O and pictures were taken with a 40x magnification. (A) Undifferentiated brown adipocytes, (B) undifferentiated white adipocytes, (C) differentiated brown adipocytes, and (D) differentiated white adipocytes.

3.4.2 *Gene expression*

Differentiation of brown and white adipocytes was further assessed by gene expression analysis. RNA was isolated from undifferentiated and mature adipocytes and processed for Real Time qPCR. As expected, the morphological changes were accompanied by induction of FABP4 mRNA in mature adipocytes (figure 32). Cells were also tested for marker genes specific of the brown (UCP1, CIDEA, PGC1α, FABP3 and SLC27A2) and white (HOXC9) phenotype. Among these, the most relevant brown marker gene, UCP1, was strongly upregulated in differentiated brown adipocytes compared to all the other groups. Very low levels were detected in mature white

adipocytes and no expression was found in white preadipocytes. Similarly, CIDEA and PGC1α were only and predominantly expressed in mature brown adipocytes, respectively. CPT-1ß and FABP3 significantly increased with differentiation in both brown and white adipocytes but were expressed at much higher extent in mature brown adipocytes compared to white adipocytes. The white marker gene HOXC9 was selectively expressed by white adipocytes and, accordingly to what observed by Carey A. *at al.,* it was slightly downregulated in differentiated white adipocytes compared to pre-adipocytes [353].

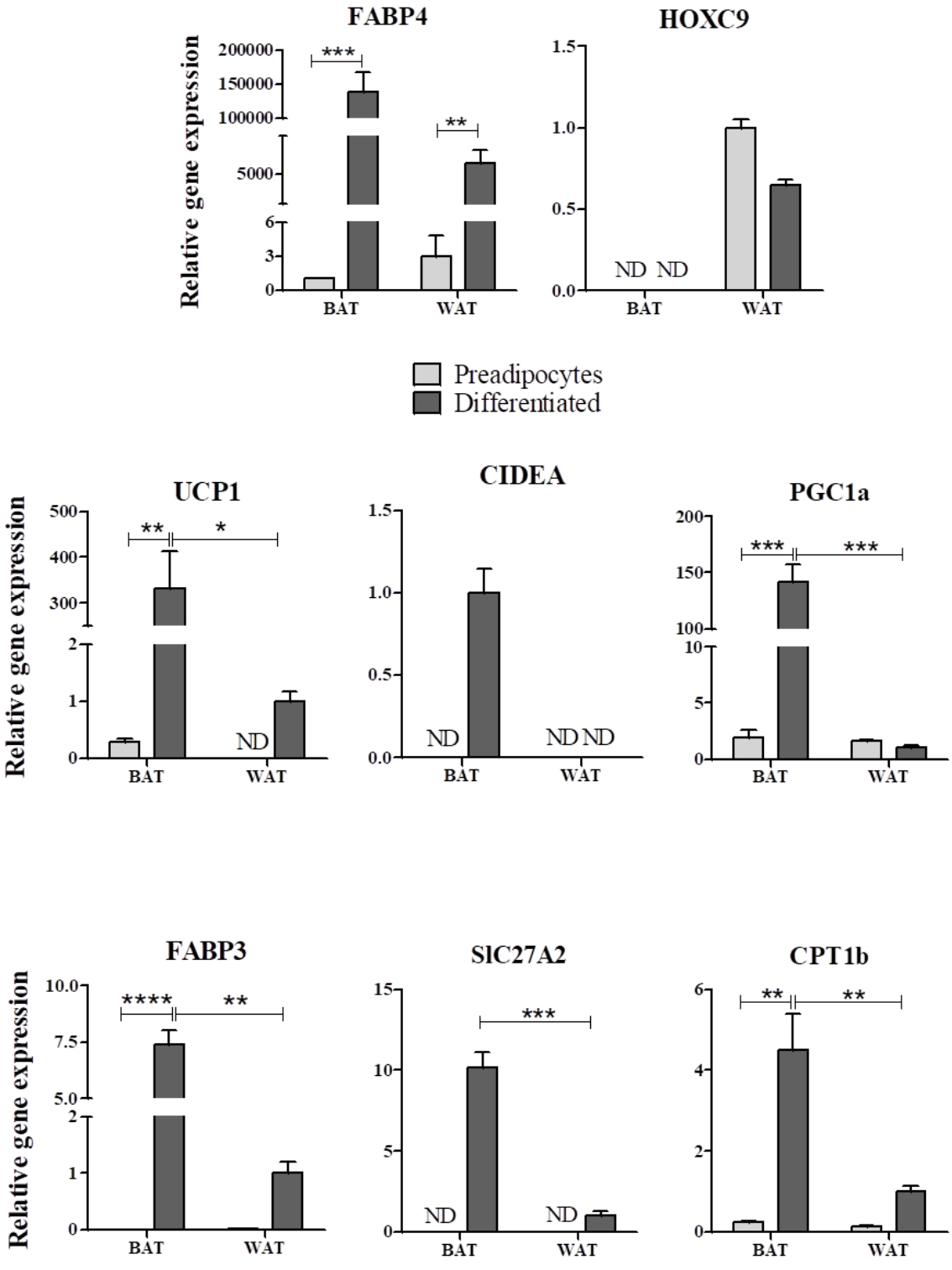

Figure 32 Gene expression in human brown and white adipose cell lines.
mRNA expression of marker genes in interscapular brown and subcutaneous white adipose cell lines before and after differentiation normalised to L19. Bars represent fold change means ±SEM of the biological triplicates and compared to BAT differentiated. * indicates p≤0.05, ** p≤0.01 *** p≤0.001 and **** p≤0.0001 according to multiple comparisons in two-way ANOVA test.

3.4.3 *UCP1 mRNA upregulation in human adipocytes upon ß-AR activation*

To evaluate the ability of the adipocytes to activate UCP1 transcription upon ß-adrenergic stimulation, differentiated brown and white adipocytes were treated for 5 hours with 10µM Isoproterenol, a non-selective ß-adrenoreceptor agonist, or DMSO (vehicle). Expression of UCP1 was analysed by Real-Time qPCR and data analysed using Student's t-test. As shown in figure 33, Isoproterenol induced UCP1 upregulation. Specifically, UCP1 levels were about 80 times significantly higher in Iso-treated brown adipocytes compared to brown control and 5 times increased in Iso-treated white adipocytes compared to white control.

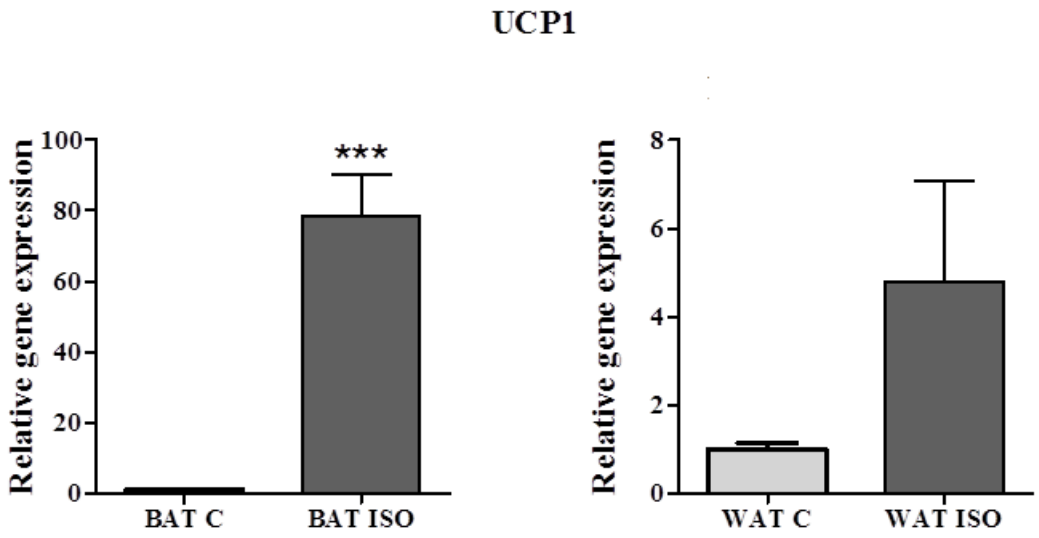

Figure 33 UCP1 mRNA induction upon Isoproterenol treatment in human differentiated brown and white adipose cell lines.
Graphs show UCP1 mRNA level of expression in brown (left panel) and white adipose cell lines (right panel) untreated (C) and treated with 10µM Isoproterenol (ISO) for 6 hours. Expression levels were normalised to L19 and bars represent the fold changes means of the triplicates ± SEM compared to BAT or WAT controls (BAT C and WAT C). *** indicates $p \leq 0.001$, according to Student's t-test.

3.4.4 *Mitochondrial content in brown and white adipocytes*

Brown adipocytes present a higher number of mitochondria than white. Indeed, uncoupling respiration takes place in these organelles where UCP1 is located. To evaluate the mitochondrial content in human adipocytes, we measured the amount of mitochondrial DNA by analysing the relative abundance of the mitochondrial genome encoded Cyt-b gene. DNA was isolated and amplified by Real time PCR. Data were then

analysed and normalised to genomic DNA levels by PCR of the nuclear encoded RIP140 gene. CYT-B levels increased with differentiation in both brown and white adipocytes (figure 34). Indeed, mitochondria play an important role also in white adipocyte metabolism [354]. However, as expected, brown adipocytes presented a significantly higher content of mitochondrial DNA compared to white adipocytes.

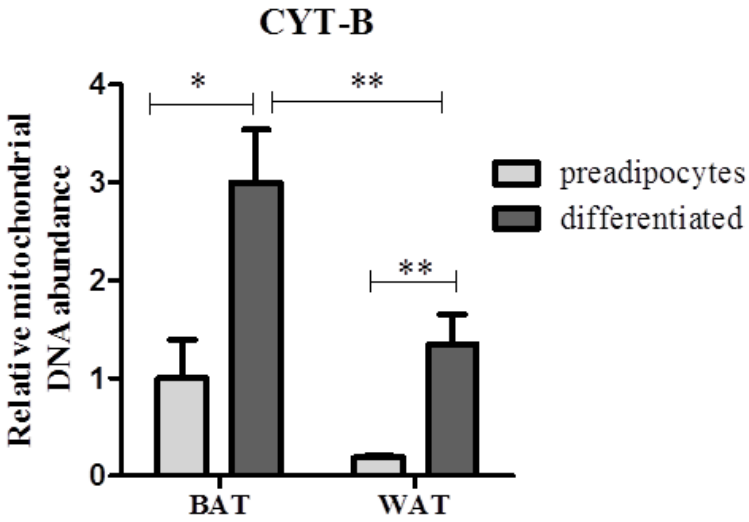

Figure 34 Mitochondrial DNA abundance.
The Graph shows abundance of the mitochondrial gene CYT-b in brown and white undifferentiated and mature adipocytes, normalised to RIP140. Bars represent fold change means ±SEM of the biological triplicates or quadruplicates and compared to BAT preadipocytes. * indicates $p \leq 0.05$ and ** $p \leq 0.01$ according to multiple comparisons in two-way ANOVA test.

3.4.5 *Oxygen consumption*

In order to test the functional activity of UCP1, basal OCR of brown and white adipocytes was measured by Seahorse technology. Brown and white adipocytes were tested simultaneously by seeding the same number of cells (50,000) into each well of a 24-well seahorse plate. As shown in figure 35, panel A, brown adipocytes presented a significant higher consumption of oxygen compared to white adipocytes. Additionally, the inducibility of UCP1 upon ß-adrenergic stimulation was assessed by measuring the oxygen consumption in brown adipocytes pre-treated with 10 µM Isoproterenol for 40 minutes or DMSO (vehicle) for controls. Oxygen consumption in treated cells was significantly greater than untreated cells suggesting increased cellular respiration,

possibly via activation of UCP1 activity under ß-adrenergic stimulation. However to confirm this hypothesis, a mitochondrial stress assay should be performed to measure the uncoupled respiration.

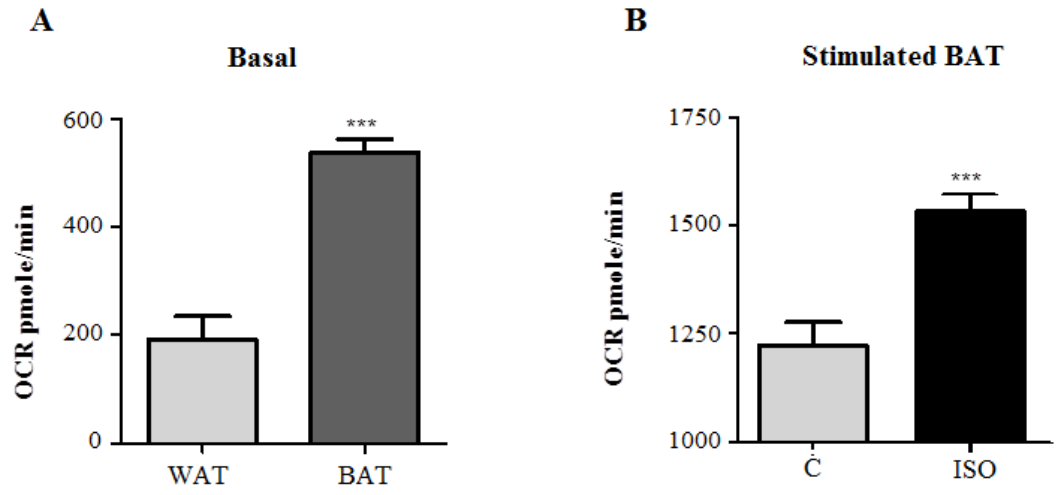

Figure 35 Oxygen consumption in adipocytes.
A) Oxygen consumed expressed in pmol/min by white and brown adipocytes at basal conditions. B) Oxygen consumption in brown adipocytes pre-treated for 40 minutes with (Iso) or with the vehicle DMSO (control). *** indicates $p \leq 0.0001$ according to Student's t-test.

3.4.6 *Gene expression of miRNA processing machinery during human adipocyte differentiation*

To explore the expression of the genes involved in miRNA maturation in human adipocyte cell lines, the mRNA levels of Ago2, Dicer1 and GW182 were monitored during adipocyte differentiation in parallel with FABP4. White and brown preadipocytes were induced to differentiate and processed for Real Time qPCR analysis at day 0, 3, 10 and 22. As represented in figure 36, FABP4 in brown adipocytes was strongly upregulated at day 3 compared to day 0. Its expression kept increasing until day 22. In white adipocytes, FABP4 reached its highest peak of expression at day 10 and decreased at day 22, still showing significant overexpression compared to day 0. Interestingly, all the miRNA processor genes tested, showed an initial downregulation in both brown and white adipocytes, although the changes in mRNA levels at day 3 were significant only for Ago2. At day 10 the expression of all the genes increased again, compared to day 3, reaching similar levels to the ones observed at day 0, except for Ago2 in white adipocytes,

which levels progressively decreased to a fold change of 0.148 ± 0.060 at day 22 compared to day 0. In brown adipocytes, at day 22, Ago2 was significantly lower expressed (fold change: 0.762 ± 0.076) compared to day 0. On the contrary, at day 22, Dicer1 and GW182 were upregulated in both cell types compared to day 0, even though Dicer1 changes in brown adipocytes were not significant.

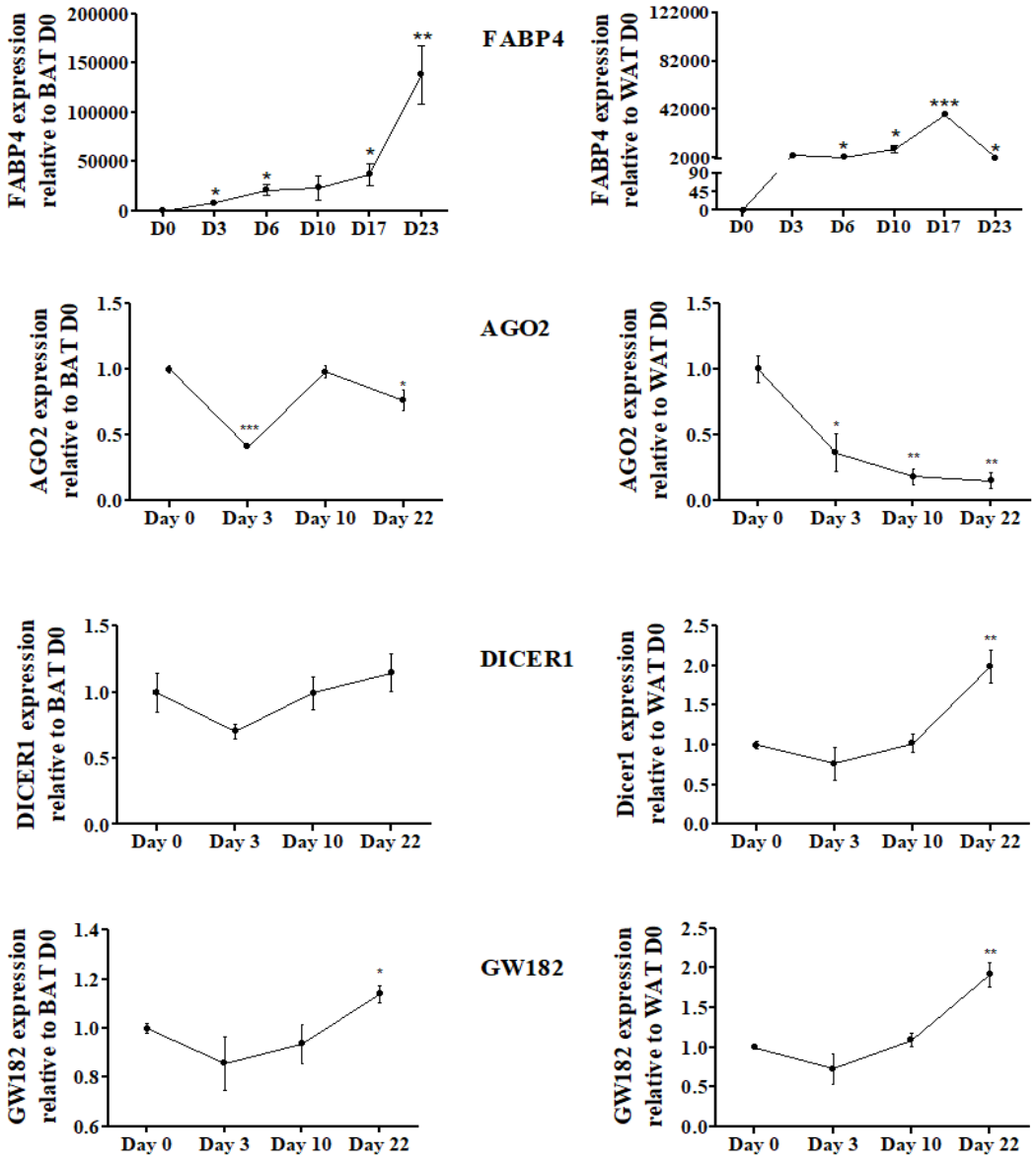

Figure 36 Regulation of genes involved in miRNA maturation during differentiation of human brown and white adipocytes.
The graphs show mRNA expression of FABP4, Ago2, Dicer1 and GW182 at day 0, 3, 11 and 22 of differentiation of brown and white adipocytes. The mRNA levels of each gene were normalised to L19. Dots represent average of fold changes of the biological triplicates ± SEM compared to day 0. Significance was assessed according to one-way ANOVA, $p \leq 0.05$ (*), $p \leq 0.01$(**) and $p \leq 0.0001$(***).

3.4.7 *Extracellular miRNAs secreted by human adipocytes*

Human undifferentiated and differentiated brown and white adipocytes were maintained in serum-free media for 24 hours. To obtain comparable data, the same number of cells ($5x10^5$) was seeded into each well of a 12-well plate. Media samples were collected as previously described. Part of the sample was sent to Exiqon service for miRNA PCR panel assay to identify miRNA differentially secreted between brown and white adipocytes in humans. The remaining part of the sample was processed for Real Time q-PCR analysis to evaluate the expression of the miRNAs previously tested in mouse experiments.

3.4.8 *MiRNA profiling of media samples from human adipocytes*

The quality control of the data obtained by the miRNA PCR panel assay was performed by analysing variation among samples. In the PCA performed on all the samples and the top 34 miRNAs with the highest standard deviation, samples from brown and white adipocytes grouped in two different areas of the graph based on the largest variation defined by PC1 (figure 37) and reflecting the different nature of brown and white adipocytes in terms of miRNA secretion. Observing the distribution of the samples based on the second largest variation specified by PC2, it is possible to note that, white adipocytes clustered very close one to each other. Brown adipocytes spread along the y-axis, suggesting, even if at low grade, variability among the brown adipocytes group. This was not necessarily due to RNA quality, but more likely to the heterogeneous nature of brown adipocytes in humans. Reassured of the good quality of the data, we proceeded with the statistical analysis to identify miRNAs differentially secreted between brown and white adipocytes.

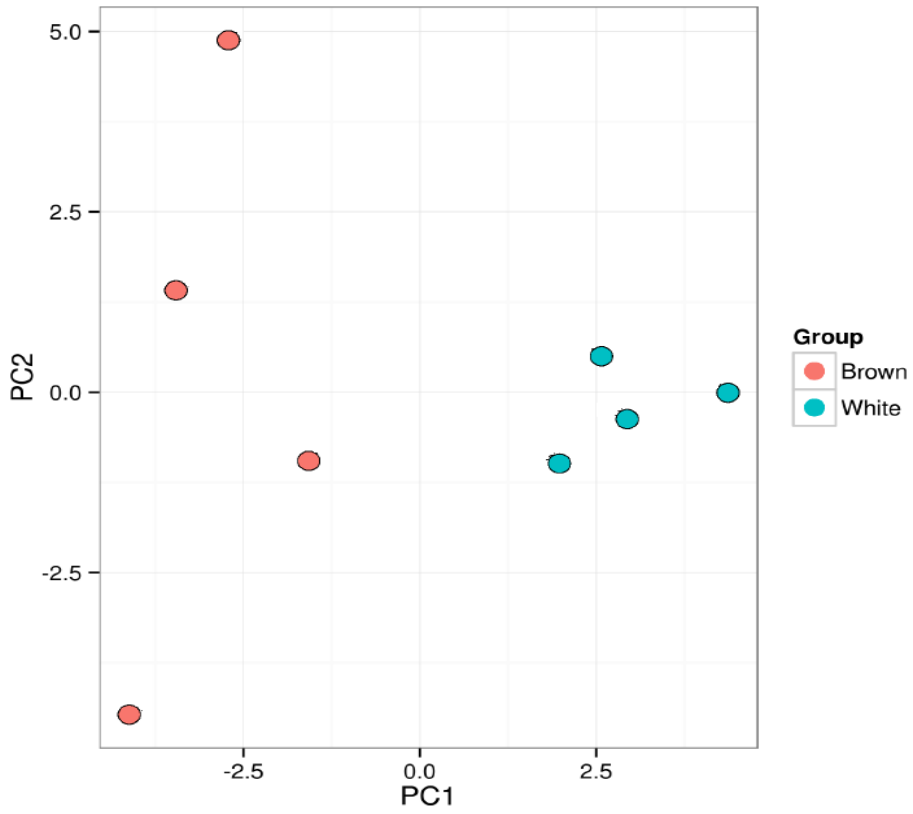

Figure 37 PCA plot.
The principal component analysis performed on all samples, and on the top 34 microRNAs with highest standard deviation. The normalized (dCq) values have been used for the analysis.

3.4.8.1 *Volcano plot*

To identify miRNAs differentially secreted between brown and white adipocytes data were analysed using Student's t-test and Benjamini-Hochberg correction. Log 2 (fold change) of brown versus white adipocytes and the –log10 (p value) were plotted on x and y axes, respectively to obtain the volcano plot in figure 38. In table 13 the top 11 miRNAs differentially expressed between brown and white adipocytes that presented a p value ≤ 0.05 are reported. Among these, there were miR-378a and miR-365, both overexpressed in media from brown adipocytes, in accordance with the results obtained by RT-qPCR. The other miRNAs overexpressed in media from brown adipocytes compared to white were: miR-335-5p and miR-92a.3p. However, of all the miRNAs identified, only miR-138-5p passed the Benjamini-Hochberg test, therefore it was included in the list of miRNAs to be tested by RT q-PCR in human adipocytes.

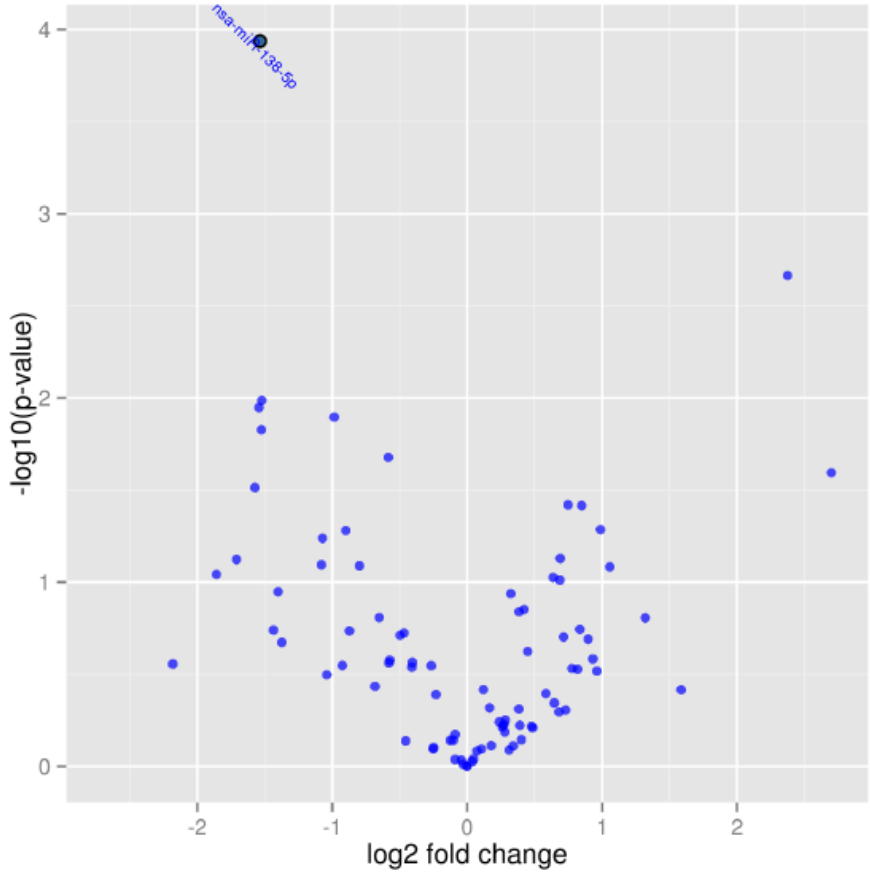

Figure 38 Volcano plot.
The graphic shows the relation between the p-values and the ddCq obtained by comparing miRNA expression in media from brown versus white adipocytes.

Table 12 miRNA differentially secreted between brown versus white adipocytes

miRName	SD Brown	SD White	Average dCq Brown	Average dCq White	FC	P-value	Adj. p value
miR-138-5p	0.25	0.18	0.28	1.80	-2.9	$1.2x10^{-4}$	0.01
miR-378a-3p	0.67	0.64	0.21	-2.20	5.2	$2.2x10^{-3}$	0.09
miR-15a-5p	0.33	0.64	-3.40	-1.90	-2.9	$1.0x10^{-2}$	0.22
miR-34a-5p	0.67	0.41	-2.20	-0.62	-2.9	$1.1x10^{-2}$	0.22
miR-320a	0.44	0.26	-0.70	0.28	-2.0	$1.3x10^{-2}$	0.22
miR-423-3p	0.71	0.37	-0.22	1.30	-2.9	$1.5x10^{-2}$	0.22
miR-23a-3p	0.06	0.27	2.00	2.60	-1.5	$2.1x10^{-2}$	0.26
miR-335-5p	0.73	1.5	-1.80	-4.50	6.5	$2.5x10^{-2}$	0.28
miR-146a-5p	0.43	0.88	-2.30	-0.71	-3.0	$3.1x10^{-2}$	0.30
miR-365a-3p	0.43	0.36	0.82	0.07	1.7	$3.8x10^{-2}$	0.30
miR-92a-3p	0.47	0.43	0.95	0.11	1.8	$3.8x10^{-2}$	0.30

3.4.9 *Extracellular miRNAs secreted by human adipocytes, validation by RT qPCR analysis*

Data obtained by RT qPCR were analysed using multiple comparison two-way ANOVA (Figure 39). Expression of secreted miR-138, miR-10b miR-365 and miR-378 increased in differentiated adipocytes versus preadipocytes. MiR-138 and miR-10b were overexpressed in media from differentiated white adipocytes compared to brown adipocytes. On the contrary, miR-378 and miR-365 were more highly expressed in media from differentiated brown adipocytes. Secreted miR-196a and miR-424 levels increased in differentiating white adipocytes and decreased in differentiated brown adipocytes compared to brown preadipocytes. Both miRNAs were more highly expressed in media from differentiated white adipocytes compared to differentiated brown adipocytes. MiR-103 secretion was downregulated in differentiated adipocytes compared to preadipocytes and was slightly higher in differentiated white adipocytes compared to differentiated brown. These data confirmed the results observed in the miRNA PCR human Panel. Most of the results shown in this analysis were also consistent with that observed for miRNA orthologues in mouse experiments. A more detailed comparison among data from human and mouse adipocytes is discussed in paragraph 14.

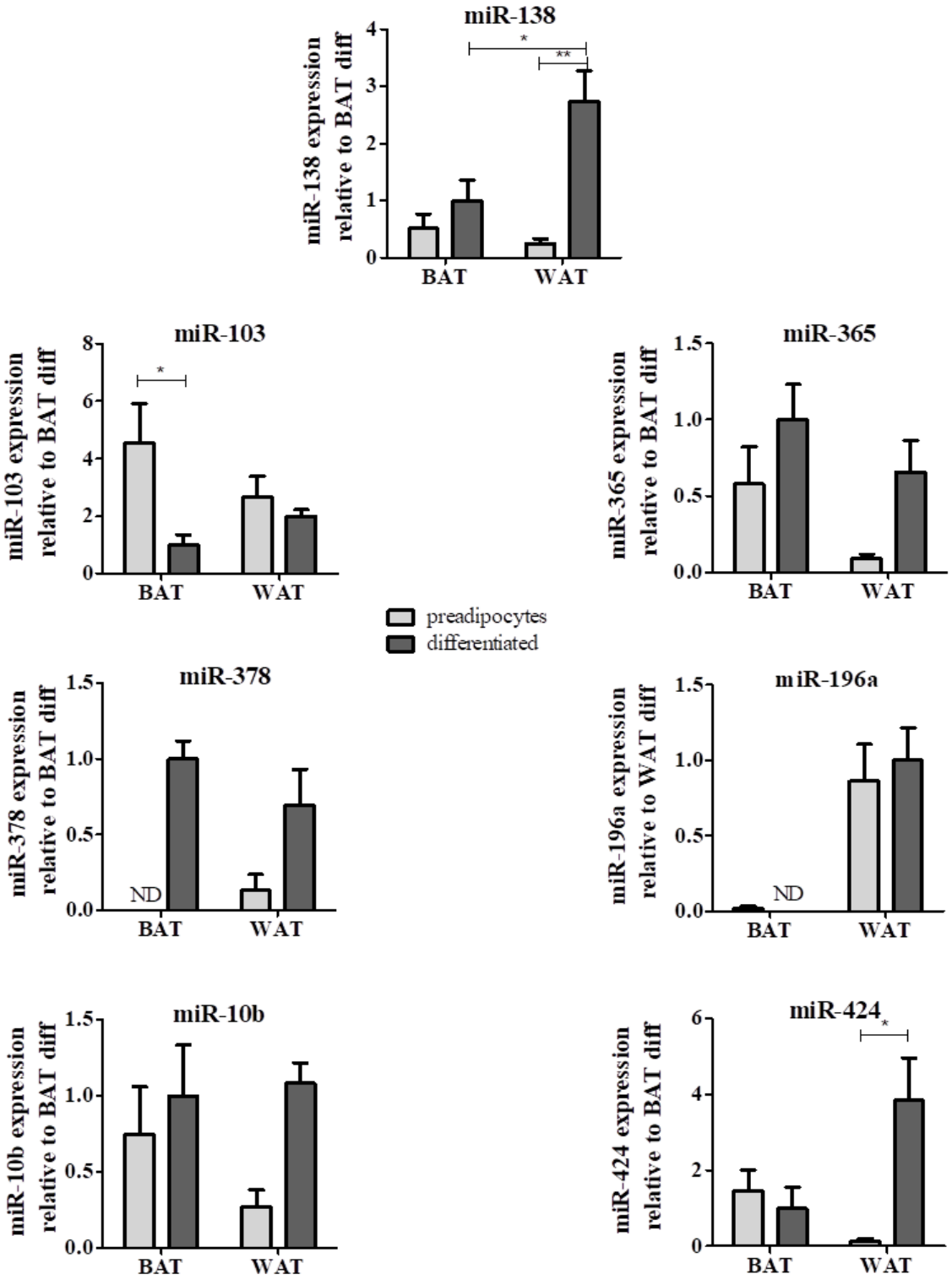

Figure 39 MiRNA expresssion in media samples from human undifferentiated and differentiated adipocytes.

Graphs show miRNA expression in serum-free media from subcutaneous white and supraclavicular brown preadipocytes and mature adipocytes, seeded all at the same cellular density. Expression levels were normalised to Unisp6 spiked-in at RNA isolation stage. Bars represent the fold changes means of triplicates ± SEM compared to BAT differentiated. ND means non-detectable. * indicates $p \leq 0.05$, and ** $p \leq 0.01$ according to multiple comparisons in two-way ANOVA test.

3.4.10 *Effect of Isoproterenol treatment on miRNAs secreted by human adipocytes*

To understand whether miRNA secretion is affected by the cold-regulated signalling pathway, we mimicked adrenergic stimulation by administrating Isoproterenol to differentiated adipocytes and measured miRNA expression in the conditioned media. The same number ($5x10^5$) of differentiated brown and white adipocytes were seeded into each well of a 12-well plate and incubated for 24 hours in serum-free media in the presence of Isoproterenol (10 μM) or DMSO (vehicle) for controls. Media samples were collected and processed for RT-qPCR assay and data was analysed using Student's t-test. As shown in figure 40, miR-103 and miR-365 were slightly upregulated in media from Iso-treated samples, while, miR-424 levels of expression were reduced. MiR-196a was only detectable in media from white adipocytes and its level of expression was moderately reduced upon Isoproterenol administration. Extracellular miR-378, mir-138 and miR-10b were downregulated in brown and upregulated in white adipocytes treated with Isoproterenol compared to controls. However, only upregulation of miR-378 in white adipocytes treated with Isoproterenol was statistically significant.

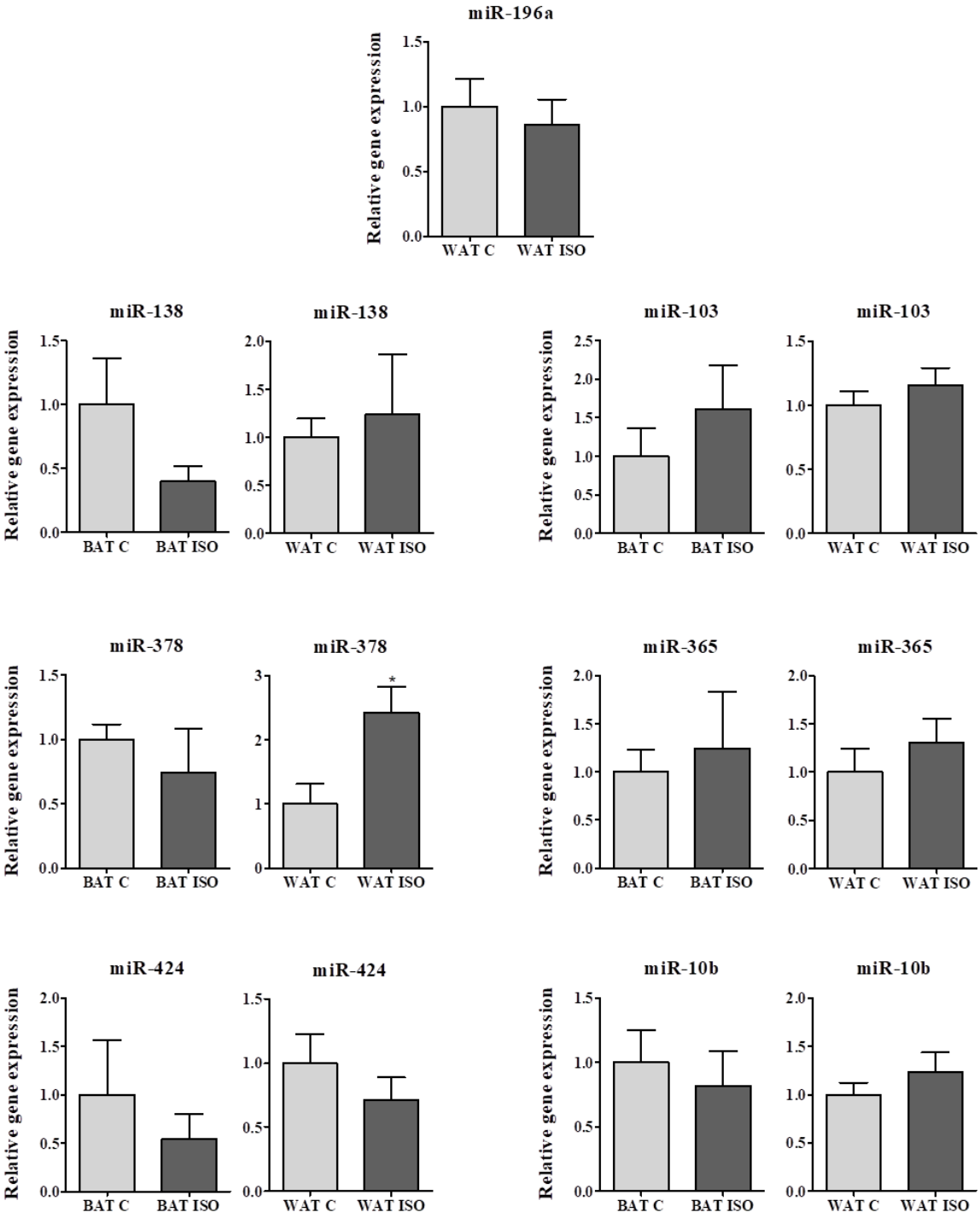

Figure 40 MiRNAs expression in media samples from differentiated human adipose cell lines upon Isoproterenol treatment.

Graphs show miRNA expression in serum-free media from supraclavicular brown (BAT) and subcutaneous white (WAT) mature adipocytes untreated (C) or treated with Isoproterenol (ISO) for 24 hours. The same number of differentiated cells were seeded for each biological triplicate. Expression levels were normalised to Unisp6 spiked-in at the RNA isolation stage. Bars represent the fold changes means of the triplicates ± SEM compared to brown or white controls (BAT C and WAT C). * indicates $p \leq 0.05$ according to Student's t-test.

3.4.11 *Intracellular miRNA expression in human adipocytes*

Human undifferentiated and differentiated brown and white adipocytes were harvested and analysed for intracellular miRNA expression by RT-qPCR. Significance was assessed by performing a two-way ANOVA test. All the miRNAs were upregulated in differentiated adipocytes compared to undifferentiated cells and in mature white adipocytes compared to differentiated brown adipocytes. Only miR-196a was not detectable in brown adipocytes.

As also observed in mouse experiments, intracellular and extracellular patterns of miRNA expression did not always go in parallel. This was particularly evident for miR-103, which secretion was downregulated in differentiated cells versus preadipocytes (figure 39), while, its intracellular abundance was upregulated in differentiated adipocytes compared to pre-adipocytes (figure 41). Extracellular and intracellular levels of miR-424 had a similar trend of expression in white adipocytes but opposite in brown adipocytes.

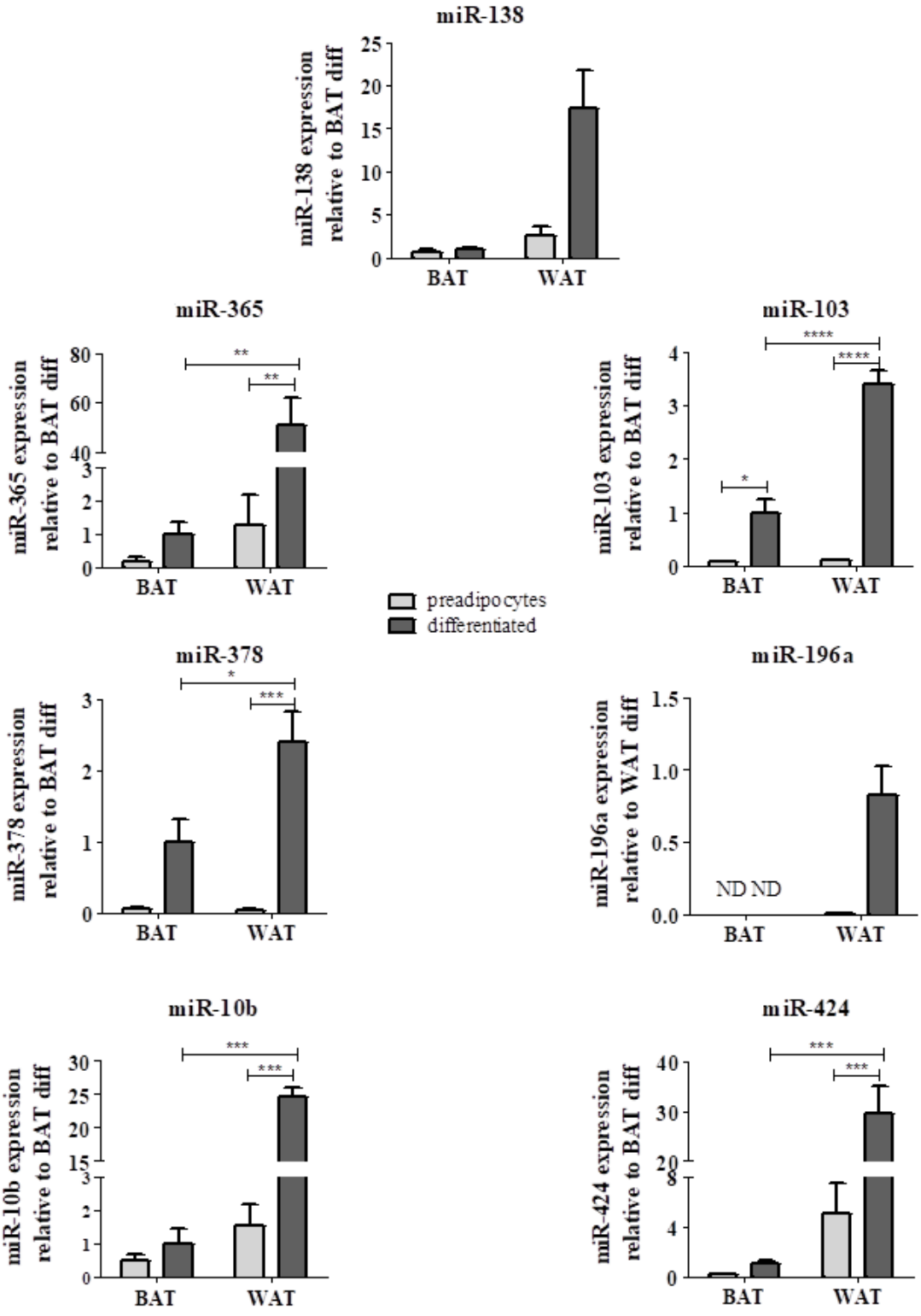

Figure 41 Intracellular miRNA expresssion in human dipocytes.
Graphs show miRNA expression in differentiated and undifferentiated supraclavicular brown and subcutaneous white adipocytes. Expression levels were normalised to Unisp6 spiked-in at the reverse transcription stage. Bars represent the fold change means of triplicates ± SEM compared to BAT differentiated. ND indicates not detectable. Significance is indicated with * for $p \leq 0.05$ ** for $p \leq 0.01$, *** for $p \leq 0.001$ and **** for $p \leq 0.0001$ according to multiple comparisons in two-way ANOVA analysis.

3.4.12 *Effect of Isoproterenol on intracellular miRNA expression in adipocytes after Isoproterenol treatment.*

Differentiated white and brown adipocytes were treated for 5 hours with Isoproterenol (10 μM) or DMSO (vehicle) for control wells. RNA was isolated from cells and processed for intracellular miRNA expression through RT-qPCR analysis. Isoproterenol induced a significant increase of miR-10b and miR-424 expression in brown adipocytes and a decrease in white adipocytes (figure 42). The same trend of expression was observed for miR-365, miR-138 and miR-378 even though the differences in miRNA expression between Iso-treated and control samples were negligible for miR-138 in brown adipocytes and miR-378 and miR-424 in white adipocytes.

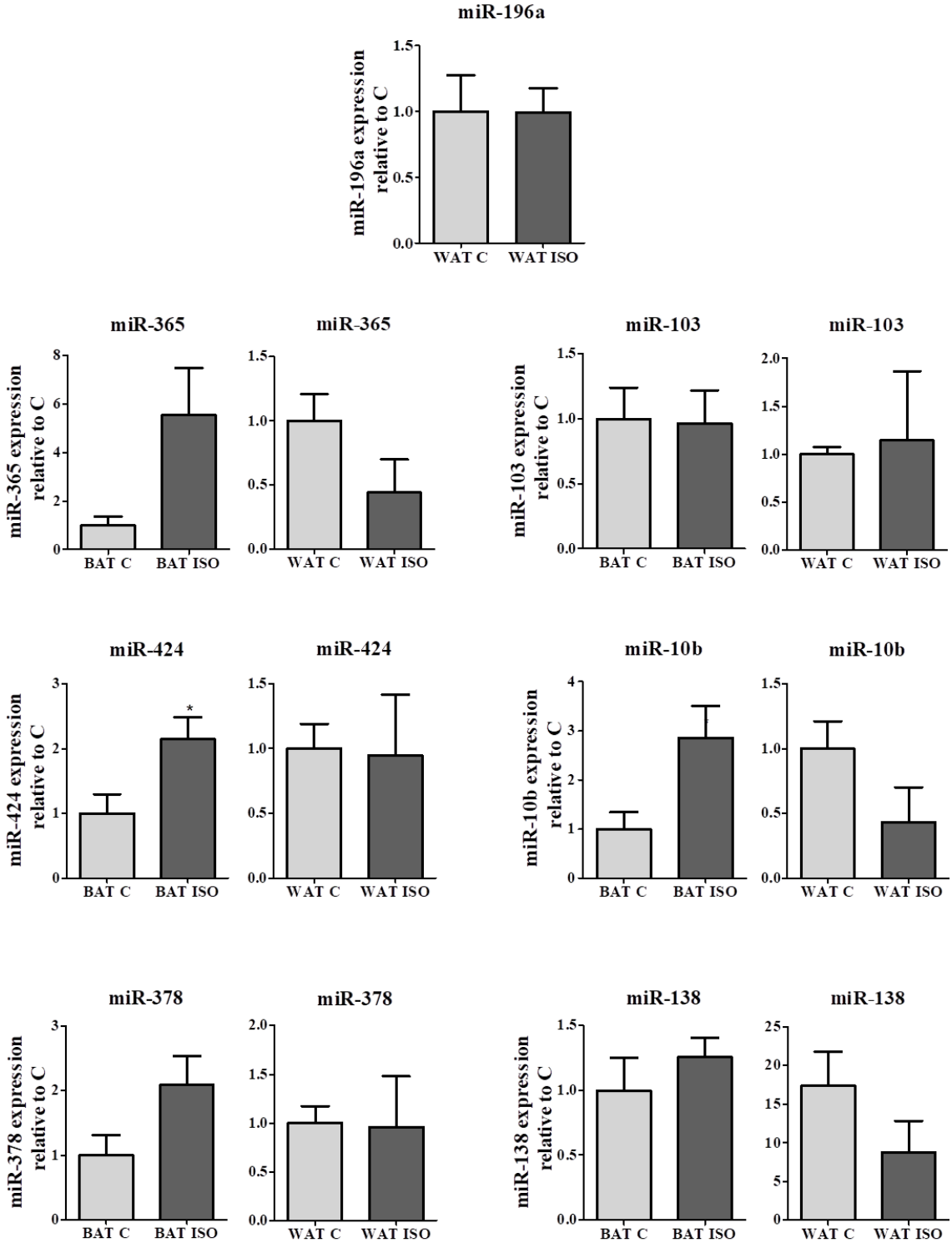

Figure 42 Effect of ß-adrenergic activation on intracellular miRNA expression in human adipose cell lines.

Differentiated adipocytes were treated for 6 hours with Isoproterenol (10µM). Graphs show miRNA expression in untreated (C) and Iso-treated (ISO) supraclavicular brown and subcutaneous white adipocytes. MiRNA levels were normalised to Unisp6 spiked-in at reverse transcription stage. Bars represent fold change means ± SEM of the biological triplicates compared to the controls BAT C or WAT C. Significance is indicated with * for $p \leq 0.05$ according to Student's t-test.

3.4.13 *Summary and overview*

In the following tables are summarised the data obtained by RT qPCR analysis of the extracellular (tables 14, 16) and intracellular (tables 15, 17) miRNA regulation across the different adipose models, both at basal conditions (tables 14 and 15) and upon ß-adrenergic stimulation (16 and 17). MiR-138 was included in the tables even though it was only tested in human adipocytes. Up (↑) and (↓) down arrows indicate miRNA upregulation and downregulation respectively, in differentiated cells versus preadipocytes (Diff vs undiff columns, BAT and WAT sub-columns) or in CL/ISO-treated cells versus control (CL vs C/ISO vs C, BAT and WAT sub-columns). For Brown (B) versus White (W) comparisons in undifferentiated and differentiated cells, B > W means that miRNA was overexpressed in brown adipocytes compared to white and vice versa. Significance is specified by * for p value ≤ 0.05, ^{2*} for $p \leq 0.01$, ^{3*} for $p \leq 0.001$ and ^{4*} for $p \leq 0.0001$. If a miRNA was undetectable in both the terms of comparison it is indicated as non-detectable (nd), while, if it was undetectable only in one on the two terms, it is indicated by the presence of the hash mark (#). Very similar level of expression is indicated by the symbol ~, assigned when the difference of the relative expression of the two comparative terms was between -0.05 and 0.05.

Intracellular quantification of the miRNAs was tested in order to verify whether the level of secretion of each miRNA could be a mere consequence of the intracellular level of expression. By observing the tables 14 and 15 it is easy to notice that intracellular and extracellular pattern of miRNA expression did not always go in parallel, as described more in details in the previous sections. This suggests that miRNA secretion is not a simply passive process but rather a controlled mechanism. Perhaps cells could use secretion to reduce intracellular level of a specific miRNA and simultaneously communicate with neighbouring cells.

The most consistent results across the adipose models were observed for extracellular miR-378a and miR-196a.

Intracellular and extracellular miR-378a was consistently upregulated in differentiated adipocytes versus preadipocytes. In differentiated cells, its extracellular levels of expression were always greater in brown adipocytes compared to white, while, intracellular levels were consistently higher in white adipocytes. In explants, both intracellular and extracellular miR-378 levels of expression were greater in BAT

compared to WAT. CL/ISO treatment increased intracellular miR-378 in all samples excluding human and mouse white adipose cell lines, on which it had no effect. Also extracellular miR-378 was consistently upregulated by the ß-adrenergic treatment, even if, in primary white adipocytes and human brown adipocytes it was slightly downregulated.

Both intracellular and extracellular miR-196a was consistently overexpressed in differentiated white adipocytes/WAT explants compared to differentiated brown adipocytes/BAT explants. It was upregulated in differentiated white adipocytes compared to preadipocytes, while, when detectable, it was downregulated in differentiated brown adipocytes versus undifferentiated. Interestingly, CL/ISO treatment inhibited miR-196a secretion in white and increased it in brown adipocytes. Intracellular miR-196a, when detectable, was induced by the treatment in all cells, human excluded, in which no differences were observed compared to control.

Extracellular miR-365 was upregulated in differentiated cells versus preadipocytes and overexpressed in brown adipocytes/explant compared to white, with the exception of primary cells. In contrast, its intracellular level of expression was consistently higher in white adipocytes compared to brown adipocytes but not in WAT compared to BAT explants. Intracellular and extracellular levels of expression of miR-365, when detectable, were increased upon ß-adrenergic stimulation, except for secreted miR-365 in primary white adipocytes and intracellular miR-365 in white human cell lines. In the first case, CL did not have any effect on miR-365 expression. In human white adipocytes intracellular miR-365 was slightly lower expressed upon ISO treatment compared to control.

Regulation of intracellular miR-103 was consistent across the adipose systems but not its secretion. Also the results obtained for all the remaining miRNAs were variable These were: miR-378a, miR-196a. MiR-138 was included as well as it was the only miRNA differentially secreted between human brown and white adipocytes. As mentioned before, these miRNAs have been found involved in adipogenesis, but their extracellular function is still largely unexplored in the cross talk between the adipose tissue and other organs.

By using miRNATap package (Bioconductor) and setting 2 as minimum source we obtained a list of the potential targets of miR-378a-3p, miR-196a-5p and miR-138-5p

(table 18). Among the potential miR-378 targets that could be most relevant for adipose tissue biology were VEGFA and SULF1 (sulfatase 1) for their involvement in angiogenesis and receptor/ligand binding mediated by heparan sulfate proteoglycans (HSP) respectively. The most interesting targets of miR-196a-5p were HIF1α which is involved in fibrosis of adipose tissue in obesity induced hypoxia, ADAM10 that has an important role in the extracellular matrix, TLR4 and NF-kB inhibitor alpha (IKBA) which are involved in inflammation and consequent impairment of insulin sensitivity in HFD – induced obesity. For the same reasons SOCS3, interleukin-6 receptor (IL6R) and interleukin-1 receptor antagonist (IL1RA) were selected among the potential targets of miR-138-5p. All these targets could be considered for future investigations on the role of the selected miRNAs secreted by adipocytes in the cross talk between adipose tissue and distal cells.

Regulation of extracellular miRNAs in mouse and human adipose models

Table 13 Regulation of extracellular miRNAs in mouse and human adipose models

miRName	Expl	Mouse cell lines				Mouse primaries				Human cell lines			
	Brown vs white	Diff vs undiff		Brown vs white		Diff vs undiff		Brown vs white		Diff vs undiff		Brown vs white	
		BAT	WAT	Undiff	Diff	BAT	WAT	Undiff	Diff	BAT	WAT	Undiff	Diff
miR-322/424	B>W*	↑2*	↑	B>W	B>W2*	↑3*	~	~	B>W3*	↓	↑*	B>W	W>B
miR-10b	W>B2*	↑3*	nd	#B>W	#B>W4*	↑	↑	B>W	~	↑	↑	B>W	W>B
miR-103	nd	#↑*	↓	#W>B	B>W2*	nd	nd	nd	nd	↓*	↓	B>W	W>B
miR-365	B>W2*	#↑	nd	nd	#B>W	#↑	#↑	# ~	W>B	↑	↑	B>W	B>W
mi R-378	B>W*	↑2*	↑	~	B>W	↑*	↑	~	B>W	#↑	↑	#W>B	B>W
miR-196a	#W>B	↓	↑2*	B>W	W>B2*	nd	↑2*	#W>B	#W>B	#↓	↑	W>B	#W>B
miR-138	-	-	-	-	-	-	-	-	-	↑	↑2*	B>W	W>B*

Table 14 Regulation of intracellular miRNAs in mouse and human adipose models

miRName	Expl	Mouse cell lines				Mouse primaries				Human cell lines			
	Brown vs white	Diff vs undiff		Brown vs white		Diff vs undiff		Brown vs white		Diff vs undiff		Brown vs white	
		BAT	WAT	Undiff	Diff	BAT	WAT	Undiff	Diff	BAT	WAT	Undiff	Diff
miR-322/424	B>W*	↓	↓	B>W	B>W	#↑	↓	#W>B	W>B	↑	↑3*	W>B	W>B3*
miR-10b	B>W	↑2*	nd	#B>W	B>W*	↑	~	W>B	~	↑	↑3*	W>B	W>B3*
miR-103	W>B	↑	↑	W>B	W>B	↑	↑	W>B	W>B	↑*	↑4*	~	W>B4*
miR-365	B>W	#↑	↑*	#W>B	W>B2*	#↑	↑	#W>B	W>B	↑	↑2*	W>B	W>B2*
miR-378	B>W	#↑	↑	#W>B	W>B	↑	↑	W>B	W>B	↑	↑3*	~	W>B*
miR-196a	W>B	↓*	↑	W>B	W>B	nd	↑	#W>B	#W>B	nd	↑	#W>B	#W>B
miR-138	-	-	-	-	-	-	-	-	-	↓	↑	W>B	W>B

Table 15 Effect of CL/ISO treatment on miRNAs secreted by human and mouse adipocytes

miRName	Mouse cell lines CL vs C		Mouse primaries CL vs C		Human cell lines ISO vs C	
	BAT	WAT	BAT	WAT	BAT	WAT
miR-322/424	↑*	↓*	↓²*	↑	↓	↓
miR-10b	↓	nd	↑	↓	↓	↑
miR-103	↓²*	↑	nd	nd	↑	↑
miR-365	↑	nd	↑	~	↑	↑
miR-378	↑	↑	↑	↓	↓	↑*
miR-196a	↑²*	↓²*	nd	↓²*	nd	↓
miR-138	-	-	-	-	↓	↑

Table 16 **Effect of CL/ISO treatment on intracellular miRNAs in human and mouse adipocytes**

miRName	Mouse cell lines		Mouse primaries		Human cell lines	
	BAT	WAT	BAT	WAT	BAT	WAT
miR-322/424	↓	↓	↑*	↑²*	↑*	↓
miR-10b	↑	#↑	↑²*	↑²*	↑*	↓
miR-103	↑*	↓	~	~	~	↑
miR-365	↑²*	↑	↑	↑*	↑	↓
miR-378	↑	~	↑²*	↑³*	↑	~
miR-196a	↑	↑	nd	↑²*	nd	~
miR-138	-	-	-	-	↑	↓

Table 17 Potential targets of selected miRNAs secreted by adipocytes

miRname	Potential target	function of target
miR-378a-3p	VEGFA	Angiogenesis
	SULF1	Receptor/ligand binding via HSP
miR-196a-5p	HIF-1α	Adipose tissue fibrosis
	ADAM10	ECM remodelling
	TLR4	Inflammation/insulin resistance
	IKBA	
miR-138-5p	SOCS3	
	IL6R	
	IL1RA	

3.5 Discussion

Brown and white preadipocytes present differences in miRNA and gene expression and the process of differentiation into mature adipocytes is characterised by a further alteration of the transcriptome. We showed for the first time that undifferentiated and differentiated brown and white adipocytes present differential profiles of secreted miRNAs, supporting the hypothesis that these molecules can mediate the cross talk between the adipose tissues and distal cells. Precisely, 45 miRNAs were differentially secreted between undifferentiated brown (UB) and undifferentiated white (UW), 118 in UW versus differentiated white (DW), 123 in UB versus differentiated brown (DB) and 12 between DB and DW (table 8). This highlights that there are significant differences among the types of adipocytes, especially between undifferentiated and differentiated adipocytes, as they presented a high number of differentially secreted miRNAs. Some of these miRNAs were selected for validation and further analysis in different adipocyte cell models. MiR-322/424-5p, miR-365-5p and miR-378a-3p were selected because they were differentially secreted between undifferentiated and differentiated adipocytes, while, miR-10b and miR-196a because they were differentially secreted between brown and white adipocytes. MiR-103 was added to the list as it was differentially secreted between preadipocytes and differentiated adipocytes and previously reported to regulate insulin sensitivity [347].

The characterization of the adipocyte systems used in this study allowed us to conclude that, the systems were good models of brown and white adipocytes and BAT and WAT. Indeed, explants showed the classical histology of BAT and WAT. BAT and brown adipocytes showed a higher UCP1 expression compared to WAT and white adipocytes respectively. Moreover, the cells were able to respond to ß-adrenergic stimuli by further raising the levels of UCP1 expression. Additionally, the functional assay performed on human adipose cell lines, characterised for the first time, confirmed that the brown adipocytes present a higher basal oxygen consumption compared to white adipocytes.

3.5.1 *Gene expression of miRNA processing machinery during human adipocyte differentiation*

Hypothesising that the switch from undifferentiated to mature status would require an increase in miRNA production to promote this process, the expression of Ago2, Dicer1 and GW182 genes was analysed in mouse and human adipocytes. Overall, the changes in expression of these genes between undifferentiated and mature adipocytes, even if statistically significant in some cases, were not as marked as expected. This suggests that miRNA production for maintaining the undifferentiated status is as much important as for inducing and maintaining maturation. Moreover, if these genes were involved in the unique function of miRNA maturation, their level of expression would be expected to vary proportionally during differentiation. Conversely, this did not happen for all the genes in the different systems. In particular, Ago2 in human WAT significantly decreased, while DICER1 and GW182 gradually and significantly increased during differentiation. In a previous study on ADMSC, Ago2 was found to translocate in the nucleus and bind to specific regions of functional genes such as of selenoprotein N1 (SEPN1), miR10b, and miR23b, regulating cell survival upon excessive ROS production [355]. This supports that fact the genes involved in miRNA biosynthesis and maturation, could be involved in other processes not strictly related to miRNA processing. Moreover, these additional functions could be different in mouse and humans as the trend in gene expression was slightly different between the adipocytes of the two species.

3.5.2 *miRNAs in different adipose models*

The analysis in parallel of the intracellular miRNA level allowed us to conclude that miRNA secretion is not a passive process but actively regulated, as extracellular and intracellular miRNA levels were not proportional. The use of adipose explants in this analysis highlighted that the pattern of intracellular and extracellular miRNA expression of BAT and WAT can show differences to that of isolated adipocytes, as cell types other than adipocytes contribute to miRNA secretion. However, it has to be considered that, in explants there is no longer blood circulation. Even though we tried to overcome this problem by cutting the tissues in small pieces (~2mm width), miRNAs could be retained in the centre of the tissue and only partially released in the media. Additionally, in explants, the different cellular components absent in isolated adipocyte cell cultures, are

likely to uptake miRNAs from the media contributing to differential concentration of circulating miRNAs.

The analysis across adipose models allowed as to identify miRNAs that display a pattern of expression in media consistent across adipose models, suggesting that their function is conserved in different species and therefore very important for the correct functioning of adipose tissue. These miRNAs were miR-196a-5p and miR-378a-3p. However, this does not imply that the remaining miRNAs tested do not play important roles in adipogenesis, adipocyte biology and in the cross talk between the adipose tissue and distal cells.

The inconsistency of miRNA expression across the different adipose models might be due to various reasons besides the intrinsic different nature of the different adipose models. Indeed, even though all the experiments were performed under the most similar controlled conditions as possible it is not possible to eliminate all the variables affecting the systems. Primarily, it has to be borne in mind that the protocols for inducing adipocyte differentiation differ in composition and the concentration of the compounds, as they are optimised specifically for each cell type. Compounds and their concentrations can have a strong impact on miRNA regulation and functioning. For example, it was observed that regulation of adipocyte differentiation by miR-378 via phosphodiesterase 1B (PED1B) was masked by the use of IBMX in the differentiation media [282]. Additionally, miRNA expression can be influenced by cellular senescence and related molecular events. The same passage number might not correspond to the same grade of senescence between human and mouse cell lines. Despite that the cell lines were all used at early passages (12-26) their level of senescence is higher than primaries (used maximum at passage number 2). An example of an age-related miRNA is miR-10b, the expression of which was demonstrated to be upregulated during human foreskin fibroblast (HEK) senescence [356]. Therefore, we focussed on miR-196a-5p and miR-378a-3p for target prediction and consideration of their potential impact on function in adipocytes, as their extracellular expression was consistent across the adipose models in spite of the variables potentially affecting miRNA expression.

3.5.2.1 *MiR-378a-3p*

Our results, in accordance with the literature, showed that intracellular miR-378a-3p was upregulated during adipocyte differentiation (figures 20, 26, 41 and table 15) [270, 282, 357]. Indeed, miR-378a-3p was found to promote adipogenesis [357]. Interestingly, a study documented that ectopic expression of miR-378a-3p, in mice, promotes enlargement of interscapular BAT but not of WAT. In vitro experiments revealed that miR-378a-3p promotes differentiation of pre-existing brown pre-adipocytes by targeting Phosphodiesterase 1B (PDE1B) [282], an enzyme that controls cAMP turnover [358]. The study pointed out that miR-378a-3p functions are likely to be tissue specific. As in our experiments, levels of miR-378a-3p were consistently greater in media from brown compared to white adipocytes, it is possible that this miRNA, besides promoting differentiation, is involved in the processes regulating BAT vascularization and ECM remodelling. Indeed, among its predicted targets there were VEGFA and Sulf1. BAT is a highly vascularized tissue and VEGFA involvement in BAT vascularization has been documented previously [302]. VEGFA expression is increased in differentiating immortalized brown adipocytes and induces cell proliferation of brown preadipocytes. In mice, neutralization of VEGFA by intravenous injection of an adenovirus expressing sFlt1 (a competitor of VEGFR that prevents VEGF signalling) provoked reduction of BAT vascularization density accompanied with tissue fibrosis, inflammation and adipocyte apoptosis. VEGFA was found to be regulated by multiple miRNAs amongst which there is miR-378a-5p, that originates from the opposite arm of miR-378a-3p. MiR-378a-5p alone induced downregulation of VEGFA, while, when in combination with miR-125, VEGFA expression was increased [359]. Therefore, miR-378a-3p might take part in this competition for VEGFA. Additionally, as previously mentioned, miR-378a-3p could participate to tissue remodelling by targeting Sulf1. This enzyme, by removing 6-O-sulfate groups from heparan sulfate hampers VEGF binding to the receptor inhibiting activation of the signal cascade [264, 360, 361]. Therefore, secreted miR-378a-3p could have a paracrine and autocrine function in regulating VEGF signalling, either by controlling sulf1 transcription in recipient endothelial cells or by directly targeting VEGFA in neighbour cells, enhancing or inhibiting vascularization depending on eventual competitors such as miR-378a-5p and miR-125. In a different study miR-378a-3p was found to prevent liver fibrosis by targeting Glioblastoma protein 3 (Gli3) in

activated hepatic stellate cells [362], supporting a role for miR-378a in shaping the extracellular matrix (ECM) and suggesting that adipose-derived circulating miR-378a-3p has a potential endocrine function.

3.5.2.2 *MiR-196a-5p*

As described in the introduction, miR-196a was found to promote a brown-like phenotype in white adipocyte progenitors by targeting the gene HOXC8 [302, 363-367] which is known to be overexpressed in white versus brown adipocytes [368, 369]. The authors speculated that miR-196a is not involved in brown adipogenesis of classical brown preadipocytes, as its levels did not vary during brown adipocyte differentiation. In accordance with their results, in our experiments, miR-196a expression was upregulated in differentiating white adipocytes even in the absence of browning stimuli and was not detectable or showed very low expression in differentiated brown adipocytes (figure 20, 26, 41 and table 15). This suggests that sustained level of miR-196a predispose the white adipocytes to acquire brown characteristics upon determined stimuli but, are also required for the activation of the white fat program independently of the brown-like features. Upon CL treatment, intracellular miR-196a, at least in mouse primary adipocytes, was significantly upregulated, suggesting involvement in activation of oxidative program upon ß-adrenergic stimuli in white adipocytes. Similar results were obtained in vivo and in vitro in Mori and colleagues' study upon acute CL treatment/cold exposure [302]. Interestingly, the levels of secretion (table 14) of this miRNA were proportional to the intracellular level of expression at basal condition (table15). In contrast, upon ß-adrenergic stimuli, intracellular miR-196a increased (table 17), while, extracellular levels were significantly reduced in white adipocytes (table 16). It is possible that at basal condition, miR-196a contributes to maintain the white differentiation status and excessive miR-196a is secreted in the extracellular environment to sustain the level of differentiation of surrounding adipocytes. Upon ß-adrenergic stimuli, secretion of miR-196a might be reduced in order to increase the intracellular levels of the miRNA and activate the brown program of already differentiated adipocytes, to provide a prompt response to the stimuli. Among the predicted targets of miR-196a there is HIF1a which may be important for the correct functioning of BAT. Indeed, BAT of transgenic mice expressing a dominant-negative form of HIF1α showed impaired

thermogenesis and energy expenditure and decreased angiogenesis [370]. The low levels of miR-196a observed in brown adipocytes may prevent HIF1α inhibition in BAT. In contrast, as previously described, HIF1α in white adipose tissue fails to trigger angiogenesis upon hypoxic stimuli and rather leads to fibrosis. In white adipocytes, where it is highly expressed, miR-196a, by inhibiting HIF-1α translation and therefore limiting the amount of the protein that can be in the active state during the hypoxic stimuli, could prevent fibrosis. Another predicted target of miR-196a is ADAM10. This metalloprotease is known to inhibit angiogenesis by modulating Notch signalling [136] and was found to be upregulated in obese mice and its silencing ameliorated insulin sensitivity [137]. A previous study showed that its deletion in endothelial cells causes defects in organ-specific vascular structures [371]. The effect of miR-196a secreted by white adipocytes on this enzyme in adipose-derived endothelial cells has not been explored and could provide additional information of the role of miR-196a in the white adipose tissue. This miRNA conferred resistance to obesity and improvement of glucose metabolism in mice [302]. TLR4 was a predicted target of miR-196a and its potential suppression induced by miR-196a could be one way through which this miR-196a protects against development of insulin resistance in obesity. However, also IKBA, was identified as a potential target of miR-196a. Therefore, whether miR-196a has a pro-inflammatory or anti-inflammatory affect in obesity via repressing IKBA or TLR4 expression respectively, should be addressed.

3.5.2.3 *MiR-138-5p*

Through the microRNA array performed on media samples from human adipocytes, we identified miR-138-5p as the unique miRNA significantly differentially secreted between brown and white adipocytes. This was probably due to the large variability observed among the brown adipose sample, which reflects the high heterogeneity of the brown human adipocytes The higher the variation and error mean, the lower are the possibilities to reach statistical significance when comparing with the white adipocytes. As previously discussed, miR-138 might inhibit white adipocytes differentiation into brown-like phenotype by targeting EID1. EID1 was found to inhibit muscle differentiation [372, 373] while its ablation in ADMSC inhibited preadipocyte differentiation [304]. Taking part in the regulation of the cell cycle the effect of EID1 on cell differentiation could vary depending on the cell type and on the stage of the

differentiation program. Therefore, at the early stages of differentiation the anti-differentiation activity of miR-138 via EID1 inhibition in adipocytes may be suppressed by downregulating miR-138 expression. Conversely, at the late stages of differentiation, re-increased levels of miR-138 in white adipocytes, in the absence of browning stimuli, could help the cells to maintain a low metabolic activity, classic of the white adipocytes. This is supported by the results obtained upon administration of Isoproterenol (figure 42). Indeed, even though statistical significance was not reached, upon ß-adrenergic stimulation miR-138 expression was reduced IN WAT, perhaps, to counteract its beige-inhibitory effect, hence permitting the activation of oxidative pathways. Isoproterenol had no particularly evident effect on miR-138 expression in brown adipocytes, and probably the very low abundance of miR-138 is insufficient to inhibit the brown fat program. However, it would be interesting to perform a time course to verify how miR-138 is expressed during differentiation of brown and white adipocytes. MiR-138 overexpression in hAMSC from obese compared to lean mothers could contribute to impair the differentiation of these cells into adipocytes able to activate an appropriated oxidative program when required, as often observed in obesity [12]. In our study, intracellular and extracellular pattern of miR-138 expression at basal condition went in parallel in both brown and white adipocytes, with miR-138 more highly expressed in and secreted by white adipocytes compared to brown adipocytes. Conversely, upon ß-adrenergic stimulation, intracellular and extracellular levels of miR-138 were negatively correlated. However, statistical significance was not reached. Interestingly, among the targets predicted for miR-138, there were genes involved in the process of inflammation and associated with insulin-resistance such as SOCS3 and Interleukin 6 receptor (IL6R). As described in the introduction, these mediators of inflammation in obesity impair insulin signalling pathway. Hence, cells that are targeted by insulin and express low levels of miR-138 may be more prone to develop insulin resistance in an inflammatory environment. Circulating miR-138 was reported to be expressed at lower levels in the serum from obese subjects compared to lean [309, 348], even though intracellular levels of miR-138 are likely to be elevated in adipocytes of obese subjects as showed by Nardelli, C., et al., [308]. Moreover, our study showed that in physiological conditions extracellular levels of miR-138 secreted by adipocytes are proportional to its intracellular levels. Therefore, it is possible that obesity affects

the ability of the adipocytes to secrete miR-138 levels sufficient to counteract inflammation and insulin resistance in peripheral tissues. Aaccording to this hypothesis, lower levels of circulating miR-138 should correspond to more severe insulin resistance. Conversely, in the same study, miR-138 was more highly expressed in peripheral blood from diabetic obese individuals compared to non-diabetic obese subjects. Another predicted target of mR-138 was Interleukin-1 receptor antagonist (IL1RA). This gene is translated into a protein that competes with IL-1α and IL-1ß for IL-1R and impeding their pro-inflammatory activity. IL-1 was found to inhibit GLUT4 translocation to the plasma membrane in response to insulin, by indirectly reducing IRS expression [374]. In a hypothetical scenario, in obese subjects, where a certain grade of inflammation is already present and activated by different factors, a decreased expression of circulating miR-138 could sustain inflammation, due to reduced ability to inhibit IL-6 signalling pathway. At the same time, low levels of circulating miR-138 may prevent inhibition of IL-RA resulting in a less severe insulin resistance. Nevertheless, further studies are required to clarify different points. Firstly, it would be interesting to verify how intracellular and extracellular miR-138 expression varies between adipocytes from different fat depots in obesity and physiological conditions. Indeed, data obtained from the analysis of serum samples do not allow determination of which is the major cell or tissue type secreting the miRNA of interest. Finally, to assess whether mR-138 could effectively induce inhibition of the predicted targets and determine its effect on the cells that are targeted by insulin and that can potentially take up circulating miR-138.

3.5.3 *Effect of ß-adrenergic stimuli on miRNA secretion*

Stimulation of ß-adrenergic receptors in adipocytes triggers a cascade that induces activation of the beta oxidative program and transcription of several factors that contribute to sustain the high metabolic activity of the cell over a prolonged period of time. As miRNAs regulate gene expression we sought to verify whether ß-adrenergic stimulation affects miRNA expression and secretion. The change of intracellular levels of miR-322/424 and miR-103 were very variable across the adipose models upon ß-adrenergic stimuli, even between mouse primary cells and mouse cell lines. The remaining miRNAs, when detectable, were generally induced after ß-adrenergic stimuli in all cells except for human white adipocytes where Isoproterenol, either reduced

miRNA levels (miR-10b, miR-365 and miR-138) or did not affect miRNA expression compared to untreated samples (miR-196a). The significant increased expression of miR-10b in white adipocytes upon CL treatment, suggests potential involvement of this miRNA in mouse white adipocyte transdifferentiation into brite adipocytes. The fact that miR-10b was not induced in human white adipocytes by ß-Adrenergic stimuli, suggests that miRNAs involved in the browning of the white adipose process could be different between mouse and humans. In general, the great variability of miRNA release upon ß-adrenergic stimuli across the different adipose models and even between mouse primaries and mouse cell lines, suggests that the changes in extracellular miRNA levels observed are not a direct effect of ß-adrenergic receptor activation. Conversely, extracellular miR-196a was consistently downregulated in white adipocytes. Previous in vivo studies showed that miR-378 and some other miRNAs were not significantly affected by acute exposure to cold [282], while miR-196a was increased in BAT and WAT of mice treated for 5 hours with CL. All together these data suggest that, in general, acute ß-adrenergic stimulation partially affects miRNA intracellular expression, while its effect on miRNA secretion could represent the results of secondary factors occurring upon the treatment. The only exception in this study is represented by miR-196a for which both extracellular and intracellular levels of expression were consistently affected by ß-adrenergic stimuli. Perhaps, greater effects for all miRNAs could be observed after a more prolonged stimulation which in white adipocytes would induce browning and in brown adipocytes would facilitate the cellular machinery to maintain high levels of ß-oxidation.

Chapter 4 – Results
MiRNA secretion by adipocytes into vesicle and vesicle-free systems

4.1 MiRNAs are depleted from conditioned media by ultracentrifugation and are detected in the ultracentrifuged pellet

MiRNAs have been found in several biological fluids incorporated into vesicles [188] and/or associated with vesicle-free systems such as Ago2 protein [375]. Ultracentrifugation is a technique widely employed to isolate vesicles from various types of fluidic sources [376]. To understand whether miRNAs secreted by adipocytes are encapsulated into vesicles and could be depleted from media by ultracentrifugation, miRNA content in serum-free conditioned media from differentiated brown adipocytes was analysed before and after ultracentrifugation at 120,000xg for 2 hours. The same number of differentiated cells was seeded for each biological replicate and kept in serum free media for 5 hours. Conditioned media was collected and processed in parallel with unconditioned media for miRNA analysis by Real Time qPCR. Figure 43 shows miRNA abundance ($2^{-\Delta Ct}$ values) before and after vesicle depletion from the media. All miRNAs investigated were detected at lower levels in the supernatant after vesicle isolation. In particular, ultracentrifugation was able to significantly deplete 44.6% of miR-196a, 41.85% of miR-322 and 19.5% of miR-378 from the media. As expected no miRNAs were detectable in unconditioned media.

The pellet obtained by the ultracentrifugation was resuspended in 2.5 ml of unconditioned media and tested for miRNA content as well. As reported in figure 44 all miRNAs were present in the pellet from conditioned media, at relatively high level, while, no miRNAs were detectable in the pellet from unconditioned media. Because the pellet is obtained by concentrating the vesicles contained in the media, miRNA levels in the two types of samples are not directly comparable. However, miRNA presence in the pellet and depletion from supernatant suggest that all the microRNAs tested are at least partially encapsulated into vesicles and in part associated with vesicle-free systems.

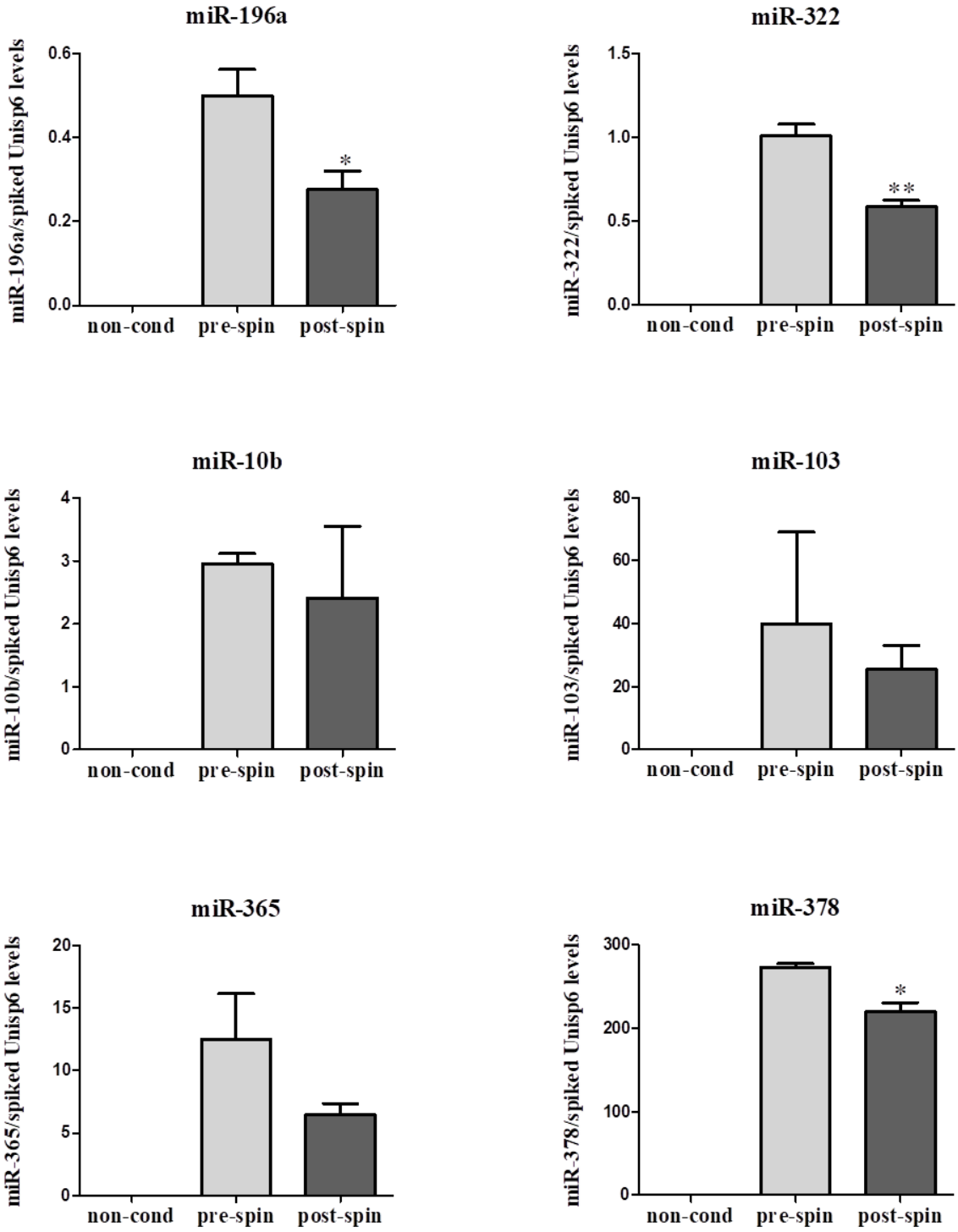

Figure 43 MiRNAs are depleted from conditioned media by ultracentrifugation.
The graphs show miRNA abundance before and after ultracentrifugation of serum free unconditioned and conditioned media samples from differentiated brown adipocytes. The same number of cells was seeded for each biological replicate. MiRNA levels were normalized to Unisp6 spiked in just prior to RNA extraction. Bars express the miRNA mean ± SEM of $2^{-\Delta Ct}$ values of the biological triplicates. Student's t-test was used to assess significance with cut-off of p-value<0.05(*). ** indicates p<0.01.

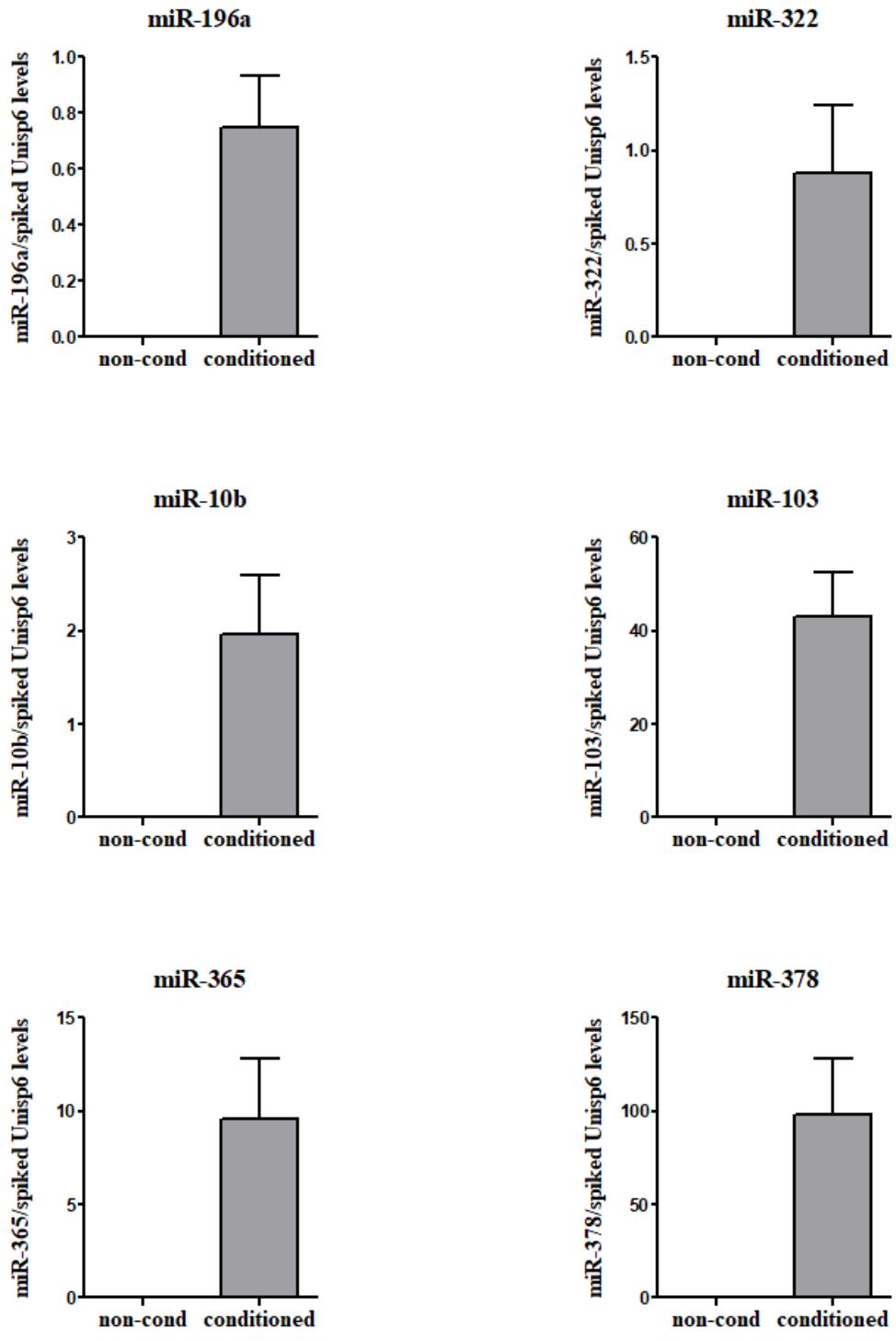

Figure 44 MiRNAs detected in the pellet of ultracentrifuged media.
The graphs show $2^{-\Delta Ct}$ values (mean of biological triplicates) of miRNAs in pellets obtained from unconditioned and conditioned media incubated with brown adipocyte for 5 hours. MiRNA levels were normalized to Unisp6 spiked in immediately prior to RNA extraction.

4.1.1 *ß3-adrenergic activation affects the level of miRNA depletion in ultracentrifuged conditioned media*

To investigate whether ß3-adrenergic activation has an effect on miRNA secretion via incorporation into vesicles or in association with vesicle-free systems, miRNA content in serum-free media from differentiated brown adipocytes treated with CL (10 μM) for 5 hours was analysed before and after ultracentrifugation. The percentage of miRNA depletion observed in untreated and CL treated samples are summarized in table 19. The first column of the table shows increment (↑) or decrement (↓) of total miRNA in media from BAT treated with CL compared to untreated from previous experiment (paragraph 4.1). Consistent with previous results, all the miRNAs were detected in the pellet (figure 46) and at least partially depleted from the media (figure 45). Little variations in the percentage of miRNA depletion were observed between CL-treated and untreated samples for miR-196a, miR-322 and miR-103. In contrast, miR-378 depletion from 19.5% in untreated samples became 42.83% in CL-treated, similar to that observed for miR-10b. In untreated brown adipocytes, 48% of miR-365 was depleted after centrifugation while its depletion in treated cells was only of 9.9%. These results suggest that CL favours miR-378 and miR-10b secretion via incorporation into vesicles while it promotes miR-365 release in association with vesicle-free systems.

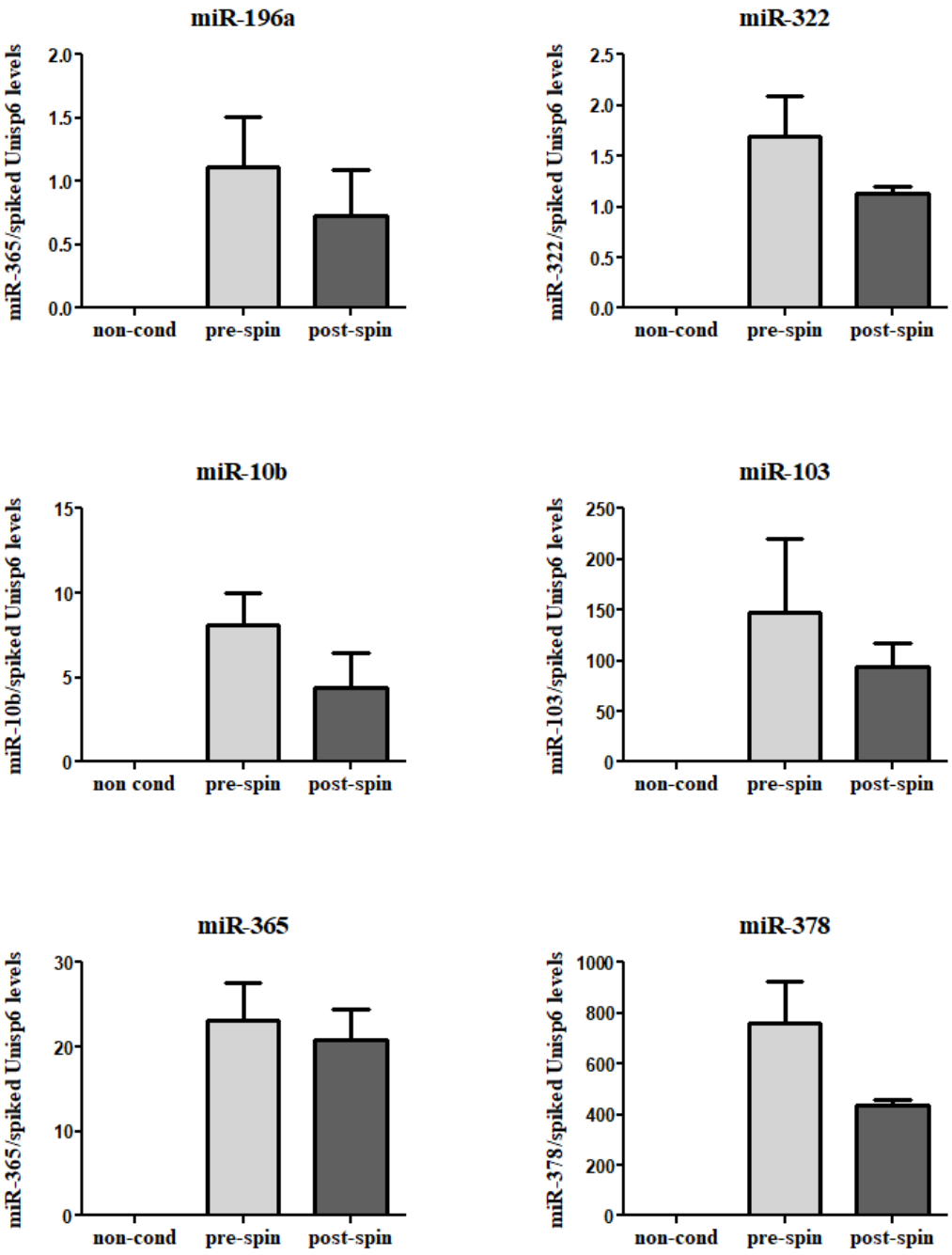

Figure 45 Treatment with CL affects the level of miRNA depletion in ultracentrifuged conditioned media

The graphs show miRNA abundance before and after ultracentrifugation of serum free unconditioned and conditioned media samples from differentiated interscapular brown adipocytes treated for 5 hours with CL (10μM). The same number of cells were seeded for each biological replicate. MiRNA levels were normalized to Unisp6 spiked in immediately prior to RNA extraction. Bars express the miRNA mean ± SEM of $2^{-\Delta Ct}$ values of the biological triplicates. Student's t-test was used to assess significance with cut-off of p-value<0.05(*).

Table 18 Percentage of miRNA depletion after ultracentrifugation of media from differentiated brown adipocytes untreated and treated with CL.

Tot miRNA CLvsC	miRName	UNTREATED		CL TREATED	
		% depletion	SEM	% depletion	SEM
↑2*	**miR-196a**	44.60	± 8.70	34.37	± 48.9
↓	**miR-10b**	18.60	± 38.70	45.74	± 35.0
↓2*	**miR-103**	36.23	± 75.39	40.41	± 25.5
↑*	**miR-322**	41.85	± 8.00	32.95	± 23.9
↑	**miR-378**	19.50	± 4.40	42.83	± 21.4
↑	**miR-365**	48.50	± 30.00	9.90	± 25.0

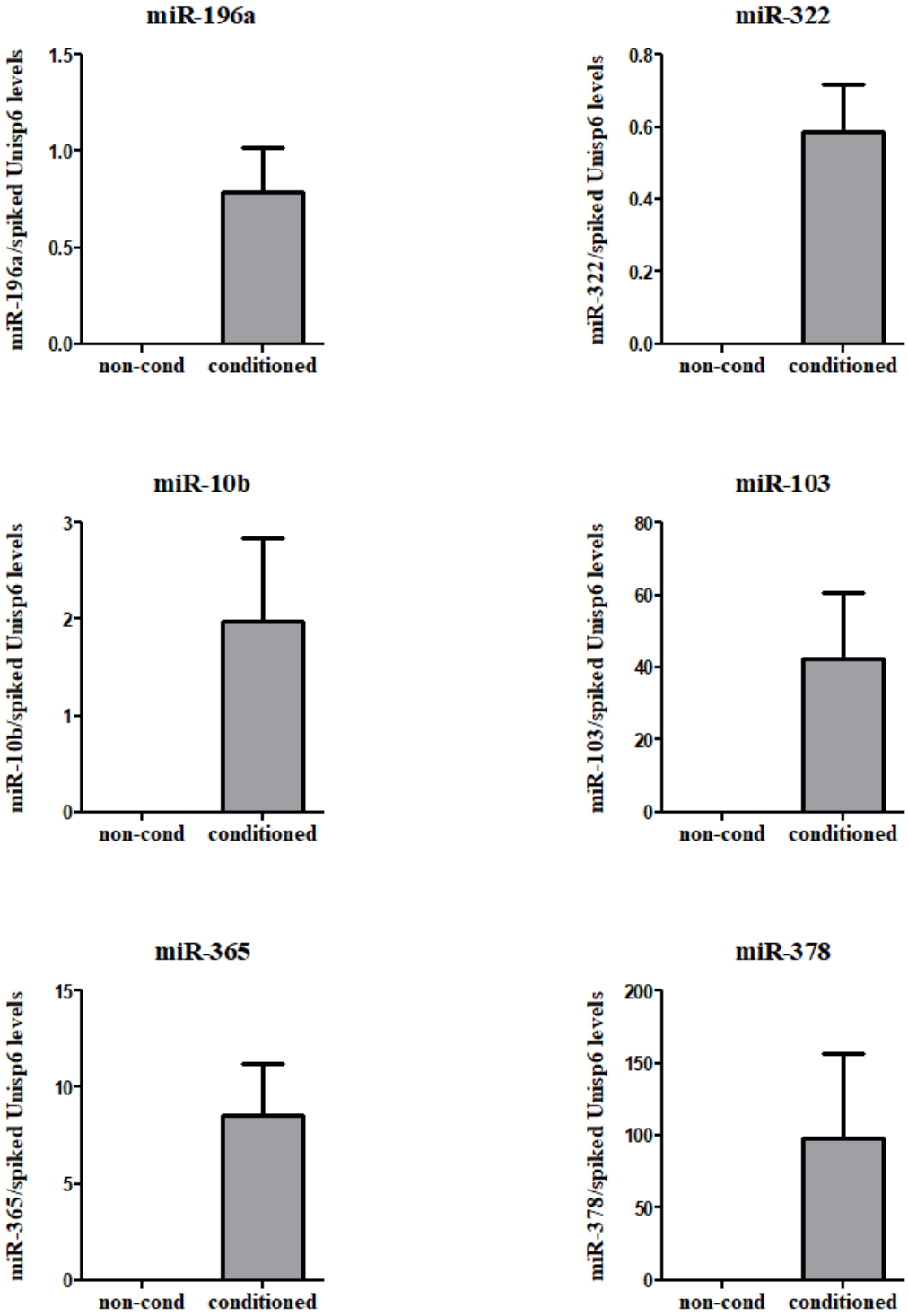

Figure 46 MiRNAs detected in the pellet of ultracentrifuged media from CL-treated adipocytes. The graphics show $2^{-\Delta Ct}$ values (mean of biological triplicates) of miRNAs in pellet obtained from unconditioned and conditioned media from brown adipocyte treated with CL for 5 hours (B). MiRNA levels were normalized to Unisp6 spiked in just prior RNA extraction

4.1.2 *Nanoparticle characterization*

To investigate the nanoparticles secreted by adipocytes, media samples from mouse and human differentiated white and brown adipocyte cell lines were analysed through NanoSight technology. This system detects particles suspended in fluids determining their concentration and profiling their size distribution. To perform the experiment, an equal number of cells was seeded into each T-175 flask and incubated for 3 days in serum-free media. However, cell density visibly decreased at day 3, probably due to long time incubation in serum-free condition. Therefore, cells were counted and data normalised to cell count so that the graphs show size distribution (figure 47 and 48 left panels) and concentration (figure 47 and 48 right panels) of particles/ml secreted by $1x10^7$ cells. Media samples were collected and processed. As the samples were analysed at the University of Cardiff, the first steps of sample preparation (serial centrifugation and filtration) were performed prior to freezing at -80 °C, to avoid large particle breakdown into smaller particles and therefore false positive results. Media samples were then analysed using NanoSight technology. As shown in the right panel of figure 47, non-conditioned media had a concentration of 1.6 (± 0.8) $x10^8$ particles per ml. As the media from brown and white adipocytes had a significantly higher concentration of nanoparticles per ml, 1.15 (± 0.5) x 10^{12} and 1.37 (± 0.3) x 10^{12} respectively, it is possible to conclude that nanoparticles in conditioned media originated from adipocytes. The analysis revealed that there were no significant differences between white and brown adipocytes and that the majority of the nanoparticles had a size of 100 nm. This suggests that a large proportion of the vesicles secreted by adipocytes consist of exosomes, which are sized 50-200 nm. The different type of vesicles such as microvesicles and exosomes, differ not only in size but also in chemical composition. Exosomes are known to express on their membrane surface the tetraspanins CD9, CD81 and CD63, which have been established as exosomes markers [377, 378]. To characterize the composition of the vesicles analysed by nanosight and confirm that adipocytes secrete exosomes, the conditioned media from mouse and human adipocytes was ultracentrifuged at 120,000xg for 2 hours to isolate vesicles. The supernatant was discarded, the pellet resuspended in 2.5 ml of PBS and analysed for exosome marker detection through Europium-based ELISA-like assay. As reported in figure 47, bottom panel, mouse vesicles were positive for CD9, CD81 and CD63 tetraspanins. CD63 was expressed only in BAT. However, no

statistical analysis was performed on these data as the replicate number was lower than 3.

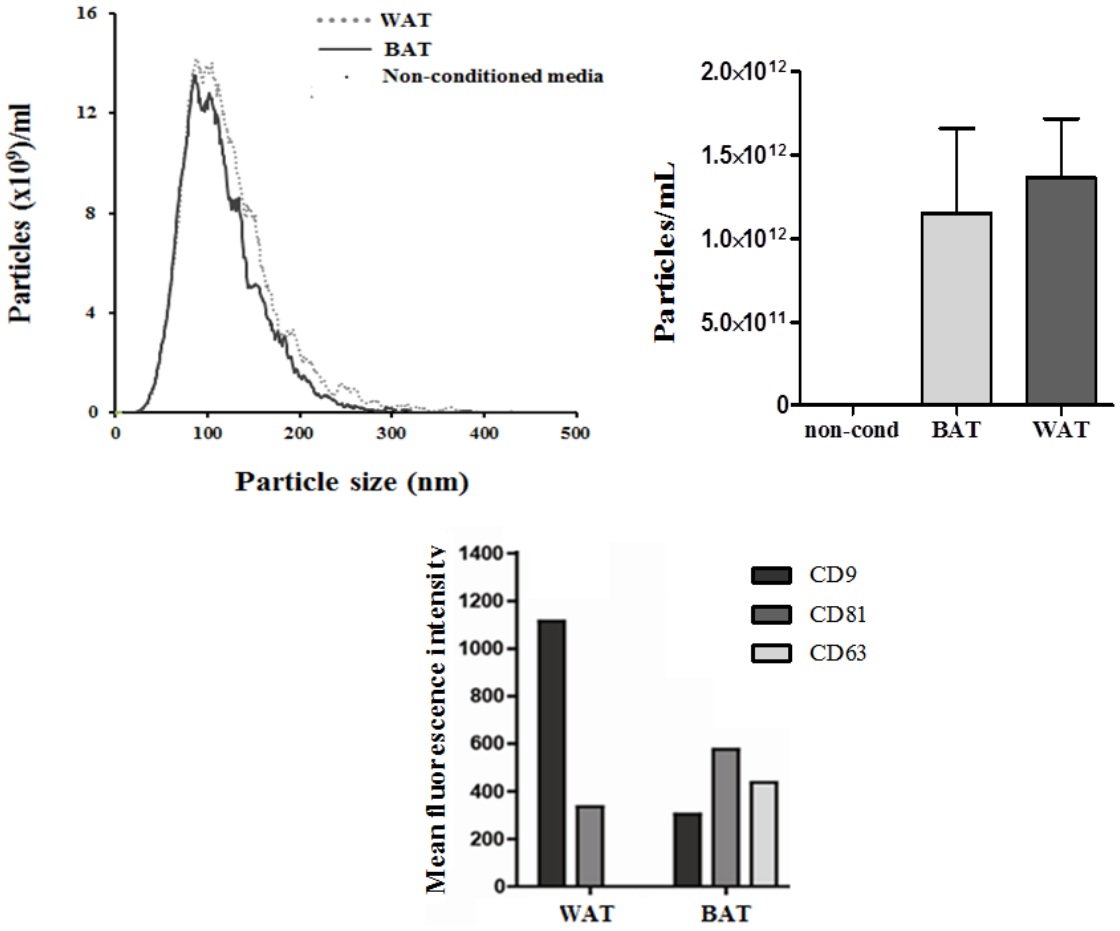

Figure 47 Mouse adipocytes secret exosome-like nanoparticles.
Media samples were collected after 3 days from mouse differentiated brown and white adipocyte cell lines. The analysis was performed at the Velindre Centre, University of Cardiff, with the assistance of Dr J. Webber. **(**A) Nanosight analysis of non-conditioned and conditioned media samples from differentiated brown and white adipocytes was adjusted for dilutions adopted when loading the samples. Left panel shows size distribution of nanoparticles. The curves represent the mean trend lines (period 11) of the 3 biological replicates of conditioned media samples for each group**.** The right panel shows mean concentration of nanoparticles and relative SEM. (B) Europium based ELISA-like assay. The graphic shows the mean fluorescence intensity for the exosomes markers (CD9, CD81 and CD63) on the surface of the nanoparticles isolated from the conditioned media samples normalised to the unconditioned media and non-specific signals for primary and secondary antibodies.

Concentration and size profiling of vesicles secreted by human adipocytes, through Nanosight analysis, revealed that, also in this case, particle concentration in conditioned media was significantly higher than in non-conditioned medium and very similar between BAT and WAT, with 2.1 (± 0.2) $x10^{10}$ and 1.8 (± 0.4) $x10^{10}$ particles per ml respectively (figure 48, right panel). However, a different profile of particle size distribution between human BAT and WAT was observed. BAT presented a high concentration of particles with a diameter of about 100 nm as shown by the sharp peak of the curve in figure 48 top left panel, while WAT is represented by the curve with a smoother peak in the range of 100 and 250 nm which reflects a higher heterogeneity in the vesicle population.

When analysed for the exosome markers expression through the Europium-based ELISA-like assay, the isolated vesicles from both human brown and white adipocytes were positive for CD9, CD63 and CD81 and showed a similar trend of expression, even if the replicates were less than 3 and no statistical analysis were performed (figure 48 bottom panel).

In conclusion, all these results suggest that both mouse and human adipocytes secrete nanoparticles and that a large part of these may consist of exosomes.

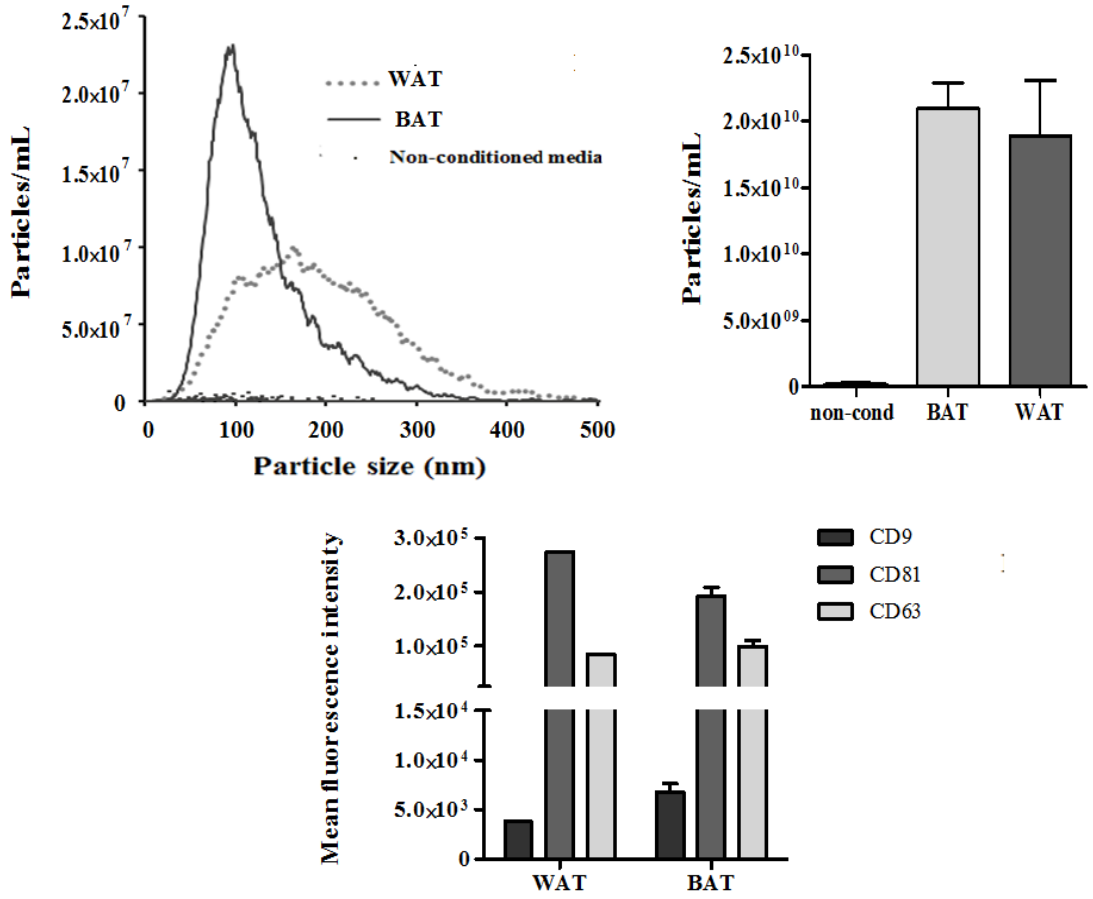

Figure 48 Human adipocytes secret exosome-like nanoparticles.
Media samples were collected after 3 days from mouse differentiated brown and white adipocyte cell lines. The analysis was performed at the Velindre Centre, University of Cardiff, with the assistance of Dr J. Webber. **(**A) Nanosight analysis of non-conditioned and conditioned media samples from differentiated brown and white adipocytes. Left panel shows size distribution of nanoparticles. The curves represent the mean trend lines (grade 11) of the 3 biological replicates of conditioned media samples for each group**.** The right panel shows mean concentration of nanoparticles and relative SEM. (B) Europium based ELISA-like assay. The graph shows the mean fluorescence intensity for the exosomes markers (CD9, CD81 and CD63) on the surface of the nanoparticles isolated from the conditioned media samples normalised to the unconditioned media and non-specific signals for primary and secondary antibodies.

4.2 Discussion

Different studies have shown that adipocytes release exosomes and miRNAs were found to be incorporated in these vesicles. Thomau T., and colleagues recently showed that adipose tissue is the major source of exosomal circulating miRNAs, which are capable of gene expression regulation in distal organs [261]. The advantages and disadvantages of the different miRNA carriers are still not fully understood. Exosomes have attracted the majority of scientists' attention over the other classes of miRNA carriers. Aiming to understand whether different adipose-derived miRNAs are preferentially incorporated into vesicles or associated to vesicle-free systems, we found out that all extracellular miRNAs tested, were in part incorporated into vesicles and in part associated to vesicle-free systems. In detail, our data suggest that adipose-derived miR-196a and miR-322 are almost equally distributed between vesicles and vesicle free-system, whereas miR-378a-3p is preferentially associated to vesicle-free systems. As the remaining miRNAs presented a large variation, it is not possible to establish their preferential way of secretion. However, miR-10b showed a similar percentage of depletion to miR-378a-3p, while miR-365 and miR-103 a similar trend to miR-196a and miR-322. As vesicles may provide a higher level of protection to the incorporated miRNAs to travel long distances, and a more specificity of target delivery, we speculate that miR-196a and miR-322 have a major chance to function as both endocrine and paracrine/autocrine miRNAs, while miR-378 might have a predominant paracrine/autocrine function. However, the knowledge on the properties of vesicle-free systems in these terms is still too poor to draw conclusions confidently.

As all miRNAs were secreted both via association to vesicle free systems and incorporation into vesicle, we aimed to understand whether ß-adrenergic stimuli favours one type of carrier for miRNA release over the other. Our results suggest that CL treatment favours incorporation of miR-378 and miR-10b into vesicles as the percentage of their depletion after ultracentrifugation was higher than in untreated samples. Conversely, a greater percentage of miR-365 was associated to vesicle free systems in media from CL treated samples compared to untreated. No particularly evident effects were observed for the remaining miRNAs. The preferential way of miRNA secretion through one type of carrier over another might implicate the necessity of a miRNA to preferentially reach a different cellular target and this aspect should be investigated.

4.2.1 *Vesicle characterization*

As previous studies have reported that adipose tissues secrete exosomes [261, 379] we characterised the vesicles isolated by ultracentracentrifugation of media samples from brown and white adipocytes. We confirmed that a large part of these vesicles consisted of exosomes as they had exosome-like size (~200 nm) and were positive for at least two of the three exosome markers tested (CD9, CD63, CD81) even though we could not perform statistical analysis on the expression of the different tetraspanins between brown and white adipocytes. Our results showed that vesicle from brown and white adipocytes present similar characteristics even though human white adipocytes secrete a more heterogeneous population of vesicles.

Chapter 5 – Results
Gene and miRNA expression in human brown and white adipocytes

5.1 MicroRNA array, mRNA sequencing and integrative analysis

The nature of the brown adipocyte in humans is not as much understood as in mice, primarily because of the scarce availability of human brown adipose tissue samples and the high heterogeneity of the tissue. Once the human cell lines used in this study were characterized, we proceeded to use Next Generation Sequencing technology (mRNA sequencing) to explore the differences in gene expression between differentiated brown and white adipocytes. In addition, to identify intracellular miRNAs differentially expressed between brown and white adipocytes we performed a microRNA array. To investigate the potential role in adipogenesis and adipose metabolism of the identified differentially expressed miRNAs we performed miRNA target prediction through bioinformatics tools and integrated the data from mRNA sequencing and miRNA array analyses as described in the following paragraphs. Both types of analysis were performed on the same RNA samples and data analysis was carried out with the assistance of Dr Mohammad Tauqeer Alam (University of Warwick).

First, we examined variation among samples. In figure 49 are reported the PCA plots performed on mRNA sequencing (Panel A) and miRNA array (Panel B) data. As shown in the graphs, in both cases, where PC1 explains the largest variation, the samples clustered similarly so that brown adipocytes grouped on the left side and the white on the right side. This is a preliminary indicator of the fact that brown and white adipocytes have clearly different gene and miRNA expression profiles, reflecting the different biological nature of the samples. PC2 explains the 2.32% and 15% of the variation among samples for mRNA sequencing and miRNA array data respectively, which might be due to secondary factors such as quality of RNA. In conclusion, the PCAs revealed the high quality of the data obtained by the mRNA sequencing and miRNA array analyses, so that all samples could be included for statistical and integrative data analysis.

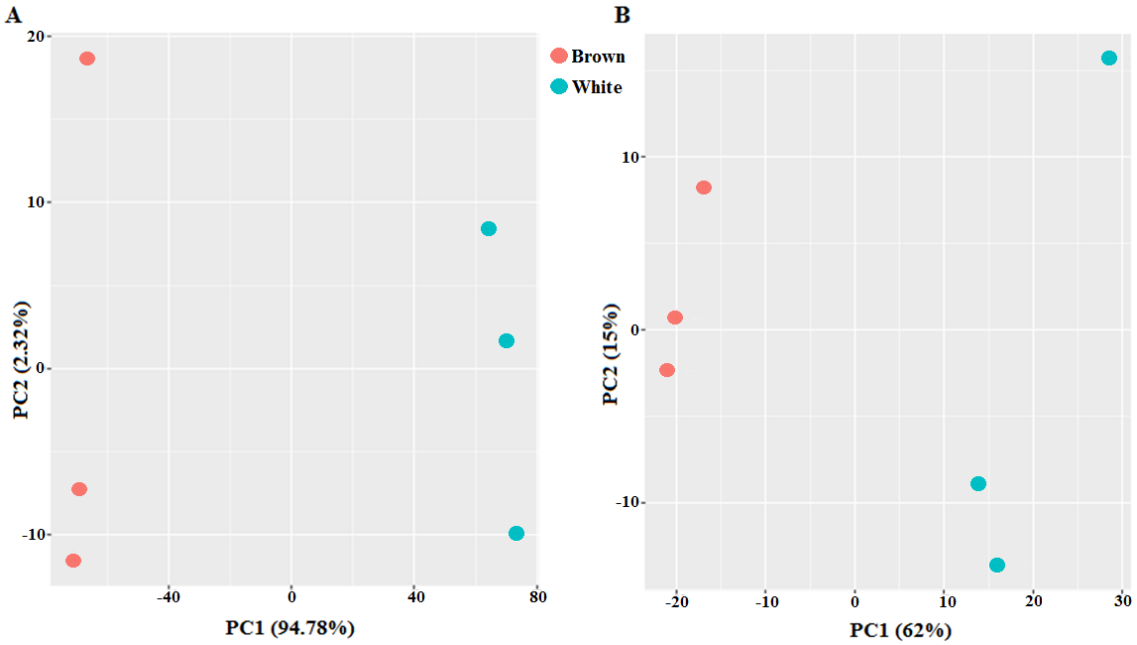

Figure 49 PCA plots in miRNA array and mRNA sequencing analysis.
A) PCA plot for brown and white adipocytes on the basis of mRNA sequencing read count data. The PCA was performed on all samples and all genes. PC1 explains 94.78% of the variation and PC2 explains 2.32% of the variation. (B) PCA performed on all samples and all miRNAs data. PC1 explains 62% of the variations and PC2 explains 15% of the variation.

5.1.1 *mRNA sequencing*

mRNA sequencing technology targets all polyadenylated (poly-A) transcripts of the transcriptome and allows identification of either known or unknown genes and their eventual novel splicing isoforms expressed in the system analysed. For the purpose of this study we compared gene expression of known genes between human mature brown and white adipocytes. Significance was assessed using Student's t-test and Benjamini-Hochberg correction. The graph in figure 50 was obtained by plotting the log2 (fold change) (brown versus white) on the abscissa and –log10 (adjusted p value) on the ordinate. Genes presenting a log2 (fold change) lower than -1 and higher than +1 with an adjusted p value lower or equal to 0.05 were considered significantly differentially expressed. This way, we identified 2463 genes upregulated and 1733 genes downregulated in brown adipocytes compared to white.

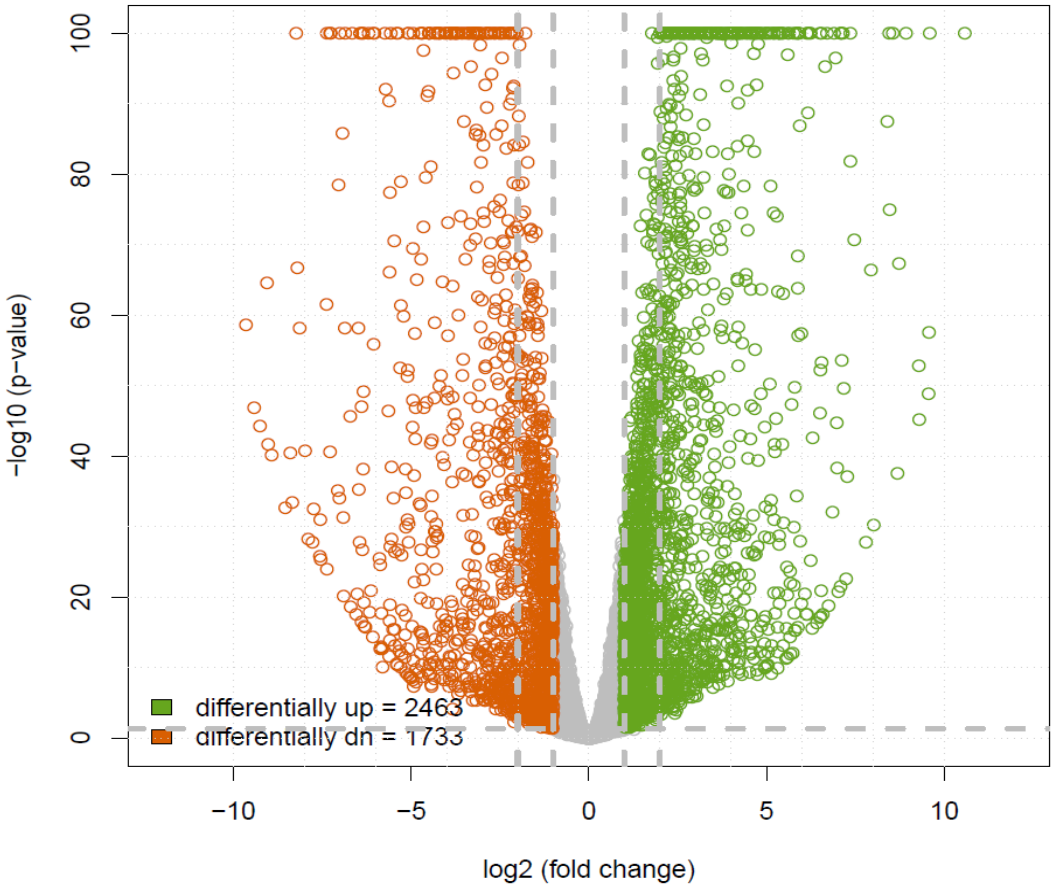

Figure 50 Genes differentially expressed between brown and white adipocytes.
Volcano plot showing the relationship between the p-values and the log2 (fold change) in RNA sequencing read count data of brown with reference to white adipocytes. Up means upregulated, dn means downregulated.

5.1.2 *KEGG enrichment in brown and white adipocytes*

We performed hypergeometric test to explore KEGG enrichment in brown versus white adipocytes. We identified 110 pathways (p values ≤ 0.05) associated with differentially expressed genes between brown and white adipocytes, of which 71 were enriched in brown and 45 in white adipocytes (Figure 51). The top 7 pathways (p value ≤ $1x10^{-8}$) associated with upregulated genes (log2 (fold change) ≥ 1, p value ≤ 0.05) in brown adipocytes were: fatty acid degradation, biosynthesis of unsaturated fatty acids, propanoate metabolism, citrate cycle, pyruvate metabolism, valine leucine and isoleucine degradation and PPAR signalling. All these pathways are known to be involved in the main function that distinguishes the brown from the white adipocytes being energy consumption. Indeed, BAT degrades fatty acids to use them as the main source of energy for heat production [77]. Moreover, polyunsatured fatty acids have been found to activate UCP1 more efficiently than saturated fatty acids [380]. This would justify the high

expression of genes involved in biosynthesis pathway of unsaturated fatty acids. As expected, pathways related to oxidative phosphorylation, insulin signalling and many others were also enriched in brown adipocytes. Indeed, BAT is known to regulate glucose homeostasis and insulin sensitivity [381]. Some other pathways may seem less obviously expected to be differentially enriched between the adipocyte cell types. For example, Huntington disease is associated with high energy expenditure and weight loss [382] and white adipose tissue of HD mice presents brown-like feature such as a high level of UCP1 [383] which would explain why the HD pathway was enriched in brown adipocytes. Many of the pathways found to be associated with the genes upregulated in white adipocytes are involved in cancer and inflammation including the top 4 ones: TNFα signalling pathway, proteoglycans in cancer, cytokine-cytokine receptor interaction and NOD-like receptors signalling. Indeed, obesity is generally characterized by low-grade chronic inflammation in white adipose depots and increases the risk of cancer (reviewed in [384] and [385]) as well as the chances to develop T2D [386]. In conclusion, these results reflected the biological nature of the brown and white adipocytes and could be used in further investigation of the differences between brown and white adipocytes. For the purpose of this study, we investigated the potential role of miRNAs in the pathways identified in this analysis as described in paragraph 5.4.

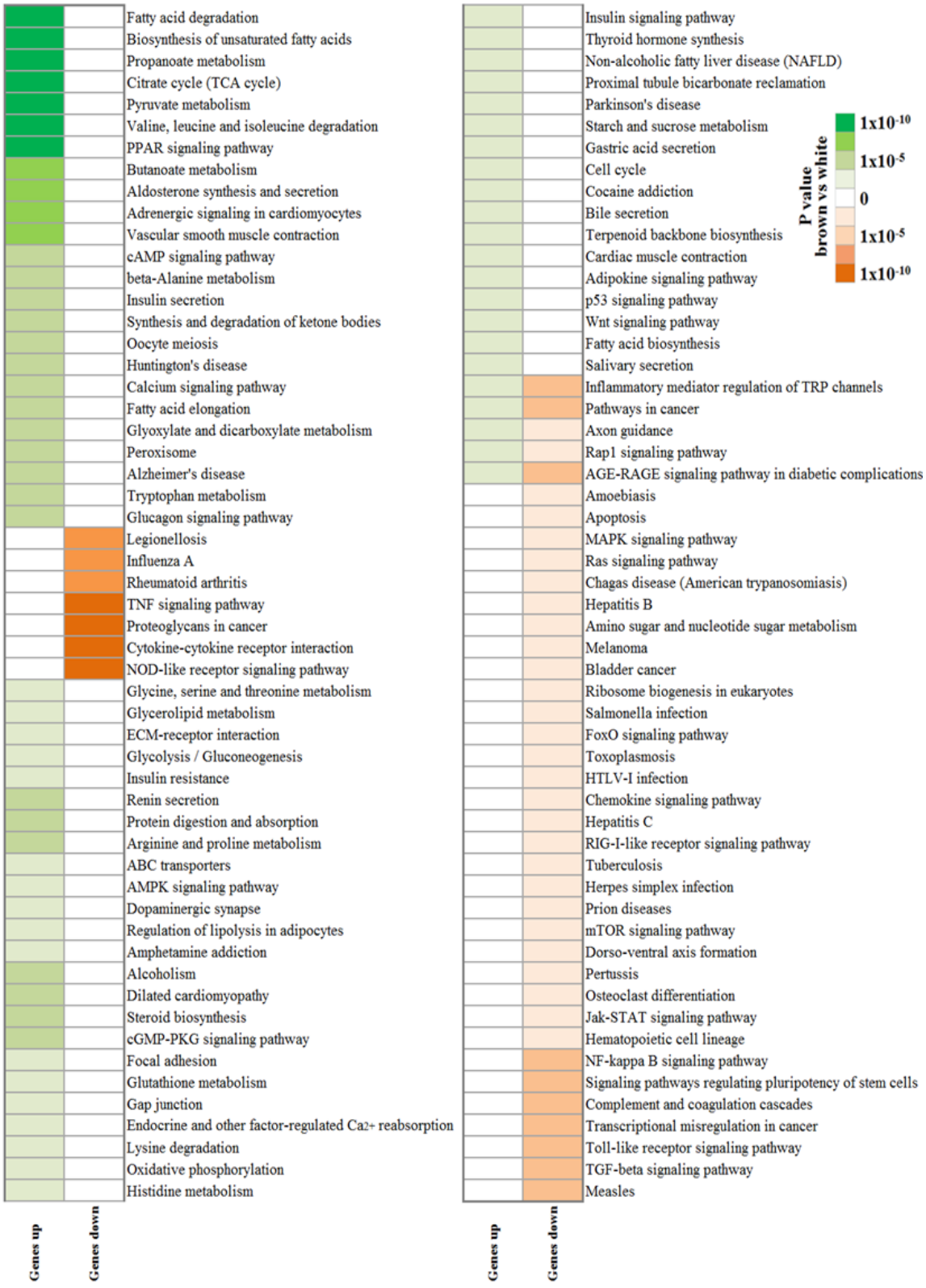

Figure 51 KEGG enrichment pheatmap.
The map shows KEGG pathways associated with genes upregulated (green) and downregulated (red) in brown versus white adipocytes obtained by hypergeometric test. Ranges of p value for each pathways are indicated by the colour scales.

5.1.3 *MiRNA array*

The heat map diagram (figure 52 panel A) shows the result of a two-way hierarchical clustering of all miRNAs and samples. The clustering was obtained using the complete-linkage method together with the Euclidean distance measure. Rows represent the different miRNAs and each column represents a sample. The clustering tree is shown on the left. For the relative miRNA expression level of each sample a different colour of the red-green scale is assigned. Red represents an expression level below the mean, green colour represents expression above the mean. The heat map reports only the top 50 miRNAs presenting the highest standard deviation, whereas the volcano plot (figure 52 panel B) reports all miRNAs tested. The thirty-three miRNAs with a log2 (fold change) ≤ -1, represented by the orange spots on the left side of the volcano plot, are significantly (adjusted p value ≤ 0.05) downregulated in brown compared to white adipocytes. The twenty green spots on the opposite side in the graphic represent the miRNAs upregulated in brown adipocytes relative to white. In tables 20 and 21 the log2 fold change values and the adjusted p values (adj.P.Value) are reported for the miRNAs upregulated and downregulated in brown adipocytes compared to white respectively. As expected, miR-196a-5p was among the miRNAs upregulated in white adipocytes. The top 5 miRNAs upregulated in brown adipocytes versus white were: miR-143-3p, the members of the miR-378 family (e, d and f) and miR-4511. The top 5 miRNA downregulated in brown adipocytes were: miR-181a-2-3p, miR-3202, miR-4306, miR-4516 and miR-4644. However, all the miRNAs identified as differentially expressed between brown and white adipocytes were included in the integrative study between the miRNA array and mRNA sequencing.

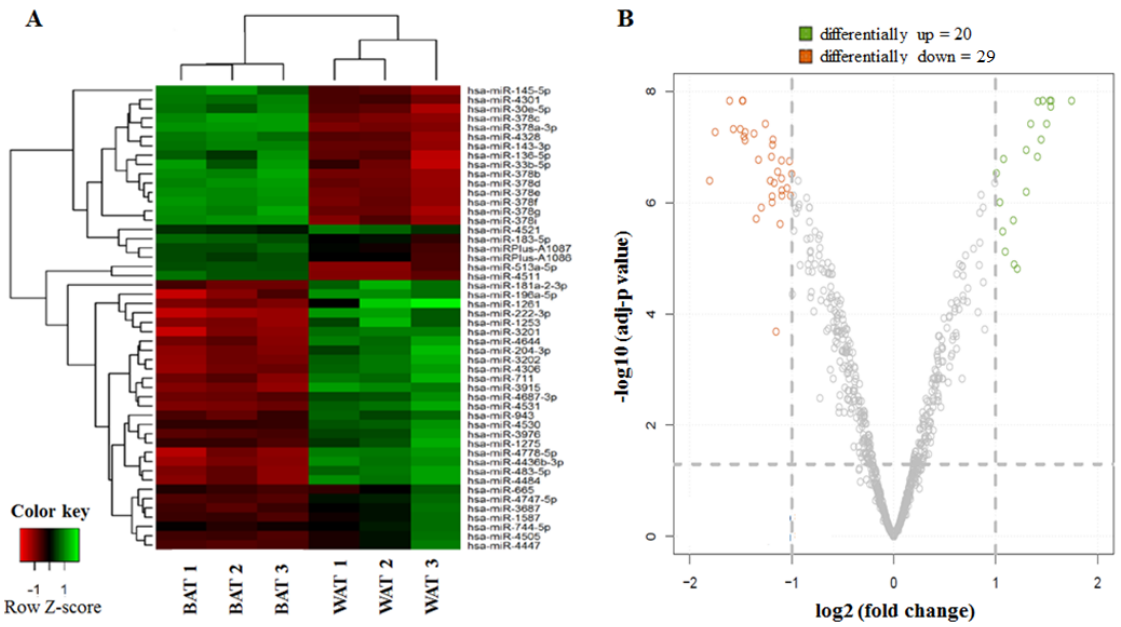

Figure 52 Differential miRNA expression in brown versus white adipocytes.
A) Heat Map performed on all samples and on the top 50 miRNAs with highest standard deviation using the normalized log ratio values for the analysis. B) Volcano plot showing the relation between the logarithm of the adjusted p-values and the log2 fold change between brown and white of all the miRNAs.

5.1.4 *Integration of data from miRNA array and mRNA sequencing analyses*

MiRNAs regulate gene expression either by promoting mRNA target degradation or by inhibiting mRNA translation into protein [177]. In the first case, assuming that there are no other factors interfering with this process, the increase of a miRNA expression should correspond to decreased expression of its mRNA targets. Therefore, if a miRNA was found to be upregulated in brown versus white adipocytes, its mRNA targets are expected to be lower expressed in brown adipocytes compared to white. Based on this principle, we investigated the potential role of miRNAs in the regulation of the pathways identified through the mRNA sequencing analysis. First we predicted the potential miRNA targets using bioinformatics tools. Next, we verified the relative level of expression of these genes, based on the results obtained through the mRNA sequencing analysis. For miRNAs downregulated in brown adipocytes, only the predicted targets that were upregulated and associated with pathways enriched in brown adipocytes were considered and vice versa. In figure 53 the log2 (fold change) of the differentially expressed miRNAs is represented by the blue-pink colour scale. The green colour scale represents the pathways associated with the genes upregulated in brown versus white

adipocytes, while, the orange scale represents the ones associated with the genes downregulated in brown adipocytes. Each different shade represents a specific range of p value of the pathways as shown in the legend. In the squares are reported the numbers of the target genes involved in the pathways with a p value exemplified by the colour of the square. In the tables below, are listed the genes upregulated (tables 22-25) and downregulated (tables 26-28) in brown versus white and the pathways in which they are involved. Tables are arranged per range of p values of the pathways. As a single gene can take part in a very high number of pathways, for each gene were reported only the ones falling in the lowest p value range. The log 2 (fold change) and p value of the gene are annotated in the third and fourth column, respectively. In the first column all the miRNAs which were predicted to target the gene are listed. However, data were rearranged in tables 20 and 21 to provide an easier visualization of the most relevant pathways in which the identified miRNAs are likely to be involved. For each miRNA only the target genes associated with the pathways falling in the lowest p value range are reported. As shown in figure 53, among all the miRNAs upregulated in brown adipocytes, miR-513a-5p was predicted to target the largest number of genes (9) downregulated in brown adipocytes and involved in the pathways falling in the lower p value range. Eight of its targets were associated with proteoglycans in cancer pathway. In the remaining pathways associated with significantly downregulated genes in brown adipocytes it was found to potentially target a total of 15 genes. Thirteen more targets were associated with the pathways presenting a p value out of the range of significance. MiR-513a-5p, miR-4511 and miR-4328 showed the highest number of targets involved in the pathways associated with downregulated genes in brown adipocytes and presenting a p value in the range of significance. Among these, the most significant ones were: cytokine-cytokine receptor interaction, proteoglycans in cancer and NOD-like receptor signalling pathways. The miRNAs downregulated in brown adipocytes targeting two or more downregulated genes involved in the most statistically significant pathways (p value) $\leq 1x10^{-8}$) were miR-4698, miR-4306 miR-4531, miR-4644, miR-4516 and miR-4306. To our knowledge, none of these miRNAs has been documented in the literature as involved in adipocyte biology. MiR-29a-3p was predicted to target the highest number of genes suggesting an important role in regulating adipogenesis and

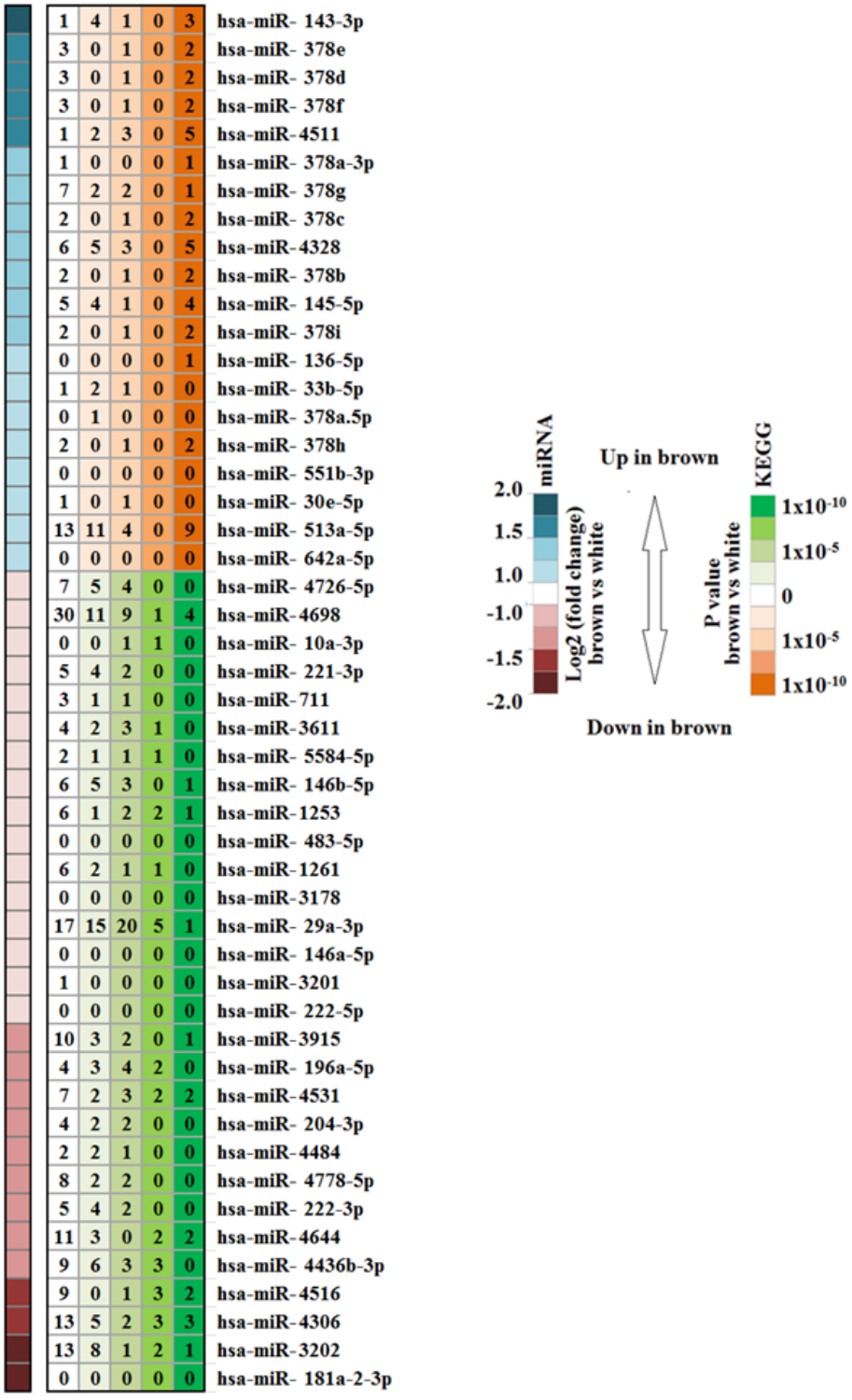

Figure 53 Integration of miRNA array and mRNA sequencing data.
The map shows for each miRNA, identified by the miRNA array analysis, the number of predicted targets belonging to the pathways associated with the genes differentially expressed between brown and white adipocytes. The p value range of the pathways is expressed by the green (for pathways enriched in brown adipocytes) and orange (for pathways enriched in white adipocytes) colour scales. Log2 (fold change) range of miRNA (brown versus white) is represented by the blue-pink color scale.

metabolism in white adipocytes. Here we identified PPARGC1α among its predicted targets. Direct regulation of this important brown adipocyte coregulator by miR-29a-3p, to our knowledge, has not been demonstrated or documented in the literature.For some miRNAs only few or no targets among the ones predicted by the bioinformatics tools and eventually involved in the pathways identified, were found to be differentially expressed in brown versus white adipocytes. This does not imply that they have a less important or no role in adipocyte biology, but it rather suggests that they might regulate gene expression without inducing mRNA target degradation. Among them miR-181a-2-3p was the most downregulated miRNA in brown compared to white adipocytes. Surprisingly, for this miRNA no targets at all were predicted by the algorithms used in this study.

Table 19 miRNAs upregulated in brown vs white adipocytes, their predicted targets and enriched pathways

miRNA up	miRNA Log2(FC)	miRNA adj.P.Val	Target down	Kegg name	KEGG pVal range
miR-143-3p	1.746	1.46E-08	PTGS2	TNF signaling pathway	$p \leq 1x10^{-8}$
			PLAUR	Proteoglycans in cancer	
			ITPR1	NOD-like receptor signaling pathway Proteoglycans in cancer	
miR-378e	1.546	1.46E-08	IGF1R	Proteoglycans in cancer	$p \leq 1x10^{-8}$
			BMP2	Cytokine-cytokine receptor interaction	$p \leq 1x10^{-8}$
miR-378d	1.543	1.89E-08	IGF1R	Proteoglycans in cancer	$p \leq 1x10^{-8}$
			BMP2	Cytokine-cytokine receptor interaction	$p \leq 1x10^{-8}$
miR-378f	1.532	1.46E-08	IGF1R	Proteoglycans in cancer	$p \leq 1x10^{-8}$
			BMP3	Cytokine-cytokine receptor interaction	$p \leq 1x10^{-8}$
miR-4511	1.502	3.82E-08	CXCL16	Cytokine-cytokine receptor interaction	$p \leq 1x10^{-8}$
			TIAM1 NRAS	Proteoglycans in cancer	$p \leq 1x10^{-8}$
			OAS3 XIAP	NOD-like receptor signaling pathway	$p \leq 1x10^{-8}$
miR-378a-3p	1.464	1.46E-08	IGF1R	Proteoglycans in cancer	$p \leq 1x10^{-8}$
miR-378g	1.448	7.22E-08	ELK1	Proteoglycans in cancer	$p \leq 1x10^{-8}$
miR-378c	1.417	1.52E-08	IGF1R	Proteoglycans in cancer	$p \leq 1x10^{-8}$
			BMP2	Cytokine-cytokine receptor interaction	$p \leq 1x10^{-8}$
miR-4328	1.412	1.48E-07	WNT5A NRAS	Proteoglycans in cancer	$p \leq 1x10^{-8}$
			PDGFA	Cytokine-cytokine receptor interaction	$p \leq 1x10^{-8}$
			DAB2IP	TNF signaling pathway	$p \leq 1x10^{-8}$
miR-378b	1.344	3.82E-08	IGF1R	Proteoglycans in cancer	$p \leq 1x10^{-8}$
			BMP2	Cytokine-cytokine receptor interaction	$p \leq 1x10^{-8}$

Continuing table 20					
miRNA up	**miRNA Log2(FC)**	**miRNA adj.P.Val**	**Target down**	**Kegg name**	**KEGG pVal range**
miR-145-5p	1.302	6.41E-07	IGF1R PXN NRAS	Proteoglycans in cancer	$p \leq 1x10^{-8}$
			FLT1	Cytokine-cytokine receptor interaction	$p \leq 1x10^{-8}$
miR-378i	1.301	1.13E-07	IGF1R PXN NRAS	Proteoglycans in cancer	$p \leq 1x10^{-8}$
			BMP3	Cytokine-cytokine receptor interaction	$p \leq 1x10^{-8}$
miR-136-5p	1.213	1.55E-05	ELK1	Proteoglycans in cancer	$p \leq 1x10^{-8}$
miR-33b-5p	1.183	1.30E-05	RUNX1T1	Pathways in cancer Transcriptional misregulation in cancer	$1x10^{-4} \leq p \leq 1x10^{-6}$
miR-378a-5p	1.174	2.05E-06	NFATC2	Axon guidance, Hepatitis B, HTLV-I infection Osteoclast differentiation	$01x10^{-2} \leq p \leq 1x10^{-4}$
miR-378h	1.094	7.67E-06	IGF1R	Proteoglycans in cancer	$p \leq 1x10^{-8}$
			BMP2	Cytokine-cytokine receptor interaction	$p \leq 1x10^{-8}$
miR-30e-5p	1.071	3.32E-06	JARID2	Signaling pathways regulating pluripotency of stem cells	$01x10^{-4} \leq p \leq 1x10^{-6}$
miR-513a-5p	1.042	9.80E-07	CD44 ITGA2 HBEGF, CAMK2A XIAP PXN NRAS	Proteoglycans in cancer	$p \leq 1x10^{-8}$
			PIK3CD	TNF signaling pathway, Proteoglycans in cancer	$p \leq 1x10^{-8}$
			ANTXR2	NOD-like receptor signaling pathway	
miR-642a-5p	1.008	2.92E-07	No targets	-	-

Table 20 miRNAs downregulated in brown vs white adipocytes, their predicted targets and enriched pathways

miRName down	**miRNA Log2(FC)**	**miRNA adj.P.Val**	**Target up**	**KEGG name (enriched in brown)**	**KEGG pVal range**
miR-4726-5p	-1.001	3.01E-07	PDE1B	Huntington's disease, Renin secretion	$1x10^{-4} \leq p \leq 1x10^{-6}$
			PKIA	Tryptophan metabolism	
			DAG1	Dilated cardiomyopathy	
			PDGFRB	Calcium signaling pathway	
miR-4698	-1.013	7.54E-07	SCD	Biosynthesis of unsaturated fatty acids	$p \leq 1x10^{-8}$
			ME1	Pyruvate metabolism	
			SORBS1	PPAR signalling pathway	
			BCAT2	Valine, leucine and isoleucine degradation	
miR-10a-3p	-1.022	1.77E-07	PLCB1	Aldosterone synthesis and secretion, Adrenergic signaling in cardiomyocytes Vascular smooth muscle contraction	$1x10^{-6} \leq p \leq 1x10^{-8}$
miR-221-3p	-1.046	5.55E-07	PPARGC1A	Huntington's disease, Glucagone signaling pathway	$1x10^{-4} \leq p \leq 1x10^{-6}$
			MAPK10	cAMP signaling pathway, Huntington disease	
miR-711	-1.096	7.54E-07	COL4A5	Protein digestion and absorption	$1x10^{-4} \leq p \leq 1x10^{-6}$
miR-3611	-1.098	6.01E-07	BDH1	Butanoate metabolism	$1x10^{-6} \leq p \leq 1x10^{-8}$
miR-5584-5p	-1.100	1.75E-07	ADCY6	Aldosterone synthesis and secretion, Adrenergic signaling in cardiomyocytes, Vascular smooth muscle contraction	$1x10^{-6} \leq p \leq 1x10^{-8}$

Continuing table 21					
miRName down	**miRNA Log2(FC)**	**miRNA adj.P.Val**	**Target up**	**KEGG name (enriched in brown)**	**KEGG pVal range**
miR-146b-5p	-1.101	3.70E-07	BCAT2	Valine, leucine and isoleucine degradation	$p \leq 1x10^{-8}$
miR-1253	-1.114	2.43E-06	HSD17B12	Biosynthesis of unsaturated fatty acids	$p \leq 1x10^{-8}$
miR-483-5p	-1.139	2.78E-07	No targets	-	-
miR-1261	-1.155	2.04E-04	CALM3	Aldosterone synthesis and secretion, Adrenergic signaling in cardiomyocytes, Vascular smooth muscle contraction	$1x10^{-6} \leq p \leq 1x10^{-8}$
miR-3178	-1.172	4.36E-07	No targets	-	$1x10^{-6} \leq p \leq 1x10^{-8}$
miR-29a-3p	-1.184	7.22E-08	LPL	PPAR signalling pathway	$p \leq 1x10^{-8}$
miR-146a-5p	-1.189	9.15E-08	No targets	-	-
miR-3201	-1.199	1.48E-07	No targets	-	-
miR-222-5p	-1.210	4.06E-07	No targets	-	-
miR-3915	-1.259	3.82E-08	ADIPOQ	PPAR signalling pathway	$p \leq 1x10^{-8}$
miR-196a-5p	-1.299	1.21E-06	CALM3	Aldosterone synthesis and secretion, Adrenergic signaling in cardiomyocytes, Vascular smooth muscle contraction	$1x10^{-6} \leq p \leq 1x10^{-8}$
miR-4531	-1.328	1.70E-07	FADS2	Biosynthesis of unsaturated fatty acids	$p \leq 1x10^{-8}$
			ACOX1	Fatty acid degradation, Biosynthesis of unsaturated fatty acids	
miR-204-3p	-1.349	1.96E-06	KCNE3	Protein digestion and absorption	$01x10^{-4} \leq p \leq 1x10^{-6}$
			RPS6KA1	Oocyte meiosis	
miR-4484	-1.372	5.71E-08	DAG1	Dilated cardiomyopathy	$01x10^{-4} \leq p \leq 1x10^{-6}$
miR-4778-5p	-1.457	5.33E-08			
miR-222-3p	-1.458	7.51E-08	PPARGC1A	Huntington's disease, Glucagone signaling pathway	$01x10^{-4} \leq p \leq 1x10^{-6}$
			MAPK10	cAMP signaling pathway, Huntington disease	
miR-4644	-1.470	6.38E-08	BCAT2	Valine, leucine and isoleucine degradation	$p \leq 1x10^{-8}$
			TECR	Biosynthesis of unsaturated fatty acids	
miR-4436b-3p	-1.479	1.46E-08	CALM1, CALM3	Aldosterone synthesis and secretion, Adrenergic signaling in cardiomyocytes, Vascular smooth muscle contraction	$1x10^{-6} \leq p \leq 1x10^{-8}$
			ATP1B1	Adrenergic signaling in cardiomyocytes	$1x10^{-6} \leq p \leq 1x10^{-8}$
miR-4516	-1.506	4.71E-08	ACOX1	Fatty acid degradation, Biosynthesis of unsaturated fatty acids	$p \leq 1x10^{-8}$
			FADS2	Biosynthesis of unsaturated fatty acids	
miR-4306	-1.574	4.71E-08	SCD	Biosynthesis of unsaturated fatty acids	$p \leq 1x10^{-8}$
			BCAT2	Valine, leucine and isoleucine degradation	
miR-3202	-1.751	5.33E-08	RXRG	PPAR signalling pathway	$p \leq 1x10^{-8}$
miR-181a-2-3p	-1.806	4.01E-07	No targets	-	-

Table 21 KEGG pathways enriched in brown versus white adipocytes with p value ≤1x10^{-8}

miRName down	Target up	Log2(FC)	Adj.pval	KEGG name (p value ≤1x10^{-8})
miR-3915	ADIPOQ	4.16	9.20E-139	PPAR signalling pathway
miR-4306 miR-4698	SCD	2.68	3.35E-112	Biosynthesis of unsaturated fatty acids
miR-4698	ME1	2.37	1.29E-62	Pyruvate metabolism
miR-4516 miR-4531	FADS2	1.57	9.67E-56	Biosynthesis of unsaturated fatty acids
miR-4306 miR-4644	TECR	1.18	4.31E-38	Biosynthesis of unsaturated fatty acids
miR-1253	HSD17B12	1.21	2.85E-23	Biosynthesis of unsaturated fatty acids
miR-4516 miR-4531	ACOX1	1.11	1.25E-21	Fatty acid degradation, Biosynthesis of unsaturated fatty acids
miR-29a-3p	LPL	1.31	1.91E-17	PPAR signalling pathway
miR-4698	SORBS1	2.48	8.84E-12	PPAR signalling pathway
miR-3202	RXRG	3.45	1.77E-09	PPAR signalling pathway
miR-4306 miR-4644 miR-146b-5p miR-4698	BCAT2	1.09	2.23E-08	Valine, leucine and isoleucine degradation

Table 22 KEGG pathways enriched in brown versus white adipocytes with p value between 1x10^{-6} and 1x10^{-8}

miRName down	Target up			KEGG name (p value 1x10^{-6}≤ p ≤1x10^{-8})
miR-4306 miR-4644	SCARB1	2.38	2.28E-107	Aldosterone synthesis and secretion
miR-4436b-3p miR-29a-3p	ATP1B1	2.25	8.43E-59	Adrenergic signaling in cardiomyocytes
miR-4306 miR-5584-5p	ADCY6	1.54	5.08E-48	Aldosterone synthesis and secretion, Adrenergic signaling in cardiomyocytes, Vascular smooth muscle contraction
miR-4436-3p	MRVI1	5.45	2.34E-42	Vascular smooth muscle contraction
miR-4436b-3p miR-29a-3p miR-196a-5p miR-1253 miR-1261	CALM3	1.32	4.66E-42	Aldosterone synthesis and secretion, Adrenergic signaling in cardiomyocytes, Vascular smooth muscle contraction
miR-29a-3p miR-1253	CAMK1D	2.97	3.12E-35	Aldosterone synthesis and secretion
miR-4516 miR-4531	PPP2R5D	1.25	3.26E-34	Adrenergic signaling in cardiomyocytes
miR-4516	PRKACA	1.32	5.48E-31	Aldosterone synthesis and secretion, Adrenergic signaling in cardiomyocytes, Vascular smooth muscle contraction
miR-196a-5b	PPP1R12B	1.43	3.68E-27	Vascular smooth muscle contraction
miR-29a-3p miR-3611	BDH1	2.01	4.60E-20	Butanoate metabolism
miR-4516	CACNB2	3.61	3.56E-16	Adrenergic signaling in cardiomyocytes
miR-10a-3p	PLCB1	1.39	3.82E-16	Aldosterone synthesis and secretion, Adrenergic signaling in cardiomyocytes Vascular smooth muscle contraction
miR-4698	L2HGDH	1.02	1.58E-15	Butanoate metabolism
miR-29a-3p miR-4531	CREB5	1.13	6.07E-15	Aldosterone synthesis and secretion, Adrenergic signaling in cardiomyocytes
miR-3202	ADCY1	1.52	7.90E-15	Aldosterone synthesis and secretion, Adrenergic signaling in cardiomyocytes, Vascular smooth muscle contraction
miR-3202	BDH2	1.17	2.81E-14	Butanoate metabolism
miR-4306 miR-4644	PLA2G2F	5.47	9.13E-14	Vascular smooth muscle contraction

Table 23 KEGG pathways enriched in brown versus white adipocytes with p value between $1x10^{-4}$ and $1x10^{-6}$

miRName (hsa-miR)	Target up	Log2 (FC)	Adj.pVal	KEGG name (p value $1x10^{-4} \leq p \leq 1x10^{-6}$)
miR-29a-3p	COL11A1	3.92	1.29E-247	Protein digestion and absorption
miR-29a-3p miR-222-3p miR-5584-5p miR-221-3p miR-4698	PPARGC1A	5.87	9.28E-242	Huntington's disease, Glucagone signaling pathway
miR-4436-3p miR-29a-3p miR-222-3p miR-221-3p	MAPK10	4.71	4.71E-154	cAMP signaling pathway, Huntington disease
miR-4726-5p miR-4698	PDE1B	2.7	2.70E-151	Huntington's disease, Renin secretion
miR-4698	AOC3	3.58	4.07E-147	beta-Alanine metabolism
miR-4306	AR	8.93	4.24E-136	Oocyte meiosis
miR-4698	FOXO1	2.6	1.06E-126	Glucagon signaling pathway
miR-29a-3p miR-3611	COL4A4	4.17	2.37E-120	Protein digestion and absorption
miR-1253	CDC25C	2.48	1.09E-71	Synthesis and degradation of ketone bodies
miR-1253	PDE5A	4.86	2.37E-64	cGMP-PKG signaling pathway
miR-29a-3p miR-196a-5p	COL1A2	2.53	1.95E-52	Protein digestion and absorption
miR-29a-3p	OXTR	3.35	1.93E-51	cAMP signaling pathway, Huntington disease
miR-204-3p	KCNE3	3.03	1.66E-50	Protein digestion and absorption
miR-3611 miR-4698	DMD	2.19	1.89E-49	Dilated cardiomyopathy
miR-4726-5p	PKIA	1.92	7.70E-49	Tryptophan metabolism
miR-29a-3p	COL5A1	2.16	1.38E-46	Protein digestion and absorption
miR-4436b-3p	CCNE1	2.47	1.10E-44	Synthesis and degradation of ketone bodies
miR-196a-5p	PDGFRA	1.5	8.16E-42	Calcium signaling pathway
miR-29a-3p	GNG2	1.72	1.02E-37	Alcoholism
miR-29a-3p	COL5A3	1.24	2.09E-36	Protein digestion and absorption
miR-29a-3p	TNFRSF1A	1.31	3.17E-36	Alzheimer's disease
miR-146b-5p	PHKB	1.62	1.06E-33	Huntington's disease
miR-3611	TSHR	4.63	3.21E-32	cAMP signaling pathway
miR-29a-3p	NFATC4	2.23	1.86E-31	cGMP-PKG signaling pathway
miR-146b-5p	MAPT	4.53	2.65E-30	Protein digestion and absorption
miR-4531	RAC3	2.23	7.89E-29	cAMP signaling pathway
miR-4436-3p miR-10a-3p miR-4698 miR-1261	MEF2C	2.1	9.61E-28	cGMP-PKG signaling pathway
miR-29a-3p	COL21A1	4.09	7.31E-25	Protein digestion and absorption
miR-4778-5p miR-4484 miR-29a-3p miR-4726-5p	DAG1	1.03	7.91E-25	Dilated cardiomyopathy
miR-146b-5p	FAXDC2	2.04	1.53E-20	Steroid biosynthesis

Continuing table 24				
miRName (hsa-miR)	**Target up**	**Log2 (FC)**	**Adj.pVal**	**KEGG name (p value $1x10^{-4} \leq p \leq 1x10^{-6}$)**
miR-4306 miR-29a-3p miR-4531 miR-4698 miR-196a-5p	COL1A1	2.5	2.33E-18	Protein digestion and absorption
miR-4516	DHCR7	1.27	2.82E-18	Steroid biosynthesis
miR-29a-3p	DRD1	6.51	9.59E-18	cAMP signaling pathway
miR-196a-5p	COL24A1	2.68	1.78E-17	Protein digestion and absorption
miR-29a-3p	ELN	3.61	2.25E-16	Protein digestion and absorption
miR-4778-5p	PTCH1	1.98	2.22E-15	cAMP signaling pathway
miR-29a-3p	COL6A3	1.1	2.57E-14	Protein digestion and absorption
miR-4726	ITPKC	1.01	5.79E-13	Calcium signaling pathway
miR-1253	PTGER4	1.98	7.24E-13	Renin secretion
miR-204-3p	RPS6KA1	1	1.55E-12	Oocyte meiosis
miR-29a-3p	COL4A3	2.97	3.57E-11	Protein digestion and absorption
miR-3915 miR-4698	SNAP25	3.16	1.13E-08	Insulin secretion
miR-4698	SOX9	1.14	1.48E-06	cAMP signaling pathway
miR-29a-3p miR-4531 miR-711	COL4A5	1.46	1.94E-05	Protein digestion and absorption
miR-3202 miR-29a-3p miR-4726-5p	PDGFRB	1.03	5.73E-04	Calcium signaling pathway

Table 24 KEGG pathways enriched in brown versus white adipocytes with p value between $1x10^{-2}$ and $1x10^{-4}$

miRName down	Target up	Gene Log2(FC)	Gene Adj.pval	KEGG name (p value $1x10^{-2} \leq p \leq 1x10^{-4}$)
miR-4698	LEPR	3.97	1.59E-259	AMPK signaling pathway, Non-alcoholic fatty liver disease (NAFLD), Adipocytokine signaling pathway
miR-711	DAAM2	4.97	3.04E-257	Wnt signaling pathway
miR-4698	PRKAR2B	3.6	6.14E-237	Histidine metabolism
miR-146b-5p	SESN3	3.65	9.71E-208	p53 signaling pathway
miR-3202	SFRP1	5.83	3.24E-137	Wnt signaling pathway
miR-29a-3p	CNR1	6.17	3.41E-120	Axon guidance
miR-4436b-3p	MLXIPL	2.27	7.07E-109	Insulin resistance, Non-alcoholic fatty liver disease (NAFLD)
miR-4484 miR-222-3p miR-4698	AXIN2	4.76	2.88E-99	p53 signaling pathway, Inflammatory mediator regulation of TRP channels
miR-1261	MITF	4.47	1.02E-92	Pathways in cancer
miR-4306 miR-222-3p miR-221-3p	SLC4A4	2.95	9.32E-86	Proximal tubule bicarbonate reclamation, Bile secretion
miR-4531	TBC1D4	2.2	6.82E-72	Insulin resistance
miR-29a-3p	GSTA4	2.57	8.99E-72	Glutathione metabolism
miR-222-3p miR-221-3p miR-196a-5p	CDKN1B	1.96	2.53E-69	Cell cycle, Inflammatory mediator regulation of TRP channels, AGE-RAGE signaling pathway in diabetic complications
miR-4698	ENPP1	2.3	4.61E-68	Starch and sucrose metabolism
miR-196a-5p	GYG2	3.14	4.74E-68	Starch and sucrose metabolism
miR-29a-3p	GPAM	2.5	6.15E-67	Glycerolipid metabolism
miR-3915 miR-3202 miR-4698	PPARGC1 B	2.88	2.79E-51	Insulin resistance
miR-3202	PLXNA4	2.91	2.33E-48	Pathways in cancer
miR-3915	G6PD	1.57	2.43E-46	Glutathione metabolism
miR-3202 miR-4726-5p	SSH2	1.5	5.54E-43	Axon guidance
miR-4778-5p miR-4698	ABCA12	3.12	7.69E-43	ABC transporters
miR-4306 miR-4644 miR-29a-3p miR-4531	CCND2	2.09	2.30E-40	Focal adhesion, Cell cycle, p53 signaling, Wnt signaling pathway
miR-4306 miR-146b-5p	FLOT2	1.54	1.01E-33	Insulin signaling pathway
miR-29a-3p	LEP	2.27	4.72E-32	AMPK signaling pathway, Thyroid hormone synthesis, Adipocytokine signaling pathway
miR-3611	TCF7L1	1.96	1.75E-29	Wnt signaling pathway, Inflammatory mediator regulation of TRP channels
miR-29a-3p	ASIC1	2.57	4.43E-28	Inflammatory mediator regulation of TRP channels
miR-4306 miR-4644	ABCG4	4.7	9.38E-27	ABC transporters
miR-4698	PCYOX1	1.24	5.83E-26	Terpenoid backbone biosynthesis
miR-29a-3p	DPYSL2	1.16	4.10E-24	Pathways in cancer
miR-4698	JAK2	1.41	5.92E-24	Adipocytokine signaling pathway AGE-RAGE signaling pathway in diabetic complications

Continuing table 25				
miRName down	**Target up**	**Gene Log2(FC)**	**Gene Adj.pval**	**KEGG name (p value $1x10^{-2} \leq p \leq 1x10^{-4}$)**
miR-4306 miR-3202 miR-4644 miR-4726-5p	EFNB1	1.28	1.17E-21	Axon guidance
miR-4436-3p miR-29a-3p	VCL	1.23	2.08E-21	Focal adhesion
miR-5584-5p	MAGI3	1.78	8.83E-20	Rap1 signaling pathway
miR-4698	TBL1XR1	1.11	8.16E-19	Wnt signaling pathway
miR-146b-5p miR-204-3p	SEMA3G	1.14	1.61E-18	Axon guidance
miR-29a-3p	DAAM1	1.04	1.20E-17	Wnt signaling pathway
miR-4778-5p miR-4698	FZD5	1.21	6.32E-16	Wnt signaling pathway, Inflammatory mediator regulation of TRP channels
miR-4436b-3p	SEMA4F	1.29	7.67E-16	Pathways in cancer
miR-29a-3p	TUBB2A	1.21	2.93E-15	Gap junction
miR-29a-3p	TUBB2B	2.18	6.13E-15	Gap junction
miR-204-3p	COLGALT2	2.7	1.06E-12	Lysine degradation
miR-29a-3p	DNM3	2.53	2.55E-11	Endocrine and other factor-regulated calcium reabsorption
miR-4698	ABCB10	1.1	9.33E-11	ABC transporters
miR-3915	NKD2	4.53	5.80E-10	Wnt signaling pathway
miR-3202	PFKFB4	1.23	6.60E-10	AMPK signaling pathway
miR-4436b-3p miR-4726-5p	TRAF1	1.19	7.77E-10	Inflammatory mediator regulation of TRP channels
miR-29a-3p	CTNNBIP1	1.17	1.43E-09	Wnt signaling pathway
miR-196a-5p	RASGRP1	2.39	6.49E-09	Inflammatory mediator regulation of TRP channels
miR-3202 miR-4726-5p	EFNA3	1.65	1.37E-08	Axon guidance, Rap1 signaling pathway
miR-29a-3p miR-146b-5p miR-3611	RARB	2.62	1.27E-07	Pathways in cancer
miR-4436b-3p	SEMA4G	1.71	2.11E-06	Axon guidance
miR-146b-5p	WNT3	1.25	4.15E-06	Wnt signaling pathway, Pathways in cancer
miR-4698	TGFA	1.43	4.37E-05	Inflammatory mediator regulation of TRP channels
miR-1261	FZD3	1.5	6.38E-05	p53 signaling pathway, Inflammatory mediator regulation of TRP channels, Pathway in cancer
miR-4484	FGFR3	1.96	2.12E-04	Inflammatory mediator regulation of TRP channels, Axon guidance
miR-222-3p miR-221-3p	CDKN1C	1.47	3.87E-04	Cell cycle
miR-4726-5p	RGS14	1.29	1.04E-03	Axon guidance
miR-29a-3p	RND1	1.28	9.80E-03	Pathways in cancer
miR-3202	EFNB3	1.13	2.42E-02	Axon guidance

Table 25 KEGG pathways enriched in white vs brown adipocytes with p value ≤1x10^{-8}

miRName up	Target down	Gene Log2(FC)	Gene Adj.pval	KEGG name (p value ≤1x10^{-8})
miR-143-3p	PTGS2	-6.35	0.00E+00	TNF signaling pathway
miR-513a-5p	CD44	-2.83	8.34E-268	Proteoglycans in cancer
miR-513a-5p	ITGA2	-4.25	6.09E-224	Proteoglycans in cancer
miR-378e miR-378f miR-378c miR-378d miR-378b miR-378i miR-378h	BMP2	-5.41	8.28E-202	Cytokine-cytokine receptor interaction
miR-4328	WNT5A	-3.8	4.09E-158	Proteoglycans in cancer
miR-4328	PDGFA	-3.59	8.92E-75	Cytokine-cytokine receptor interaction
miR-143-3p	PLAUR	-2.39	6.03E-68	Proteoglycans in cancer
miR-513a-5p	ANTXR2	-1.27	8.39E-41	NOD-like receptor signaling pathway
miR-513a-5p miR-145-5p	PXN	-1.07	7.96E-28	Proteoglycans in cancer
miR-513a-5p	HBEGF	-1.49	6.72E-27	Proteoglycans in cancer
miR-143-3p	ITPR1	-1.1	2.07E-25	NOD-like receptor signaling pathway and proteoglycans in cancer
miR-4511	CXCL16	-2.13	5.05E-24	Cytokine-cytokine receptor interaction
miR-513a-5p miR-4328 miR-4511 miR-145-5p	NRAS	-1.08	9.42E-24	Proteoglycans in cancer
miR-513a-5p miR-4511	XIAP	-1.09	8.25E-22	NOD-like receptor signaling pathway
miR-378a-3p miR-378e miR-378f miR-378c miR-378d miR-378b miR-378i miR-378h miR-145-5p	IGF1R	-1.06	6.73E-21	Proteoglycans in cancer
miR-136-5p miR-378g	ELK1	-1	4.43E-16	Proteoglycans in cancer
miR-4328 miR-145-5p	FLT1	-2.39	1.46E-10	Cytokine-cytokine receptor interaction
miR-4328	DAB2IP	-1.05	2.88E-10	TNF signaling pathway
miR-513a-5p	PIK3CD	-1.29	1.62E-09	TNF signaling pathway, Proteoglycans in cancer
miR-513a-5p	CAMK2A	-3.92	3.97E-09	Proteoglycans in cancer
miR-4511	TIAM1	-1.01	3.16E-05	Proteoglycans in cancer
miR-4511	OAS3	-1.18	1.40E-04	NOD-like receptor signaling pathway

Table 26 KEGG pathways enriched in white vs brown adipocytes with p value between $1x10^{-4}$ and $1x10^{-6}$

miRName up	Target down	Gene Log2(FC)	Gene Adj.pval	KEGG name (p value $1x10^{-4} \leq p \leq 1x10^{-6}$)
miR-4511	HRH1	-3.4	1.64E-106	Inflammatory mediator regulation of TRP channels
miR-4511	TBX3	-2.4	3.19E-97	Signaling pathways regulating pluripotency of stem cells
miR-4328	FGF7	-2.9	1.86E-90	Pathways in cancer
miR-4511	FGF5	-3.5	3.12E-88	Pathways in cancer
miR-513a-5p	RUNX1	-1.7	1.43E-72	Pathways in cancer, transcriptional misregulation in cancer
30e.5p	JARID2	-2.2	1.76E-49	Signaling pathways regulating pluripotency of stem cells
miR-378g	SKIL	-1.9	3.28E-41	Signaling pathways regulating pluripotency of stem cells
miR-145-5p	SMAD3	-1.5	1.14E-34	Pathways in cancer, AGE-RAGE signaling pathway in diabetic complications, signaling pathways regulating pluripotency of stem cells and TGF-beta signaling pathway
miR-143-3p	FGF1	-1.5	2.46E-23	Pathways in cancer
miR-378e miR-378f miR-378c miR-378d miR-378b miR-378i miR-378h	REST	-1	3.47E-17	Signaling pathways regulating pluripotency of stem cells
miR-4328	PTGER2	-1.3	8.09E-14	Inflammatory mediator regulation of TRP channels, pathways in cancer
miR-513a-5p	HOXA10	-1	4.79E-13	Transcriptional misregulation in cancer
miR-513a-5p	PRKCH	-1.2	5.04E-08	Inflammatory mediator regulation of TRP channels
miR-513a-5p miR-4328 miR-378g miR-33b-5p	RUNX1T1	-1.3	1.89E-07	Pathways in cancer, transcriptional misregulation in cancer

Table 27 KEGG pathways enriched in white vs brown adipocytes with p value between $1x10^{-2}$ and $1x10^{-4}$

miRName up	Target down	Gene Log2(FC)	Gene Adj.pval	KEGG name (p value $1x10^{-2} \leq p \leq 1x10^{-4}$)
miR-513a-5p miR-4328 miR-33b-5p	SEMA7A	-3.2	8.82E-127	Axon guidance
miR-513a-5p miR-143-3p	GFPT2	-1.6	1.40E-71	Amino sugar and nucleotide sugar metabolism
miR-4328	SEMA3A	-3.83	1.22E-64	Axon guidance
miR-513a-5p miR-4328	GRB10	-1.65	1.19E-62	mTOR signaling pathway
miR-4328	EGR2	-4.34	7.49E-49	Hepatitis B HTLV-I infection
miR-513a-5p	RAPGEF3	-3.97	1.02E-48	Rap1 signaling pathway, salmonella infection
miR-513a-5p miR-143-3p miR-4511	ABL2	-2.28	2.91E-44	Ras signaling pathway
miR-145-5p	SIRPA	-1.56	4.41E-41	Osteoclast differentiation
miR-33b-5p miR-145-5p	RASA1	-1.56	5.60E-39	Axon guidance, MAPK signaling pathway
miR-378a.5p	NFATC2	-4.29	3.42E-31	Axon guidance Hepatitis B HTLV-I infection, osteoclast differentiation
miR-513a-5p	WDR43	-1.09	4.15E-29	Ribosome biogenesis in eukaryotes
miR-378g	NOTCH2	-1.15	5.08E-29	Dorso-ventral axis formation
miR-143-3p	RAB7A	-1.02	4.83E-28	Rap1 signaling pathway, salmonella infection ,tuberculosis
miR-513a-5p	ADORA2B	-1.46	1.10E-27	Rap1 signaling pathway
miR-513a-5p miR-4328 miR-143-3p	LIMK1	-1.29	8.72E-26	Axon guidance
miR-513a-5p	RICTOR	-1.11	4.95E-23	mTOR signaling pathway
miR-145-5p	RASA2	-1.55	1.61E-21	MAPK signaling pathway
miR-513a-5p	SESN2	-1.1	1.11E-14	mTOR signaling pathway
miR-513a-5p	FOSB	-3.69	1.15E-14	Osteoclast differentiation
miR-145-5p	CPEB1	-2.29	2.35E-13	Amoebiasis
miR-4511	EPHA5	-4.99	2.79E-09	Axon guidance

5.2 Discussion

As the nature of human brown adipocytes is still poorly understood, we performed mRNA sequencing and miRNA array analysis on human brown and white adipocytes to explore their differential gene and miRNA expression and KEGG enrichment. This allowed us to identify 2463 genes and 20 miRNAs upregulated in brown versus white adipocytes and 1733 genes and 29 miRNAs upregulated in white versus brown adipocytes. The KEGG enrichment analysis reflected the nature of brown adipocytes highlighting the pathways that are involved in the development and functioning of the two types of cells. Integrating the data from miRNA array and mRNA sequencing analysis we identified miRNAs that potentially control the KEGG pathways differentially enriched between brown and white adipocytes by targeting the associated genes. In this section the miRNAs targeting genes of particular interest or with the highest number of predicted target associated to the top differentially expressed pathways will be discussed.

5.2.1 *miRNAs downregulated in brown adipocytes potentially involved in the top pathways enriched in brown adipocytes*

The top pathways enriched in brown versus white adipocytes were: fatty acid degradation, biosynthesis of unsaturated fatty acids, propanoate metabolism, citrate cycle, pyruvate metabolism, valine leucine and isoleucine degradation and PPAR signalling. In total 10 miRNAs downregulated in brown versus white adipocytes (miR-4516, miR-4531, miR-4306, miR-4698, miR-4644, miR-146b.5p, miR-3915, miR-1253, miR-29a-3p and miR-3202) were predicted to control some of the genes associated to these pathways.

Of these miRNAs, miR-4698 was predicted to target a total of twenty four genes associated to the pathways enriched in brown adipocytes with a significant p value, four of which were among the top ones. Among these genes there was (SCD). This enzyme, as previously described, participates in de novo lipogenesis, the second main source of fatty acid of brown adipocytes [77]. This gene was also predicted to be targeted by miR-4306. Another two important enzymes involved in fatty acid degradation are acyl- CoA oxidase 1 (ACOX1) and fatty acid desaturase 2 (FADS2). Both were predicted to be targeted by miR-4516 and miR-4531. Therefore, the downregulation of these miRNAs in brown adipocytes may be very important to allow the high oxidative activity typical of BAT.

MiR-29a-3p was predicted to target the highest number of genes associated with the significant pathways enriched in brown adipocytes. Accordingly to the literature, miR-29 was predicted to target LPL [387], the enzyme responsible for FAs uptake from the blood stream, the main source of energy of brown adipocytes. Even if LPL is important in white adipocytes as well, its expression is known to be increased during high metabolic activity, which would justify its higher expression in brown versus white adipocytes. Interestingly, among the targets of miR-29a-3p there was also PGC1α. MiR-29a-3p might play an important role by repressing a large number of genes involved in brown adipogenesis and metabolism in order to promote the white phenotype.

Finally, we identified miR-3915 as a potential repressor of ADIPOQ, the gene encoding adiponectin. This adipokine, presenting an anti-inflammatory function, and promoting lipid oxidation protects against obesity and associated insulin resistance [70-72]. As levels of circulating adiponectin are reduced in obese subjects [73] it would be interesting to investigate whether the expression of this miRNA is altered in adipose tissue of obese subjects.

5.2.2 *MiRNAs upregulated in brown versus white adipocytes potentially involved in suppression of the genes associated the top pathways enriched in white adipocytes*

The top pathways enriched in white adipocytes associated to the downregulated genes in brown adipocytes were: TNFα signalling pathway, proteoglycans in cancer, cytokine-cytokine receptor interaction and NOD-like receptors signalling. We identified six miRNAs (miR-143-3p, miR-4328, miR-513a-3p, miR-145 and miR-4511) plus the members of the miR-378 family, to potentially control these pathways by targeting some of the associated genes.

MiR-513a-3p was predicted to target the highest number of genes (9) involved in these pathways. Interestingly, it was found to potentially target both CD44 and ITGA2, which encodes integrin-α2 subunit. CD44 and integrins are involved in cell motility [122, 388]. CD44 was reported to play a role in gonadal WAT remodelling as a subpopulation of adipose-precursors expressing PDGFRα and CD44 started proliferating after being attracted by recruited macrophages overexpressing osteopontin [389]. As both CD44 and integrins were found to be involved in insulin resistance [125, 128] miR-513a-3p may play an important role in regulating these genes in obesity. Another predicted target of miR-513a-3p potentially involved in obesity is XIAP (X-linked inhibitor of apoptosis).

XIAP was found upregulated in squirrel adipose tissue during hibernation, when the respiratory rate is dramatically reduced, to prevent hypoxia-induced apoptosis [390]. This gene was predicted to be also targeted by miR-4511. Another interesting potential target of miR-513a-3p HB-EGF (Heparin-binding EGF-like growth factor) which was found to be involved in cellular plasticity and to promote brown-like phenotype in mouse fibroblasts [391].

Also miR-4511 presented a high number of potential targets (5) associated to the pathways enriched in white adipocytes. Among its predicted targets, besides XIAP, there is Chemokine (C-X-C motif) ligand 16 (CXCL16). This membrane-bound chemokine, in the soluble form, attracts immune cells expressing Chemokine (C-X-C Motif) Receptor 6 (CXCR6) such as natural killer cells, CD8T and Th1-polarized T cells [392, 393]. CXCL16 was also found to have antimicrobial action against Staphylococcus aureus and Escherichia coli [394] therefore, its activation could be related to toll-like receptors upon LPS stimulation and play a role in the HFD-induced inflammation.

Finally, miR-4328 could be another miRNA with important functions in obesity. Indeed, among its predicted targets there were Wnt5α and PDGFA. Wnt5α is a non-canonical Wnt protein as it triggers β-catenin–independent signalling activation. Importantly, it was found to promote adipose tissue inflammation and insulin resistance in obesity [395]. PDGFA was found to promote adipose stem cell self-renewal via PI3K/AKT2 (phosphoinositide 3-kinase/protein kinase B) in dermal WAT [396]. PDGFA is increased in subcutaneous WAT of obese compared to lean and may be involved in obesity-induced fibrosis by activating the pro-fibrotic pathway mediated by PDGFRα in $CD9^{high}$ PDGFRα+ progenitors [397].

Chapter 6 – General Discussion

6.1 Discussion

The incidence of obesity and associated metabolic disorders constantly increases worldwide [398-400] and challenges the health care systems. BAT, with its ability to burn energy and counteract obesity has become a candidate target for the development of new treatments against metabolic disorders. An increasing number of studies aim to investigate the complex network among the metabolic organs in order to understand the mechanisms underlying energy homeostasis balance. MiRNAs are potent regulator of gene expression and, as previously discussed, many of them have been identified as modulators of adipogenesis and adipose metabolism, some miRNAs are known to promote or inhibit differentiation, some others to enhance the development of a specific adipose phenotype. Their potential ability to induce brown adipogenesis or white transdifferentiation into brite adipocytes has attracted scientific interest and novel adipose miRNAs are constantly identified. However, there are sometimes discrepancies among studies, mainly due to the utilization of different types of adipose models, but also because the effect of one miRNA can vary depending on the stage of the differentiation. Cell maturation requires an alteration of the transcriptome. MiRNAs are known to regulate these changes, but recent studies have shown that genes in turn regulate miRNA function [227-229]. Moreover, several miRNAs have been identified as inhibitors of adipogenesis even though they can be upregulated during differentiation. This is the case of let-7 and miR-488 in 3T3-L1 cells [310, 401]. This indicates that differentiation is not simply a process where all the players act towards one single direction, but is rather a complex mechanism where the balance of contrasting forces is shifted towards maturation, as this last never relies on one single factor. Therefore, the function of a miRNA taken in isolation might be considered as anti-adipogenic, but contextualized into a system where the balance is shifted towards differentiation by other factors, it may be relevant for the definition of one adipose phenotype over another, such as brown, beige and white. This could be true for miR-138-5p, which, as previously discussed, could either inhibit differentiation or promote the white phenotype by suppressing brown gene expression, depending on the stage of differentiation. The hypothesis that the environment defines the final function of a given miRNA and hence its tissue specificity is further supported by the case of miR-378a-3p, which promotes BAT but not WAT expansion [282], even though it is overexpressed in both brown and white adipocytes during differentiation.

Similarly, miR-196a-5p promotes the beige phenotype in white adipocytes by targeting HOXC8 but had no evident effect in BAT [302]. Additionally, miRNAs could be upregulated in order to be secreted into the extracellular environment and explicate their function in distal cells. For example, Let-7 inhibits adipogenesis by downregulating high-mobility group AT-hook 2 (HMGA) [401]. This miRNA is also known to promote angiogenesis [402, 403], therefore, despite its anti-adipogenic function it might be upregulated during differentiation in order to be secreted and stimulate angiogenesis to support tissue expansion.

Another source of discrepancies among results from different studies is represented by the inconsistency of miRNA nomenclature and by the fact that the arm from which the miRNA of interest generates is not always specified [281]. Even though lead and passenger miRNA strands, when almost equally expressed, generally take part in similar processes, they can have opposite functions, therefore it is important to specify the strand of interest. One example is represented by miR-378a-3p and mir-378-5p, which, as previously mentioned, were found to have opposing effects on LDHA regulation [280]. Moreover, miRNAs with very similar sequences can target the same genes. Once again, miR-378 provides a good example. The members of miR-378 family, as also demonstrated in our results, are predicted to share many gene targets. In experiments where the effect of a miRNA is studied by its forced expression or deletion, the other members of the miRNA family should be taken into consideration, as they could be responsible for compensatory action. Additionally, having very similar but not equal sequences, their affinity for the same target might be different and it would be interesting to explore their combinatorial effect. This could help in predicting the effect of a secreted miRNA taken up by a different cell, where the expression of the members of the miRNA family might be different from the donor cell. The mechanism of function of miRNAs, as revealed by an increasing number of studies, is very complex and intricate. Many factors can interfere with miRNA effects. This can mask miRNA actions or lead to false results when performing experiments. The development of always more sophisticated bioinformatics algorithms and databases provides a potent tool for predicting miRNA functions. In particular, miRegulome (http://bnet.egr.vcu.edu/miRegulome), an online miRNA data and analysis repository, incorporates miRNA dynamics, upstream and downstream targets and the regulatory effect of chemicals on these targets [404].

Therefore, before approaching experimental miRNA studies, the usage of this type of tool, would be strongly recommended.

The importance of miRNAs in the cross-talk between adipose tissue and distal cells is further supported by the fact that in obesity levels of circulating miRNAs are altered compared to lean subjects. However, the majority of the studies on extracellular miRNA secreted by adipocytes mainly focused on mouse models or on analysis of blood samples, which does not allow to determinate which cellular component contributes to miRNA secretion. In this study, we identified miRNAs differentially secreted specifically by undifferentiated and differentiated brown and white adipocytes. Among these miR-322-5p, miR-10b, miR-103, miR-365-5p, miR-378a-3p and miR-196a-5p were selected and considered for further analysis. Even though only extracellular miR-378a-3p and miR-196a-5p showed consistent results across the adipose models, all these miRNAs could play an important role in cell-to-cell communication. Still poorly explored in adipogenesis, they have been reported to be involved in processes such as angiogenesis, insulin resistance inflammation and their secretion by adipocytes might be of relevant contribution in obesity and associated disorders. For instance, miR-365, in a study on HEK293 and HeLa cells inhibited IL-6 expression. Moreover, the miR-365 promoter presents consensus sites for NF-kB. This last in cooperation with Sp1 was found to highly upregulate miR-365 [405]. Our data show that miR-365 is more highly secreted by BAT/brown adipocytes in most of the adipose models and it would be interesting to investigate whether BAT-secreted miR-365 has any effect on inflammation and insulin resistance in obesity via regulating IL-6.

MiR-10b besides promoting angiogenesis [406, 407], and cell migration in several types of cancer [407-411], and was found to be induced by and to suppress IL-17 by targeting MAP3K7 [412]. IL-17 is required to maintain Th-17 immune cells functional activity against altered microbiota flora in the intestine upon HFD and IL-17 absence was reported to promote obesity [413]. To our knowledge, no studies have demonstrated the effect of miR-10b on IL-17 and consequently on Th-17 in adipose tissue and obesity. According to our results and previous studies, miR-103 is upregulated in adipocytes during differentiation in physiological conditions (table 15) but downregulated in obesity [414, 415]. TNFα was found to inhibit miR-103 expression [414]. RaeAnna et al., showed that miR-103 suppresses angiogenesis in a tumor environment by inhibiting non-

canonical DNA repair enzymes, three prime exonucleases (TREX) 1 and 2 in endothelial cells [416]. Whether miR-103 also inhibits angiogenesis in adipose tissue has not been proven yet. If this was the case, downregulation of miR-103 during inflammatory status in obesity might be a strategy adopted by the cells to prevent inhibition of angiogenesis and reduce the grade of obesity-induced hypoxia.

MiR-424 was found to be induced by hypoxic stimuli in endothelial cells and to prevent HIF-1α degradation by inhibiting expression of Cullin-2 [417], important in the ubiquitin ligase system [418]. MiR-424 was also reported to promote differentiation of the monocytes that infiltrate in atherosclerotic plaque sites by inhibiting miR-9, a repressor of differentiation [419]. Therefore, miR-424 could play an important role in sustaining inflammation and HIF-1α-induced fibrosis in obesity. As previously discussed miR-196a-5p, miR-378a-3p and miR-138-5p were predicted to target genes involved in inflammation fibrosis and angiogenesis, therefore all the aforementioned miRNAs may be implicated in obesity and associated dysfunctions. Some of them are predicted to share some gene targets and their effect could be different depending on the acceptor cell. For example, targeting HIF1α in BAT could result in impaired angiogenesis, while in WAT it could prevent adipose tissue fibrosis. PPARɣ expression in endothelial cells has an antiproliferative effect, hence it inhibits angiogenesis. Conversely, its expression in adipocytes induces expression of the pro-angiogenic factor VEGFA [114]. Therefore, a miRNA targeting PPARɣ has the potential to induce or inhibit angiogenesis, depending on the host cell. Most of the targets that we predicted in this study for miR-378a-3p, miR-196a-5p and miR-138-5p are expressed in different cell types, either in cellular components of the adipose tissue adipocytes included, or of other different organs. Our analysis also demonstrated that miRNAs are secreted both via incorporation into vesicles and in association to vesicle free system. The preference of one type of carrier over the other could implicate specificity of acceptor cell for miRNA delivery and this aspect together with the endocrine, autocrine and paracrine potential miRNA functions should be further investigated. As previously discussed, the properties of vesicle free system are still largely unknown. Moreover, so far the most explored vesicular miRNA carriers are exosomes, but a large variety of vesicles exist and they could be relevant as well in conferring specificity of miRNA delivery.

The mRNA sequencing and miRNA array analyses provided a large amount of information. In this study we have only discussed some of the novel miRNAs identified as potentially involved in brown and white adipogenesis/metabolism. We mainly focussed on the miRNAs that were predicted to target genes associated to the differentially enriched pathways between brown and white adipocytes falling in the most significant p value. However, we provided the full list of miRNAs targeting the genes associated to all the pathways identified and these can be used for future analysis as well. One of the limits of this analysis consists in the fact that it does not consider miRNAs targeting genes which level of expression remains unvaried or is only slightly reduced even though their translation into protein is inhibited [420, 421]. Therefore, each miRNA can target many other genes, besides the ones reported by us. Through the mRNA sequencing analysis, we also identified isoforms of genes that are differentially expressed between brown and white adipocytes, besides identifying novel genes. These will be considered in future work to verify whether the different isoforms of a gene can compete for miRNA interaction. Moreover, our findings could be integrated with total transcriptome analyses performed on human adipocytes by other groups, in order to further improve the knowledge on the nature of human adipocytes.

6.2 Next experimental steps

This study has provided many results that could be used as a starting point for future experiments that aim to improve the knowledge on miRNA function in adipocyte biology and their role in the cell-to-cell communication among adipocytes and the distal organs involved in maintaining the energy homeostasis balance. Here we list the next immediate steps in continuation of this work, that can constitute a possible initial approach.

Experimental validation of miRNA target identification

There exist different strategies to validate a predicted target of a determined miRNA, which have been reviewed in different publications [422-424]. The most direct way to check the actual activity of a miRNA on its predicted mRNA target would be to control the downstream production of the translated protein. In this study we particularly focussed on miR-196a-5p, miR-378a-3p and miR-138-5p for their potential role in cell to communication. As discussed in paragraphs these secreted miRNAs could have both

an autocrine and paracrine role, therefore, the effect of the miRNAs will be investigated in both adipocytes and endothelial cells blood vessels from adipose tissue. Specifically, in separate experiments, miR-196a will be exogenously expressed through miRNA transfection and knocked down using antisense miRNA (antagomiR) in adipocytes and endothelial cells. The protein and mRNA expression of TLR4, IKBA, HIF-1α and ADAM10 will be then analysed and compared to controls. If these genes are under the control of miR-196a their protein expression will be decreased after exogenous miRNA expression and increased after miRNA knock down. Measuring both mRNA and protein changes in these experiments will provide further information on the mechanism through which the miRNA inhibits gene expression. Indeed changes in the protein expression of the miRNA target and unvaried mRNA expression upon miRNA knock down or transfection would suggest that the miRNA induces gene silencing without mRNA degradation, providing further elucidation on miRNA mechanism of action. The same experiment will be performed for miR-138 and miR-378 with their respective targets (table 18) in both endothelial cells and adipocytes. With regard to the intracellular miRNAs identified in this study, as differentially expressed between brown and white adipocytes, we focussed on miR-513a-3p, miR-4511, miR-4328 miR-4698, miR-4516, miR-4531, miR-29a-3p and miR-3915 as they are novel miRNAs with potential function in adipocytes or because we identified targets that were not predicted before for these miRNAs, as discussed in paragraphs 5.1.4 and 5.2. For these miRNAs, the results obtained by the microRNA array analysis will be first validated through q-RT PCR to confirm their differential expression between human brown and white adipocytes. Afterwards, their predicted targets considered in this study, (paragraph 5.2) will be experimentally validated in adipocytes, as explained above.

Investigation on feedback regulation

In the cases where the miRNA target regulation is experimentally confirmed, the experiments will be repeated in the opposite direction. Therefore, to investigate whether the expression of a predicted target gene at both protein and mRNA level can induce or inhibit miRNA expression, in separate experiments, the target will be transfected into the target cell (adipocyte and/or endothelial cell) to force its expression or knocked down

using short interference RNAs. Alteration of miRNA expression will reveal the existence of positive/negative feedback regulation.

MiRNA transfer into recipient cells

To investigate whether the adipose miR-196a, miR-378 and miR-138 can be transferred into the hypothesised recipient cells, distal adipocytes and endothelial cells, and to test autocrine and paracrine action respectively, the function of the miRNA processor machine will be compromised in the acceptor cells by depleting or knocking down DICER in two different ways as explained below. This would induce the blockage of endogenous mature miRNA production, at least, of those miRNA which maturation relies on DICER activity. Subsequently, the cells will be incubated with conditioned media from adipocytes. Intracellular content of the miRNAs of interest and expression of their targets will be measured through qRT-PCR in both cells exposed to conditioned media and non-exposed cells. The target protein expression will be analysed by western blot. To assess adipose miRNA uptake in adipocytes the BAT DicerF/F Cre-LBD and subcutaneous WAT DicerF/F Cre-LBD cell lines will be employed. In the DNA of these cells, Dicer gene is flanked by loxP (lox) sites. These sequences are recognized by Cre recombinase enzyme which is fused to the ligand binding domain of the estrogen receptor (LBD ER). Only upon tamoxifen administration, Cre recombinase protein, previously confined in the cytoplasm, translocates to the nucleus where it catalyses recombination of the target DNA sequence flanked by lox in the same orientation [425]. In this way it will be possible to deplete Dicer only when required. Dicer ablation would be permanent and the cells could be exposed to conditioned media for a longer period of time, allowing the clearance of the cell from the pre-existing DICER protein. Moreover, it will be possible to explore the function of the miRNA uptaken miRNAs at different points of the differentiation process, that in total takes around 10 days. Alternatively, if such a cell system is not available, such as in our case for endothelial cells, transient DICER knock down will be obtained using siRNAs and the protein DICER product will be monitored.

Effect of multiple miRNA interaction on target genes

Through the use of the Cre recombinase models, the interaction of multiple miRNAs predicted to target the same gene will be evaluated. In particular, after depleting dicer, via tamoxifen administration, the cells will be co-transfected with different combinations of miRNAs and the expression of the target will be assed via RT qPCR and western blot. This will allow us to identify the presence of miRNA competitors. The choice of the miRNAs will be based on the data obtained through the integration of microRNA array-mRNA seq and the results that will be provided from the experiments described before.

Active release of miRNAs

Inducible vesicle secretion is dependent on intracellular Ca^{2+} [237]. Intracellular Ca^{2+} concentration is regulated by purinergic receptors in response to extracellular ATP [238]. Brown adipocytes response to ATP through multiple P2 receptors. Brown adipocytes have been found to be positive for 9 purinergic receptor mRNAs (P2Y2, P2Y6, P2Y12, P2X1, P2X2, P2X1, P2X2, P2X3, P2X4, P2X5 and P2X7) [426]. After testing the presence of these receptors in both brown and white adipocytes, the involvement of these purinergic receptor in the process of miRNA-vesicle secretion will be investigated. P2 receptor expression will be inhibited using single or a combination of specific short interference RNA (siRNA) for receptor silencing. Afterwards, the expression of the miRNAs that will give us the best results in the experiments previously described for testing miRNA transfer into recipient cells, will be measured. both in the medium and in the ultracentrifugation pellet. This experiment will be performed in the presence and absence of Isoproterenol/CL, to investigate whether the ability of ß-adrenergic stimulation to directly affect miR-196a-5p observed in this study, involves these receptors.

6.3 Conclusion and future prospective

This study allowed us to conclude that undifferentiated and differentiated brown adipocytes present differential profiles of secreted miRNAs. The analysis of the intracellular and extracellular expression of the selected miRNAs in different adipose

models revealed that miRNA secretion is not a passive process but rather actively controlled. The use of different adipose models also revealed that the expression of intracellular and extracellular miRNAs in adipose tissue does not reflect the patterns of miRNA expression of the corresponding adipocytes. Moreover, among the miRNAs selected, miR-10b, miR-322/424, miR-103, miR-365, miR-378a-3p and miR-196a, only the last two showed a consistent pattern of extracellular expression across adipose models, suggesting that they play important roles in adipose cross-talk to be conserved across species. As mouse and human adipocytes displayed differences in miRNA expression, a miRNA PCR array was performed on media samples from human adipocytes and miR-138-5p was identified as the most differentially secreted miRNA between human brown and white adipocytes. By predicting miRNA targets through bioinformatics tools and correlating our results with scientific studies in the literature we hypothesised the potential functions of miR-378a, miR-196a and miR-138-5p. In particular, different types of evidence led us to think that miR-378a-3p is potentially involved in BAT angiogenesis and ECM remodelling by targeting VEGFA and Sulf1. MiR-196a-5p may play an important role in inflammation, ECM remodelling and adipose tissue fibrosis in obesity as it is predicted to target ADAM10, HIF1α, TLR4 and IKBA. Finally, miR-138-5p, the unique miRNA identified as significantly differentially secreted miRNAs between human brown and white adipocytes, could be involved in inflammation and the associated insulin resistance in obesity. The analysis of miRNA depletion from media by ultracentrifugation revealed that all the miRNAs tested are secreted both via incorporation into vesicles and in association with vesicle free systems. As miR-378a-3p and miR-10b-5p were mostly associated with vesicle free systems while the other miRNAs showed equal distribution between the types of carriers we speculate that vesicle-free systems are important miRNA carriers as much as vesicles and their characteristics should be further explored. We found out that ß-adrenergic stimulation can affect miRNA expression and secretion, probably due to secondary events triggered by the stimuli, while, miR-196a-5p secretion could be under its direct control. The ß-adrenergic agonist CL affects the modality by which miRNAs are secreted even though it can favour one carrier over another one depending on the miRNAs. Finally, through the microRNA array and mRNA sequencing analysis, we identified 2463 genes and 20 miRNAs upregulated in brown versus white adipocytes and 1733 genes and 29 miRNAs

upregulated in white versus brown adipocytes. This analysis allowed us to identify poorly studied or novel miRNAs that potentially control the most significant pathways differentially enriched between brown and white adipocytes. Among the significantly downregulated miRNAs in brown versus white adipocytes we highlighted miR-513a-3p, miR-4511 and miR-4328. While, among the significantly upregulated miRNAs in brown versus white we highlighted miR-4698, miR-4516, miR-4531, miR-29a-3p and miR-3915.

In conclusion, these results provide new insight and further work is warranted to more precisely define miRNA roles in adipocytes and cells that take up adipocyte-secreted miRNAs. Experimental tests will be needed to prove that miRNAs and their predicted target can actually interact. Further investigation of the mRNAs highlighted in this study should be done in consideration of the language dictated by the MRE sequence miRNA interactions between miRNAs and potential competitors. Alternative mechanisms for miRNA production should be investigated, as well as the potential additional functions of the genes involved in miRNA biosynthesis/maturation. As the adipose models in this study were representative of healthy adipocytes, further analysis should be performed in models of obesity to investigate if, the expression of the miRNAs identified in this study, is different between adipocytes from obese and lean subjects/mice. More attention should be directed towards the different miRNA carriers and their characteristics, as knowledge is still lacking on the modality by which miRNAs are taken up. All together our data provided encouraging results for the importance of further investigating miRNAs for future development of treatments against metabolic disorders.

References

1. Cinti, S., *The adipose organ.* Prostaglandins Leukot Essent Fatty Acids, 2005. **73**(1): p. 9-15.
2. Collins, S., E. Yehuda-Shnaidman, and H. Wang, *Positive and negative control of Ucp1 gene transcription and the role of beta-adrenergic signaling networks.* Int J Obes (Lond), 2010. **34 Suppl 1**: p. S28-33.
3. Skurk, T., et al., *Relationship between adipocyte size and adipokine expression and secretion.* J Clin Endocrinol Metab, 2007. **92**(3): p. 1023-33.
4. Adamczak, M. and A. Wiecek, *The adipose tissue as an endocrine organ.* Semin Nephrol. **33**(1): p. 2-13.
5. Meritxell Rosell, M.K., Andrea Fortini, Anthony Okolo, Yi-Wah Chan, Evanthia Nikolopoulou, Steven Millership, Matthew E Fenech, David MacIntyre, Jeremy O Turner, Jonathan D Moore, Edith Blackburn, William J Gullick, Saverio Cinti, Giovanna Montana, Malcom G Parker, Mark Christian, *Cold-induced transcriptional changes in gene expression nd response to cold exposure in mice.* 2014.
6. Fenzl, A. and F.W. Kiefer, *Brown adipose tissue and thermogenesis.* Horm Mol Biol Clin Investig, 2014. **19**(1): p. 25-37.
7. Ito, T., et al., *Morphological studies on brown adipose tissue in the bat and in humans of various ages.* Arch Histol Cytol, 1991. **54**(1): p. 1-39.
8. Cannon, B. and J. Nedergaard, *Brown adipose tissue: function and physiological significance.* Physiol Rev, 2004. **84**(1): p. 277-359.
9. Drubach, L.A., et al., *Pediatric brown adipose tissue: detection, epidemiology, and differences from adults.* J Pediatr. **159**(6): p. 939-44.
10. Cypess, A.M., et al., *Identification and importance of brown adipose tissue in adult humans.* N Engl J Med, 2009. **360**(15): p. 1509-17.
11. Nedergaard, J., T. Bengtsson, and B. Cannon, *Unexpected evidence for active brown adipose tissue in adult humans.* Am J Physiol Endocrinol Metab, 2007. **293**(2): p. E444-52.
12. van Marken Lichtenbelt, W.D., et al., *Cold-activated brown adipose tissue in healthy men.* N Engl J Med, 2009. **360**(15): p. 1500-8.
13. Reddy, N.L., et al., *Identification of brown adipose tissue using MR imaging in a human adult with histological and immunohistochemical confirmation.* J Clin Endocrinol Metab. **99**(1): p. E117-21.
14. Timmons, J.A. and B.K. Pedersen, *The importance of brown adipose tissue.* N Engl J Med, 2009. **361**(4): p. 415-6; author reply 418-21.
15. Petrovic, N., et al., *Chronic peroxisome proliferator-activated receptor gamma (PPARgamma) activation of epididymally derived white adipocyte cultures reveals a population of thermogenically competent, UCP1-containing adipocytes molecularly distinct from classic brown adipocytes.* J Biol Chem. **285**(10): p. 7153-64.
16. Wu, J., et al., *Beige adipocytes are a distinct type of thermogenic fat cell in mouse and human.* Cell. **150**(2): p. 366-76.
17. Rosenwald, M., et al., *Bi-directional interconversion of brite and white adipocytes.* Nat Cell Biol, 2013. **15**(6): p. 659-67.
18. Poissonnet, C.M., A.R. Burdi, and S.M. Garn, *The chronology of adipose tissue appearance and distribution in the human fetus.* Early Hum Dev, 1984. **10**(1-2): p. 1-11.

19. Chamberlain, G., et al., *Concise review: mesenchymal stem cells: their phenotype, differentiation capacity, immunological features, and potential for homing.* Stem Cells, 2007. **25**(11): p. 2739-49.
20. Kajimura, S., et al., *Initiation of myoblast to brown fat switch by a PRDM16-C/EBP-beta transcriptional complex.* Nature, 2009. **460**(7259): p. 1154-8.
21. Ali, A.T., et al., *Adipocyte and adipogenesis.* Eur J Cell Biol. **92**(6-7): p. 229-36.
22. Lefterova, M.I. and M.A. Lazar, *New developments in adipogenesis.* Trends Endocrinol Metab, 2009. **20**(3): p. 107-14.
23. Wang, Y., C. Hudak, and H.S. Sul, *Role of preadipocyte factor 1 in adipocyte differentiation.* Clin Lipidol. **5**(1): p. 109-115.
24. Fajas, L., et al., *E2Fs regulate adipocyte differentiation.* Dev Cell, 2002. **3**(1): p. 39-49.
25. Scime, A., et al., *Rb and p107 regulate preadipocyte differentiation into white versus brown fat through repression of PGC-1alpha.* Cell Metab, 2005. **2**(5): p. 283-95.
26. Lehmann, J.M., et al., *An antidiabetic thiazolidinedione is a high affinity ligand for peroxisome proliferator-activated receptor gamma (PPAR gamma).* J Biol Chem, 1995. **270**(22): p. 12953-6.
27. Zhang, J.W., et al., *Role of CREB in transcriptional regulation of CCAAT/enhancer-binding protein beta gene during adipogenesis.* J Biol Chem, 2004. **279**(6): p. 4471-8.
28. Tang, Q.Q., et al., *Sequential phosphorylation of CCAAT enhancer-binding protein beta by MAPK and glycogen synthase kinase 3beta is required for adipogenesis.* Proc Natl Acad Sci U S A, 2005. **102**(28): p. 9766-71.
29. Hamm, J.K., et al., *Role of PPAR gamma in regulating adipocyte differentiation and insulin-responsive glucose uptake.* Ann N Y Acad Sci, 1999. **892**: p. 134-45.
30. Darlington, G.J., S.E. Ross, and O.A. MacDougald, *The role of C/EBP genes in adipocyte differentiation.* J Biol Chem, 1998. **273**(46): p. 30057-60.
31. Langin, D., *Recruitment of brown fat and conversion of white into brown adipocytes: strategies to fight the metabolic complications of obesity?* Biochim Biophys Acta. **1801**(3): p. 372-6.
32. Stanford, K.I., et al., *Brown adipose tissue regulates glucose homeostasis and insulin sensitivity.* J Clin Invest. **123**(1): p. 215-23.
33. Guerra, C., et al., *Emergence of brown adipocytes in white fat in mice is under genetic control. Effects on body weight and adiposity.* J Clin Invest, 1998. **102**(2): p. 412-20.
34. Seale, P., et al., *Prdm16 determines the thermogenic program of subcutaneous white adipose tissue in mice.* J Clin Invest. **121**(1): p. 96-105.
35. Gburcik, V., et al., *An essential role for Tbx15 in the differentiation of brown and "brite" but not white adipocytes.* Am J Physiol Endocrinol Metab. **303**(8): p. E1053-60.
36. Lee, Y.H., et al., *In vivo identification of bipotential adipocyte progenitors recruited by beta3-adrenoceptor activation and high-fat feeding.* Cell Metab. **15**(4): p. 480-91.
37. Wu, J., P. Cohen, and B.M. Spiegelman, *Adaptive thermogenesis in adipocytes: is beige the new brown?* Genes Dev. **27**(3): p. 234-50.
38. Crossno, J.T., Jr., et al., *Rosiglitazone promotes development of a novel adipocyte population from bone marrow-derived circulating progenitor cells.* J Clin Invest, 2006. **116**(12): p. 3220-8.
39. Himms-Hagen, J., et al., *Multilocular fat cells in WAT of CL-316243-treated rats derive directly from white adipocytes.* Am J Physiol Cell Physiol, 2000. **279**(3): p. C670-81.
40. Vegiopoulos, A., et al., *Cyclooxygenase-2 controls energy homeostasis in mice by de novo recruitment of brown adipocytes.* Science. **328**(5982): p. 1158-61.
41. Kharitonenkov, A., et al., *FGF-21 as a novel metabolic regulator.* J Clin Invest, 2005. **115**(6): p. 1627-35.

42. Hondares, E., et al., *Thermogenic activation induces FGF21 expression and release in brown adipose tissue.* J Biol Chem. **286**(15): p. 12983-90.
43. Fisher, F.M., et al., *FGF21 regulates PGC-1alpha and browning of white adipose tissues in adaptive thermogenesis.* Genes Dev. **26**(3): p. 271-81.
44. Algire, C., D. Medrikova, and S. Herzig, *White and brown adipose stem cells: from signaling to clinical implications.* Biochim Biophys Acta. **1831**(5): p. 896-904.
45. Farmer, S.R., *Transcriptional control of adipocyte formation.* Cell Metab, 2006. **4**(4): p. 263-73.
46. Lin, J., et al., *Defects in adaptive energy metabolism with CNS-linked hyperactivity in PGC-1alpha null mice.* Cell, 2004. **119**(1): p. 121-35.
47. Uldry, M., et al., *Complementary action of the PGC-1 coactivators in mitochondrial biogenesis and brown fat differentiation.* Cell Metab, 2006. **3**(5): p. 333-41.
48. Seale, P., et al., *PRDM16 controls a brown fat/skeletal muscle switch.* Nature, 2008. **454**(7207): p. 961-7.
49. Herzig, S., et al., *CREB regulates hepatic gluconeogenesis through the coactivator PGC-1.* Nature, 2001. **413**(6852): p. 179-83.
50. Cao, W., et al., *p38 mitogen-activated protein kinase is the central regulator of cyclic AMP-dependent transcription of the brown fat uncoupling protein 1 gene.* Mol Cell Biol, 2004. **24**(7): p. 3057-67.
51. Tiraby, C., et al., *Acquirement of brown fat cell features by human white adipocytes.* J Biol Chem, 2003. **278**(35): p. 33370-6.
52. Hallberg, M., et al., *A functional interaction between RIP140 and PGC-1alpha regulates the expression of the lipid droplet protein CIDEA.* Mol Cell Biol, 2008. **28**(22): p. 6785-95.
53. Picard, F., et al., *SRC-1 and TIF2 control energy balance between white and brown adipose tissues.* Cell, 2002. **111**(7): p. 931-41.
54. Bostrom, P., et al., *A PGC1-alpha-dependent myokine that drives brown-fat-like development of white fat and thermogenesis.* Nature. **481**(7382): p. 463-8.
55. Nishikata, I., et al., *A novel EVI1 gene family, MEL1, lacking a PR domain (MEL1S) is expressed mainly in t(1;3)(p36;q21)-positive AML and blocks G-CSF-induced myeloid differentiation.* Blood, 2003. **102**(9): p. 3323-32.
56. Seale, P., et al., *Transcriptional control of brown fat determination by PRDM16.* Cell Metab, 2007. **6**(1): p. 38-54.
57. Kajimura, S., et al., *Regulation of the brown and white fat gene programs through a PRDM16/CtBP transcriptional complex.* Genes Dev, 2008. **22**(10): p. 1397-409.
58. Reshef, R., M. Maroto, and A.B. Lassar, *Regulation of dorsal somitic cell fates: BMPs and Noggin control the timing and pattern of myogenic regulator expression.* Genes Dev, 1998. **12**(3): p. 290-303.
59. Tseng, Y.H., et al., *New role of bone morphogenetic protein 7 in brown adipogenesis and energy expenditure.* Nature, 2008. **454**(7207): p. 1000-4.
60. McKay, R.M., et al., *C elegans: a model for exploring the genetics of fat storage.* Dev Cell, 2003. **4**(1): p. 131-42.
61. Miller, J.M., et al., *Identification of fat-cell enhancer regions in Drosophila melanogaster.* Insect Mol Biol, 2002. **11**(1): p. 67-77.
62. Van Vleet, E.S., et al., *Neutral lipid components of eleven species of Caribbean sharks.* Comp Biochem Physiol B, 1984. **79**(4): p. 549-54.
63. Rondinone, C.M., *Adipocyte-derived hormones, cytokines, and mediators.* Endocrine, 2006. **29**(1): p. 81-90.
64. Vaisse, C., et al., *Leptin activation of Stat3 in the hypothalamus of wild-type and ob/ob mice but not db/db mice.* Nat Genet, 1996. **14**(1): p. 95-7.

65. Munzberg, H., J.S. Flier, and C. Bjorbaek, *Region-specific leptin resistance within the hypothalamus of diet-induced obese mice.* Endocrinology, 2004. **145**(11): p. 4880-9.
66. Myers, M.G., Jr., et al., *Obesity and leptin resistance: distinguishing cause from effect.* Trends Endocrinol Metab, 2010. **21**(11): p. 643-51.
67. Pelleymounter, M.A., et al., *Effects of the obese gene product on body weight regulation in ob/ob mice.* Science, 1995. **269**(5223): p. 540-3.
68. Chen, H., et al., *Evidence that the diabetes gene encodes the leptin receptor: identification of a mutation in the leptin receptor gene in db/db mice.* Cell, 1996. **84**(3): p. 491-5.
69. Scherer, P.E., et al., *A novel serum protein similar to C1q, produced exclusively in adipocytes.* J Biol Chem, 1995. **270**(45): p. 26746-9.
70. Berg, A.H., et al., *The adipocyte-secreted protein Acrp30 enhances hepatic insulin action.* Nat Med, 2001. **7**(8): p. 947-53.
71. Yamauchi, T., et al., *Adiponectin stimulates glucose utilization and fatty-acid oxidation by activating AMP-activated protein kinase.* Nat Med, 2002. **8**(11): p. 1288-95.
72. Folco, E.J., et al., *Adiponectin inhibits pro-inflammatory signaling in human macrophages independent of interleukin-10.* J Biol Chem, 2009. **284**(38): p. 25569-75.
73. De Rosa, A., et al., *Adiponectin oligomers as potential indicators of adipose tissue improvement in obese subjects.* Eur J Endocrinol, 2013. **169**(1): p. 37-43.
74. Glatz, J.F., J.J. Luiken, and A. Bonen, *Membrane fatty acid transporters as regulators of lipid metabolism: implications for metabolic disease.* Physiol Rev, 2010. **90**(1): p. 367-417.
75. Yamamoto, T., et al., *Classification of FABP isoforms and tissues based on quantitative evaluation of transcript levels of these isoforms in various rat tissues.* Biotechnol Lett, 2009. **31**(11): p. 1695-701.
76. LaLonde, J.M., D.A. Bernlohr, and L.J. Banaszak, *The up-and-down beta-barrel proteins.* FASEB J, 1994. **8**(15): p. 1240-7.
77. Calderon-Dominguez, M., et al., *Fatty acid metabolism and the basis of brown adipose tissue function.* Adipocyte, 2016. **5**(2): p. 98-118.
78. Shimizu, T. and K. Yokotani, *Acute cold exposure-induced down-regulation of CIDEA, cell death-inducing DNA fragmentation factor-alpha-like effector A, in rat interscapular brown adipose tissue by sympathetically activated beta3-adrenoreceptors.* Biochem Biophys Res Commun, 2009. **387**(2): p. 294-9.
79. Zhou, Z., et al., *Cidea-deficient mice have lean phenotype and are resistant to obesity.* Nat Genet, 2003. **35**(1): p. 49-56.
80. Silva, J.E., *Thermogenic mechanisms and their hormonal regulation.* Physiol Rev, 2006. **86**(2): p. 435-64.
81. Himms-Hagen, J., *Does brown adipose tissue (BAT) have a role in the physiology or treatment of human obesity?* Rev Endocr Metab Disord, 2001. **2**(4): p. 395-401.
82. Feldmann, H.M., et al., *UCP1 ablation induces obesity and abolishes diet-induced thermogenesis in mice exempt from thermal stress by living at thermoneutrality.* Cell Metab, 2009. **9**(2): p. 203-9.
83. Westerterp, K.R., *Diet induced thermogenesis.* Nutr Metab (Lond), 2004. **1**(1): p. 5.
84. Dalgaard, L.T. and O. Pedersen, *Uncoupling proteins: functional characteristics and role in the pathogenesis of obesity and Type II diabetes.* Diabetologia, 2001. **44**(8): p. 946-65.
85. Wu, J., P. Cohen, and B.M. Spiegelman, *Adaptive thermogenesis in adipocytes: is beige the new brown?* Genes Dev, 2013. **27**(3): p. 234-50.
86. Harris, R.B., *Sympathetic denervation of one white fat depot changes norepinephrine content and turnover in intact white and brown fat depots.* Obesity (Silver Spring). **20**(7): p. 1355-64.

87. Bengtsson, T., B. Cannon, and J. Nedergaard, *Differential adrenergic regulation of the gene expression of the beta-adrenoceptor subtypes beta1, beta2 and beta3 in brown adipocytes.* Biochem J, 2000. **347 Pt 3**: p. 643-51.
88. Bartelt, A., et al., *Brown adipose tissue activity controls triglyceride clearance.* Nat Med, 2011. **17**(2): p. 200-5.
89. Bartelt, A., M. Merkel, and J. Heeren, *A new, powerful player in lipoprotein metabolism: brown adipose tissue.* J Mol Med (Berl), 2012. **90**(8): p. 887-93.
90. Mottillo, E.P., et al., *Coupling of lipolysis and de novo lipogenesis in brown, beige, and white adipose tissues during chronic beta3-adrenergic receptor activation.* J Lipid Res, 2014. **55**(11): p. 2276-86.
91. Hardy, O.T., M.P. Czech, and S. Corvera, *What causes the insulin resistance underlying obesity?* Curr Opin Endocrinol Diabetes Obes, 2012. **19**(2): p. 81-7.
92. Lovren, F., H. Teoh, and S. Verma, *Obesity and atherosclerosis: mechanistic insights.* Can J Cardiol, 2015. **31**(2): p. 177-83.
93. Wang, Q.A., et al., *Tracking adipogenesis during white adipose tissue development, expansion and regeneration.* Nat Med, 2013. **19**(10): p. 1338-44.
94. Joe, A.W., et al., *Depot-specific differences in adipogenic progenitor abundance and proliferative response to high-fat diet.* Stem Cells, 2009. **27**(10): p. 2563-70.
95. Salans, L.B., S.W. Cushman, and R.E. Weismann, *Studies of human adipose tissue. Adipose cell size and number in nonobese and obese patients.* J Clin Invest, 1973. **52**(4): p. 929-41.
96. Choe, S.S., et al., *Adipose Tissue Remodeling: Its Role in Energy Metabolism and Metabolic Disorders.* Front Endocrinol (Lausanne), 2016. **7**: p. 30.
97. Hirsch, J. and J.L. Knittle, *Cellularity of obese and nonobese human adipose tissue.* Fed Proc, 1970. **29**(4): p. 1516-21.
98. Stern, J.S., et al., *Adipose-cell size and immunoreactive insulin levels in obese and normal-weight adults.* Lancet, 1972. **2**(7784): p. 948-51.
99. Rausch, M.E., et al., *Obesity in C57BL/6J mice is characterized by adipose tissue hypoxia and cytotoxic T-cell infiltration.* Int J Obes (Lond), 2008. **32**(3): p. 451-63.
100. Hosogai, N., et al., *Adipose tissue hypoxia in obesity and its impact on adipocytokine dysregulation.* Diabetes, 2007. **56**(4): p. 901-11.
101. Mazzatti, D., et al., *A microarray analysis of the hypoxia-induced modulation of gene expression in human adipocytes.* Arch Physiol Biochem, 2012. **118**(3): p. 112-20.
102. Pasarica, M., et al., *Reduced adipose tissue oxygenation in human obesity: evidence for rarefaction, macrophage chemotaxis, and inflammation without an angiogenic response.* Diabetes, 2009. **58**(3): p. 718-25.
103. Goossens, G.H., et al., *Increased adipose tissue oxygen tension in obese compared with lean men is accompanied by insulin resistance, impaired adipose tissue capillarization, and inflammation.* Circulation, 2011. **124**(1): p. 67-76.
104. Karpe, F., et al., *Impaired postprandial adipose tissue blood flow response is related to aspects of insulin sensitivity.* Diabetes, 2002. **51**(8): p. 2467-73.
105. Halberg, N., et al., *Hypoxia-inducible factor 1alpha induces fibrosis and insulin resistance in white adipose tissue.* Mol Cell Biol, 2009. **29**(16): p. 4467-83.
106. Wree, A., et al., *Adipokine expression in brown and white adipocytes in response to hypoxia.* J Endocrinol Invest, 2012. **35**(5): p. 522-7.
107. Michailidou, Z., et al., *Increased angiogenesis protects against adipose hypoxia and fibrosis in metabolic disease-resistant 11beta-hydroxysteroid dehydrogenase type 1 (HSD1)-deficient mice.* J Biol Chem, 2012. **287**(6): p. 4188-97.
108. Sung, H.K., et al., *Adipose vascular endothelial growth factor regulates metabolic homeostasis through angiogenesis.* Cell Metab, 2013. **17**(1): p. 61-72.

109. Tinahones, F.J., et al., *Obesity-associated insulin resistance is correlated to adipose tissue vascular endothelial growth factors and metalloproteinase levels.* BMC Physiol, 2012. **12**: p. 4.
110. Elias, I., S. Franckhauser, and F. Bosch, *New insights into adipose tissue VEGF-A actions in the control of obesity and insulin resistance.* Adipocyte, 2013. **2**(2): p. 109-12.
111. Fraisl, P., et al., *Regulation of angiogenesis by oxygen and metabolism.* Dev Cell, 2009. **16**(2): p. 167-79.
112. Aragones, J., et al., *Deficiency or inhibition of oxygen sensor Phd1 induces hypoxia tolerance by reprogramming basal metabolism.* Nat Genet, 2008. **40**(2): p. 170-80.
113. Saint-Geniez, M., et al., *PGC-1alpha regulates normal and pathological angiogenesis in the retina.* Am J Pathol, 2013. **182**(1): p. 255-65.
114. Gealekman, O., et al., *Enhanced angiogenesis in obesity and in response to PPARgamma activators through adipocyte VEGF and ANGPTL4 production.* Am J Physiol Endocrinol Metab, 2008. **295**(5): p. E1056-64.
115. Aumailley, M. and B. Gayraud, *Structure and biological activity of the extracellular matrix.* J Mol Med (Berl), 1998. **76**(3-4): p. 253-65.
116. Divoux, A., et al., *Fibrosis in human adipose tissue: composition, distribution, and link with lipid metabolism and fat mass loss.* Diabetes, 2010. **59**(11): p. 2817-25.
117. Sun, K., et al., *Fibrosis and adipose tissue dysfunction.* Cell Metab, 2013. **18**(4): p. 470-7.
118. Khan, T., et al., *Metabolic dysregulation and adipose tissue fibrosis: role of collagen VI.* Mol Cell Biol, 2009. **29**(6): p. 1575-91.
119. Spencer, M., et al., *Adipose tissue extracellular matrix and vascular abnormalities in obesity and insulin resistance.* J Clin Endocrinol Metab, 2011. **96**(12): p. E1990-8.
120. Lawler, H.M., et al., *Adipose Tissue Hypoxia, Inflammation, and Fibrosis in Obese Insulin-Sensitive and Obese Insulin-Resistant Subjects.* J Clin Endocrinol Metab, 2016. **101**(4): p. 1422-8.
121. Kahles, F., H.M. Findeisen, and D. Bruemmer, *Osteopontin: A novel regulator at the cross roads of inflammation, obesity and diabetes.* Mol Metab, 2014. **3**(4): p. 384-93.
122. Lin, T.H. Chun, and L. Kang, *Adipose extracellular matrix remodelling in obesity and insulin resistance.* Biochem Pharmacol, 2016. **119**: p. 8-16.
123. Naor, D., R.V. Sionov, and D. Ish-Shalom, *CD44: structure, function, and association with the malignant process.* Adv Cancer Res, 1997. **71**: p. 241-319.
124. Zoller, M., *CD44: can a cancer-initiating cell profit from an abundantly expressed molecule?* Nat Rev Cancer, 2011. **11**(4): p. 254-67.
125. Kang, H.S., et al., *CD44 plays a critical role in regulating diet-induced adipose inflammation, hepatic steatosis, and insulin resistance.* PLoS One, 2013. **8**(3): p. e58417.
126. Hynes, R.O., *Integrins: bidirectional, allosteric signaling machines.* Cell, 2002. **110**(6): p. 673-87.
127. Meakin, P.J., et al., *Mice Lacking beta2-Integrin Function Remain Glucose Tolerant in Spite of Insulin Resistance, Neutrophil Infiltration and Inflammation.* PLoS One, 2015. **10**(9): p. e0138872.
128. Kang, L., et al., *Diet-induced muscle insulin resistance is associated with extracellular matrix remodeling and interaction with integrin alpha2beta1 in mice.* Diabetes, 2011. **60**(2): p. 416-26.
129. Sarrazin, S., W.C. Lamanna, and J.D. Esko, *Heparan sulfate proteoglycans.* Cold Spring Harb Perspect Biol, 2011. **3**(7).
130. Wilsie, L.C., et al., *Cell surface heparan sulfate proteoglycans contribute to intracellular lipid accumulation in adipocytes.* Lipids Health Dis, 2005. **4**: p. 2.
131. Mulcahy, L.A., R.C. Pink, and D.R. Carter, *Routes and mechanisms of extracellular vesicle uptake.* J Extracell Vesicles, 2014. **3**.

132. Poulain, F.E. and H.J. Yost, *Heparan sulfate proteoglycans: a sugar code for vertebrate development?* Development, 2015. **142**(20): p. 3456-67.
133. Bonnans, C., J. Chou, and Z. Werb, *Remodelling the extracellular matrix in development and disease.* Nat Rev Mol Cell Biol, 2014. **15**(12): p. 786-801.
134. Nagase, H., R. Visse, and G. Murphy, *Structure and function of matrix metalloproteinases and TIMPs.* Cardiovasc Res, 2006. **69**(3): p. 562-73.
135. Chavey, C., et al., *Matrix metalloproteinases are differentially expressed in adipose tissue during obesity and modulate adipocyte differentiation.* J Biol Chem, 2003. **278**(14): p. 11888-96.
136. Caolo, V., et al., *ADAM10 and ADAM17 have opposite roles during sprouting angiogenesis.* Angiogenesis, 2015. **18**(1): p. 13-22.
137. Moest, H., et al., *Malfunctioning of adipocytes in obesity is linked to quantitative surfaceome changes.* Biochim Biophys Acta, 2013. **1831**(7): p. 1208-16.
138. Strissel, K.J., et al., *Adipocyte death, adipose tissue remodeling, and obesity complications.* Diabetes, 2007. **56**(12): p. 2910-8.
139. Kahn, S.E., *The relative contributions of insulin resistance and beta-cell dysfunction to the pathophysiology of Type 2 diabetes.* Diabetologia, 2003. **46**(1): p. 3-19.
140. Butler, A.E., et al., *Beta-cell deficit and increased beta-cell apoptosis in humans with type 2 diabetes.* Diabetes, 2003. **52**(1): p. 102-10.
141. Rhodes, C.J., *Type 2 diabetes-a matter of beta-cell life and death?* Science, 2005. **307**(5708): p. 380-4.
142. Frayn, K.N., et al., *Regulation of fatty acid movement in human adipose tissue in the postabsorptive-to-postprandial transition.* Am J Physiol, 1994. **266**(3 Pt 1): p. E308-17.
143. Christianson, J.L., et al., *Stearoyl-CoA desaturase 2 is required for peroxisome proliferator-activated receptor gamma expression and adipogenesis in cultured 3T3-L1 cells.* J Biol Chem, 2008. **283**(5): p. 2906-16.
144. Hotamisligil, G.S., *Inflammation and metabolic disorders.* Nature, 2006. **444**(7121): p. 860-7.
145. Hulsmans, M. and P. Holvoet, *The vicious circle between oxidative stress and inflammation in atherosclerosis.* J Cell Mol Med, 2010. **14**(1-2): p. 70-8.
146. Hu, E., et al., *Inhibition of adipogenesis through MAP kinase-mediated phosphorylation of PPARgamma.* Science, 1996. **274**(5295): p. 2100-3.
147. Camp, H.S. and S.R. Tafuri, *Regulation of peroxisome proliferator-activated receptor gamma activity by mitogen-activated protein kinase.* J Biol Chem, 1997. **272**(16): p. 10811-6.
148. He, F., J.A. Doucet, and J.M. Stephens, *Caspase-mediated degradation of PPARgamma proteins in adipocytes.* Obesity (Silver Spring), 2008. **16**(8): p. 1735-41.
149. Makki, K., P. Froguel, and I. Wolowczuk, *Adipose tissue in obesity-related inflammation and insulin resistance: cells, cytokines, and chemokines.* ISRN Inflamm, 2013. **2013**: p. 139239.
150. Simon, M.C., et al., *Fatty acids modulate cytokine and chemokine secretion of stimulated human whole blood cultures in diabetes.* Clin Exp Immunol, 2013. **172**(3): p. 383-93.
151. Bulua, A.C., et al., *Mitochondrial reactive oxygen species promote production of proinflammatory cytokines and are elevated in TNFR1-associated periodic syndrome (TRAPS).* J Exp Med, 2011. **208**(3): p. 519-33.
152. Kim, J.J. and D.D. Sears, *TLR4 and Insulin Resistance.* Gastroenterol Res Pract, 2010. **2010**.
153. Leow-Dyke, S., et al., *Neuronal Toll-like receptor 4 signaling induces brain endothelial activation and neutrophil transmigration in vitro.* J Neuroinflammation, 2012. **9**: p. 230.

154. Soares, J.B., et al., *The role of lipopolysaccharide/toll-like receptor 4 signaling in chronic liver diseases.* Hepatol Int, 2010. **4**(4): p. 659-72.
155. Hirata, T., et al., *Evidence for the presence of toll-like receptor 4 system in the human endometrium.* J Clin Endocrinol Metab, 2005. **90**(1): p. 548-56.
156. Hijiya, N., et al., *Possible involvement of toll-like receptor 4 in endothelial cell activation of larger vessels in response to lipopolysaccharide.* Pathobiology, 2002. **70**(1): p. 18-25.
157. Garay-Malpartida, H.M., et al., *Toll-like receptor 4 (TLR4) expression in human and murine pancreatic beta-cells affects cell viability and insulin homeostasis.* BMC Immunol, 2011. **12**: p. 18.
158. Nicola, J.P., et al., *Functional toll-like receptor 4 conferring lipopolysaccharide responsiveness is expressed in thyroid cells.* Endocrinology, 2009. **150**(1): p. 500-8.
159. Frisard, M.I., et al., *Toll-like receptor 4 modulates skeletal muscle substrate metabolism.* Am J Physiol Endocrinol Metab, 2010. **298**(5): p. E988-98.
160. Vitseva, O.I., et al., *Inducible Toll-like receptor and NF-kappaB regulatory pathway expression in human adipose tissue.* Obesity (Silver Spring), 2008. **16**(5): p. 932-7.
161. Ehrchen, J.M., et al., *The endogenous Toll-like receptor 4 agonist S100A8/S100A9 (calprotectin) as innate amplifier of infection, autoimmunity, and cancer.* J Leukoc Biol, 2009. **86**(3): p. 557-66.
162. Bianchi, M.E., *HMGB1 loves company.* J Leukoc Biol, 2009. **86**(3): p. 573-6.
163. Gondokaryono, S.P., et al., *The extra domain A of fibronectin stimulates murine mast cells via toll-like receptor 4.* J Leukoc Biol, 2007. **82**(3): p. 657-65.
164. Rietschel, E.T., et al., *Bacterial endotoxin: molecular relationships of structure to activity and function.* FASEB J, 1994. **8**(2): p. 217-25.
165. Brun, P., et al., *Increased intestinal permeability in obese mice: new evidence in the pathogenesis of nonalcoholic steatohepatitis.* Am J Physiol Gastrointest Liver Physiol, 2007. **292**(2): p. G518-25.
166. Erridge, C., et al., *A high-fat meal induces low-grade endotoxemia: evidence of a novel mechanism of postprandial inflammation.* Am J Clin Nutr, 2007. **86**(5): p. 1286-92.
167. Spruss, A., et al., *Toll-like receptor 4 is involved in the development of fructose-induced hepatic steatosis in mice.* Hepatology, 2009. **50**(4): p. 1094-104.
168. Broz, P. and D.M. Monack, *Molecular mechanisms of inflammasome activation during microbial infections.* Immunol Rev, 2011. **243**(1): p. 174-90.
169. Proell, M., et al., *The Nod-like receptor (NLR) family: a tale of similarities and differences.* PLoS One, 2008. **3**(4): p. e2119.
170. Franchi, L., et al., *The inflammasome: a caspase-1-activation platform that regulates immune responses and disease pathogenesis.* Nat Immunol, 2009. **10**(3): p. 241-7.
171. Ye, Z. and J.P. Ting, *NLR, the nucleotide-binding domain leucine-rich repeat containing gene family.* Curr Opin Immunol, 2008. **20**(1): p. 3-9.
172. Schertzer, J.D. and A. Klip, *Give a NOD to insulin resistance.* Am J Physiol Endocrinol Metab, 2011. **301**(4): p. E585-6.
173. Zhao, L., et al., *Differential modulation of Nods signaling pathways by fatty acids in human colonic epithelial HCT116 cells.* J Biol Chem, 2007. **282**(16): p. 11618-28.
174. Schertzer, J.D., et al., *NOD1 activators link innate immunity to insulin resistance.* Diabetes, 2011. **60**(9): p. 2206-15.
175. Tamrakar, A.K., et al., *NOD2 activation induces muscle cell-autonomous innate immune responses and insulin resistance.* Endocrinology, 2010. **151**(12): p. 5624-37.
176. Watanabe, Y., Y. Nagai, and K. Takatsu, *Activation and regulation of the pattern recognition receptors in obesity-induced adipose tissue inflammation and insulin resistance.* Nutrients, 2013. **5**(9): p. 3757-78.

177. Valencia-Sanchez, M.A., et al., *Control of translation and mRNA degradation by miRNAs and siRNAs.* Genes Dev, 2006. **20**(5): p. 515-24.
178. Yuan, Z., et al., *MicroRNA genes derived from repetitive elements and expanded by segmental duplication events in mammalian genomes.* PLoS One, 2011. **6**(3): p. e17666.
179. Corcoran, D.L., et al., *Features of mammalian microRNA promoters emerge from polymerase II chromatin immunoprecipitation data.* PLoS One, 2009. **4**(4): p. e5279.
180. Lee, Y., et al., *MicroRNA genes are transcribed by RNA polymerase II.* Embo J, 2004. **23**(20): p. 4051-60.
181. Borchert, G.M., W. Lanier, and B.L. Davidson, *RNA polymerase III transcribes human microRNAs.* Nat Struct Mol Biol, 2006. **13**(12): p. 1097-101.
182. Morlando, M., et al., *Primary microRNA transcripts are processed co-transcriptionally.* Nat Struct Mol Biol, 2008. **15**(9): p. 902-9.
183. Kim, Y.K. and V.N. Kim, *Processing of intronic microRNAs.* Embo J, 2007. **26**(3): p. 775-83.
184. Zeng, Y. and B.R. Cullen, *Structural requirements for pre-microRNA binding and nuclear export by Exportin 5.* Nucleic Acids Res, 2004. **32**(16): p. 4776-85.
185. Bohnsack, M.T., K. Czaplinski, and D. Gorlich, *Exportin 5 is a RanGTP-dependent dsRNA-binding protein that mediates nuclear export of pre-miRNAs.* Rna, 2004. **10**(2): p. 185-91.
186. Shah, K., *The Role of MicroRNAs in the Endometrium*.
187. Chendrimada, T.P., et al., *TRBP recruits the Dicer complex to Ago2 for microRNA processing and gene silencing.* Nature, 2005. **436**(7051): p. 740-4.
188. Xu, L., B.F. Yang, and J. Ai, *MicroRNA transport: a new way in cell communication.* J Cell Physiol. **228**(8): p. 1713-9.
189. Paroo, Z., et al., *Phosphorylation of the human microRNA-generating complex mediates MAPK/Erk signaling.* Cell, 2009. **139**(1): p. 112-22.
190. Iwasaki, S., et al., *Hsc70/Hsp90 chaperone machinery mediates ATP-dependent RISC loading of small RNA duplexes.* Mol Cell. **39**(2): p. 292-9.
191. Iwasaki, S., et al., *Hsc70/Hsp90 chaperone machinery mediates ATP-dependent RISC loading of small RNA duplexes.* Mol Cell, 2010. **39**(2): p. 292-9.
192. Khvorova, A., A. Reynolds, and S.D. Jayasena, *Functional siRNAs and miRNAs exhibit strand bias.* Cell, 2003. **115**(2): p. 209-16.
193. Schwarz, D.S., et al., *Asymmetry in the assembly of the RNAi enzyme complex.* Cell, 2003. **115**(2): p. 199-208.
194. Cifuentes, D., et al., *A novel miRNA processing pathway independent of Dicer requires Argonaute2 catalytic activity.* Science. **328**(5986): p. 1694-8.
195. Mudhasani, R., et al., *Dicer is required for the formation of white but not brown adipose tissue.* J Cell Physiol. **226**(5): p. 1399-406.
196. Salzman, D.W., et al., *miR-34 activity is modulated through 5'-end phosphorylation in response to DNA damage.* Nat Commun, 2016. **7**: p. 10954.
197. Kim, Y. and V.N. Kim, *MicroRNA factory: RISC assembly from precursor microRNAs.* Mol Cell, 2012. **46**(4): p. 384-6.
198. Kawamata, T. and Y. Tomari, *Making RISC.* Trends Biochem Sci, 2010. **35**(7): p. 368-76.
199. Lai, E.C., *Micro RNAs are complementary to 3' UTR sequence motifs that mediate negative post-transcriptional regulation.* Nat Genet, 2002. **30**(4): p. 363-4.
200. Lewis, B.P., C.B. Burge, and D.P. Bartel, *Conserved seed pairing, often flanked by adenosines, indicates that thousands of human genes are microRNA targets.* Cell, 2005. **120**(1): p. 15-20.
201. Orom, U.A., F.C. Nielsen, and A.H. Lund, *MicroRNA-10a binds the 5'UTR of ribosomal protein mRNAs and enhances their translation.* Mol Cell, 2008. **30**(4): p. 460-71.

202. Enright, A.J., et al., *MicroRNA targets in Drosophila.* Genome Biol, 2003. **5**(1): p. R1.
203. Krek, A., et al., *Combinatorial microRNA target predictions.* Nat Genet, 2005. **37**(5): p. 495-500.
204. Lall, S., et al., *A genome-wide map of conserved microRNA targets in C. elegans.* Curr Biol, 2006. **16**(5): p. 460-71.
205. Kiriakidou, M., et al., *A combined computational-experimental approach predicts human microRNA targets.* Genes Dev, 2004. **18**(10): p. 1165-78.
206. Hutvagner, G. and M.J. Simard, *Argonaute proteins: key players in RNA silencing.* Nat Rev Mol Cell Biol, 2008. **9**(1): p. 22-32.
207. Macfarlane, L.A. and P.R. Murphy, *MicroRNA: Biogenesis, Function and Role in Cancer.* Curr Genomics, 2010. **11**(7): p. 537-61.
208. Nottrott, S., M.J. Simard, and J.D. Richter, *Human let-7a miRNA blocks protein production on actively translating polyribosomes.* Nat Struct Mol Biol, 2006. **13**(12): p. 1108-14.
209. Petersen, C.P., et al., *Short RNAs repress translation after initiation in mammalian cells.* Mol Cell, 2006. **21**(4): p. 533-42.
210. Olsen, P.H. and V. Ambros, *The lin-4 regulatory RNA controls developmental timing in Caenorhabditis elegans by blocking LIN-14 protein synthesis after the initiation of translation.* Dev Biol, 1999. **216**(2): p. 671-80.
211. Seggerson, K., L. Tang, and E.G. Moss, *Two genetic circuits repress the Caenorhabditis elegans heterochronic gene lin-28 after translation initiation.* Dev Biol, 2002. **243**(2): p. 215-25.
212. Sonenberg, N., et al., *Eukaryotic mRNA cap binding protein: purification by affinity chromatography on sepharose-coupled m7GDP.* Proc Natl Acad Sci U S A, 1979. **76**(9): p. 4345-9.
213. Kahvejian, A., et al., *Mammalian poly(A)-binding protein is a eukaryotic translation initiation factor, which acts via multiple mechanisms.* Genes Dev, 2005. **19**(1): p. 104-13.
214. Braun, J.E., et al., *GW182 proteins directly recruit cytoplasmic deadenylase complexes to miRNA targets.* Mol Cell, 2011. **44**(1): p. 120-33.
215. Zekri, L., et al., *The silencing domain of GW182 interacts with PABPC1 to promote translational repression and degradation of microRNA targets and is required for target release.* Mol Cell Biol, 2009. **29**(23): p. 6220-31.
216. Kedersha, N., et al., *Stress granules and processing bodies are dynamically linked sites of mRNP remodeling.* J Cell Biol, 2005. **169**(6): p. 871-84.
217. Mittal, S., et al., *The Ccr4a (CNOT6) and Ccr4b (CNOT6L) deadenylase subunits of the human Ccr4-Not complex contribute to the prevention of cell death and senescence.* Mol Biol Cell. **22**(6): p. 748-58.
218. Gibbings, D.J., et al., *Multivesicular bodies associate with components of miRNA effector complexes and modulate miRNA activity.* Nat Cell Biol, 2009. **11**(9): p. 1143-9.
219. Simons, M. and G. Raposo, *Exosomes--vesicular carriers for intercellular communication.* Curr Opin Cell Biol, 2009. **21**(4): p. 575-81.
220. Tahbaz, N., et al., *Characterization of the interactions between mammalian PAZ PIWI domain proteins and Dicer.* EMBO Rep, 2004. **5**(2): p. 189-94.
221. Johnston, M., et al., *HSP90 protein stabilizes unloaded argonaute complexes and microscopic P-bodies in human cells.* Mol Biol Cell. **21**(9): p. 1462-9.
222. Salmena, L., et al., *A ceRNA hypothesis: the Rosetta Stone of a hidden RNA language?* Cell, 2011. **146**(3): p. 353-8.
223. D'Errico, I., G. Gadaleta, and C. Saccone, *Pseudogenes in metazoa: origin and features.* Brief Funct Genomic Proteomic, 2004. **3**(2): p. 157-67.

224. Poliseno, L., et al., *A coding-independent function of gene and pseudogene mRNAs regulates tumour biology.* Nature, 2010. **465**(7301): p. 1033-8.
225. Chi, S.W., et al., *Argonaute HITS-CLIP decodes microRNA-mRNA interaction maps.* Nature, 2009. **460**(7254): p. 479-86.
226. Licatalosi, D.D., et al., *HITS-CLIP yields genome-wide insights into brain alternative RNA processing.* Nature, 2008. **456**(7221): p. 464-9.
227. Cazalla, D., T. Yario, and J.A. Steitz, *Down-regulation of a host microRNA by a Herpesvirus saimiri noncoding RNA.* Science, 2010. **328**(5985): p. 1563-6.
228. Lee, D.Y., et al., *Expression of versican 3'-untranslated region modulates endogenous microRNA functions.* PLoS One, 2010. **5**(10): p. e13599.
229. Wang, J., et al., *CREB up-regulates long non-coding RNA, HULC expression through interaction with microRNA-372 in liver cancer.* Nucleic Acids Res, 2010. **38**(16): p. 5366-83.
230. Guo, L., et al., *Integrative analysis of miRNA-mRNA and miRNA-miRNA interactions.* Biomed Res Int, 2014. **2014**: p. 907420.
231. Xu, J., et al., *MiRNA-miRNA synergistic network: construction via co-regulating functional modules and disease miRNA topological features.* Nucleic Acids Res, 2011. **39**(3): p. 825-36.
232. Harvey Lodish, A.B., S Lawrence Zipursky, Paul Matsudaira, David Baltimore and james Darnell, *Overview of extracellular Signalling*, in *Molecular Cell Biology*. 2000: new York.
233. Kawa, D., et al., *Inhibition of viral gene expression by human ribonuclease P.* Rna, 1998. **4**(11): p. 1397-406.
234. Chen, X., et al., *Characterization of microRNAs in serum: a novel class of biomarkers for diagnosis of cancer and other diseases.* Cell Res, 2008. **18**(10): p. 997-1006.
235. Mitchell, P.S., et al., *Circulating microRNAs as stable blood-based markers for cancer detection.* Proc Natl Acad Sci U S A, 2008. **105**(30): p. 10513-8.
236. Kooijmans, S.A., et al., *Exosome mimetics: a novel class of drug delivery systems.* Int J Nanomedicine. **7**: p. 1525-41.
237. Thery, C., M. Ostrowski, and E. Segura, *Membrane vesicles as conveyors of immune responses.* Nat Rev Immunol, 2009. **9**(8): p. 581-93.
238. Dubyak, G.R., *P2X7 receptor regulation of non-classical secretion from immune effector cells.* Cell Microbiol. **14**(11): p. 1697-706.
239. Joop, K., et al., *Microparticles from patients with multiple organ dysfunction syndrome and sepsis support coagulation through multiple mechanisms.* Thromb Haemost, 2001. **85**(5): p. 810-20.
240. Sabatier, F., et al., *Interaction of endothelial microparticles with monocytic cells in vitro induces tissue factor-dependent procoagulant activity.* Blood, 2002. **99**(11): p. 3962-70.
241. Alais, S., et al., *Mouse neuroblastoma cells release prion infectivity associated with exosomal vesicles.* Biol Cell, 2008. **100**(10): p. 603-15.
242. Fevrier, B., et al., *Cells release prions in association with exosomes.* Proc Natl Acad Sci U S A, 2004. **101**(26): p. 9683-8.
243. Raposo, G. and W. Stoorvogel, *Extracellular vesicles: exosomes, microvesicles, and friends.* J Cell Biol. **200**(4): p. 373-83.
244. Keller, S., et al., *Exosomes: from biogenesis and secretion to biological function.* Immunol Lett, 2006. **107**(2): p. 102-8.
245. Eystathioy, T., et al., *The GW182 protein colocalizes with mRNA degradation associated proteins hDcp1 and hLSm4 in cytoplasmic GW bodies.* RNA, 2003. **9**(10): p. 1171-3.
246. M, R., *Exosomes as intercelluar signalosomes and pharmacological effectors*, in *Biochemical Pharmacology*. 2010.

247. Kosaka, N., et al., *Secretory mechanisms and intercellular transfer of microRNAs in living cells.* J Biol Chem. **285**(23): p. 17442-52.
248. Mittelbrunn, M., et al., *Unidirectional transfer of microRNA-loaded exosomes from T cells to antigen-presenting cells.* Nat Commun. **2**: p. 282.
249. Vickers, K.C., et al., *MicroRNAs are transported in plasma and delivered to recipient cells by high-density lipoproteins.* Nat Cell Biol. **13**(4): p. 423-33.
250. Arroyo, J.D., et al., *Argonaute2 complexes carry a population of circulating microRNAs independent of vesicles in human plasma.* Proc Natl Acad Sci U S A. **108**(12): p. 5003-8.
251. Gallo, A., et al., *The majority of microRNAs detectable in serum and saliva is concentrated in exosomes.* PLoS One. **7**(3): p. e30679.
252. Li, L., et al., *Argonaute 2 complexes selectively protect the circulating microRNAs in cell-secreted microvesicles.* PLoS One. **7**(10): p. e46957.
253. Chevillet, J.R., et al., *Quantitative and stoichiometric analysis of the microRNA content of exosomes.* Proc Natl Acad Sci U S A, 2014. **111**(41): p. 14888-93.
254. Svensson, K.J., et al., *Exosome uptake depends on ERK1/2-heat shock protein 27 signaling and lipid Raft-mediated endocytosis negatively regulated by caveolin-1.* J Biol Chem, 2013. **288**(24): p. 17713-24.
255. Naslund, T.I., et al., *Exosomes from breast milk inhibit HIV-1 infection of dendritic cells and subsequent viral transfer to CD4+ T cells.* AIDS, 2014. **28**(2): p. 171-80.
256. Zernecke, A., et al., *Delivery of microRNA-126 by apoptotic bodies induces CXCL12-dependent vascular protection.* Sci Signal, 2009. **2**(100): p. ra81.
257. Pegtel, D.M., et al., *Functional delivery of viral miRNAs via exosomes.* Proc Natl Acad Sci U S A, 2010. **107**(14): p. 6328-33.
258. Zhang, Y., et al., *Secreted monocytic miR-150 enhances targeted endothelial cell migration.* Mol Cell, 2010. **39**(1): p. 133-44.
259. Fabbri, M., et al., *MicroRNAs bind to Toll-like receptors to induce prometastatic inflammatory response.* Proc Natl Acad Sci U S A, 2012. **109**(31): p. E2110-6.
260. Ogawa, R., et al., *Adipocyte-derived microvesicles contain RNA that is transported into macrophages and might be secreted into blood circulation.* Biochem Biophys Res Commun, 2010. **398**(4): p. 723-9.
261. Thomou, T., et al., *Adipose-derived circulating miRNAs regulate gene expression in other tissues.* Nature, 2017. **542**(7642): p. 450-455.
262. Prud'homme, G.J., et al., *Neuropilin-1 is a receptor for extracellular miRNA and AGO2/miRNA complexes and mediates the internalization of miRNAs that modulate cell function.* Oncotarget, 2016. **7**(42): p. 68057-68071.
263. Prud'homme, G.J. and Y. Glinka, *Neuropilins are multifunctional coreceptors involved in tumor initiation, growth, metastasis and immunity.* Oncotarget, 2012. **3**(9): p. 921-39.
264. Wang, S., et al., *QSulf1, a heparan sulfate 6-O-endosulfatase, inhibits fibroblast growth factor signaling in mesoderm induction and angiogenesis.* Proc Natl Acad Sci U S A, 2004. **101**(14): p. 4833-8.
265. Huang, J., et al., *MicroRNA-204 regulates Runx2 protein expression and mesenchymal progenitor cell differentiation.* Stem Cells, 2010. **28**(2): p. 357-64.
266. Kim, D.S., et al., *MicroRNA-103a-3p controls proliferation and osteogenic differentiation of human adipose tissue-derived stromal cells.* Exp Mol Med, 2015. **47**: p. e172.
267. Kajimoto, K., H. Naraba, and N. Iwai, *MicroRNA and 3T3-L1 pre-adipocyte differentiation.* RNA, 2006. **12**(9): p. 1626-32.
268. Chen, L., et al., *MicroRNA-143 regulates adipogenesis by modulating the MAP2K5-ERK5 signaling.* Sci Rep, 2014. **4**: p. 3819.
269. Li, M., et al., *miR-103 promotes 3T3-L1 cell adipogenesis through AKT/mTOR signal pathway with its target being MEF2D.* Biol Chem, 2015. **396**(3): p. 235-44.

270. Gerin, I., et al., *Roles for miRNA-378/378* in adipocyte gene expression and lipogenesis.* Am J Physiol Endocrinol Metab, 2010. **299**(2): p. E198-206.
271. Lee, D.Y., et al., *MicroRNA-378 promotes cell survival, tumor growth, and angiogenesis by targeting SuFu and Fus-1 expression.* Proc Natl Acad Sci U S A, 2007. **104**(51): p. 20350-5.
272. Krist, B., et al., *The Role of miR-378a in Metabolism, Angiogenesis, and Muscle Biology.* Int J Endocrinol, 2015. **2015**: p. 281756.
273. Eichner, L.J., et al., *miR-378(*) mediates metabolic shift in breast cancer cells via the PGC-1beta/ERRgamma transcriptional pathway.* Cell Metab, 2010. **12**(4): p. 352-61.
274. Stark, M.S., et al., *Characterization of the Melanoma miRNAome by Deep Sequencing.* PLoS One, 2010. **5**(3): p. e9685.
275. Jima, D.D., et al., *Deep sequencing of the small RNA transcriptome of normal and malignant human B cells identifies hundreds of novel microRNAs.* Blood, 2010. **116**(23): p. e118-27.
276. Berezikov, E., et al., *Many novel mammalian microRNA candidates identified by extensive cloning and RAKE analysis.* Genome Res, 2006. **16**(10): p. 1289-98.
277. Goff, L.A., et al., *Ago2 immunoprecipitation identifies predicted microRNAs in human embryonic stem cells and neural precursors.* PLoS One, 2009. **4**(9): p. e7192.
278. Dannemann, M., et al., *Transcription factors are targeted by differentially expressed miRNAs in primates.* Genome Biol Evol, 2012. **4**(4): p. 552-64.
279. Carrer, M., et al., *Control of mitochondrial metabolism and systemic energy homeostasis by microRNAs 378 and 378*.* Proc Natl Acad Sci U S A, 2012. **109**(38): p. 15330-5.
280. Mallat, Y., et al., *Proteome modulation in H9c2 cardiac cells by microRNAs miR-378 and miR-378.* Mol Cell Proteomics, 2014. **13**(1): p. 18-29.
281. Davidsen, P.K., et al., *High responders to resistance exercise training demonstrate differential regulation of skeletal muscle microRNA expression.* J Appl Physiol (1985), 2011. **110**(2): p. 309-17.
282. Pan, D., et al., *MicroRNA-378 controls classical brown fat expansion to counteract obesity.* Nat Commun, 2014. **5**: p. 4725.
283. Trajkovski, M. and H. Lodish, *MicroRNA networks regulate development of brown adipocytes.* Trends Endocrinol Metab. **24**(9): p. 442-50.
284. Sun, L., et al., *Mir193b-365 is essential for brown fat differentiation.* Nat Cell Biol. **13**(8): p. 958-65.
285. Cole, F., et al., *Positive regulation of myogenic bHLH factors and skeletal muscle development by the cell surface receptor CDO.* Dev Cell, 2004. **7**(6): p. 843-54.
286. Kang, J.S., et al., *CDO, a robo-related cell surface protein that mediates myogenic differentiation.* J Cell Biol, 1998. **143**(2): p. 403-13.
287. Feuermann, Y., et al., *MiR-193b and miR-365-1 are not required for the development and function of brown fat in the mouse.* RNA Biol. **10**(12): p. 1807-14.
288. Karbiener, M., et al., *MicroRNA-26 family is required for human adipogenesis and drives characteristics of brown adipocytes.* Stem Cells.
289. Wang, Y. and H.S. Sul, *Ectodomain shedding of preadipocyte factor 1 (Pref-1) by tumor necrosis factor alpha converting enzyme (TACE) and inhibition of adipocyte differentiation.* Mol Cell Biol, 2006. **26**(14): p. 5421-35.
290. Walden, T.B., et al., *Distinct expression of muscle-specific microRNAs (myomirs) in brown adipocytes.* J Cell Physiol, 2009. **218**(2): p. 444-9.
291. Trajkovski, M., et al., *MyomiR-133 regulates brown fat differentiation through Prdm16.* Nat Cell Biol. **14**(12): p. 1330-5.
292. Yin, H., F. Price, and M.A. Rudnicki, *Satellite cells and the muscle stem cell niche.* Physiol Rev. **93**(1): p. 23-67.

293. Chen, Y., et al., *miR-155 regulates differentiation of brown and beige adipocytes via a bistable circuit.* Nat Commun. **4**: p. 1769.
294. Kong, W., et al., *MicroRNA-155 is regulated by the transforming growth factor beta/Smad pathway and contributes to epithelial cell plasticity by targeting RhoA.* Mol Cell Biol, 2008. **28**(22): p. 6773-84.
295. Ignotz, R.A. and J. Massague, *Type beta transforming growth factor controls the adipogenic differentiation of 3T3 fibroblasts.* Proc Natl Acad Sci U S A, 1985. **82**(24): p. 8530-4.
296. Ramirez, C.M., et al., *MicroRNA 33 regulates glucose metabolism.* Mol Cell Biol. **33**(15): p. 2891-902.
297. Goedeke, L., et al., *A regulatory role for microRNA 33* in controlling lipid metabolism gene expression.* Mol Cell Biol. **33**(11): p. 2339-52.
298. Kiskinis, E., et al., *RIP140 represses the "brown-in-white" adipocyte program including a futile cycle of triacylglycerol breakdown and synthesis.* Mol Endocrinol, 2014. **28**(3): p. 344-56.
299. Sun, L. and M. Trajkovski, *MiR-27 orchestrates the transcriptional regulation of brown adipogenesis.* Metabolism. **63**(2): p. 272-82.
300. Lin, Q., et al., *A role of miR-27 in the regulation of adipogenesis.* Febs J, 2009. **276**(8): p. 2348-58.
301. Zhang, H., et al., *MicroRNA-455 regulates brown adipogenesis via a novel HIF1an-AMPK-PGC1alpha signaling network.* EMBO Rep, 2015. **16**(10): p. 1378-93.
302. Mori, M., et al., *Essential role for miR-196a in brown adipogenesis of white fat progenitor cells.* PLoS Biol, 2012. **10**(4): p. e1001314.
303. Yekta, S., I.H. Shih, and D.P. Bartel, *MicroRNA-directed cleavage of HOXB8 mRNA.* Science, 2004. **304**(5670): p. 594-6.
304. Liu, X., et al., *MicroRNA-138 suppresses invasion and promotes apoptosis in head and neck squamous cell carcinoma cell lines.* Cancer Lett, 2009. **286**(2): p. 217-22.
305. Yang, Z., et al., *MicroRNA hsa-miR-138 inhibits adipogenic differentiation of human adipose tissue-derived mesenchymal stem cells through adenovirus EID-1.* Stem Cells Dev, 2011. **20**(2): p. 259-67.
306. Lizcano, F. and D. Vargas, *EID1-induces brown-like adipocyte traits in white 3T3-L1 pre-adipocytes.* Biochem Biophys Res Commun, 2010. **398**(2): p. 160-5.
307. Vargas, D., et al., *Regulation of human subcutaneous adipocyte differentiation by EID1.* J Mol Endocrinol, 2016. **56**(2): p. 113-22.
308. Nardelli, C., et al., *miR-138/miR-222 Overexpression Characterizes the miRNome of Amniotic Mesenchymal Stem Cells in Obesity.* Stem Cells Dev, 2017. **26**(1): p. 4-14.
309. Wu, L., et al., *Profiling peripheral microRNAs in obesity and type 2 diabetes mellitus.* APMIS, 2015. **123**(7): p. 580-5.
310. Kinoshita, M., et al., *Regulation of adipocyte differentiation by activation of serotonin (5-HT) receptors 5-HT2AR and 5-HT2CR and involvement of microRNA-448-mediated repression of KLF5.* Mol Endocrinol, 2010. **24**(10): p. 1978-87.
311. Bork, S., et al., *Adipogenic differentiation of human mesenchymal stromal cells is down-regulated by microRNA-369-5p and up-regulated by microRNA-371.* J Cell Physiol, 2011. **226**(9): p. 2226-34.
312. Lee, E.K., et al., *miR-130 suppresses adipogenesis by inhibiting peroxisome proliferator-activated receptor gamma expression.* Mol Cell Biol, 2011. **31**(4): p. 626-38.
313. Zhu, Y., et al., *Downregulated miR-29a/b/c during Contact Inhibition Stage Promote 3T3-L1 Adipogenesis by Targeting DNMT3A.* PLoS One, 2017. **12**(1): p. e0170636.
314. Guo, W., et al., *Adipogenesis licensing and execution are disparately linked to cell proliferation.* Cell Res, 2009. **19**(2): p. 216-23.

315. Lee, M.J., Y. Wu, and S.K. Fried, *A modified protocol to maximize differentiation of human preadipocytes and improve metabolic phenotypes.* Obesity (Silver Spring). **20**(12): p. 2334-40.
316. Klemm, D.J., et al., *Insulin-induced adipocyte differentiation. Activation of CREB rescues adipogenesis from the arrest caused by inhibition of prenylation.* J Biol Chem, 2001. **276**(30): p. 28430-5.
317. Hancock, J.F., et al., *All ras proteins are polyisoprenylated but only some are palmitoylated.* Cell, 1989. **57**(7): p. 1167-77.
318. Chapman, A.B., et al., *Analysis of gene expression during differentiation of adipogenic cells in culture and hormonal control of the developmental program.* J Biol Chem, 1984. **259**(24): p. 15548-55.
319. Essayan, D.M., *Cyclic nucleotide phosphodiesterases.* J Allergy Clin Immunol, 2001. **108**(5): p. 671-80.
320. Obregon, M.J., *Thyroid hormone and adipocyte differentiation.* Thyroid, 2008. **18**(2): p. 185-95.
321. Guerra, C., et al., *Triiodothyronine induces the transcription of the uncoupling protein gene and stabilizes its mRNA in fetal rat brown adipocyte primary cultures.* J Biol Chem, 1996. **271**(4): p. 2076-81.
322. Styner, M., et al., *Indomethacin promotes adipogenesis of mesenchymal stem cells through a cyclooxygenase independent mechanism.* J Cell Biochem. **111**(4): p. 1042-50.
323. Irshad, Z., et al., *Diacylglycerol acyltransferase 2 (DGAT2) links glucose utilization to fatty acid oxidation in the brown adipocytes.* J Lipid Res, 2016.
324. Rosell, M., et al., *Brown and white adipose tissues: intrinsic differences in gene expression and response to cold exposure in mice.* Am J Physiol Endocrinol Metab. **306**(8): p. E945-64.
325. Collins, J.M., et al., *De novo lipogenesis and stearoyl-CoA desaturase are coordinately regulated in the human adipocyte and protect against palmitate-induced cell injury.* J Biol Chem, 2010. **285**(9): p. 6044-52.
326. Pinnick, K.E., et al., *Distinct developmental profile of lower-body adipose tissue defines resistance against obesity-associated metabolic complications.* Diabetes, 2014. **63**(11): p. 3785-97.
327. Kauppinen, S., B. Vester, and J. Wengel, *Locked nucleic acid (LNA): High affinity targeting of RNA for diagnostics and therapeutics.* Drug Discov Today Technol, 2005. **2**(3): p. 287-90.
328. Mestdagh, P., et al., *A novel and universal method for microRNA RT-qPCR data normalization.* Genome Biol, 2009. **10**(6): p. R64.
329. Ritchie, M.E., et al., *A comparison of background correction methods for two-colour microarrays.* Bioinformatics, 2007. **23**(20): p. 2700-7.
330. Sanger, F., S. Nicklen, and A.R. Coulson, *DNA sequencing with chain-terminating inhibitors.* Proc Natl Acad Sci U S A, 1977. **74**(12): p. 5463-7.
331. Maragkakis, M., et al., *DIANA-microT Web server upgrade supports Fly and Worm miRNA target prediction and bibliographic miRNA to disease association.* Nucleic Acids Res, 2011. **39**(Web Server issue): p. W145-8.
332. Friedman, R.C., et al., *Most mammalian mRNAs are conserved targets of microRNAs.* Genome Res, 2009. **19**(1): p. 92-105.
333. Webber, J. and A. Clayton, *How pure are your vesicles?* J Extracell Vesicles, 2013. **2**.
334. Kao, L.S. and C.E. Green, *Analysis of variance: is there a difference in means and what does it mean?* J Surg Res, 2008. **144**(1): p. 158-70.
335. Tukey, J.W., *Comparing individual means in the analysis of variance.* Biometrics, 1949. **5**(2): p. 99-114.

336. Dunnett, C.W., Journal of the American Statistical Association. **75**: p. 789-795.
337. Kanehisa, M., et al., *KEGG for integration and interpretation of large-scale molecular data sets.* Nucleic Acids Res, 2012. **40**(Database issue): p. D109-14.
338. Guller, I., et al., *Comparative analysis of microRNA expression in mouse and human brown adipose tissue.* BMC Genomics, 2015. **16**: p. 820.
339. Hu, J., et al., *Short-Chain Fatty Acid Acetate Stimulates Adipogenesis and Mitochondrial Biogenesis via GPR43 in Brown Adipocytes.* Endocrinology, 2016. **157**(5): p. 1881-94.
340. Liu, S.Y., et al., *MiR-378 Plays an Important Role in the Differentiation of Bovine Preadipocytes.* Cell Physiol Biochem, 2015. **36**(4): p. 1552-62.
341. Zhang, Y., et al., *miR-378 Activates the Pyruvate-PEP Futile Cycle and Enhances Lipolysis to Ameliorate Obesity in Mice.* EBioMedicine, 2016. **5**: p. 93-104.
342. Sun, L., et al., *Mir193b-365 is essential for brown fat differentiation.* Nat Cell Biol, 2011. **13**(8): p. 958-65.
343. Feuermann, Y., et al., *MiR-193b and miR-365-1 are not required for the development and function of brown fat in the mouse.* RNA Biol, 2013. **10**(12): p. 1807-14.
344. Gamez, B., et al., *MicroRNA-322 (miR-322) and its target protein Tob2 modulate Osterix (Osx) mRNA stability.* J Biol Chem, 2013. **288**(20): p. 14264-75.
345. Zhang, K., et al., *MicroRNA-322 inhibits inflammatory cytokine expression and promotes cell proliferation in LPS-stimulated murine macrophages by targeting NF-kappaB1 (p50).* Biosci Rep, 2017. **37**(1).
346. Marchand, A., et al., *miR-322 regulates insulin signaling pathway and protects against metabolic syndrome-induced cardiac dysfunction in mice.* Biochim Biophys Acta, 2016. **1862**(4): p. 611-21.
347. Trajkovski, M., et al., *MicroRNAs 103 and 107 regulate insulin sensitivity.* Nature, 2011. **474**(7353): p. 649-53.
348. Pescador, N., et al., *Serum circulating microRNA profiling for identification of potential type 2 diabetes and obesity biomarkers.* PLoS One, 2013. **8**(10): p. e77251.
349. Shinoda, K., et al., *Genetic and functional characterization of clonally derived adult human brown adipocytes.* Nat Med, 2015. **21**(4): p. 389-94.
350. Kazantzis, M., et al., *PAZ6 cells constitute a representative model for human brown pre-adipocytes.* Front Endocrinol (Lausanne), 2012. **3**: p. 13.
351. Xue, R., et al., *Clonal analyses and gene profiling identify genetic biomarkers of the thermogenic potential of human brown and white preadipocytes.* Nat Med, 2015. **21**(7): p. 760-8.
352. Liu, W., et al., *A heterogeneous lineage origin underlies the phenotypic and molecular differences of white and beige adipocytes.* J Cell Sci, 2013. **126**(Pt 16): p. 3527-32.
353. Carey, A.L., et al., *Reduced UCP-1 content in in vitro differentiated beige/brite adipocytes derived from preadipocytes of human subcutaneous white adipose tissues in obesity.* PLoS One, 2014. **9**(3): p. e91997.
354. Kusminski, C.M. and P.E. Scherer, *Mitochondrial dysfunction in white adipose tissue.* Trends Endocrinol Metab, 2012. **23**(9): p. 435-43.
355. Kim, B.S., et al., *Nuclear Argonaute 2 regulates adipose tissue-derived stem cell survival through direct control of miR10b and selenoprotein N1 expression.* Aging Cell, 2011. **10**(2): p. 277-91.
356. Bonifacio, L.N. and M.B. Jarstfer, *MiRNA profile associated with replicative senescence, extended cell culture, and ectopic telomerase expression in human foreskin fibroblasts.* PLoS One, 2010. **5**(9).
357. Huang, N., et al., *MiR-378a-3p enhances adipogenesis by targeting mitogen-activated protein kinase 1.* Biochem Biophys Res Commun, 2015. **457**(1): p. 37-42.

358. Francis, S.H., M.A. Blount, and J.D. Corbin, *Mammalian cyclic nucleotide phosphodiesterases: molecular mechanisms and physiological functions.* Physiol Rev, 2011. **91**(2): p. 651-90.
359. Hua, Z., et al., *MiRNA-directed regulation of VEGF and other angiogenic factors under hypoxia.* PLoS One, 2006. **1**: p. e116.
360. Narita, K., et al., *HSulf-1 inhibits angiogenesis and tumorigenesis in vivo.* Cancer Res, 2006. **66**(12): p. 6025-32.
361. Rosen, S.D. and H. Lemjabbar-Alaoui, *Sulf-2: an extracellular modulator of cell signaling and a cancer target candidate.* Expert Opin Ther Targets, 2010. **14**(9): p. 935-49.
362. Hyun, J., et al., *MicroRNA-378 limits activation of hepatic stellate cells and liver fibrosis by suppressing Gli3 expression.* Nat Commun, 2016. **7**: p. 10993.
363. Tanzer, A., et al., *Evolution of microRNAs located within Hox gene clusters.* J Exp Zool B Mol Dev Evol, 2005. **304**(1): p. 75-85.
364. Luthra, R., et al., *MicroRNA-196a targets annexin A1: a microRNA-mediated mechanism of annexin A1 downregulation in cancers.* Oncogene, 2008. **27**(52): p. 6667-78.
365. Zhang, J., et al., *miR-196a targets netrin 4 and regulates cell proliferation and migration of cervical cancer cells.* Biochem Biophys Res Commun, 2013. **440**(4): p. 582-8.
366. Hou, T., et al., *MicroRNA-196a promotes cervical cancer proliferation through the regulation of FOXO1 and p27Kip1.* Br J Cancer, 2014. **110**(5): p. 1260-8.
367. Mueller, D.W. and A.K. Bosserhoff, *MicroRNA miR-196a controls melanoma-associated genes by regulating HOX-C8 expression.* Int J Cancer, 2011. **129**(5): p. 1064-74.
368. Gesta, S., Y.H. Tseng, and C.R. Kahn, *Developmental origin of fat: tracking obesity to its source.* Cell, 2007. **131**(2): p. 242-56.
369. Schulz, T.J., et al., *Identification of inducible brown adipocyte progenitors residing in skeletal muscle and white fat.* Proc Natl Acad Sci U S A, 2011. **108**(1): p. 143-8.
370. Zhang, X., et al., *Adipose tissue-specific inhibition of hypoxia-inducible factor 1{alpha} induces obesity and glucose intolerance by impeding energy expenditure in mice.* J Biol Chem, 2010. **285**(43): p. 32869-77.
371. Glomski, K., et al., *Deletion of Adam10 in endothelial cells leads to defects in organ-specific vascular structures.* Blood, 2011. **118**(4): p. 1163-74.
372. MacLellan, W.R., et al., *A novel Rb- and p300-binding protein inhibits transactivation by MyoD.* Mol Cell Biol, 2000. **20**(23): p. 8903-15.
373. Miyake, S., et al., *Cells degrade a novel inhibitor of differentiation with E1A-like properties upon exiting the cell cycle.* Mol Cell Biol, 2000. **20**(23): p. 8889-902.
374. Jager, J., et al., *Interleukin-1beta-induced insulin resistance in adipocytes through down-regulation of insulin receptor substrate-1 expression.* Endocrinology, 2007. **148**(1): p. 241-51.
375. Arroyo, J.D., et al., *Argonaute2 complexes carry a population of circulating microRNAs independent of vesicles in human plasma.* Proc Natl Acad Sci U S A, 2011. **108**(12): p. 5003-8.
376. Thery, C., et al., *Isolation and characterization of exosomes from cell culture supernatants and biological fluids.* Curr Protoc Cell Biol, 2006. **Chapter 3**: p. Unit 3 22.
377. Escola, J.M., et al., *Selective enrichment of tetraspan proteins on the internal vesicles of multivesicular endosomes and on exosomes secreted by human B-lymphocytes.* J Biol Chem, 1998. **273**(32): p. 20121-7.
378. Fevrier, B. and G. Raposo, *Exosomes: endosomal-derived vesicles shipping extracellular messages.* Curr Opin Cell Biol, 2004. **16**(4): p. 415-21.
379. Ferrante, S.C., et al., *Adipocyte-derived exosomal miRNAs: a novel mechanism for obesity-related disease.* Pediatr Res, 2015. **77**(3): p. 447-54.

380. Beck, V., et al., *Polyunsaturated fatty acids activate human uncoupling proteins 1 and 2 in planar lipid bilayers.* FASEB J, 2007. **21**(4): p. 1137-44.
381. Stanford, K.I., et al., *Brown adipose tissue regulates glucose homeostasis and insulin sensitivity.* J Clin Invest, 2013. **123**(1): p. 215-23.
382. van der Burg, J.M., et al., *Increased metabolism in the R6/2 mouse model of Huntington's disease.* Neurobiol Dis, 2008. **29**(1): p. 41-51.
383. McCourt, A.C., et al., *White Adipose Tissue Browning in the R6/2 Mouse Model of Huntington's Disease.* PLoS One, 2016. **11**(8): p. e0159870.
384. Gutierrez, D.A., M.J. Puglisi, and A.H. Hasty, *Impact of increased adipose tissue mass on inflammation, insulin resistance, and dyslipidemia.* Curr Diab Rep, 2009. **9**(1): p. 26-32.
385. van Kruijsdijk, R.C., E. van der Wall, and F.L. Visseren, *Obesity and cancer: the role of dysfunctional adipose tissue.* Cancer Epidemiol Biomarkers Prev, 2009. **18**(10): p. 2569-78.
386. Must, A. and N.M. McKeown, *The Disease Burden Associated with Overweight and Obesity*, in *Endotext*, L.J. De Groot, et al., Editors. 2000: South Dartmouth (MA).
387. Yang, Y., et al., *miR-29b Targets LPL and TDG Genes and Regulates Apoptosis and Triglyceride Production in MECs.* DNA Cell Biol, 2016. **35**(12): p. 758-765.
388. Hiraga, T., S. Ito, and H. Nakamura, *Cancer stem-like cell marker CD44 promotes bone metastases by enhancing tumorigenicity, cell motility, and hyaluronan production.* Cancer Res, 2013. **73**(13): p. 4112-22.
389. Lee, Y.H., A.P. Petkova, and J.G. Granneman, *Identification of an adipogenic niche for adipose tissue remodeling and restoration.* Cell Metab, 2013. **18**(3): p. 355-67.
390. Logan, S.M., B.E. Luu, and K.B. Storey, *Turn down genes for WAT? Activation of anti-apoptosis pathways protects white adipose tissue in metabolically depressed thirteen-lined ground squirrels.* Mol Cell Biochem, 2016. **416**(1-2): p. 47-62.
391. Zhou, Z., et al., *Cellular reprogramming into a brown adipose tissue-like phenotype by co-expression of HB-EGF and ADAM 12S.* Growth Factors, 2013. **31**(6): p. 185-98.
392. Matloubian, M., et al., *A transmembrane CXC chemokine is a ligand for HIV-coreceptor Bonzo.* Nat Immunol, 2000. **1**(4): p. 298-304.
393. Wilbanks, A., et al., *Expression cloning of the STRL33/BONZO/TYMSTRligand reveals elements of CC, CXC, and CX3C chemokines.* J Immunol, 2001. **166**(8): p. 5145-54.
394. Tohyama, M., et al., *CXCL16 is a novel mediator of the innate immunity of epidermal keratinocytes.* Int Immunol, 2007. **19**(9): p. 1095-102.
395. Rauner, M., et al., *WNT5A is induced by inflammatory mediators in bone marrow stromal cells and regulates cytokine and chemokine production.* J Bone Miner Res, 2012. **27**(3): p. 575-85.
396. Rivera-Gonzalez, G.C., et al., *Skin Adipocyte Stem Cell Self-Renewal Is Regulated by a PDGFA/AKT-Signaling Axis.* Cell Stem Cell, 2016. **19**(6): p. 738-751.
397. Marcelin, G., et al., *A PDGFRalpha-Mediated Switch toward CD9high Adipocyte Progenitors Controls Obesity-Induced Adipose Tissue Fibrosis.* Cell Metab, 2017. **25**(3): p. 673-685.
398. Ng, M., et al., *Global, regional, and national prevalence of overweight and obesity in children and adults during 1980-2013: a systematic analysis for the Global Burden of Disease Study 2013.* Lancet, 2014. **384**(9945): p. 766-81.
399. Kahlmeier, S., et al., *National physical activity recommendations: systematic overview and analysis of the situation in European countries.* BMC Public Health, 2015. **15**: p. 133.
400. Ruiz, M., et al., *Impact of Low Maternal Education on Early Childhood Overweight and Obesity in Europe.* Paediatr Perinat Epidemiol, 2016. **30**(3): p. 274-84.
401. Sun, T., et al., *MicroRNA let-7 regulates 3T3-L1 adipogenesis.* Mol Endocrinol, 2009. **23**(6): p. 925-31.

402. Kuehbacher, A., et al., *Role of Dicer and Drosha for endothelial microRNA expression and angiogenesis.* Circ Res, 2007. **101**(1): p. 59-68.
403. Bonauer, A., R.A. Boon, and S. Dimmeler, *Vascular microRNAs.* Curr Drug Targets, 2010. **11**(8): p. 943-9.
404. Barh, D., et al., *miRegulome: a knowledge-base of miRNA regulomics and analysis.* Sci Rep, 2015. **5**: p. 12832.
405. Xu, Z., et al., *miR-365, a novel negative regulator of interleukin-6 gene expression, is cooperatively regulated by Sp1 and NF-kappaB.* J Biol Chem, 2011. **286**(24): p. 21401-12.
406. Shen, X., et al., *Heparin impairs angiogenesis through inhibition of microRNA-10b.* J Biol Chem, 2011. **286**(30): p. 26616-27.
407. Wang, X., et al., *MicroRNA-10a/10b represses a novel target gene mib1 to regulate angiogenesis.* Cardiovasc Res, 2016. **110**(1): p. 140-50.
408. Sun, X.J., et al., *miR-10b promotes migration and invasion in nasopharyngeal carcinoma cells.* Asian Pac J Cancer Prev, 2013. **14**(9): p. 5533-7.
409. Wang, Y.Y., et al., *MicroRNA-10b promotes migration and invasion through Hoxd10 in human gastric cancer.* World J Surg Oncol, 2015. **13**: p. 259.
410. Li, Q.J., et al., *MicroRNA-10b promotes migration and invasion through CADM1 in human hepatocellular carcinoma cells.* Tumour Biol, 2012. **33**(5): p. 1455-65.
411. Liu, Y., et al., *MicroRNA-10b overexpression promotes non-small cell lung cancer cell proliferation and invasion.* Eur J Med Res, 2013. **18**: p. 41.
412. Chen, L., et al., *miR-10b-5p is a novel Th17 regulator present in Th17 cells from ankylosing spondylitis.* Ann Rheum Dis, 2017. **76**(3): p. 620-625.
413. Garidou, L., et al., *The Gut Microbiota Regulates Intestinal CD4 T Cells Expressing RORgammat and Controls Metabolic Disease.* Cell Metab, 2015. **22**(1): p. 100-12.
414. Xie, H., B. Lim, and H.F. Lodish, *MicroRNAs induced during adipogenesis that accelerate fat cell development are downregulated in obesity.* Diabetes, 2009. **58**(5): p. 1050-7.
415. Ortega, F.J., et al., *MiRNA expression profile of human subcutaneous adipose and during adipocyte differentiation.* PLoS One, 2010. **5**(2): p. e9022.
416. Wilson, R., et al., *MicroRNA regulation of endothelial TREX1 reprograms the tumour microenvironment.* Nat Commun, 2016. **7**: p. 13597.
417. Ghosh, G., et al., *Hypoxia-induced microRNA-424 expression in human endothelial cells regulates HIF-alpha isoforms and promotes angiogenesis.* J Clin Invest, 2010. **120**(11): p. 4141-54.
418. Kamura, T., et al., *VHL-box and SOCS-box domains determine binding specificity for Cul2-Rbx1 and Cul5-Rbx2 modules of ubiquitin ligases.* Genes Dev, 2004. **18**(24): p. 3055-65.
419. Forrest, A.R., et al., *Induction of microRNAs, mir-155, mir-222, mir-424 and mir-503, promotes monocytic differentiation through combinatorial regulation.* Leukemia, 2010. **24**(2): p. 460-6.
420. Chen, X., *A microRNA as a translational repressor of APETALA2 in Arabidopsis flower development.* Science, 2004. **303**(5666): p. 2022-5.
421. Poy, M.N., et al., *A pancreatic islet-specific microRNA regulates insulin secretion.* Nature, 2004. **432**(7014): p. 226-30.
422. Kuhn, D.E., et al., *Experimental validation of miRNA targets.* Methods, 2008. **44**(1): p. 47-54.
423. Thomson, D.W., C.P. Bracken, and G.J. Goodall, *Experimental strategies for microRNA target identification.* Nucleic Acids Res, 2011. **39**(16): p. 6845-53.
424. Huang, Y., et al., *A study of miRNAs targets prediction and experimental validation.* Protein Cell, 2010. **1**(11): p. 979-86.

425. Kohan, D.E., *Progress in gene targeting: using mutant mice to study renal function and disease.* Kidney Int, 2008. **74**(4): p. 427-37.
426. Lee, S.C., et al., *Differential regulation of ca(2+) signaling and membrane trafficking by multiple p2 receptors in brown adipocytes.* J Membr Biol, 2005. **207**(3): p. 131-42.